N+3 Aircraft Concept Designs and Trade Studies, Final Report

Volume 1

E.M. Greitzer, P.A. Bonnefoy, E. De la Rosa Blanco, C.S. Dorbian, M. Drela,
D.K. Hall, R.J. Hansman, J.I. Hileman, R.H. Liebeck, J. Lovegren, P. Mody,
J.A. Pertuze, S. Sato, Z.S. Spakovszky, and C.S. Tan
Massachusetts Institute of Technology, Cambridge, Massachusetts

J.S. Hollman, J.E. Duda, N. Fitzgerald, J. Houghton, J.L. Kerrebrock, G.F. Kiwada,
D. Kordonowy, J.C. Parrish, J. Tylko, and E.A. Wen
Aurora Flight Sciences, Cambridge, Massachusetts

W.K. Lord
Pratt & Whitney, East Hartford, Connecticut

NASA STI Program . . . in Profile

Since its founding, NASA has been dedicated to the advancement of aeronautics and space science. The NASA Scientific and Technical Information (STI) program plays a key part in helping NASA maintain this important role.

The NASA STI Program operates under the auspices of the Agency Chief Information Officer. It collects, organizes, provides for archiving, and disseminates NASA's STI. The NASA STI program provides access to the NASA Aeronautics and Space Database and its public interface, the NASA Technical Reports Server, thus providing one of the largest collections of aeronautical and space science STI in the world. Results are published in both non-NASA channels and by NASA in the NASA STI Report Series, which includes the following report types:

- TECHNICAL PUBLICATION. Reports of completed research or a major significant phase of research that present the results of NASA programs and include extensive data or theoretical analysis. Includes compilations of significant scientific and technical data and information deemed to be of continuing reference value. NASA counterpart of peer-reviewed formal professional papers but has less stringent limitations on manuscript length and extent of graphic presentations.

- TECHNICAL MEMORANDUM. Scientific and technical findings that are preliminary or of specialized interest, e.g., quick release reports, working papers, and bibliographies that contain minimal annotation. Does not contain extensive analysis.

- CONTRACTOR REPORT. Scientific and technical findings by NASA-sponsored contractors and grantees.

- CONFERENCE PUBLICATION. Collected papers from scientific and technical conferences, symposia, seminars, or other meetings sponsored or cosponsored by NASA.

- SPECIAL PUBLICATION. Scientific, technical, or historical information from NASA programs, projects, and missions, often concerned with subjects having substantial public interest.

- TECHNICAL TRANSLATION. English-language translations of foreign scientific and technical material pertinent to NASA's mission.

Specialized services also include creating custom thesauri, building customized databases, organizing and publishing research results.

For more information about the NASA STI program, see the following:

- Access the NASA STI program home page at *http://www.sti.nasa.gov*

- E-mail your question via the Internet to *help@sti.nasa.gov*

- Fax your question to the NASA STI Help Desk at 443–757–5803

- Telephone the NASA STI Help Desk at 443–757–5802

- Write to:
  NASA Center for AeroSpace Information (CASI)
  7115 Standard Drive
  Hanover, MD 21076–1320

N+3 Aircraft Concept Designs and Trade Studies, Final Report
Volume 1

E.M. Greitzer, P.A. Bonnefoy, E. De la Rosa Blanco, C.S. Dorbian, M. Drela,
D.K. Hall, R.J. Hansman, J.I. Hileman, R.H. Liebeck, J. Lovegren, P. Mody,
J.A. Pertuze, S. Sato, Z.S. Spakovszky, and C.S. Tan
Massachusetts Institute of Technology, Cambridge, Massachusetts

J.S. Hollman, J.E. Duda, N. Fitzgerald, J. Houghton, J.L. Kerrebrock, G.F. Kiwada,
D. Kordonowy, J.C. Parrish, J. Tylko, and E.A. Wen
Aurora Flight Sciences, Cambridge, Massachusetts

W.K. Lord
Pratt & Whitney, East Hartford, Connecticut

National Aeronautics and
Space Administration

Glenn Research Center
Cleveland, Ohio 44135

December 2010

Acknowledgments

This report contains preliminary findings, subject to revision as analysis proceeds.

This work was sponsored by the Fundamental Aeronautics Program at the NASA Glenn Research Center.

Level of Review: This material has been technically reviewed by NASA technical management.

Available from

NASA Center for Aerospace Information	National Technical Information Service
7115 Standard Drive	5301 Shawnee Road
Hanover, MD 21076–1320	Alexandria, VA 22312

Available electronically at http://gltrs.grc.nasa.gov

Program Abstract

MIT, Aerodyne Research, Aurora Flight Sciences, and Pratt & Whitney have collaborated to address NASA's desire to pursue revolutionary conceptual designs for a subsonic commercial transport that could enter service in the 2035 timeframe. The MIT team brings together multidisciplinary expertise and cutting-edge technologies to determine, in a rigorous and objective manner, the potential for improvements in noise, emissions and performance for subsonic fixed wing transport aircraft. The collaboration incorporates assessment of the trade space in aerodynamics, propulsion, operations, and structures to ensure that the full spectrum of improvements is identified. Although the analysis focuses on these key areas, the team has taken a *system-level approach* to find the integrated solutions that offer the best balance in performance enhancements. Based on the trade space analyses and system-level assessment, two aircraft have been identified and carried through *conceptual design* to show both the *in-depth engineering* that underpins the benefits envisioned and also the *technology paths* that need to be followed to enable, within the next 25 years, the development of aircraft three generations ahead in capabilities from those flying today.

Table of Contents

Appendices included in separate volume, "Design Methodologies for Aerodynamics, Structures, Weight, and Thermodynamic Cycles."

1 Executive Summary

Content and Scope of the Report

This final report for the NASA N+3 Phase 1 project "Aircraft and Technology Concepts for an N+3 Subsonic Transport" represents the results of research carried out from 1 September 2008 to 31 March 2010 by a team from MIT, Aerodyne Research, Aurora Flight Sciences, and Pratt&Whitney.

This research included development of the conceptual design of two advanced civil aircraft for the 2030-2035 time period, as well as trade studies relating aircraft performance (fuel burn, field length requirement), noise, and emissions for the defined mission to each of the identified advanced technologies, and specific steps needed to advance these technologies. The principal findings are summarized in this section.

Scenario Development as a Driver for Aircraft Selection

To define the conditions that aircraft attributes must address in the 2030-2035 timeframe, we have developed a scenario that adopts the economic, environmental, and mobility issues expected to exist at that time. This scenario drove the requirements specifications for the design of two conceptual aircraft that targeted the NASA N+3 goals. The missions of the two were selected from different market segments, but chosen so together they would represent a substantial fraction of the commercial fleet; this in turn implies that adoption of such a design could have major impact on fleet-wide fuel burn, noise, emissions, and airport utilization. One aircraft addresses the role currently filled by the B737/Airbus A320 class, accommodating 180 passengers for 500 nm to transcontinental range trip length. The other is aimed at the market served by a B777, accommodating 350 passengers in a multiclass configuration with cargo and a range of at least 7000 nm. For both, the passenger trip time was also taken into account in the design of the concept aircraft.

N+3 Aircraft Configurations

The two aircraft designs developed to carry out these missions have very different configurations. The aircraft intended to serve the B737/A320 mission is a "double-bubble", i.e. a double-tube and wing design, referred to as the D8 Series. The aircraft intended to serve the B777 mission is a hybrid wing body, referred to as the H3 Series. The two aircraft concepts are shown in Figure 1.

Figure 1: Double-bubble (D8 Series) and hybrid wing body (H3 Series) conceptual aircraft.

Aircraft Performance in Terms of NASA N+3 Metrics

The capabilities of the two aircraft are given in Tables 1a and 1b, which show the NASA metrics, the baseline aircraft, the N+3 goals and the calculated performance. The items in italics in the fourth column are those in which the N+3 goals were met or exceeded. The D8 Series (double-bubble) can be seen to

achieve three of the NASA N+3 metrics and nearly achieves the fourth (noise.) The H3 (hybrid wing body) meets only one of the goals (emissions), although there are substantial gains towards the other three aggressive targets. The potential of the hybrid wing body configuration has been recognized by NASA and others, but the D8 Series is a new configuration whose design was developed as a direct result of the N+3 Phase 1 program. *The performance levels achieved by the two configurations are the first major finding from the Phase 1 project.*

Table 1a: Performance of Double-Bubble (D8 Series) Aircraft (B737-800 Baseline)

NASA Metric	Baseline (B737-800)	N+3 Goals	Double-bubble (D8.5)
Fuel Burn (Represented by Payload Fuel Energy Intensity, PFEI, in [KJ/kg-km])	7.43	2.23 (70% reduction)	*2.17 (70.87% reduction)*
Noise [EPNdB] (EPNdB below Stage 4)	277	202 (-71 EPNdB)	213 (-60 EPNdB)
LTO NOx [g/KN] (% below CAEP 6)	43.28 (31% below CAEP 6)	>75% reduction	*10.5 (87.3% reduction)*
Field Length [ft]	7680 ft for 300 nm mission	Metroplex	*5000*

Table 1b: Performance of Hybrid Wing Body (H3) Aircraft (B777-200LR Baseline)

NASA Metric	Baseline (B777-200LR)	N+3 Goals	Hybrid Wing-Body (H3.2)
Fuel Burn [KJ/kg-km]	5.94	1.78 (70% reduction)	2.75 (53.7% reduction)
Noise [EPNdB] (EPNdB below Stage 4)	288	217 (-71 EPNdB)	242 (-46 EPNdB)
LTO NOx [g/KN] (% below CAEP 6)	67.9	>75% reduction	*18.6 (81% reduction)*
Field Length [ft]	10000	Metroplex	9000

Aircraft Performance Trends (Scaling) with Payload

The trade studies we conducted show that the two aircraft configurations scale differently in terms of size and payload. One example is given in Figure 2, showing fuel burn as a function of payload. In this case, over the range examined, the double-bubble gives better fuel burn at the B737 size and payload than at the higher payload, whereas the hybrid wing body achieves its best fuel burn at the B777 size and payload. However, even at the larger size the double-bubble configuration gives essentially the same performance (NASA metrics) as the hybrid-wing body. Put more strongly, *the second major finding is that although both configurations gave substantial benefits compared to the baselines, for the range of aircraft we examined the double-bubble configuration exhibited better performance (or equal performance for very large sizes/payloads) compared to the hybrid wing body.*
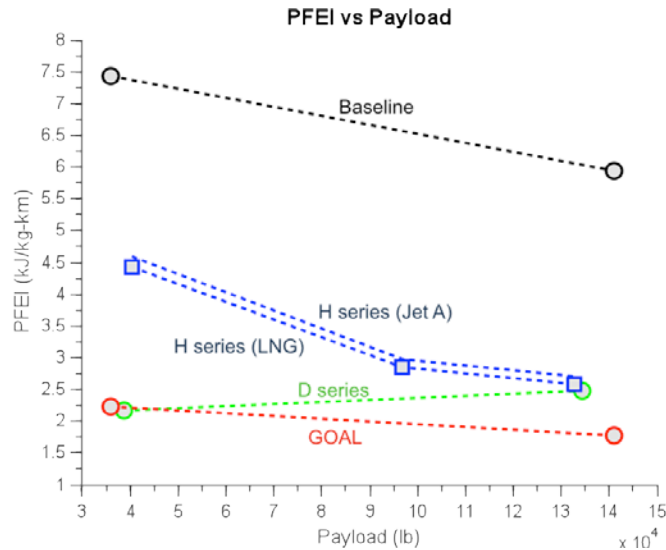
Figure 2: Fuel burn performance of double-bubble and hybrid wing body aircraft versus payload.

Benefits from Configuration Changes vs. Benefits from Technology Advancements

A third result stems from our investigation of specific contributions to the performance of the D8 Series aircraft. The benefits seen in the N+3 aircraft concepts are from two sources: first, advances in specific technologies, such as stronger and lighter materials, higher efficiency engine components, turbine materials with increased temperature capability, others; second, the inherent benefit of the *aircraft configuration*. In other words, even given today's technologies (aluminum wings and fuselage, current technology engines with current bypass ratios, etc.), there is a major performance benefit from the use of the configuration alone. This is demonstrated explicitly in the report through calculations that "morph" a B737 into a D8, so the contribution of each element of the configuration change can be determined.

This finding relating to the benefit of the configuration change is shown in Figure 3, which compares benefits of configuration change with benefits due to advanced technologies for fuel burn, noise, and LTO NOx (all D8 aircraft meet the 5000 foot takeoff goal). There is a 49% reduction in fuel burn compared to the baseline, a 40 EPNdB decrease in noise relative to Stage 4, and a 52% reduction in LTO NOx compared to the CAEP 6 standard, provided by the configuration alone for the D8 Series; the technology improvements then bring this number to the total level of improvement given in Table 1. The D8.1 configuration includes the benefits of boundary layer ingestion on the top surface of the fuselage, a slightly increased OPR from the B737 baseline, and a present day but optimized engine cycle for the D8.1 application. *The significant step change in capability provided by the D8 Series configuration is the third, but perhaps the most important, finding of this project.* It implies that an aircraft configuration change has the potential to alter the face of commercial aviation. Further, as the development of the configuration itself is fairly straightforward, this change could occur on a much shorter time scale than required for maturation of many separate technologies.
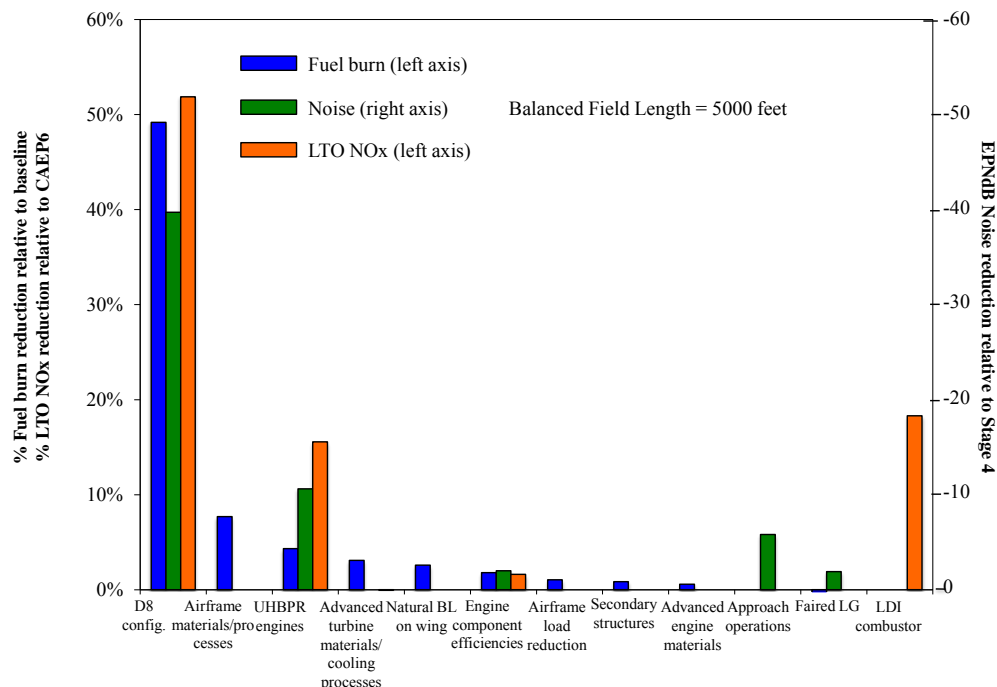
Figure 3: Improvement in N+3 metrics from configuration change and from technology advances.

Determination of Critical Technology Issues

An important complement to the design process was an impact analysis various technologies on aircraft performance. The conclusion of the previous section, that aircraft configuration is the major contributor to the N+3 goals, illustrates what we see as the critical technology challenge to be resolved: propulsion system-airframe integration.

The D8 Series is an integrated configuration that makes use of boundary layer ingestion and unconventional engine placement, with three engines on top of the aft end of the fuselage. Engine placement is such that there is little diffusion upstream of the inlet or in the inlet, so the influence of ingestion can be considerably less than for an S-duct inlet. However, the configuration results in an exhaust flow geometry with three adjacent streams and, for example, a possibility of base drag. The parameters that are affected as part of this integration include aircraft drag, engine performance in the resulting inlet distortion (effect on fuel burn and thrust, effect on aerodynamic stability, effect on aeromechanics), and noise due to the non-uniformity. *The fourth major finding is that the consideration of propulsion system-airframe integration issues, and thus the in-depth assessment of the D8 Series feasibility, is the highest priority for future study.*

While the above stands out as the main technology topic, there are other technology areas of high interest that are described in the report. A second important challenge is the capability for development of high-efficiency cores at the small sizes that are implied by the interlocking requirements of ultra high bypass ratio, increases in cycle pressure ratio, and aircraft with much improved drag characteristics and thus lower thrust requirements.

University-Industry Collaboration: Process and Results

As a final point, there are two related aspects of the university-industry collaboration that are worth describing. The first was the virtually seamless interaction between the different organizations. The second, enabled by the first, was the strong emphasis on what is perhaps best described as the *primacy of ideas* rather than of organization or hierarchy. In other words, concepts and suggestions were considered directly on merit (e.g. content, strategic value, or impact) rather than the originator of the idea, or the legacy of the idea. From the start of the project (and as described in our proposal in 2008) this was emphasized and fostered explicitly in team discussions. The consequence was that the team functioned with open-mindedness to new ideas and, as a direct corollary, a willingness to subject even cherished concepts to in-depth scrutiny; there were several strongly held beliefs that were challenged and altered during the course of the project.

In sum, the goal was to create a team in which "the whole was greater than the sum of the parts" because of strong interactions between participants. *Capacity for achievement of this type of enterprise involving students, staff, faculty, and engineers in industry from a number of fields is also a major finding of the project.*

1.1 Configuration Definition

Throughout this report several aircraft configurations will be used to describe the performance of the different aircraft concepts as combined with the mission scenarios and various advanced technologies. Table 2 details the various configurations with a description of the purpose of that.

Table 2: Concept aircraft configurations

Configuration	Description
737-800	D series baseline aircraft for NASA Goal Comparison
B777-200LR	H series baseline aircraft for NASA goal comparison
D8.1	D8 "double bubble" fuselage with cantilever wing, Pi tail, aluminum structure, CFM-56 class optimized engines with boundary layer ingestion
D8.5	D8 "double bubble fuselage" with cantilever wing, Pi tail, advanced composite structures, ultra high-bypass engines, advanced materials and components, with BLI and with natural laminar flow on the bottom wing and other 2035 advanced technology insertion.
SD8.1	Strut-braced version of D8.1 that examines feasibility of a strut-braced wing with aluminum structure
SD8.5	Strut-braced version of D8.5 that examines feasibility of a strut-braced wing with advanced composite structures
H3.B	Hybrid Wing Body fuselage with three podded, high-bypass ratio geared engines
H3.2	Hybrid Wing Body fuselage with advanced composite materials, with an ultra high-bypass ratio distributed propulsion system (two turbogenerators and four propulsors), and boundary layer ingestion.
H3.2Q	Hybrid Wing Body fuselage with advanced composite materials, with an ultra high-bypass ratio distributed propulsion system (three turbogenerators and nine propulsors), and boundary layer ingestion.

2 Scenario

2.1 Introduction

The high level design requirements for the N+3 vehicle were developed based on a combination of the NASA defined performance improvements (Table 3) and a future air transportation scenario based on an analysis of the key trends and drivers influencing the air transportation system. The scenario was targeted for a 2035 entry into service of an N+3 vehicle driven by project assumptions of technologies which would reach a TRL of 4 by 2025.

Table 3: NASA Performance Goals

CORNERS OF THE TRADE SPACE	N+1 (2015 EIS) Generation Conventional Tube and Wing (relative to B737/CFM56)	N+2 (2020 IOC) Generation Unconventional Hybrid Wing Body (relative to B777/GE90)	N+3 (2030-2035 EIS) Advanced Aircraft Concepts (relative to B737/CFM56)
Noise (cum below Stage 3)	- 42 dB	- 52 dB	better than -81 dB (55 LDN at average boundary)
LTO NOx Emissions (below CAEP 2)	-70%	-80%	better than -80% plus mitigate formation of contrails
Performance: Aircraft Fuel Burn	-33%***	-40%***	better than -70% plus non-fossil fuel sources
Performance: Field Length	-33%	-50%	exploit metro-plex concepts

2.2 Method

The general methodology is shown in Figure 4. The scenario analysis was based on five primary dimensions: Demand, Operations, Infrastructure, Energy, and Environment. Historical data in these dimensions were collected and analyzed to develop past trends. These trends were then combined with projected drivers to develop the 2035 scenario. The scenario was then used as a basis to develop the market concept and the relevant aircraft design requirements, which reflect characteristics of a vehicle positioned to operate most effectively under the assumed future circumstances.
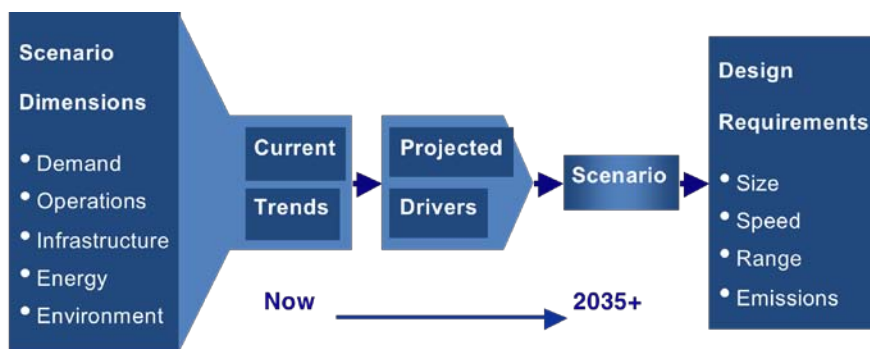
Figure 4: Scenario and requirements development methodology.

2.3 Scenario Dimensions

2.3.1 Demand

The overall demand for air transportation has historically been correlated with GDP and population density. As the world population grows and both developed and developing economies mature, the demand for air transportation is expected to continue to increase. Figure 5 shows the total revenue passenger kilometers (RPK) flown each year for several key regions. Figure 6 similarly shows the freight trends. Except for a short downturn of passenger traffic after 9/11, air travel in North America, Asia, and Europe has grown rapidly over the past 40 years. The traffic growth has risen past the high point before the 9/11 downturn and has a positive slope.
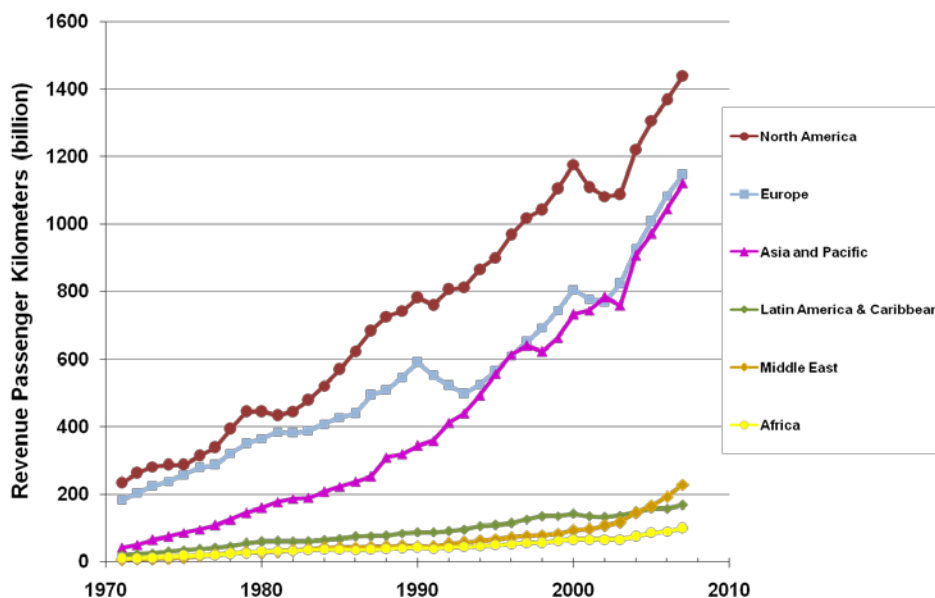
Figure 5: Passenger air travel trends by region[1].

_____

[1] Data source: ICAO Scheduled Services of Commercial Air Carriers (through 2006), IATA Annual Traffic Growth Data for Year 2007 (Jan.-Oct.).

Growth of demand in developing regions such as China, India and the Middle East is expected to outpace growth in more mature regions, such as the U.S. and Europe, as the former connect more strongly into the world economy and the standard of living improves. The potential for strong growth in these regions can be seen in Figure 7 which plots the 2004 RPK per capita vs. the GDP per capita for countries around the world. The size of the bubble represents the population. As the GDP per capita rises in the developing regions the demand is expected to grow strongly (note the logarithmic scale). Those countries such as China and India, which have both large populations and significant economic growth potential, are expected to become dominant markets in the 2035 timeframe.
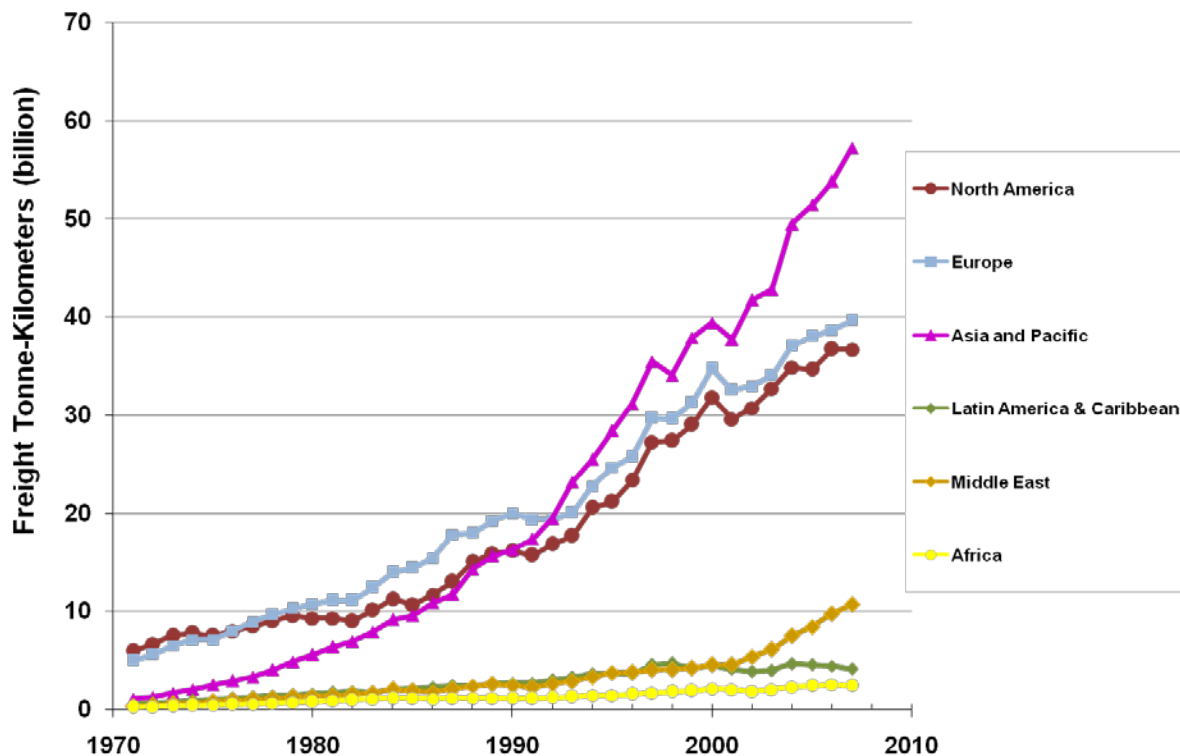
Figure 6: Freight air traffic by region[2].

---

[2] See Footnote 1.
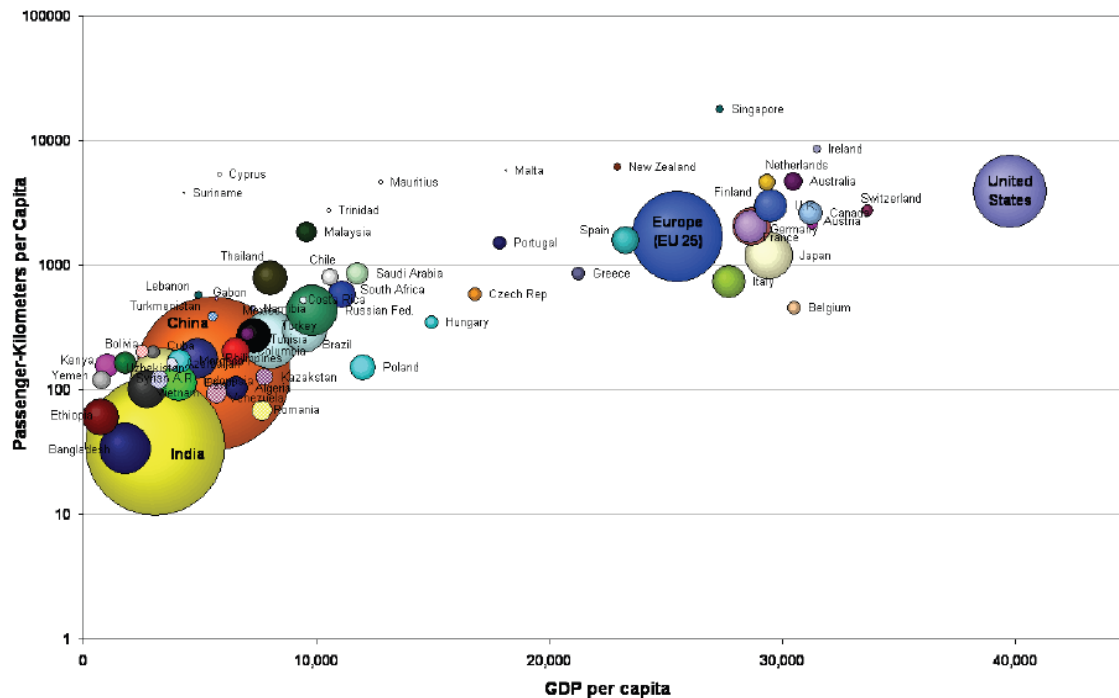
Figure 7: Relationship between GDP and air travel, where the size of the bubble represents the population[3].

Unless there is sustained major economic recession or geopolitical conflict it is reasonable to assume that demand will continue to grow. A linear extrapolation to 2035 of the North American RPK growth rate during the 1990s, shown in Figure 8, projects a doubling of demand in North America by 2035. As noted, higher growth is expected in developing regions which is consistent with the Airbus projection of a doubling of world air traffic in 15 years shown in Figure 9.

---

[3] Bonnefoy, P., 2007; data sources: ICAO Traffic Data, 2006, and CIA World Fact Book, 2006.
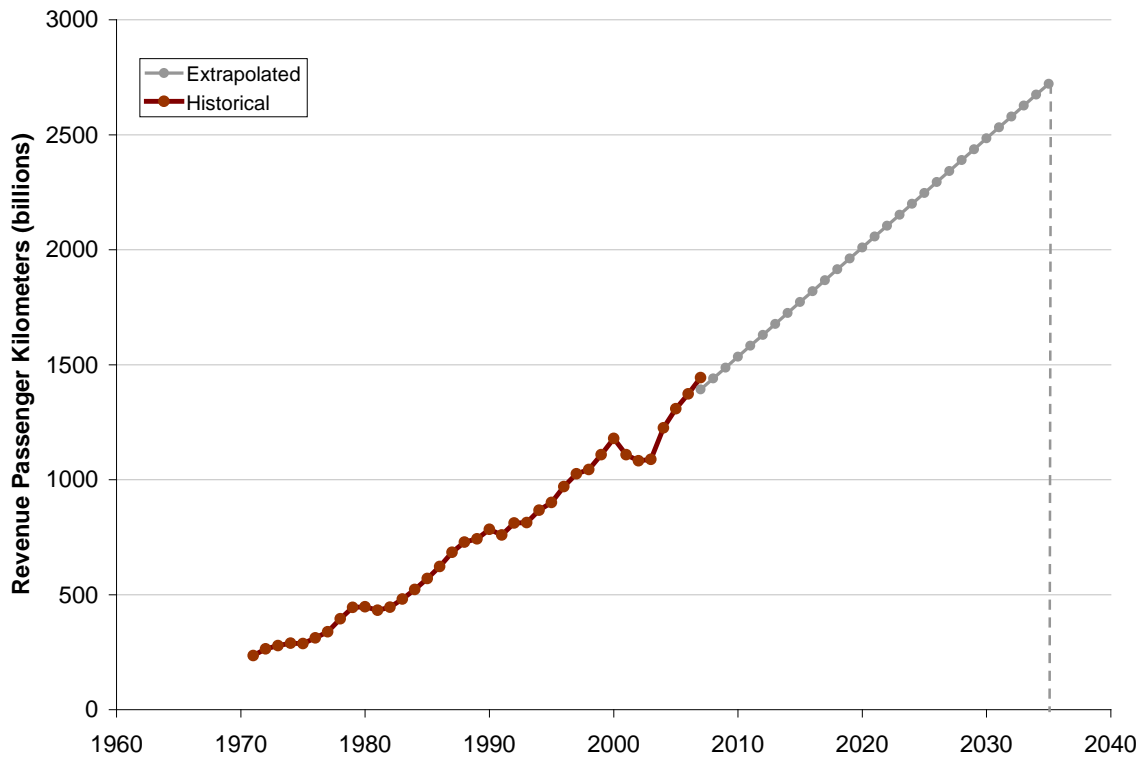
Figure 8: Linear extrapolation of North American passenger travel to 2035 based on 1990's growth rate[4].

The spatial distribution of demand is strongly coupled to the spatial distribution of the traveling population. In developed regions of the world such as the U.S., major changes in population density or travel behavior are not expected and the spatial distribution of domestic flights should be similar to the current operating patterns. Current schedules have a significant number of high frequency routes between populous regions, as demonstrated by the route density chart in Figure 10. Approximately 70% of Americans live in metropolitan areas and, as a result, most population growth will occur in these dense regions. The current population centers are not expected to change dramatically. As cities become larger, the increase in air traffic will be focused between these cities.

---

[4] See Footnote 1.

World annual traffic - RPKs trillion

Source: ICAO, Airbus
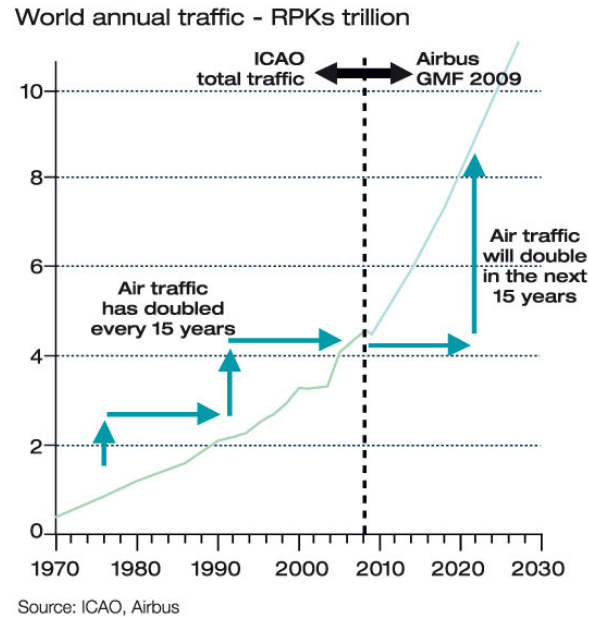
Figure 9: Airbus prediction of world air traffic doubling within 15 years[5].
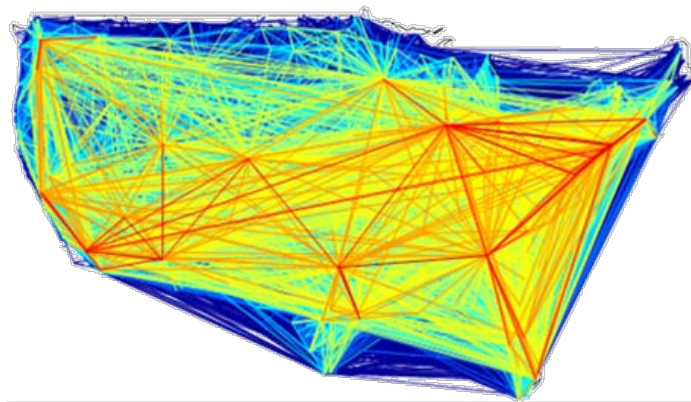
Figure 10: Flight density in the U.S., with blue being the lowest and red being the highest density[6].

While most domestic travel patterns will remain stable, some shifts are expected in the international and leisure markets. Leisure travel may decline as transportation costs increase and high-carbon-footprint flights to distant locations become unpopular in an ever-critical "green" society. The overall distribution of flights throughout the world is, as previously mentioned, expected to grow with GDP. However, the growth will not be uniform. As air travel expands, most increases are expected to occur in Asia, specifically China and India, which have demonstrated rapid GDP growth in recent years. Figure 11 shows an example of the rapid recent growth of both passenger and freight air traffic in the Asia Pacific region indicating that these will be important future markets.

---

[5] Airbus Market Outlook (2008-2028).

[6] Bonnefoy, P., 2007; Data source: Enhanced Traffic Management System (ETMS), 2008.
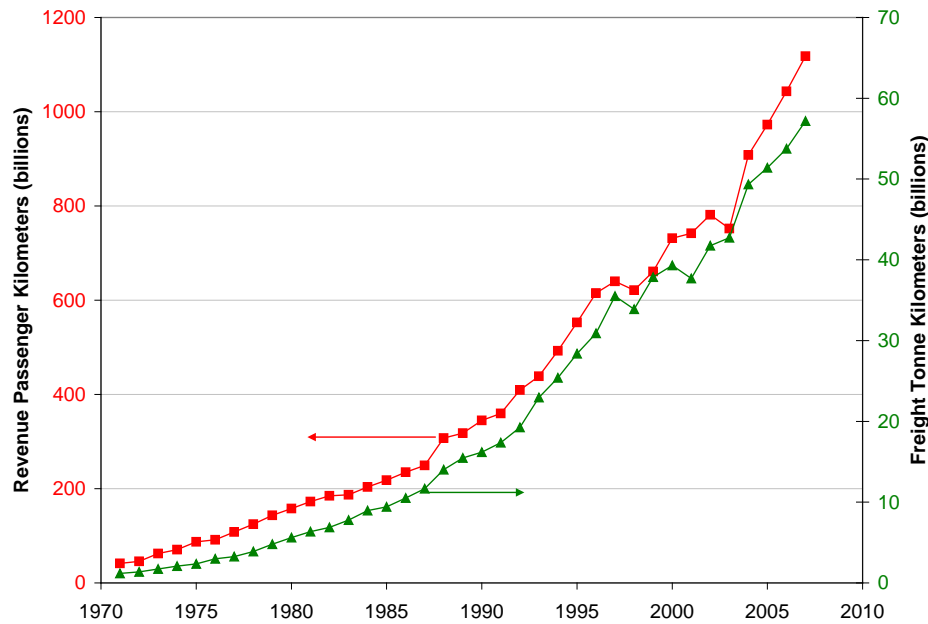
Figure 11: The growing air travel and air freight trends in the Asia Pacific region[7].

Other factors such as congestion, fuel cost, security delays, and environmental considerations are expected to reduce demand for short haul flights (less than 400 miles). Longer flights will be less affected as long as aviation remains the only reasonable means of high speed long distance travel. However, while short-haul flights are sometimes convenient, they face competition from slower means such as road and rail. Aviation is expected to remain a target for terrorism, thus security measures are likely to remain high, increasing the door-to-gate times in airports. Additionally, as ground vehicles become more energy efficient, they are expected to gain popularity over the short flights that emit more pollution and provide little time saving.

2.3.1.1 Airline operations

The general operating structure of Airlines for inter-city and international markets is not expected to change significantly in the 2035 timeframe. Most of the flight procedures are well established and are specified by regulatory requirements, which will change slowly (if at all). The exception is NextGen (discussed in Section 2.3.2.2), which is expected to change some ATC and flight procedures.

2.3.1.2 Business Models

Airline business models are expected to be driven by efforts to improve operating efficiency and to generate market share. There will be some modifications to marketing and passenger service driven by information technology and competitive factors but the core transportation service model should remain stable. Low Cost Carrier (LCC) and Traditional Network Carrier (TNC) business models have already begun to coalesce. The emergent model is expected to be a high efficiency network airline with high emphasis on efficiency and reduced operating costs.

There will be a high emphasis on increasing aircraft utilization by reducing turn times (loading and unloading), increasing dispatch reliability and reducing maintenance down time. New vehicle concepts

---

[7] See Footnote 1.

will have to demonstrate operating cost savings or significant market generation potential if their operating and maintenance costs are high.

2.3.1.3 Network Structure

The general airline network structure is expected to remain based on a modified hub and spoke system due to the operational and market efficiency of this structure[8]. Hubs are useful for maintenance and crew management and have been shown to improve fuel efficiency and equipment utilization[9]. Point to point service will exist but will be concentrated on high demand routes. At the high end, network size and density will grow with consolidation and the expected strengthening of network alliances. It is likely that three or four "super airlines" will emerge. At the low end, there will continue to be new entrant start-up airlines, with a limited network, focused on niche markets.

The spatial distribution of the network and the key hubs will shift slightly. The general structure will continue to be driven by the population distribution; however, capacity limits may prevent current hubs from expanding, resulting in emergence of new hub airports. In addition immature networks in developing regions (such as India and China) will grow.

2.3.1.4 IT Impact

Information technology will significantly impact airline marketing and distribution, passenger services, scheduling and flight operations. Electronic marketing and ticking distribution will dominate through the evolved web infrastructure with ubiquitous personal communication and computation devices linked to electronic ticketing systems. Because of the high transparency in the electronic marketing and distribution environment, price will continue to be the driver for on-line sales. Passenger entertainment will be based on individual portable devices, so In Flight Entertainment (IFE) infrastructure will be more focused on providing connectivity and power rather than expensive and unreliable in-seat systems.

Scheduling and pricing will be more flexible and based on sophisticated robust optimization algorithms which will be able to broaden the utility space to directly include operating and environmental costs as well as market impact and profitability considerations. The revenue management systems will keep load factors at high levels near 80%. Flight operations will be highly integrated with System Wide Information Management (SWIM) linking aircraft, ATC, dispatch, station, maintenance and scheduling functions enabling more flexible and efficient response to weather, traffic and other flight disruptions.

2.3.1.5 Passenger Baggage and Cargo

Although the cabin load factor (percent of seats that are occupied) for aircraft types flown in the U.S. is typically between 70 and 80%, the belly freight capacity is less utilized. From Bureau of Transportation Statistics (BTS) database, one can ascertain the belly freight utilization because airlines report payload weight from both mail and cargo as well as the number of passengers. The BTS database assumes an average passenger weight of 200 lbs.

---

[8] Schipper, Y., and P. Rietveld. "Economic and environmental effects of airline deregulation," in C. Capineri and P. Rietveld (eds), *Networks in Transport and Communications*, Aldershot: Ashgate, 325–344.

Peeters, P., Rietveld, P. and Schipper, Y., "Environmental impacts of hub and spoke networks in European aviation", September, 2001. (http://airneth.nl/index.php/doc_download/309-environmental-impacts-of-hub-and-spoke-networks-in-aviation.html)

[9] Azzam, M., P. Bonnefoy, and R.J. Hansman. "Investigation of the Fuel Efficiency of the US Air Transportation Network Structure" (submitted to AIAA Air Transportation Integration and Operations Conference, 2010.)

Figure 12 presents load factors for the cabin, belly where revenue cargo is held, and the overall weight capacity for several aircraft types that are operated by U.S. carriers. The passenger cabins for all of these aircraft are nearly 80% full. However, the belly freight load factor for the two narrow body aircraft (B737 and B757) was less than 10% while the wide-body aircraft (B767, B777, and B747) was between 25 and 40%. The net result is that all of these aircraft take off with payload that is roughly 60% of the maximum allowable.
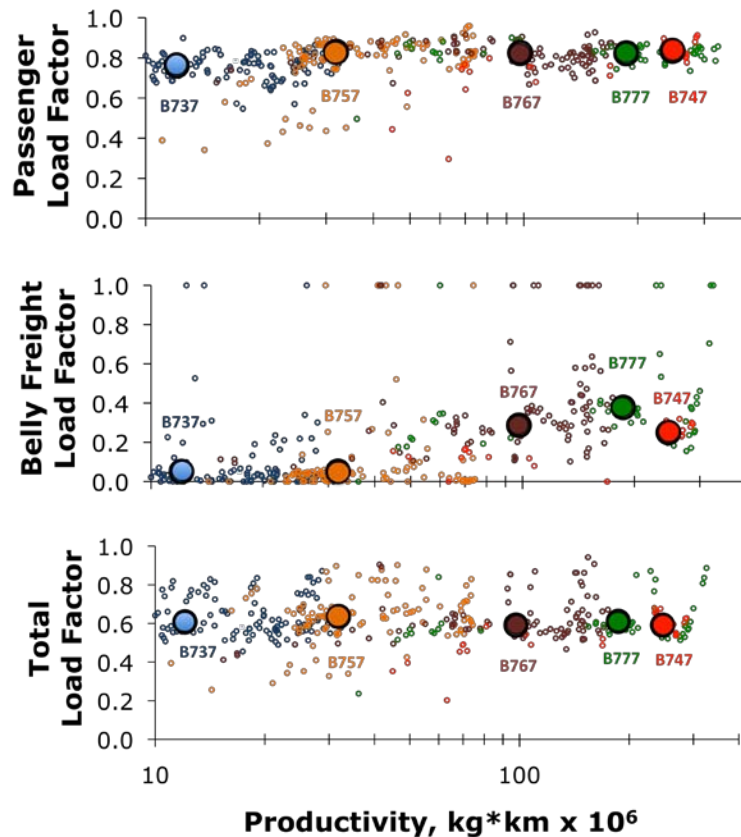
Figure 12: Load factors for select U.S. aircraft in 2007. The smaller circles reflect individual airlines operating the aircraft during each quarter during the year. The larger circles are the average for all operations for that aircraft type[10].

The difference in belly freight utilization has implications for the design for future narrow body and wide body aircraft. Since belly freight capacity is not being utilized in single aisle passenger aircraft, there is an argument for future single aisle passenger aircraft being designed with a minimum of freight capacity. Conversely, the belly freight of wide body passenger aircraft is utilized; therefore, it is likely that future airlines would use belly-freight capacity in their wide body passenger aircraft and by extension there is an argument that this capacity be maintained in future wide body aircraft designs.

Passenger baggage management is a major area of logistical challenge in current airline operations both for baggage transfer and security considerations. More efficient passenger baggage management will be developed and the current trend of shifting from checked to carry-on baggage will continue. Increased

---

[10] Data from U.S. BTS Form 41 database, 2007.

carry-on baggage capacity will be expected in future aircraft configurations as well as more efficient carry-on loading schemes to reduce aircraft turn times.

Cargo and belly freight loads are expected to be lower in 2035 for domestic markets where security considerations and screening have shifted much air cargo such as the U.S. mail from passenger to dedicated air cargo flights or surface transportation. International markets will continue to carry significant air cargo loads.

2.3.1.6 Security

Air transportation will continue to be a potential terrorism target within the 2035 timeframe and the security burden is expected to increase particularly following failed or successful attempts. Increased security policies following 9/11 and subsequent attempts have resulted in longer waits at airport terminals and increased "hassle factor"[11]. This has and will continue to erode the demand for short haul flights. While there will be improvement in streamlining security protocols, these gains are expected to be offset by additional requirements over time.

2.3.2 Infrastructure

The ability of the air transportation system to grow to accommodate demand will be limited by the ability of the infrastructure to accommodate this growth. In mature air transportation markets such as the U.S., the infrastructure is already approaching its capacity limits at key points as can be seen in increasing magnitude and volatility of delays in Figure 13. The infrastructure can be limited by airport capacity and airspace capacity, both of which will be a factor in the 2035 timeframe.
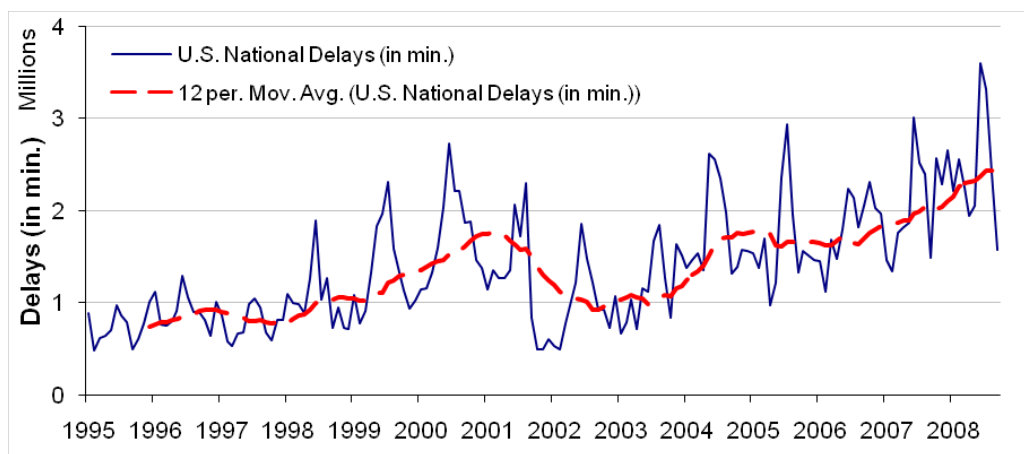
Figure 13: Increasing delays of U.S. flights[12].

2.3.2.1 Airport Capacity

Currently the major infrastructure constraint in the U.S. system is airport capacity, particularly at key locations in the system such as New York. Airport capacity is generally limited by the runway capacity of the airport although gates and landside constraints can also be a factor. The capacity of a single runway is

---

[11] Blalock, G., V. Kadiyali, and D.H. Simon. "The Impact of Post-9/11 Airport Security Measures on the Demand for Air Travel." *The Journal of Law and Economics,* vol. 50 (2007).

[12] Data source: FAA Operational Network (OPSNET).

limited due to the wake vortex separation requirements between aircraft. Reducing the wake vortex or making aircraft less vulnerable to wake vortex would significantly improve single airport capacity.

The ability of the U.S. system to add new airports or runways has severely diminished after the National Environmental Policy Act (NEPA) was signed into law in 1970. Since that time new airport and runway growth has plummeted. As a consequence, it is assumed that there will only be less than 20 new runways added to the U.S. system by 2035. Similar limits will apply in Europe. There will be significant new airport and runway expansion in developing regions such as China and India. In 2008, China began an initiative to build 97 regional airports by 2020, up from the 147 civilian airports that existed in 2006[13]. India has recently built or upgraded 5 major airport systems and has plans for significant expansion.

The key mechanism for increasing airport capacity over the past decade has been the emergence of secondary airports, which can offload traffic from congested primary airports. This results in a multi-airport metroplex system around the major metropolitan areas. An example of the New York Airport system is shown in Figure 14.
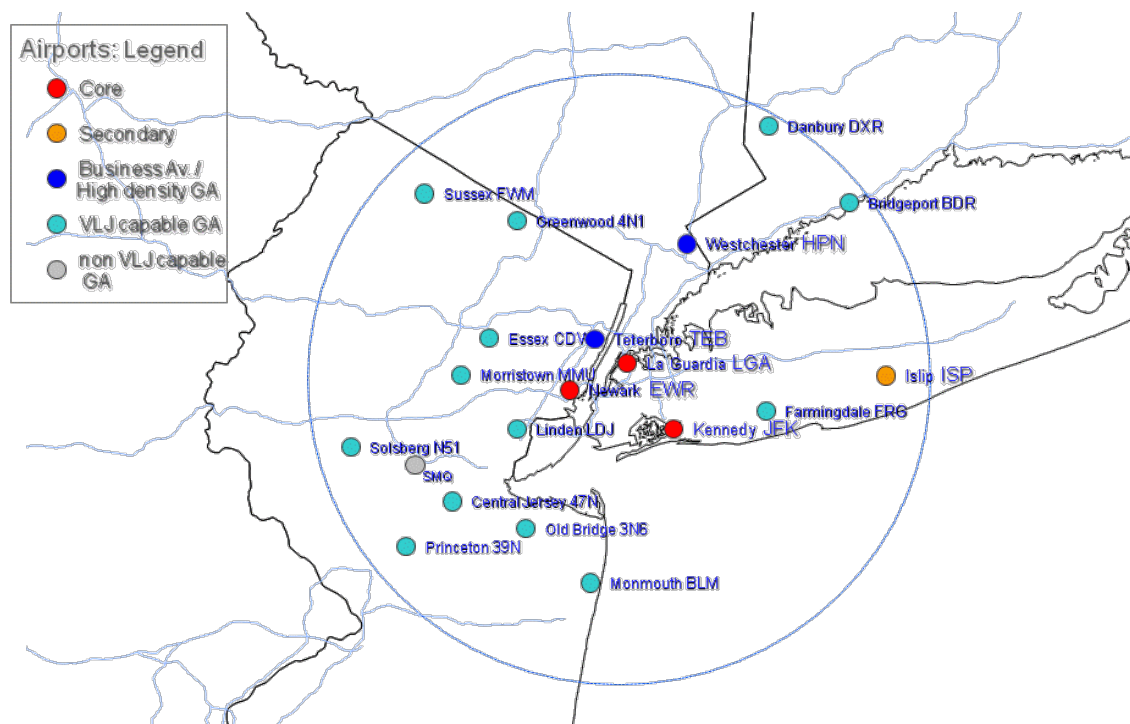
Figure 14: New York multi-airport system[14].

The trend toward multi-airport systems has been observed worldwide. In the U.S. and Europe the expansion is limited to existing airports for the reasons discussed above. This trend is expected to continue into the 2035 time period.

---

[13] "China sanctions massive airport building programme." (http://www.travelmole.com/stories)

[14] Bonnefoy, P., Hansman, R., "Scalability of the Air Transportation System and Development of Multi-Airport Systems: A Worldwide Perspective," 2008.

In determining the available runway infrastructure for secondary or tertiary airport growth in the 2035 time period, the existing runway infrastructure was used as a baseline. Figure 15 shows the distance from a current runway for the U.S. population as a function of runway length, which gives insight into the required runway performance for the N+3 vehicle. It can be seen that nearly 80% of the U.S. population lives within 15 miles of a 5,000 ft long runway.
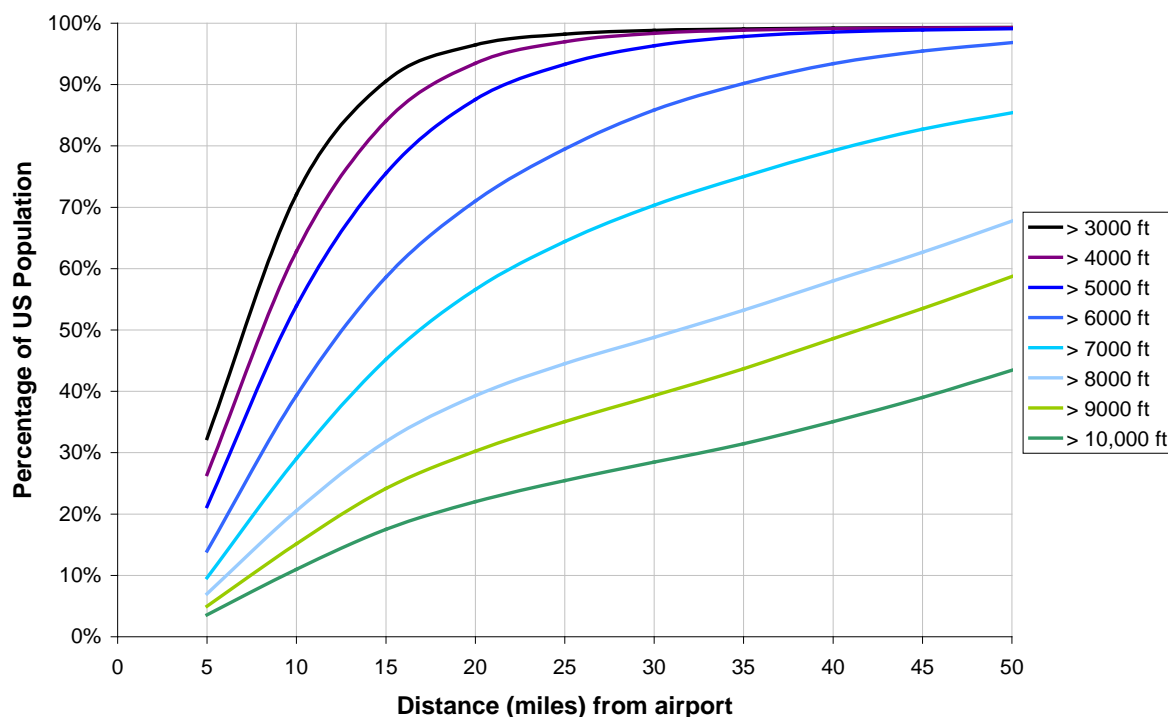
Figure 15: Distribution of U.S. population distance from secondary airports[15].

The results of a similar analysis, focused on the top metropolitan areas, are shown in Figure 16. The analysis indicates that, based on a 5000ft runway requirement, there is significant secondary airport growth potential within 50 miles of all major metropolitan areas with the possible exception of Las Vegas.

---

[15] Data source: FAA Form 5010 Airport Database and 2000 U.S. Census.
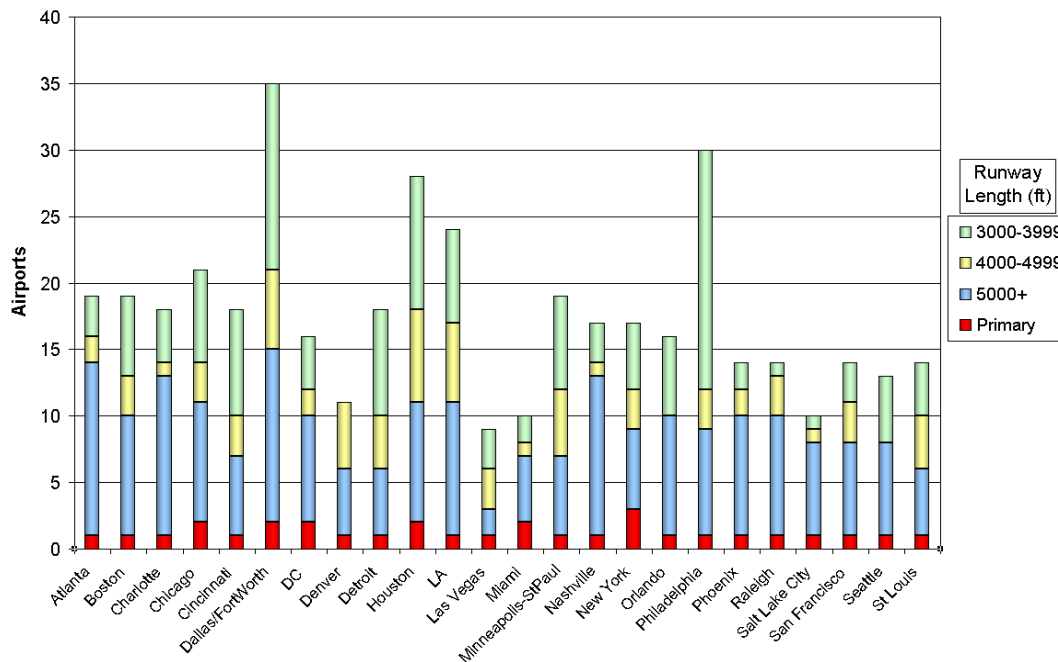
Figure 16: Airports within 50 miles of major city centers, separated by runway length[16].

2.3.2.2 Airspace Capacity and NextGen

Airspace capacity is also a limiting infrastructure factor to system growth, both in the enroute airspace and increasingly in the terminal airspace within metroplex systems[17]. This limitation has been identified and in response the U.S. is implementing the Next Generation Air Transportation System (NextGen), a system-wide plan to upgrade the National Airspace System (NAS) via technological and operational enhancements, with the ultimate goal of increased system capacity and performance. A parallel modernization effort is underway in Europe with the Single European Sky ATM Research (SESAR) program. Recent plans indicate that mid-term goals of NextGen may be met by 2018 and by 2035, NextGen will likely be deployed[18]. By switching from legacy ground-based systems to satellite-based network information sharing and navigation, pilots and controllers will be provided with a common and complete situational picture, allowing for more precise control and enhanced flexibility. NextGen has the potential to relieve workload of air traffic controllers and increase airspace efficiency by reducing separation minimums and allowing for more direct routes. NextGen also promises to enable more environmentally friendly procedures in virtually all phases of flight. The operational benefits offered by NextGen will reduce congestion to some extent, relieving pressure on key airports.

---

[16] Same as Footnote 15.

[17] Hansman, R.J. "The impact of information technologies on air transportation." AIAA 43rd Aerospace Sciences Meeting and Exhibit, Reno, NV, Jan 2005.

[18] Aviation Week website:
http://www.aviationweek.com/aw/generic/story.jsp?id=news/FAA020309.xml&headline=FAA%20Updates%20NextGen%20Plan,%20Targets%202018&channel=comm (as of March 29, 2010).

2.3.3 Energy

The cost and availability of fuel will be a major factor in the 2035 timeframe. Fuel costs have been trending up and are the single largest contributor to airline Direct Operating Costs (DOC). Fuel costs are expected to continue to increase and remain the dominant operating cost factor[19].

2.3.3.1 Petroleum Outlook

As the world's energy demand increases, so does the need for production. As shown in Figure 17, increasing demand has led to a steady increase in oil prices over the past decade with a peak being achieved in 2008 of over $140 per barrel. Even though the world economy has subsequently suffered its worst recession since the Great Depression, oil has stabilized at a price between $70 and $80 per barrel. The peak in 2008 and the recent relatively high prices during a global downturn both indicate a likely end to the era of cheap oil. Continued high prices for petroleum will force airlines to adopt more efficient practices, which includes operating greener aircraft.

As oil prices increased, previously inaccessible petroleum resources became economically viable thus increasing petroleum reserves. This includes the extraction of conventional petroleum (a.k.a., crude oil) from previously inaccessible locations farther offshore in the ocean and the development of unconventional petroleum resources such as Canadian oil sands and Venezuelan very heavy oils. On top of the development of conventional and unconventional petroleum, energy companies have responded to increased oil prices with increased investment in facilities to create synthetic liquid fuels from natural gas using Fischer-Tropsch (F-T) synthesis and expanded ethanol production. If not for the large greenhouse gases that would result from their production, it is likely there would be extensive interest in creating synthetic fuels from coal as the estimated cost of production is below the current price of conventional petroleum[20]. F-T synthesis is attractive for aviation in that it can be used to create Synthetic Paraffinic Kerosene (SPK) fuels that are already certified for use as a 50-50 blending stock with conventional jet fuel[21].

---

[19] Quarterly Cost Index: U.S. Passenger Airlines, Web page with data through third quarter 2009, last modified Jan 8, 2010. As of March 28, 2010: http://www.airlines.org/economics/finance/Cost+Index.htm.

[20] Hileman, J., Ortiz, D., Bartis. J., Wong, H.M., Donohoo, P., Weiss, M., and Waitz, I., "Near-Term Feasibility of Alternative Jet Fuels, jointly published by the RAND Corporation" (Report No. TR-554-FAA) and the Partnership for AiR Transportation Noise and Emissions Reduction (Report No. PARTNER-COE-2009-001), 2009. http://web.mit.edu/aeroastro/partner/reports/proj17/altfuelfeasrpt.pdf.

[21] ASTM Standard D7566-09, 2009, "Standard Specification for Aviation Turbine Fuel Containing Synthesized Hydrocarbons," ASTM International, West Conshohocken, PA, 2009, DOI: 10.1520/D7566-0, www.astm.org.
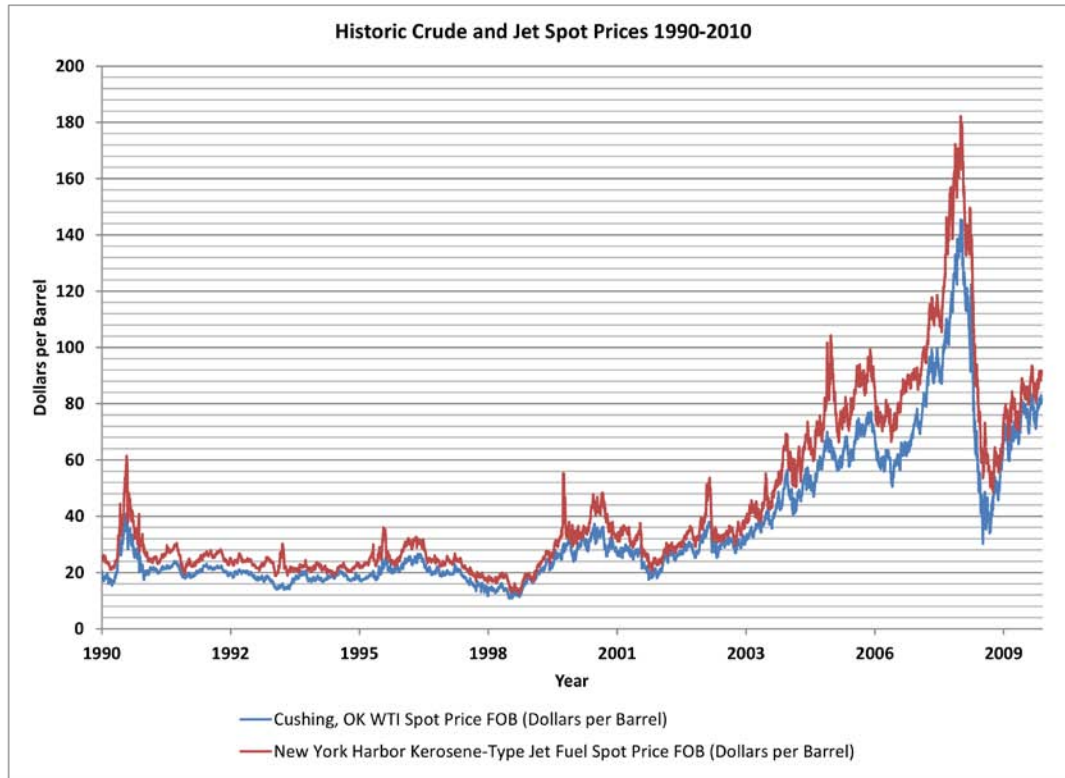
Figure 17: Crude and jet price history in the U.S. gulf coast region[22].

2.3.3.2 Future Fuels and Energy Sources

With oil extraction becoming more difficult, and environmental pressure on aviation increasing, cleaner alternative jet fuels are being considered to augment or even replace fuels derived from petroleum. Out of the options mentioned above, jet fuel derived from conventional petroleum has the lowest life cycle greenhouse gases.[23] This is a consequence of the relative efficiency in extracting jet fuel from conventional petroleum[24]. However, there are other options for future energy sources that one could envision in the 2035 time frame including biofuels, cryogenic methane, and cryogenic hydrogen. These are discussed below in terms of their technical, environmental, and economic viability.

Biofuels

Biofuels offer an opportunity to reduce the life cycle greenhouse gases from transportation fuels because the biomass used in their creation extracts CO_2 from the atmosphere. This carbon uptake is generally equal to the carbon dioxide released during fuel combustion. The life cycle greenhouse gases from biofuels are thus set by the emissions from changes in land usage, resource and fuel transportation, and

---

[22] Energy Information Administration, "Spot Prices for Crude Oil and Petroleum Products," March 2010. http://tonto.eia.doe.gov/dnav/pet/pet_pri_spt_s1_d.htm.

[23] The fuel life cycle considers all aspects of fuel production and use including resource extraction, transportation, refinement, and combustion.

[24] Stratton, R., Wong, H.M., Hileman, J., "PARTNER Project 28 Report: Life Cycle Greenhouse Gas Emissions from Alternative Jet Fuels," published by the Partnership for AiR Transportation Noise and Emissions Reduction (Report No. PARTNER-COE-2010-001), 2010.

fuel processing. Biofuels are potentially limited in their ability to augment or replace petroleum by production cost, growth rate, and the land and water resources required for their growth[25].

Although ground transportation can use a variety of biofuel compositions such as ethanol, butanol, and fatty acid methyl esters (FAME), aviation requires fuels with a high specific energy that are safe to handle on the ground and can withstand cruise altitude conditions. In addition to safety concerns with their use, the reduced specific energy of ethanol and butanol would lead to an increase in fuel energy consumption. Such an increase is not experienced with their use in ground transportation. In addition to a similar problem with its reduced specific energy, thermal stability concerns preclude FAME use in aviation. Because of these concerns and the fact that fuel production pathways exist to create hydrocarbon fuels from biomass resources, alcohols and FAMEs are not considered further.

A variety of feedstock-to-fuel pathways exist to create aviation biofuels that are similar in composition to conventional jet fuel. These pathways include the use of F-T synthesis with any biomass resource to create an SPK fuel, hydroprocessing of renewable plant oils to a Hydroprocessed Renewable Jet (HRJ) fuel which is similar to an SPK fuel, the fermentation of sugars to alkanes which is again similar to an SPK fuel, and the pyrolysis of cellulosic biomass to synthetic aromatics that can be mixed with SPK fuels to make a fully synthetic jet fuel. These fuels could all be blended with conventional jet fuel in today's aircraft as well as the N+3 aircraft concept.

Because of the wide range of opportunities for making biofuels that are compatible with current and future aircraft, the N+3 aircraft concepts that are developed herein for conventional jet fuel would be compatible with aviation biofuels.

Liquefied Natural Gas

Liquefied natural gas (LNG) is simply natural gas that has been cooled to its liquid state at about -260 F. Natural gas consists mostly of methane, with small amounts of ethane, propane, and butane, as well as other hydrocarbons. LNG has been used as an intermediary for natural gas transport for over 50 years and its use is currently growing. Natural gas is one of our most abundant energy resources with considerable new unconventional resources, such as coal bed methane and shale gas, being developed around the world. These new resources are such that North America could become a net exporter of LNG instead of an importer[26]. In addition to these resources, methane hydrates could provide more energy, in the form of methane, than is contained in all other fossil fuels. Methane hydrates are methane molecules encased in ice and are potentially available around the world[27]. At present, the extraction of methane hydrates is difficult due to the location of deposits. Also, handling the ice must be done with caution so that the methane, a potent GreenHouse Gas (GHG), is not released into the atmosphere.

The primary advantage of LNG relative to conventional jet fuel is the potential vastness of the reserves. As will be discussed later, LNG results in fewer life cycle GHG emissions than either conventional jet fuel or F-T fuels produced from natural gas, making it attractive environmentally. The main disadvantage is the storage requirement in terms of dealing with a fuel that not only has lower energy density than conventional jet fuel, but also is cryogenic. LNG would not be compatible with existing aircraft and it would require considerable expansion of the existing worldwide distribution network. Further, LNG is non-renewable like conventional petroleum. In spite of these concerns, LNG is evaluated in this work as a

---

[25] See Footnotes 20 and 24.

[26] The Economist Newspaper, "An unconventional glut," March 11, 2010. As of March 28, http://www.economist.com/business-finance/displaystory.cfm?story_id=15661889

[27] http://www.netl.doe.gov/technologies/oil-gas/FutureSupply/MethaneHydrates/about-hydrates/occurrences.htm.

potential fuel for the N+3 aircraft concepts because of the reduction in GHG emissions and the large methane hydrate resources.

Liquefied Hydrogen

Hydrogen has been discussed as a future "fuel" for several decades. Because energy is required to produce hydrogen, it is not technically a fuel, but instead a means of storing energy from a primary source such as nuclear, wind or solar. The low density of gaseous hydrogen means it would need to be liquefied at a temperature of -420°F for use as an energy source for aviation. An aircraft could then harness the primary energy source stored in the cryogenic hydrogen and through combustion or perhaps via a fuel cell.

The success of hydrogen ultimately relies on the ability to produce clean, cheap electricity. Aviation requires cryogenic hydrogen and not gaseous hydrogen, and it is unlikely that hydrogen will be used as an aviation fuel in the 2035 timeframe. Any clean and cheap electricity would first be used to displace fossil fuels for making electricity, as this is the most efficient use of the resource from both an economic and environmental standpoint. For this reason, nuclear, wind and solar resources are being used to replace electricity generation from fossil resources, although these resources will not replace all electricity from fossil fuels before 2035[28]. If some new form of energy such as fusion were developed that could meet the demand for electricity, excess electricity might be used to create gaseous hydrogen for use in fuel cells or internal combustion engines for ground transportation. It is only after all of the energy requirements for electricity and ground transportation sectors are met that it might be economically viable to create cryogenic hydrogen because liquefied hydrogen would be more expensive to produce and would require a specialized infrastructure for storage and transportation. Although it is outside of the scope of the work considered here, it might ultimately prove cheaper and greener to convert carbon dioxide in the atmosphere to liquid fuels than to create cryogenic hydrogen. As such, cryogenic hydrogen was not considered as an aviation energy source for the N+3 aircraft concepts in this study.

2.3.4 Environmental Considerations

Environmental impacts of aviation have become increasingly important over the last 50 years with the rapid growth of commercial jet aviation. Aircraft noise—the most easily perceived environmental impact—is regulated by the International Civil Aviation Organization (ICAO). Aircraft built today are required to meet noise certification standards adopted by ICAO as contained in the Annex 16: Environmental Protection, Volume I – International Noise Standards[29]. ICAO also regulates emissions to improve air quality in the vicinity of airports. These emissions standards are detailed in the Annex 16: Environmental Protection, Volume II – Aircraft Engine Emissions for nitrogen oxides, hydrocarbons, carbon monoxide and smoke[30]. Lastly, ICAO has recently established the Group on International Aviation and Climate Change, which is responsible for providing guidance to ICAO on policies to addresses aviation's impact on climate[31]. The United States' stance on greenhouse gas emissions is reflected in

---

[28] International Energy Agency, "World Energy Outlook," Paris: Organisation for Economic Co-Operation and Development and International Energy Agency, 2009.

[29] International Civil Aviation Organization (ICAO), "Annex 16: Environmental Protection Volume I: Aircraft Noise," 4th Edition, 2005.

[30] International Civil Aviation Organization (ICAO), "Annex 16: Environmental Protection Volume II: Aircraft Engine Emissions," 2nd Edition, 2006.

[31] International Civil Aviation Organization's Group on International Aviation and Climate Change (GIACC) First Meeting, Summary of Discussions of Day 3, GIACC/1-SD/3, February, 2008. Available at http://www.icao.int/icao/en/env/Meetings/Giacc/sd3 en.pdf.

President Obama's stated goal of reducing carbon emissions to 1990 levels by 2020 and to 80% below 1990 levels by 2050.

This direction of increased environmental regulation and more environmentally conscious policymaking makes it highly likely that environmental considerations will be a major constraint on aviation and other transportation sectors in the 2035 timeframe. The IPCC Fourth Assessment Report estimates the total GHG emissions attributable to aviation to be about 3% of total anthropogenic emissions; however this fraction is expected to increase as other sectors reduce their footprint[32]. Due to strict power, range, and weight demands on aircraft, these vehicles require high performance fuel, power plants, and materials for which economical "greener" substitutes are difficult to find. Meanwhile, for example, the automotive industry will much more easily adapt to alternative fuels and hybrid power trains with lower power-to-weight but increased fuel efficiency. The resulting relative reduction in other sectors will increase aviation's share of the global carbon footprint, generating further pressure on aviation to reduce emissions.

NASA has set aggressive noise, landing and takeoff (LTO) NOx, and fuel burn targets for the N+3 timeline that aim to address these environmental concerns. It is useful to compare the hypothetical impact of meeting these environmental goals to see where the greatest benefit is felt. One tool that can be of assistance for this type of environmental impact modeling is the Aviation environmental Portfolio Management Tool (APMT). APMT-Impacts—developed and run by MIT—is a component of the FAA's Aviation Environmental Tools Suite that uses a flexible, probabilistic framework for estimating the physical and socio-economic (or monetized) environmental impacts of aviation[33]. An APMT-Impacts study of the impact of the three NASA N+3 targets as applied to the present-day air transportation fleet can be used to help inform the definition of the scenario in this project and thus to inform the aircraft design process. A summary of the APMT-Impacts, Noise, Air Quality, and Climate modules can be found at http://apmt.aero.

To assess the impact of the N+3 targets, a sample noise and emissions scenario was acquired from the Volpe National Transportation Systems Center. This captures the noise contours and emissions inventories produced by the U.S. air transportation fleet in the year 2006. This was used as a baseline case and was run through the three APMT-Impacts modules as a means to benchmark the policy scenario in which the three targets are implemented.

Applying the noise goal of -71 EPNdB (cumulative below Stage 4) was not feasible with the data at hand. Instead, the impact of eliminating aviation noise from the system entirely was used as a proxy for measuring the impact of the N+3 noise goal. This approach overestimates the noise benefits, but suffices for the purposes of comparing impacts across noise, air quality, and climate. Indeed, N+3 noise targets are aggressive, as shown in the noise regulation history diagram in Figure 18.

---

[32] Solomon, S., Intergovernmental Panel on Climate Change, and Intergovernmental Panel on Climate Change. Working Group I, "Climate Change 2007: the physical science basis: contribution of Working Group I to the Fourth Assessment Report of the Intergovernmental Panel on Climate Change," Cambridge University Press, Cambridge; New York, 2007.

[33] Aviation environment Portfolio Management Tool http://apmt.aero/.
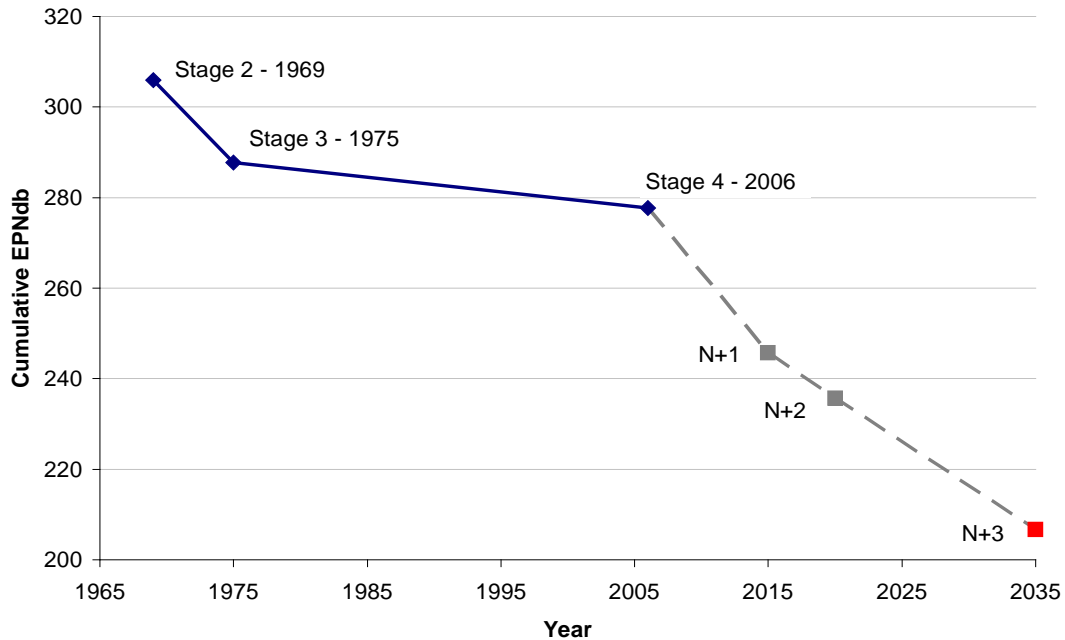
Figure 18: Cumulative noise restriction history for a B737-700 (150,000 lbs) class aircraft[34].

The LTO NOx target is constructed by NASA as a percent change from CAEP/6 levels. These ICAO engine standards are listed by in units of grams NOx produced per kN thrust over the ICAO reference landing and takeoff cycle. Accompanying these standards for each engine is also a value for NOx emissions index (EI) in units of grams NOx per kilogram of fuel burn.

For this study, the LTO NOx target was applied as a change in the NOx EI for all of the different engines in the emissions inventory. This change was only applied to NOx emissions below 3,000 feet, i.e. emissions in the landing-takeoff area. The 70% fuel burn reduction was applied to the full-flight fuel levels in the data and was translated to absolute reductions CO_2, NOx, SOx, and non-volatile particulate matter through the use of constant emissions indices. Scenarios were created for each of the LTO NOx and fuel burn goals, and these were examined in relation to the baseline cases within APMT-Impacts.

The results of the analysis are presented in Figure 19. In the chart, the monetized environmental benefit of implementing the N+3 goals is broken down in terms of noise, air quality, and climate impact, each with a low, mid, and high estimate.

---

[34] See Footnote 29.
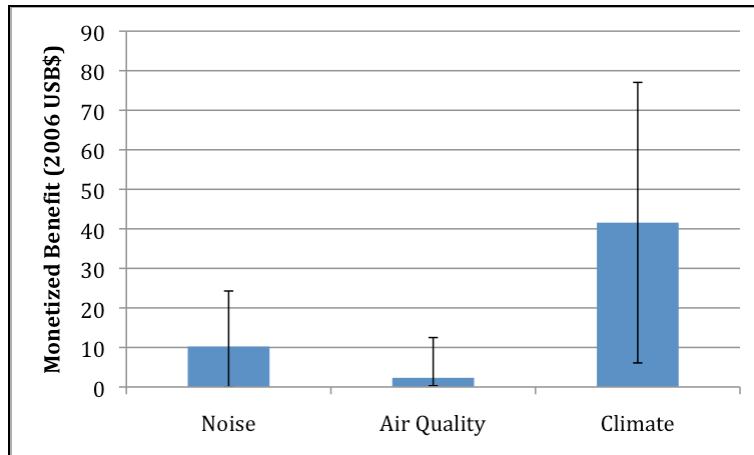
Figure 19: Monetized environmental benefit of N+3 goals implementation.

It can be inferred from Figure 19 that meeting the climate goal has a larger monetized benefit than meeting the other environmental goals. The benefit of eliminating aviation's noise impact entirely—an overestimate of the N+3 goal—is still a fraction of the climate benefit that results from a 70% fleet-wide fuel burn reduction. It should be noted also that the air quality benefit in Figure 19 is potentially underrepresented as a result of NASA's focus on LTO NOx only. The impact of cruise emissions on air quality, though more uncertain than LTO impacts at this time, are expected to be non-zero. In fact, Barrett et al.[35] estimate that including cruise impacts may lead to an increase in total air quality impacts by a factor from two to twelve. The impact of U.S. cruise emissions is realized both within the U.S. and also globally, due to strong zonal westerly winds aloft that lead to significant trans-boundary air pollution.

Historically, regulation of the environmental impact of aviation has largely consisted of certification standards aimed at reducing aviation's impact on noise and air quality. It is clear from this analysis and trends in environmental policymaking, however, that it will become increasingly important to design aircraft for a climate-constrained world. The most effective way of making environmental strides in this area from the perspective of innovative aircraft design is to focus on full-flight fuel burn and emissions reductions rather than noise and LTO emissions standards.

2.4   Requirements

Based on the trend and 2035 scenario analysis as well as the NASA specified performance goals and their potential fleet wide impact, the high level requirements for the N+3 design effort were established.

In the impact analysis, it was found that there are two high impact points for the N+3 technology. One is for a mid-size domestic transport in the 150-180 seat class for aircraft capable of U.S Transcontinental range. The second is for a long haul international transport in the 301 + class capable of intercontinental missions. Because the potential N+3 vehicle configurations and technologies optimize differently at the two high impact leverage points it was decided to carry two sets of vehicle requirements into the initial N+3 design phase.

The high level aircraft design requirements are summarized in Table 4. For the mid-size domestic vehicle the Boeing B737-800 was taken as the current technology baseline. For the long-haul international

---

[35] Barrett, S., Britter, R. & Waitz, I., "Global Mortality Attributable to Aircraft Cruise Emissions," (forthcoming).

vehicle the Boeing B777-200LR was used as the current technology baseline. More discussion on the individual requirements is included below.

Table 4: Design Requirements Summary

	Mid-Sized Domestic Vehicle	**Long-Haul International Vehicle**
Capacity	180 passengers	350 passengers
Design Range	3000 nm	7600 nm
Speed	greater than Mach 0.72	greater than Mach 0.8
Runway Length	5,000 ft balanced field	9,000 ft balanced field
Noise	At least 71 EPNdB cumulative reduction below FAA Stage 4 At most 55 dB LDN at average airport boundary	
Fuel Burn	70% below baseline aircraft	
NOx	75% below CAEP 6	
Compliance	FAA and JAA safety standards, NextGen compatibility	

2.4.1 Vehicle Capacity

Under the 2035 scenario assumption of similar airline networks and operating patterns, the current fleet and operating patterns were used to determine where the N+3 technologies would have the most impact. To provide insight, the existing fleet was evaluated. Figure 20 depicts the number of aircraft by type in the world commercial aircraft fleet. In terms of number of aircraft, the mid size domestic transport represented by the B737 and A320 class aircraft dominates the fleet. These aircraft range from 130-180 in passenger capacity. Their popularity stems from the route flexibility and scheduling frequency they offer operators.
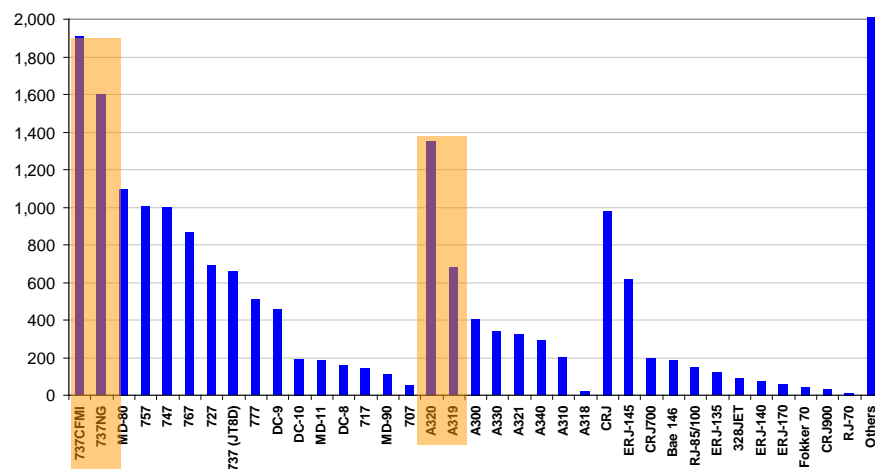
Figure 20: World aircraft fleet inventory in 2005[36].

---

[36] Credit Suisse Report, "Aerospace and Defense – Civil Aerospace Cycle Themes and Sensitivities," 2007.

In addition to the number of aircraft, it is also important to consider how much these aircraft fly and what might be the potential aggregate impact of the NASA N+3 goals are at a fleet-wide level. To estimate this total impact on the aircraft fleet, flight data was acquired from Volpe National Transportation Systems Center for all operations worldwide for each aircraft type over the period of one day on January 7, 2006. Aircraft were grouped into seat classes, and the total fuel burn and NOx emissions for each seat class group were reduced by the N+3 goal targets, while holding the other seat class groups constant. This simulates the effect of various aircraft sizes being completely replaced by N+3 aircraft. The results are presented in Figure 21.
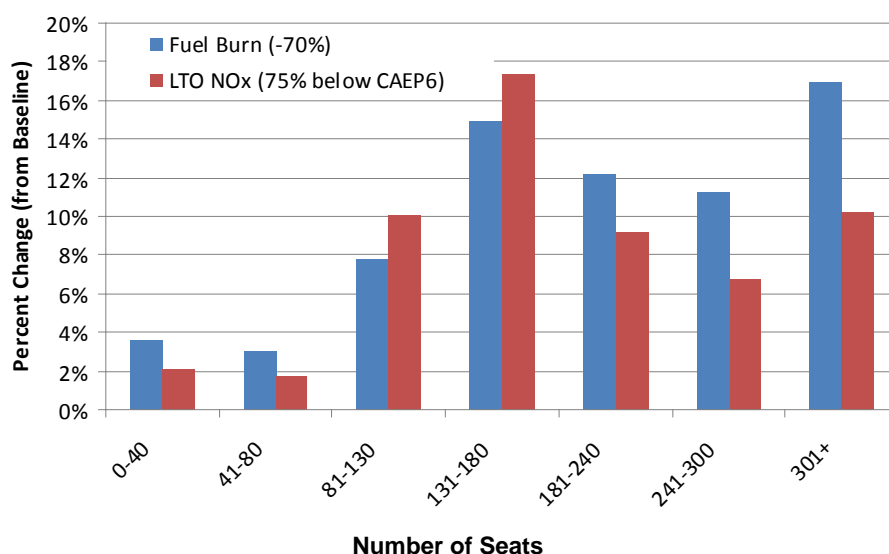
Figure 21: Total fleet-wide fuel burn and NOx reduction given total N+3 market penetration. Data created by analysis of worldwide data for Jan. 7, 2006.

The analysis confirmed that the mid-range domestic transport class (131-180 seats) was a high leverage impact point with the highest aggregate LTO NOx impact and high fuel burn impact. However the analysis also indicated the potential impact for a 301+ seat class long-haul international vehicle. This class, while smaller in number, had the highest potential fuel impact due to their long stage lengths and the second highest LTO NOx impact.

Based on these results, it was decided to address both classes of aircraft in the N+3 requirements. For the mid range domestic class a passenger capability of 180 was selected. This value is on the high side of the current passenger capability of this type of aircraft and represents an assumption that there will be a slight trend up in payload due to market demand and capacity restrictions. For the long-haul international class a payload capability of 350 was selected.

2.4.2 Range

The design mission for the 180-passenger aircraft was based on an the longest U.S domestic transcontinental mission of Miami, FL to Seattle, WA with a great circle distance of 2370 nm. Assuming 65 kt headwinds to account for winter westbound headwinds and NBAA IFR reserves the design range for the 180-passenger aircraft was 3200 nm, which is comparable to the B737-800.

The design missions for the 350-passenger aircraft were New York to Hong Kong and Los Angeles to Sydney. Using a similar approach of the range requirement for the 350-passenger aircraft was set as 7,600 nm. This is consistent with the Boeing 777-200LR, which was used as a performance baseline.

2.4.3 Cruise Speed

A number of factors in the 2035 scenario motivated opening up the design space in terms of cruise speed. In this timeframe it is expected that the Cost Index (CI) for airlines will decrease. The Cost Index is a parameter used to determine optimal cruise speed and is effectively the ratio to the value of time over the value of DOC. The expected increase in fuel and environmental costs in the future will cause the CI to decrease, translating to lower optimal cruise speeds because higher fuel efficiency can be achieved with reduced speed. While this optimization is normally done for an existing airframe, the concept translates to determining the optimal design value. As such, a decrease in cruise speed was considered for the 180 passenger aircraft to help improve fuel efficiency and increase environmental benefit. However, because of the long distances that would be flown, decreased cruise speed was not considered for the 350 passenger aircraft.

A reduction in speed raises concerns about disrupting airline operational capability. In order to evaluate this, an analysis was conducted on the schedule impact of lower cruise Mach number for the mid range fleet of 2 current U.S. Airlines. Results are shown in Figure 22. JetBlue is a low cost carrier with the highest current aircraft utilization rates in the U.S. and represents a worst case for the impact of schedule impact, while American Airlines is more representative of a traditional network carrier. The analysis also considers the potential impact of reduced turn-around times, which would mitigate the impact of reduced cruise speeds. The analysis shows that even at speeds as low as 10% below the design speed for these aircraft, the cumulative daily schedule slip is still generally less than 30 minutes.

It is also important to consider the impact of reduced cruise speed from the passenger perspective. The passengers would see lower cruise Mach numbers as slightly longer block times but given the continued airport congestion and security requirements, this is likely to be a relatively small factor and is not thought to be a market concern, especially on flights less than 1000 nm. Currently there is significant variation in cruise Mach number (Figure 23) and little evidence that passengers select on minimal block time. Passengers are more likely to select flights based on price or departure time. There may also be a marketing advantage if the aircraft is considered environmentally attractive, although this is speculative.

Figure 22: Total daily schedule slip based on cruise speed reduction for two types of operations.

Figure 23: Cruise Mach number history.[37]

Based on the analysis of these factors, it was determined to open up the cruise speed design space and allow cruise Mach number to be a design variable from Mach 0.83 to Mach 0.72.

2.4.4 Fuel and Emissions

The 2035 scenario highlighted the importance of improved fuel efficiency and reducing environmental impact both through reducing Green House Gas emissions through reduced fuel burn and reducing NOx. Due to long-term concerns on fuel availability, alternative fuel sources should be considered. The baseline requirement for fuel efficiency and emissions were established by the N+3 goal targets of fuel burn 70% reduction from the baseline aircraft and a 75% NOx reduction below CAEP 6. In evaluating fuel efficiency performance the Payload Fuel Energy Intensity PFEI was chosen as the performance metric. PFEI is the ratio of fuel energy burned divided by payload times the range. PFEI is not linked to a specific fuel so the metric is useful for evaluating performance between aircraft with different fuel assumptions. PFEI will be discussed in section 3.1.4.

2.4.5 Runway Length

Based on the infrastructure analysis (Figure 16) it was determined that for the existing U.S runways there is marginal gain in airport accessibility below 5,000 ft runways and that there is an adequate supply of airports with 5,000 ft or greater runways to accommodate the expected growth in demand. Lowering runway length, however, reduces cruise performance and a 5,000 ft balanced field length (sea level, standard temperature and pressure) was thus chosen as the runway length requirement for the B737-800 mission. A balanced field length requirement of 9,000 ft was set for the B777-200LR mission.

---

[37] Yutko, B., 2009. Data sources: *Jane's All the World's Aircraft*.

2.4.6 Noise

Noise performance will influence the airport accessibility and community response to airport operations. The 2035 scenario expects expansion into secondary airports where there are limited turbine and air carrier operations so it will be important to minimize the noise footprint. The N+3 goals specify a requirement of 71 EPNdB Cumulative below FAA Stage 4 noise limits, as well as a day-night sound level (LDN) of 55 dB or less at the average airport boundary.

2.4.7 Safety

The aircraft will be required to meet or exceed the FAA and JAA certification standards in the 2035 timeframe, which are expected to be more stringent than current certification standards.

2.4.8 Other

NextGen is assumed to be fully implemented by the 2035 timeframe so the N+3 aircraft should be fully compliant with NextGen requirements and be optimized for the NextGen operating environment of Optimal Profile Descents, 4D trajectory management, close parallel approaches, as well as other emergent Operational Concepts.

Because airport capacity will continue to be limited in the 2035 scenario, a desirable requirement would be to reduce the required vortex separation for the N+3 aircraft either by reducing the vehicle wake or reducing the vulnerability of the N+3 aircraft to wake encounters.

3 Figures of Merit

3.1 NASA N+3 Metrics

3.1.1 Noise

The noise certification analysis was performed according to Federal Aviation Regulation Part 36 (FAR 36) using Matlab noise scripts based on NASA LaRC's Aircraft NOise Prediction Program (ANOPP) for all the noise sources. Peak value attenuation as a function of duct length-to-diameter ratio, based on the results of the Silent Aircraft Initiative (SAI) project[38], was used for the prediction of noise attenuation due to acoustic liners. For the proposed highly integrated N+3 airframe-engine configurations, shielding is an important contributor for noise reduction. For the prediction of turbomachinery noise shielding, a diffraction integral method was employed[39]. This method was developed at MIT under a Boeing Phantom Works led NASA N+2 Subsonic Fixed Wing project entitled "Acoustic Assessment of Very Quiet Hybrid Wing Body Subsonic Transport".

The noise certification measurement locations are shown in Figure 24 below.
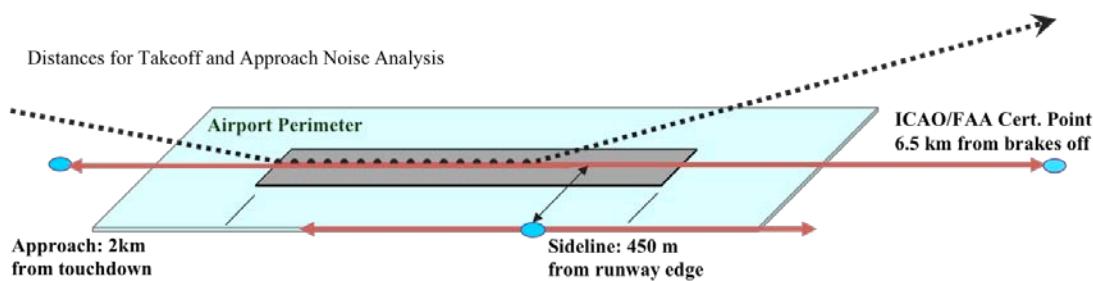
Figure 24: FAR Part 36 noise measurement locations.

For the sideline condition, the peak lateral noise was determined by changing the axial position of the observer along the runway edge and estimating noise at each location. The loudest position was taken as the sideline certification point. This is specified for each of the vehicles in sections 5.5.1 (D configuration) and 6.5.1 (HWB configuration).

Table 5 shows the noise sources considered and the estimation methods that have been used to determine the total noise for sideline, flyover and approach certification conditions, and therefore the cumulative EPNdB which is the metric used by NASA to evaluate the aircraft noise performance.

---

[38] Law, T.R., Dowling, A.P., "Optimization of Annular and Cylindrical Liners for Mixed Exhaust Aeroengines," AIAA 2007-3546, 13th AIAA/CEAS Aeroacoustics Conference (28th AIAA Aeroacoustics Conference), 2007.

[39] Ng, L.W-T., "Design and Acoustic Shielding Prediction of Hybrid Wing-Body Aircraft," MS Thesis. Massachusetts Institute of Technology, 2009.

Table 5: Noise Sources and Estimation Methods

Noise Source	Estimation method
Jet	ANOPP Stone 2 Jet Module
Fan forward	ANOPP Large fan module Diffraction Integral Method by MIT for shielding Acoustic liner treatment from SAI
Fan rearward	ANOPP Large fan module Diffraction Integral Method by MIT for shielding Acoustic liner treatment from SAI
Undercarriage	ANOPP Fink module Faired landing gear reduction from SAI
Vertical Tail	ANOPP Fink module
Horizontal Tail	ANOPP Fink module
Elevon	ANOPP Fink module (modeled as aileron)
Aileron	ANOPP Fink module
Flap	ANOPP Fink module

3.1.2 Balanced Field Length Calculation

3.1.2.1 Thrust Model

A high-bypass turbofan engine, operating at fixed fan and compressor pressure ratios during the takeoff, has its thrust decrease nearly linearly with velocity. The thrust dependence on velocity can be assumed to be quadratic without a large error and this allows an analytic derivation of takeoff velocity versus distance.

$$F(V) = F_0 - K_V \tfrac{1}{2} V^2 \tag{1}$$

$$F_0 = n_{eng} \frac{F_{\max} + F_{ref}}{2} \tag{2}$$

$$K_V = n_{eng} \frac{F_{\max} - F_{ref}}{V_{ref}^2} \tag{3}$$

The F_0 and K_V constants are set to give the actual thrust and also the actual thrust lapse rate at the V_{ref} takeoff reference airspeed, as shown in Figure 25. Because of the tangent fit at $V = V_{ref}$, the exact choice of V_{ref} is not critical, and a suitable choice is $V_{ref} = V_{stall}$, for example.
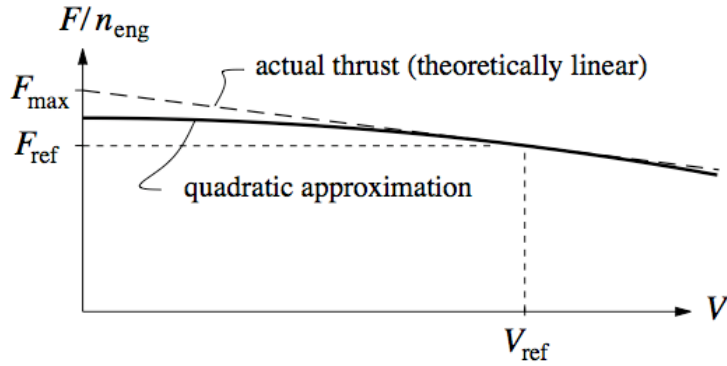
Figure 25: Thrust dependence on velocity, and assumed quadratic fit.

3.1.2.2 Velocity-Distance Relation

The equation for the ground-roll acceleration or deceleration is as follows.

$$m\frac{dV}{dt} = F - mg\,\mu - \frac{1}{2}\rho V^2 S\,C_D \ . \tag{4}$$

The lefthand side can be manipulated to yield

$$\frac{dV}{dt} = \frac{V}{V}\frac{dV}{dt} = \frac{d\left(\frac{1}{2}V^2\right)}{dl} , \tag{5}$$

and the quadratic thrust model is substituted for F, converting the acceleration equation (4) to the following equivalent form.

$$\frac{d\left(V^2\right)}{dl} = 2\frac{F_0 - mg\,\mu}{m} - \frac{K_V + \rho SC_D}{m}V^2 \tag{6}$$

This is a first-order ODE for V^2, whose solution is

$$k = \frac{K_V + \rho SC_D}{m} \tag{7}$$

$$V_{\text{lim}}^2 = \frac{2}{k}\frac{F_0 - mg\,\mu}{m} = 2\frac{F_0 - mg\,\mu}{K_V + \rho SC_D} \tag{8}$$

$$V^2{}_{(l)} = V_{\text{lim}}^2\left[1 - \cancel{c}\,\exp(-kl\,)\right] \tag{9}$$

where $\cancel{c}$ is an appropriate integration constant.

3.1.2.3 Takeoff Profiles

Figure 26 shows three different takeoff profiles, with the decaying-exponential V^2 plotted versus distance. Each of the three V_A, V_B, V_C segments is defined by (7)–(9), but with different constants. The relatively

simple Normal Takeoff will be considered first. The Engine-out and Aborted Takeoffs will then be considered, as these typically set the aircraft's takeoff performance requirements.

Takeoff Length Definitions

The normal takeoff length ℓ_{TO} is shown in Figure 26. This is simply the distance needed to accelerate to the initial climb speed V_2 (= 1.2 V_{stall}) which for transport aircraft is specified by FAR-25 regulation. The balanced field length ℓ_{BF} definition results from the situation where the distance needed to clear a 35 ft obstacle with one engine inoperative is equal to the distance needed to decelerate to a stop after the takeoff run is aborted. The situation is sketched in Figure 26, which also shows the as yet unknown abort-decision distance ℓ_1, and corresponding abort-decision speed V_1. For simplicity, one $V_B^2(l)$ function is assumed for the final roll and short climb in the Engine-out takeoff case. This is an appropriate simplification, since after liftoff the lost rolling resistance is comparable to the gained induced drag, so the net thrust does not change appreciably. Table 1 gives the constant values for the three velocity segments. Reverse thrust is assumed to be unavailable for the braking segment, as required by FAR-25 regulations. $C_{D_{eng}}$ is the drag of one windmilling engine, $C_{D_{i_{vert}}}$ is the induced drag of the vertical tail balancing the engine-out yaw moment, and $C_{D_{spoiler}}$ is the added drag of any deployed spoilers.
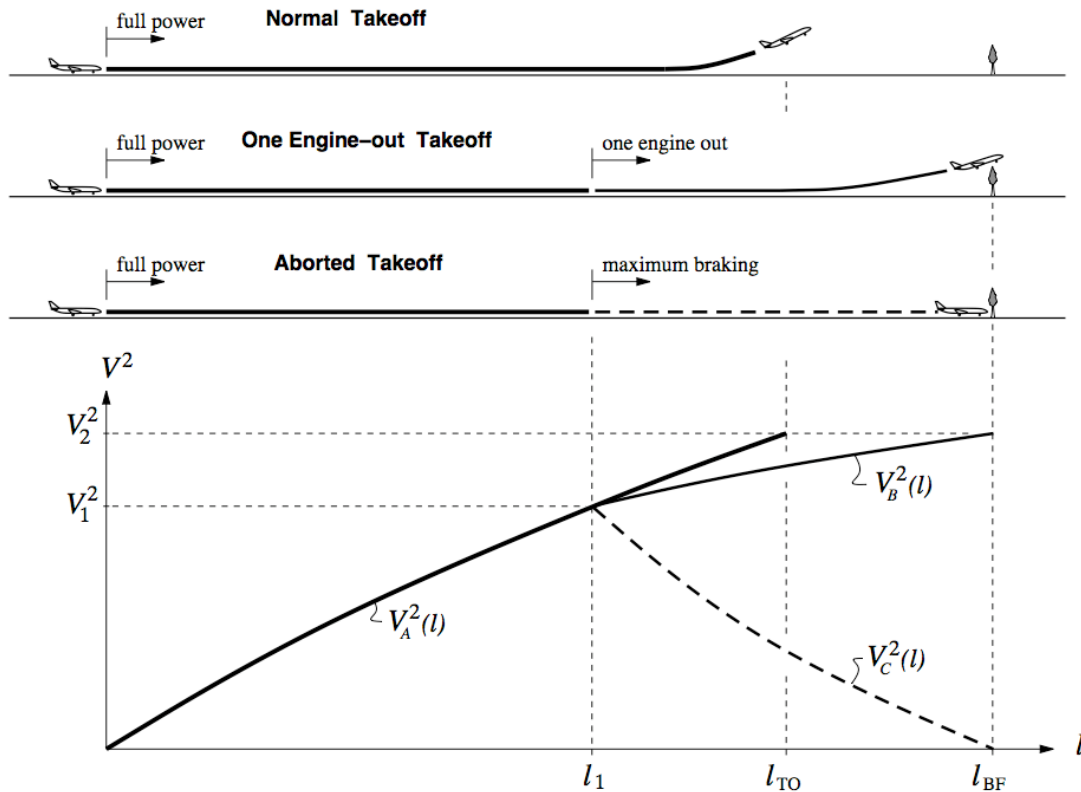
Figure 26: Engine-out takeoff and aborted takeoff over balanced-field length.

The known initial and end conditions

$$V_A(0) = 0, \tag{10}$$

$$V_B(\ell_{BF}) = V_2, \tag{11}$$

$$V_C(\ell_{BF}) = 0, \tag{12}$$

allow elimination of the integration constants ¢ for $V_A(\ell)$, $V_B(\ell)$, $V_C(\ell)$.

$$V_A^2(\ell) = V_{A_{lim}}^2 \left\{ 1 - \exp[-k_A \ell] \right\} \tag{13}$$

$$V_B^2(\ell) = V_{B_{lim}}^2 - \left(V_{B_{lim}}^2 - V_2^2 \right) \exp[k_B(\ell_{BF} - \ell)] \tag{14}$$

$$V_C^2(\ell) = V_{C_{lim}}^2 \left\{ 1 - \exp[k_C(\ell_{BF} - \ell)] \right\} \tag{15}$$

The k_A, k_B, k_C and $V_{A_{lim}}^2$, $V_{B_{lim}}^2$, $V_{C_{lim}}^2$ constants are calculated via their definitions (7) and (8), using the appropriate constants in Table 6 for each of the three A,B,C cases. Note that $V_{C_{lim}}^2$ is negative. The balanced field length ℓ_{BF} is still to be determined.

Table 6: Constants for Computing k and V$_{lim}$ for Each of the three A,B,C Takeoff Segments

		$V_A(\ell)$	$V_B(\ell)$	$V_C(\ell)$
F_0	=	$n_{eng} \dfrac{F_{max} + F_{ref}}{2}$	$(n_{eng} - 1) \dfrac{F_{max} + F_{ref}}{2}$	0
K_V	=	$n_{eng} \dfrac{F_{max} - F_{ref}}{V_{ref}^2}$	$(n_{eng} - 1) \dfrac{F_{max} - F_{ref}}{V_{ref}^2}$	0
μ	=	μ_{roll}	μ_{roll}	μ_{brake}
C_D	=	C_{D_p}	$C_{D_p} + C_{D_{eng}} + C_{D_{ivert}}$	$C_{D_p} + n_{eng} C_{D_{eng}} + C_{D_{spoiler}}$

Normal Takeoff Distance

The full-power Normal Takeoff distance ℓ_{TO} is completely determined by setting $V_A(\ell_{TO}) = V_2$, and solving for ℓ_{TO}.

$$\ell_{TO} = -\frac{1}{k_A} \ln\left[1 - (V_2/V_{A_{lim}})^2 \right] \tag{16}$$

The time required for the normal takeoff can also be determined by integration.

$$
\begin{aligned}
t_{\mathrm{TO}} \;=\; \int_0^{\ell_{\mathrm{TO}}} \frac{d\ell}{V_A(\ell)} \;&=\; \frac{1}{V_{A\,\mathrm{lim}}} \int_0^{\ell_{\mathrm{TO}}} \frac{d\ell}{\sqrt{1-\exp(-k_A\ell)}} \\
&=\; \frac{1}{k_A V_{A\,\mathrm{lim}}} \ln\!\left(\frac{1+\sqrt{1-\exp(-k_A\ell_{\mathrm{TO}})}}{1-\sqrt{1-\exp(-k_A\ell_{\mathrm{TO}})}} \right) \\
&=\; \frac{1}{k_A V_{A\,\mathrm{lim}}} \ln\!\left(\frac{1+V_2/V_{A\,\mathrm{lim}}}{1-V_2/V_{A\,\mathrm{lim}}} \right)
\end{aligned}
\tag{17}
$$

The above equations require that $V_{A\,\mathrm{lim}} > V_2$, otherwise takeoff cannot occur, and ℓ_{TO} and t_{TO} are not defined.

Balanced-Field Distance

The Balanced-Field case has ℓ_{BF} and also ℓ_1 as unknowns. The necessary two equations for determining them are the V_A, V_B, V_C segment matching conditions at $\ell = \ell_1$,

$$
V_A(\ell_1) = V_B(\ell_1)
\tag{18}
$$

$$
V_A(\ell_1) = V_C(\ell_1)
\tag{19}
$$

or equivalently,

$$
V_{A\,\mathrm{lim}}^2 \left\{ 1 - \exp[-k_A\ell_1] \right\} \;=\; V_{B\,\mathrm{lim}}^2 - \left(V_{B\,\mathrm{lim}}^2 - V_2^2 \right) \exp[k_B(\ell_{\mathrm{BF}} - \ell_1)]
\tag{20}
$$

$$
V_{A\,\mathrm{lim}}^2 \left\{ 1 - \exp[-k_A\ell_1] \right\} \;=\; V_{C\,\mathrm{lim}}^2 \left\{ 1 - \exp[k_C(\ell_{\mathrm{BF}} - \ell_1)] \right\}
\tag{21}
$$

Equations (20) and (21) can be simultaneously solved for ℓ_1 and ℓ_{BF} by Newton iteration. The initial guesses $\ell_1 = \ell_{\mathrm{BF}} = \ell_{\mathrm{TO}}$ are adequate for starting the iteration. As with the normal-takeoff case, the requirement $V_{B\,\mathrm{lim}} > V_2$ is necessary for a solution to exist.

As a final step, the V_1 abort-decision speed can be calculated from any of the three segment velocities, e.g.

$$
V_1^2 \;=\; V_{A\,\mathrm{lim}}^2 \left\{ 1 - \exp[-k_A\ell_1] \right\}
\tag{22}
$$

3.1.3   LTO NOx

Nitrogen Oxides (NOx) emissions from Gas Turbine engines have a negative impact on air quality, particularly at low altitude near airports[40]. A major goal of the N+3 program is to reduce low altitude NOx emissions by greater than 75% compared to the CAEP6 standard. NOx is a particularly important

---

[40] Kerrebrock, J. L., *Aircraft Engines and Gas Turbines,* The MIT Press, Cambridge, MA, second edition, 1992.

pollutant to regulate because unlike other harmful gas turbine emissions, NOx production is unrelated to the fuel efficiency of the engine. Other pollutants, such as unburned hydrocarbons and overall carbon output are directly related to the amount of fuel burned in the engine and therefore benefit from the pressure to reduce fuel burn. New technologies, such as higher pressure ratios and more efficient combustors that improve engine fuel burn, also reduce the emissions of fuel related pollutants. NOx emissions, however, are a function of combustor temperature, and can therefore be adversely affected by technologies designed to improve engine efficiency such as increased pressure ratio.

Currently the most stringent NOx emission standards were set during the 6th meeting of the Committee on Aviation Environmental Protection (CAEP) for engines produced after 2007. The NOx standards are structured to even out the inherent differences in NOx production in different engine classes and types, so that all engine designers face a similarly challenging emissions target. These standards are expressed per-unit thrust (D_p/F_∞) and are a function of overall pressure ratio (OPR) and engine thrust class. Engine emissions are measured on a static test stand during a simulated landing/takeoff (LTO) cycle in an effort to quantify the potential NOx impact from low altitude aircraft operation. The standards are [41]:

> "for engines of a type or model of which the date of manufacture of the first individual production model was after 31 December 2007:
> 1) for engines with a pressure ratio of 30 or less:
> > i. for engines with a maximum rated thrust of more than 89.0 kN:
> > > • $D_p/F_{oo} = 16.72 + 1.4080\pi_{oo}$
> > ii. for engines with a maximum rated thrust of more than 26.7 kN but not more than 89.0 kN:
> > > • $D_p/F_{oo} = 38.5486 + 1.6823\pi_{oo} - 0.2453F_{oo} - 0.00308 \pi_{oo} \times F_{oo}$
> 2) for engines with a pressure ratio of more than 30 but less than 82.6:
> > i. for engines with a maximum rated thrust of more than 89.0 kN:
> > > • $D_p/F_{oo} = -1.04 + 2.0\pi_{oo}$
> > ii. for engines with a maximum rated thrust of more than 26.7 kN but not more than 89.0 kN:
> > > • $D_p/F_{oo} = 46.1600 + 1.4286\pi_{oo} - 0.5303F_{oo} + 0.00642\pi_{oo} \times F_{oo}$
> 3) for engines with a pressure ratio of 82.6 or more:
> > $D_p/F_{oo} = 32 + 1.6\pi_{oo}$"

> Where: D_p = mass of pollutant emitted during LTO cycle (g), F_{oo} = rated thrust (kN), π_{oo} = rated OPR

An important feature of the CAEP emissions standards is their airframe independence. Utilizing a standard static test cycle forces engine designers to reduce emissions through engine specific technology development, as opposed to taking credit for engine airframe interactions. For N+3 this regulatory approach does not fully capture the emissions benefit of the design concept because embedded propulsion systems lead to reductions in required thrust, irrespective of engine efficiency, and therefore reductions in NOx released in the atmosphere on a per passenger or per operation basis. Coupling the inherent emissions reduction from an N+3 airframe concept with the engine specific emissions reductions leads to a dramatic reduction in the overall environmental impact. The reported NOx reductions are specific to the

---

[41] International Civil Aviation Organization, Annex 16 Volume II, *Aircraft Engine Emissions*, second edition, 1993, amended 2005.

N+3 engine technologies, while the overall emissions impact of the N+3 concept is captured via a climate analysis, described in Section 3.2.

NOx production is a complex chemical process that occurs at high temperature and is dependent on both the engine cycle parameters, such as Tt3 and fuel flow, and the physical structure of the flame front in the combustors. Improvement in combustor designs generally relates to changing the flame structure within the combustor to reduce residence time in high temperature regions while maintaining combustion efficiency. The NOx emissions have been estimated by using empirical combustor models that correlate NOx production to engine cycle parameters, with different combustor technology levels represented by different correlations. Changes to the engine cycle, such as higher bypass ratio, can be a major NOx reduction approach by producing more thrust per unit heat released in the combustor. For this program two correlations are presented, one representing the current combustor technology level, the other representing the latest low emissions combustor concepts from NASA's Ultra Efficient Engine Technology (UEET)[42] program. Comparing the predicted NOx emissions from these two correlations applied to N+3 concepts allows the impact of engine cycle changes and combustion technology changes to be independently bounded.
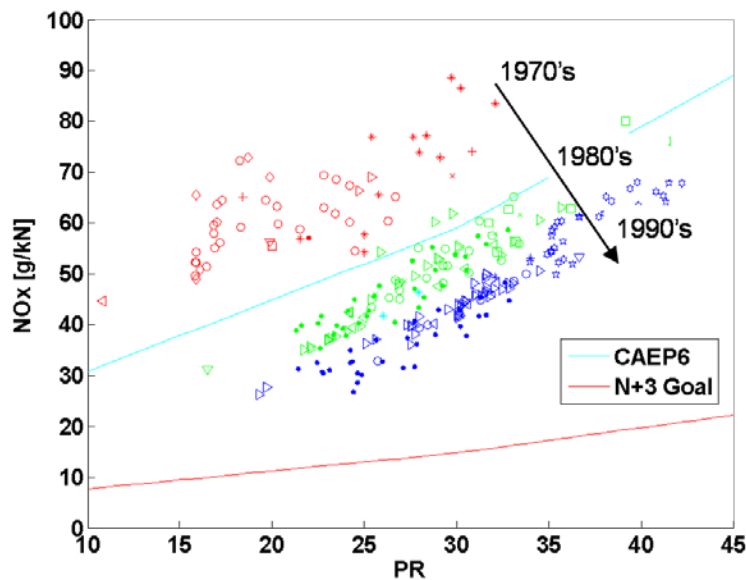
Figure 27: ICAO database LTO NOx emissions with pressure ratio for different combustor technology levels[43].

For engines using current technology level combustors a fit was produced using the International Civil Aviation Organization (ICAO) database of reported engine qualification tests[44]. Engines were grouped by

---

technology level, shown in Figure 27, using an approach similar to that of Mongia[45]. A NOx model of the form first proposed by Lefebvre[46] was fitted to each combustor technology level, shown in Figure 28. The model depends on compressor exit pressure and stoichiometric combustion temperature along with the empirical constants; this assumes combustors of the same technology level have similar mixing and residence times. The exponent on pressure was held fixed at 0.5 for all fits as suggested in related literature.[47][48] During low power engine operations NOx production mechanisms not captured by this modeling approach become important, therefore a limit of 4 g/kg of fuel was set as minimum NOx produced based on the idle behavior of current engines. Applying this correlation to existing engines such as the CFM56-7B series estimates NOx production within ~10% of the actual values.

$$NO_x \left[\frac{g}{kg} \right] = 2.7392E - 13 * P_3^{0.5} * e^{0.0108*T_{st}}$$

Figure 28: NOx production correlation for current generation combustors.

In NASA's UEET program advanced combustors with extremely low NOx production were produced by both industry and NASA. All these combustors successfully met the program NOx reduction goals and are representative of the combustor technology level expected in the N+3 timeframe. The performance of NASA's UEET combustor, the multipoint Lean Direct Injection (LDI) concept, is publicly available. The published NOx fit for the NASA LDI combustor, shown in Figure 29, is used to represent the potential NOx reduction expected when the UEET combustors enter into service. The model has limited applicability during low power operations, so the same minimum NOx production limit of 4 g/kg was used as in the conventional combustor model. The pressure loss due to mixing was assumed to be 4% and the minimum equivalence ratio was set at 0.45 as suggested by the published literature.

$$EINOx = 0.0092 * P_3^{0.59} * e^{T_3} * \varphi^{1.69} * \left(\frac{\Delta P}{P} \% \right)^{-0.56}$$

Figure 29: NASA LDI Combustor NOx data fit[49].

3.1.3.1 Cruise NOx

While NOx standards focus on low altitude NOx the impact of NOx emissions during cruise is also of interest and the same modeling approach can be used to bound the quantity of pollutants emitted. The engine cycle parameters and fuel flow at cruise are combined with the same NOx correlations used for the LTO NOx estimation. This approach is conceptually similar to the "P3T3" approach described as the

---

[45] Mongia, Hukam C. *Data Reduction and Analysis (DRA) for Emissions and Lean Blowout Part 1: Mostly Empirical Analysis (MEA)*, AIAA paper 2003-0822, 2003.

[46] Lefebvre, A.H., "Fuel effects on gas turbine combustion - linear temperature, pattern factor and pollutant emissions," AIAA paper 1984-1491, 1984.

[47] Zarzalis, N., Joos, F., Glaeser, B., Ripplinger, T., "NO(x)-reduction by rich-lean combustion," AIAA paper 1992-3339, 1992.

[48] Tacina, R., Mao, C.-P., Wey, C., "Experimental Investigation of a Multiplex Fuel Injector Module for Low Emissions Combustors," AIAA paper 2003-827, 2003.

[49] Tacina, R., Mao, C.-P., Wey, C., "Experimental Investigation of a Multiplex Fuel Injector Module for Low Emissions Combustors*," AIAA paper 2003-827, 2003.

Boeing Fuel Flow Method[50]. It is expected that the correlations will have less accuracy in the cruise regime, however the estimated values are presented to bound the potential emissions and suggest trends between aircraft configurations.

3.1.4 PFEI/Fuel Burn

The team used an energy intensity metric to allow for a fair comparison of 'fuel burn' for different aircraft concepts and fuel compositions, (e.g., conventional, alternative fuel, cryogenic, electric, etc.). Because the productivity of an aircraft can be defined as the movement of payload over a distance, the Payload Fuel Energy Intensity (PFEI) metric was chosen[51]. PFEI is defined as follows:

$$PFEI = \frac{\text{fuel energy consumed}}{\text{total payload x great circle distance}} \qquad (23)$$

For reference the PFEI for the fifty most fuel efficient aircraft in the current aircraft fleet have been plotted in Figure 30 which shows PFEI for 50 best existing aircraft within global fleet, computed using Piano-X software[52] as a function of the productivity (payload × range). Each line represents an aircraft type operating at 100% of its payload capacity over varied flight distances. The PFEI curves for the reference aircraft are noted in Figure 30. The goal of achieving a 70% reduction in fuel burn is shown for the two aircraft sizes being considered in this work.
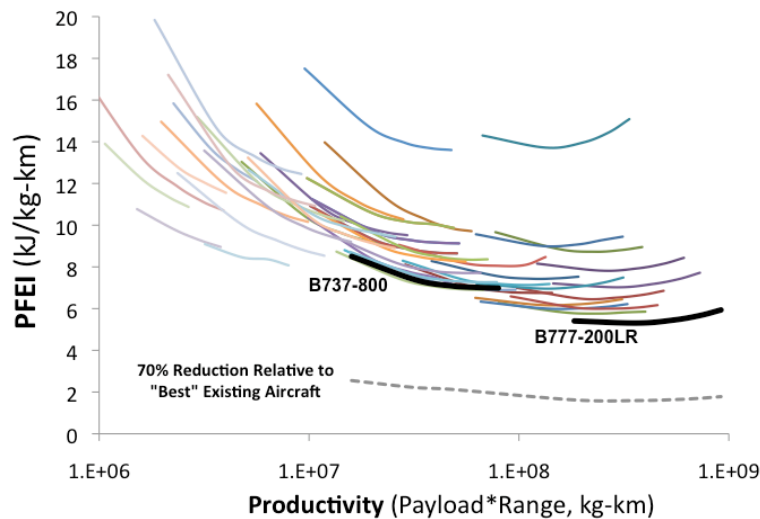
Figure 30: PFEI for 50 best existing aircraft within global fleet computed using Piano-X software[53].

---

[50] DuBois, D., Paynter, G.C., "Fuel Flow Method2 for Estimating Aircraft Emissions," SAE paper 2006-01-1987, 2006.

[51] Hileman, J.I., Katz, J.B., Mantilla, J., Fleming, G., "Payload Fuel Energy Efficiency as a Metric for Aviation Environmental Performance," Proceedings of the 26th International Congress of the Aeronautical Sciences, Anchorage Alaska, September, 2008.

[52] "Piano.Aero aircraft performance and design software," as of March 28, 2010, http://www.lissys.demon.co.uk/.

[53] As presented in the MIT Team NASA N+3 12 Month Presentation October 2009.

3.2 Climate

In Section 2, where the scenario developed for this project was discussed, the notion of including climate impact as part of the suite of parameters for evaluating aircraft concepts was introduced. In addition to the progressive warming of the planet, the upward trend in environmental policymaking and regulation motivates the expectation that it will become increasingly important to design aircraft for a climate-constrained world. The environmental analysis in Section 2 also indicated that climate is the largest environmental impact area to address and the area in which there is the greatest potential to make significant environmental strides, particularly through full-flight fuel burn and emissions reductions.

3.2.1 CO_2 Intensity

A metric of CO_2 Intensity combines PFEI with the fuel's carbon footprint to yield the total greenhouse gas emissions per payload range by considering the life cycle greenhouse gas emissions. The fuel life cycle includes the resource extraction, transportation of the resource to the production facility, the creation of the fuel from various raw materials, the transportation of the fuel to the airport, and then its use to power the aircraft. The summation of all of these emissions, as well as the emissions that result from each of the side processes is determined via a life cycle analysis with the result being the grams carbon dioxide equivalent per MJ (LHV) of fuel consumed by the aircraft:

$$g\ LC\ CO_2e = (g\ CO_2 + GWP_{CH4}*g\ CH_4 + GWP_{N2O}*g\ N_2O)_{WtT} + (g\ CO_2)_{TtW} \qquad (24)$$

Figure 31 presents the life cycle greenhouse gas emissions for liquefied natural gas using conventional technology from today as well as a wide range of liquid fuels that could be used in today's fleet of aircraft.
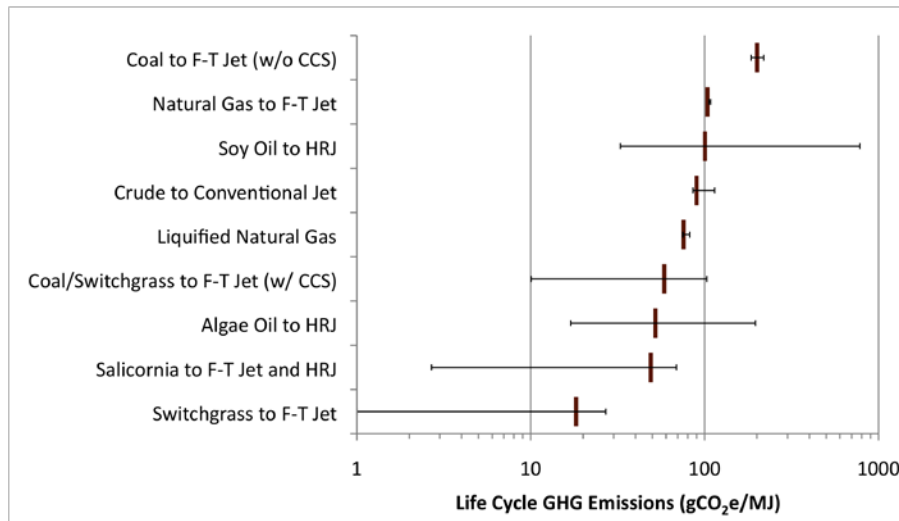
Figure 31: Life cycle greenhouse gas emissions from various alternative jet fuels as well as liquefied natural gas. Alternative jet fuel results from Stratton et al.[54] while the LNG results were derived in Appendix K.

---

[54] Stratton, R., Wong, H.M., Hileman, J., "PARTNER Project 28 Report: Life Cycle Greenhouse Gas Emissions from Alternative Jet Fuels," published by the Partnership for AiR Transportation Noise and Emissions Reduction (Report No. PARTNER-COE-2010-001), 2010.

The life Cycle CO_2 Intensity combines life cycle CO_2 emissions with PFEI:

$$LC\text{-}CO_2I = (g\ LC\ CO_2e/MJ) * (PFEI,\ MJ/kg\text{-}km) \tag{25}$$

Using the life cycle GHG emissions of conventional jet fuel, as presented by Stratton et al.[55], and the PFEI value from Figure 30, a fully loaded single aisle aircraft, such as the Boeing 737-800, produces roughly 0.6 g CO2e/kg-km. This can be compared to the 2005 fleetwide U.S. average value of 1.37 g CO_2e/kg-km, which was computed using data from the U.S. Bureau of Transportation Statistics[56] and the life cycle GHG emissions from Stratton et al.

3.2.2 Global Delta Temperature Change

To quantitatively assess the effects on climate, instead of simply accounting for an inventory, it is necessary to specify an appropriate climate metric. Using APMT-Impacts—an environmental impact modeling tool developed by MIT and funded by the FAA Office of Environment and Energy, NASA, and Transport Canada—the research team can look at the impact pathway of a unit of CO_2 emissions on climate, as depicted in Figure 32.

---

[55] Stratton, R., Wong, H.M., Hileman, J., "PARTNER Project 28 Report: Life Cycle Greenhouse Gas Emissions from Alternative Jet Fuels," published by the Partnership for AiR Transportation Noise and Emissions Reduction (Report No. PARTNER-COE-2010-001), 2010.

[56] U.S. Department of Transportation, Bureau of Transportation Statistics. Air Carrier Summary Data, Form 41 Schedule T-2 for 1991-2008. Washington DC: Department of Transportation.
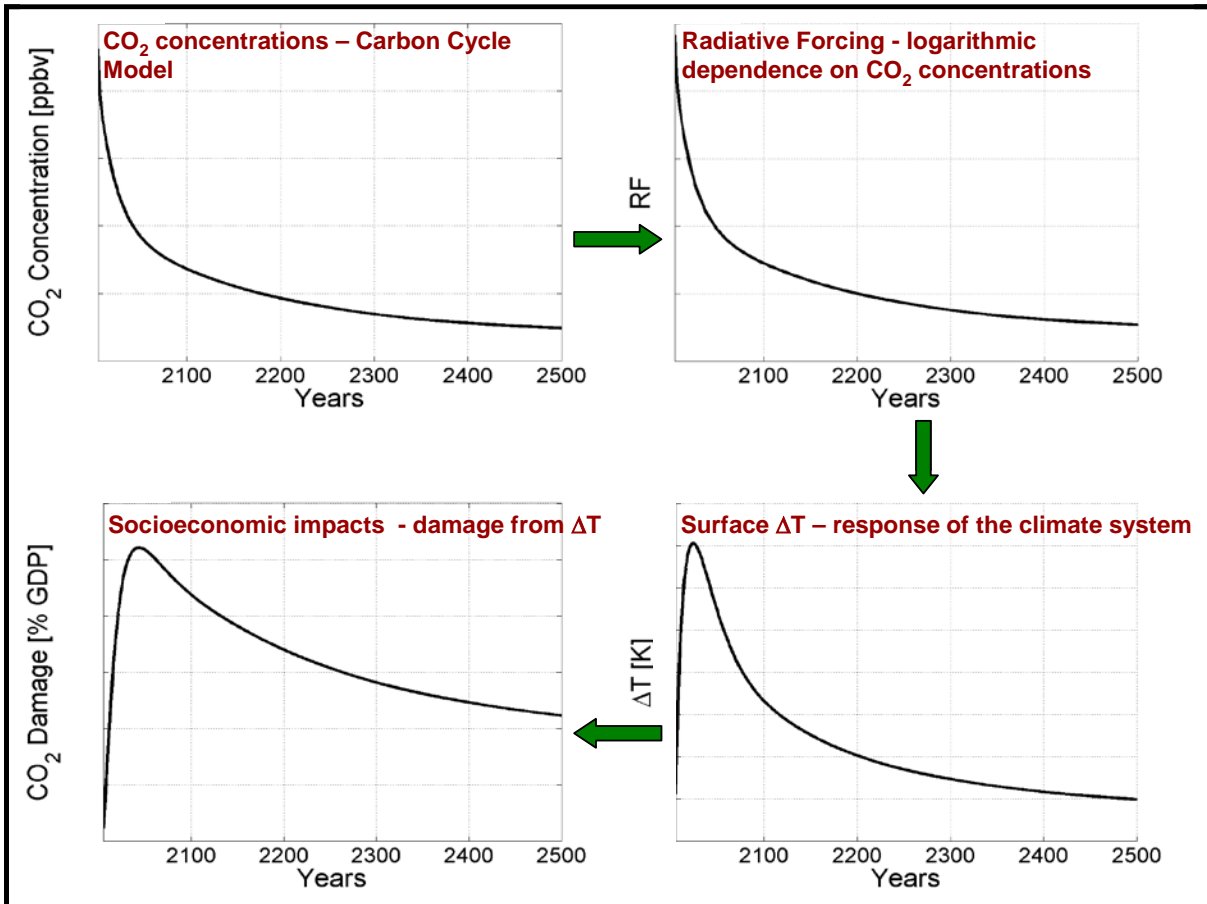
Figure 32: Evolution of a pulse of CO_2 on climate.

In the above figure, it is clear that there are a number of options to choose from in selecting a climate metric. Starting with aviation emissions, one can proceed along the impact pathway to change in atmospheric concentration, globally-averaged radiative forcing (RF), surface temperature change, and associated socio-economic damage. For this project, we used globally-averaged surface temperature change to assess different aircraft concepts. This metric was chosen because it lies the farthest down the impact pathway (apart from monetization of damages, which is often a source of contention in environmental analyses) and the information is thus more easily interpreted and more relevant to the decision-making community.

In looking at climate impacts, there is also choice to be made concerning time window (or, equivalently, discount rate for economic damages) that represents an implicit valuation of long- versus short-lived effects. The emissions from aircraft engines impact climate over varying timescales, as shown in Figure 33.
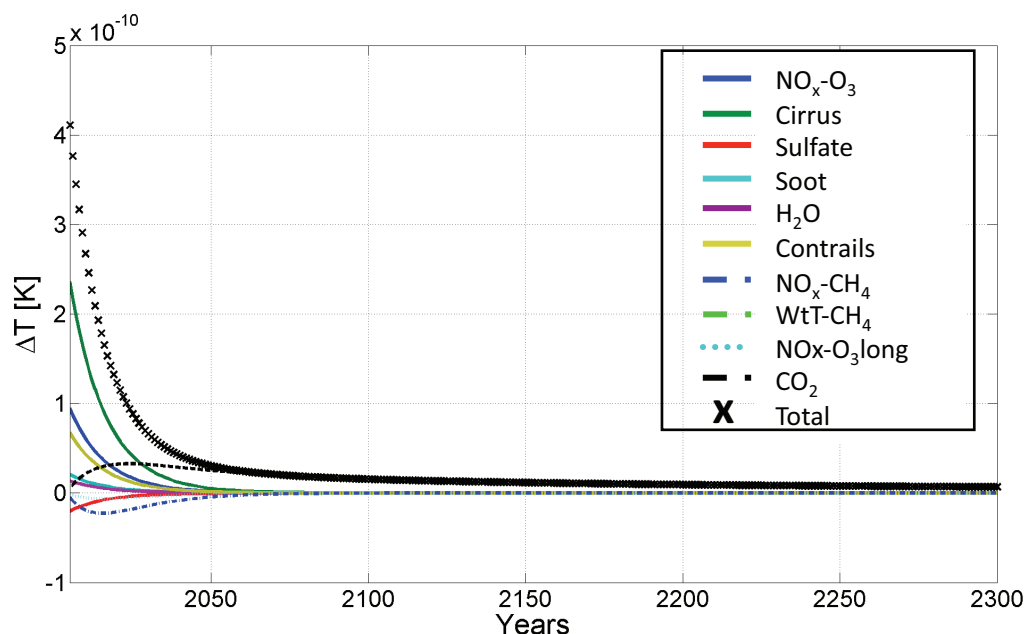
Figure 33: Climate impacts for a 30-year aviation scenario. Well-to-tank emissions are not included.

In Figure 33, a one-year aviation impulse was assessed, after which all emissions were set to zero. While some effects result in higher initial warming, the CO_2 impact is seen to persist on the order of hundreds of years. For this reason, the team used APMT-Impacts to calculate surface temperature change for each aircraft concept out to 800 years in order to capture the full lifetime of CO_2 impacts. The extent of climate impacts that will be captured include lifecycle CO_2 (production and combustion), well-to-tank methane (CH_4), the short- and long-term impact of NOx on ozone (O_3) as well as the impact of NOx on methane, contrails and contrail-induced cirrus cloudiness, sulfates, soot, and water vapor (H_2O). For a given aircraft concept, the climate metric will be calculated as temperature change normalized by aircraft productivity for a given mission (payload times distance). These concepts will then be compared on a climate basis to baseline aircraft of a similar class performing a similar mission.

4 Program Approach

4.1   Overall Process

The N+3 Phase 1 project was an 18 month collaborative effort between MIT, Aerodyne Research (for the first year), Aurora Flight Sciences, and Pratt & Whitney. The overall program was structured to accomplish the following tasks:

Task 1: Scenario Development
Task 2: Feasibility Assessment and Requirements Definition
Task 3: Operational Concept Definition
Task 4: Advanced Vehicle Conceptual Design
Task 5: Trade Studies
Task 6: Environmental, Economic, and Mobility Impact Assessment
Task 7: Credibility Establishment
Task 8: Pros/Cons Identification
Task 9: Risk Assessment and Development Challenge Identification
Task 10: Technology Roadmap Development
Task 11: Phase 2 Proposal Development
Task 12: Reviews
Task 13: Reporting

These thirteen tasks were grouped into process steps and organized into three primary phases of the program:

- Development of requirement, tools, concepts, and metrics.
- Trade Studies: Including trading the combination of technologies and aircraft concepts, trading the level of technology to use, as well as trading performance of the aircraft in regard to the various metrics against each other.
- Performance assessment and Evaluation. This including evaluating the performance against the baseline mission as well as evaluating the risk and technology maturation of each concept and included technology.

The following are the different steps in the overall process followed to accomplish the program tasks:

Step 1: Determine a baseline reference aircraft that can be used as the basis of comparison for each of the concepts generated.
Step 2: Establish a well-documented mission scenario (including aircraft requirements such as payload capacity, range) to establish comparative parameters of the different aircraft concepts.
Step 3: Develop metrics and tools for designing and evaluating vastly different aircraft configurations (architectures)
Step 4: Develop candidate technologies and concepts of the technologies that could have the greatest impact in terms of the evaluated metrics
Step 5: Group the technologies into aircraft concepts that employ the most favorable technology concepts
Step 6: Evaluate aircraft performance using mission scenario from Step 2
Step 7: Compare and contrast aircraft concepts based on program objectives and metrics

Although the list captures the steps, what is not captured in any sequential listing is the degree of iteration that is needed in a design process with four metrics and with a number of design constraints that must be closed. Figure 34 thus shows a more realistic (and more complex) view of the process. In addition to the

four metrics, as described in Chapter 3, a fifth quantity, climate impact, is also evaluated as part of the design loop.
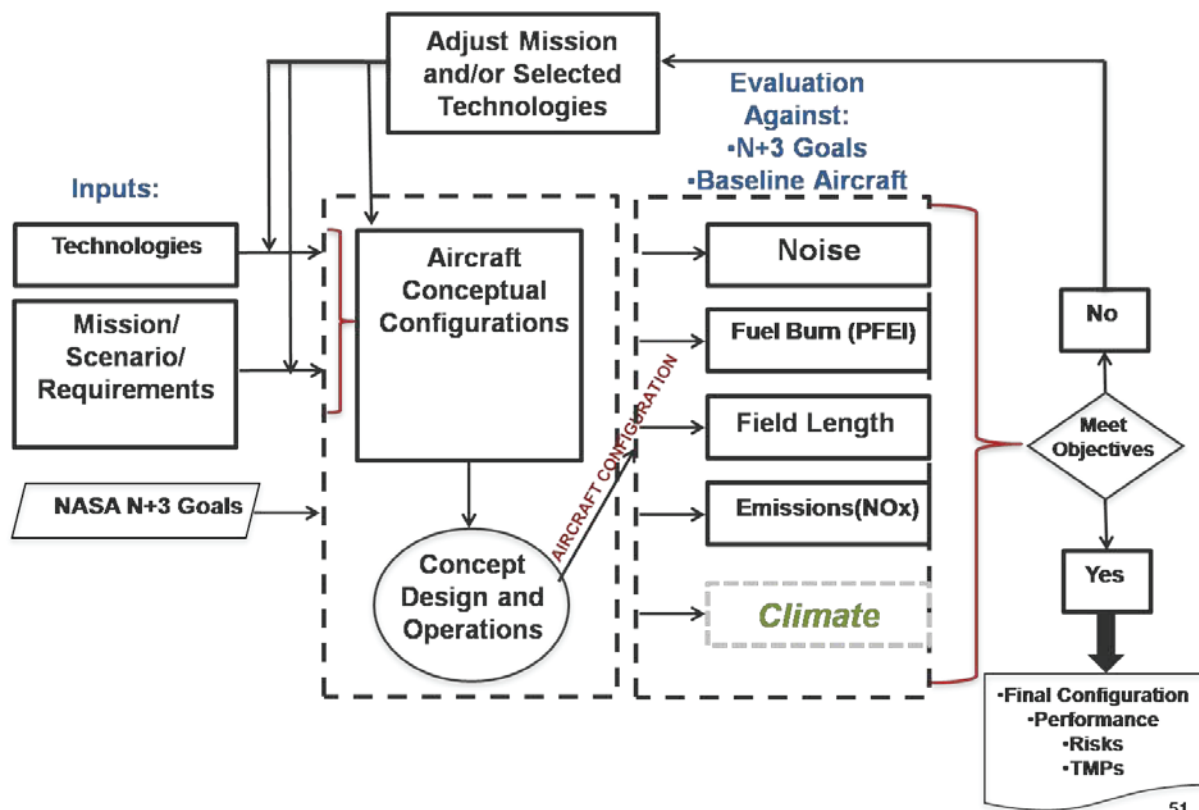
Figure 34: Overall program process flow[57].

4.2   Rationale for Examination of Two Different Aircraft Configurations

In the N+3 Phase 1 program the team investigated technologies and performance of two distinct aircraft configurations: (i) a Hybrid Wing Body (HWB) configuration that builds on information obtained from the Silent Aircraft Initiative but greatly modifies the design to address the NASA N+3 goals, and (ii) an innovative advanced tube and wing aircraft with a double-bubble fuselage, referred to as the "D8" series (or "D13" for the larger size) aircraft. The overall program process and execution for each of these two separate aircraft architectures was followed independently. As a result of the difference in configuration, different requirements and tools were needed to develop the separate aircraft concepts and to assess their performance. These two configurations have been pursued throughout the program in regards to scenario development and identification, technology evaluation, performance assessment and risk identification.

An important result of the program concerns the applicability of each of the two architectures to different scenarios. As the two configurations were designed and the performance assessed against various baseline missions and scenarios, we found the HWB aircraft was more applicable to a larger payload and longer range baseline aircraft, such as the B777-200LR, than to a smaller payload, shorter range aircraft such as the B737. We thus use the B777-200LR aircraft and mission as the baseline for the HWB. The D8 series

---

[57] MIT N+3 12 Month Review Presentation.

aircraft has as its baseline comparison scenario the B737-800, for which mission it performs extremely well.

We chose to develop and evaluate *both concepts* thoroughly, because of the different targets of each aircraft in the transport aircraft scenario. The two aircraft are presented in separate sections of this document, with the specific technologies that establish the performance of the aircraft described when appropriate. Section 5 describes the D8 series aircraft. It also gives a summary of the design modifications that lead to the performance differences between the baseline B737 and the D8 series. Section 6 then describes the HWB.

5 D8 "Double-Bubble" Design Concept

5.1   Design Overview

The D8 series aircraft configuration is an advanced tube and wing aircraft that has been designed in a newly developed process (referred to as TASOPT) that is built up from a first principles perspective and that incorporates the design and optimization of the mission, the airframe, operations, and the propulsion system. This process has as its objective the global optimization of aircraft fuel burn with other NASA requirements (e.g., field length) either appearing as constraints or being evaluated in a post processing step (noise and emissions) for reinsertion into the design loop. The D8 aircraft is targeted at a comparable mission as the B737-800.

Two versions of the D8 series aircraft will be discussed and described in this report. *The D8.1 aircraft is an aircraft optimized for minimum fuel burn while incorporating technologies available currently*. This provides a basis of comparison as to the final impact of the inclusion of each advanced technology on the performance in regards to each metric considered. It also provides a sense of the overall contribution to the accomplishment of the goals through the configuration alone. *The D8.5 is the final advanced vehicle configuration optimized to meet the N+3 program goals.* This includes the insertion of advanced technologies, processes, and designs that may not be available or ready to include in an aircraft until the N+3 timeframe.

The D8 series aircraft concept includes a "double-bubble" fuselage that allows for the inclusion of a lifting nose. (The D designation is provided as homage to the chief designer and originator of the concept design, Prof Mark Drela.) The concept features embedded aft engines with pi tail arrangement while designed around a reduced Mach number operation that allows for a nearly-unswept wing and eliminates the need for LE slats.

Figure 35: D8 Series aircraft rendering.
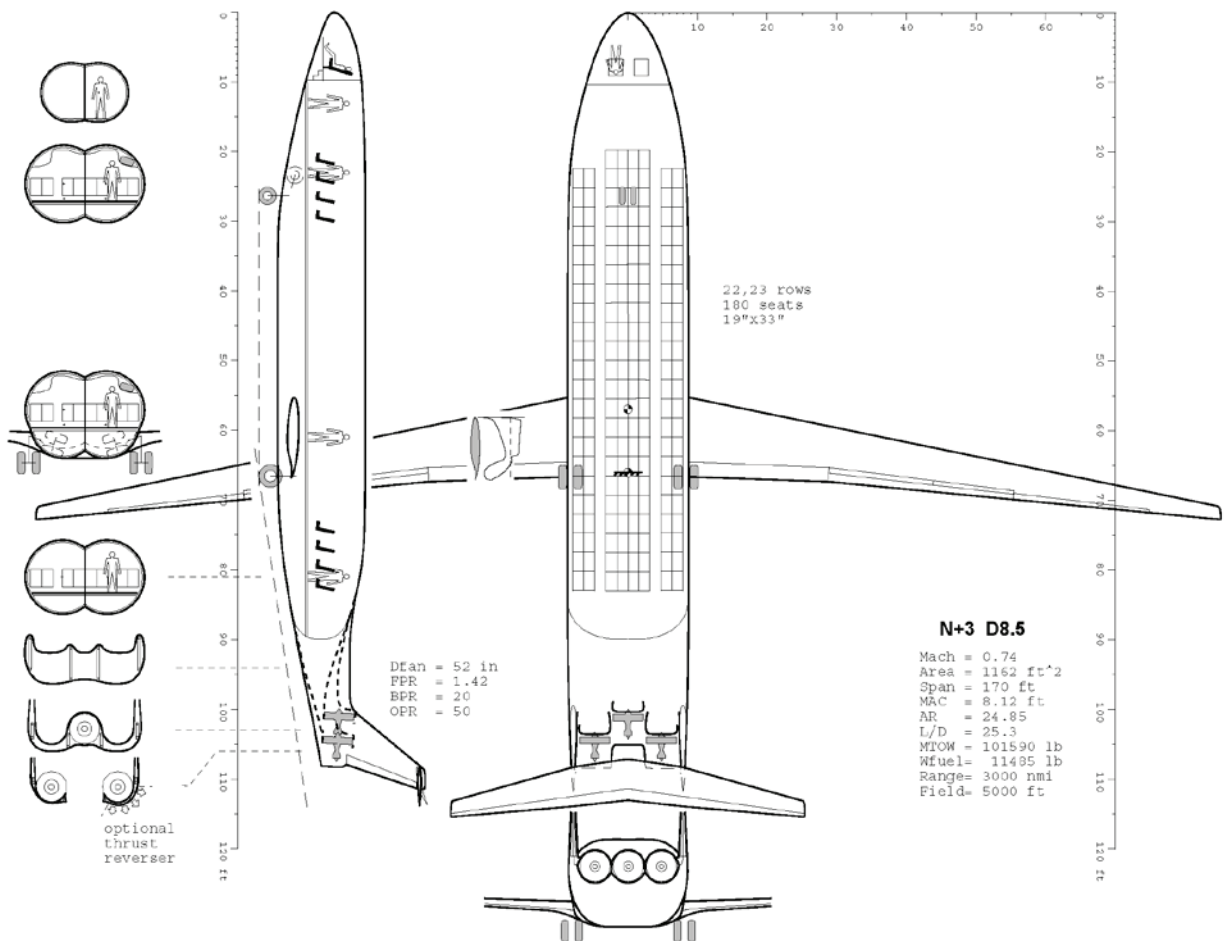
Figure 36: D8.5 layout.

Figure 36 provides a geometric three view layout of the D8.5 showing the major features. The aircraft is a twin aisle 2 X 4 X 2 seat arrangement within the double bubble fuselage. Various fuselage cross sections are laid out along the left of the figure to outline features of interest such as the landing gear retraction, luggage volume, and engine layout. Table 7 describes the D8.5 performance in regard to the baseline B737-800 aircraft for each of the four primary metrics of interest defined by NASA. The table gives the baseline performance, the design objective or goal and the final performance of the D8.5 aircraft both in terms of absolute values and in percent reduction from the reference.

Table 7: Performance of D8.5 in Relation to N+3 Program Metrics

Metric	737-800 Baseline	N+3 Goals % of Baseline	D8.5
Fuel Burn (PFEI) [KJ/kg-km]	7.43	2.23 (70% reduction)	2.17 (70.87% reduction)
Noise [EPNdB] (EPNdB below Stage 4)	277	202 (-71 EPN dB)	213 (-60 EPNdB)
LTO NOx [g/kN] (% Below CAEP 6)	43.28 (31% below CAEP 6)	>75% reduction	10.5 (87.3% reduction)
Field Length [ft]	7680 ft for 3000 nm mission	5000 ft (metroplex)	5000 ft

Table 8 shows the baseline mission for which the D8.5 aircraft design was optimized. The mission parameters are either variable's that were determined based upon the scenario developed for the 2035 mission (payload, range, etc. details in Section 2.0) or optimized in the design process (cruise altitude).

Table 8: D8.5 Aircraft Mission Parameters

Range (nm) (Plus 5% fuel reserves)	3000
Payload (lb)	38700
Cruise Mach number	0.74
Takeoff distance balanced field length (feet)	5001
Dry landing distance (CLmax =3) (feet)	2768[58]
Dry landing distance (CLmax =2) (feet)	3555
Wet landing distance (CLmax =3) (feet)	4185
Wet landing distance (CLmax =2) (feet)	5684
Cruise altitude beginning (feet)	44,653
Cruise altitude end (feet)	46,415

---

[58] Assumes 3 deg approach path over 50 foot obstacle, plus 3 second delay to full braking.

5.2   Design Concept and Technologies
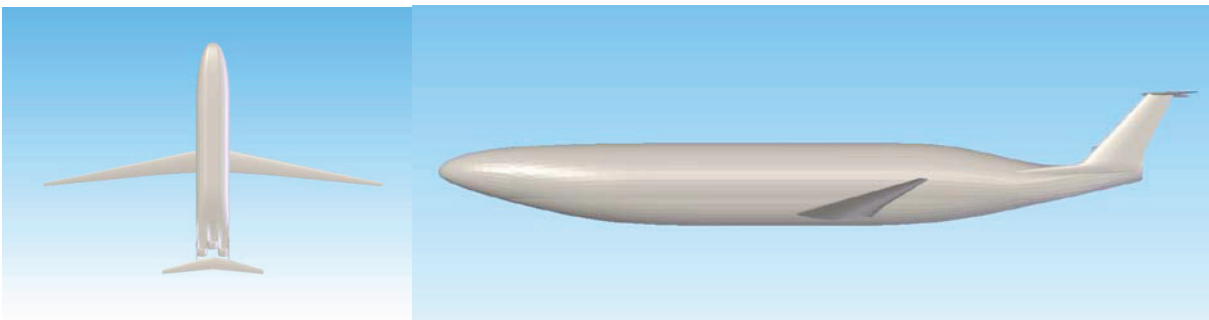
Figure 37: D8.5 top and side views.

D8.5 Configuration Primary Design Features

The D8 series configuration is a modified tube and wing configuration, with the following features:

- Double Bubble Fuselage with lifting nose:
    - Increases optimum carryover lift and effective span, via flat rear fuselage
    - Produces nose-up trimming moment, via fuselage lift on nose region
    - Provides roomier coach cabin than B737 coach, similar to A300 business class
    - Provides weight advantage of fewer windows, via 22.5 seat rows (vs. 30 seat rows)
    - Allows for *span loading* (i.e., fuselage lift) via 216" wide fuselage (vs. 154")
    - Reduces floor-beam weight via center floor support
    - Allows for shorter landing gear via better tail clearance
    - Improves propulsive efficiency via *fuselage boundary layer ingestion* (BLI)
- Embedded aft engines:
    - Allows use of pi-tail (π-tail) unit with surface flush-mounted engines
    - Improves propulsive efficiency via fuselage boundary layer ingestion
    - Enables lightweight minimal nacelles, via engine flow alignment by aft fuselage and fin strakes
    - Provides reduced susceptibility to bird strike, since engines are invisible head-on, especially at takeoff angle of attack
- Reduced cruise Mach = 0.72 (D8.1) or Mach = 0.74 (D8.5) with unswept wing (versus Mach = 0.80, sweep = 25 deg of B737-800):
    - Reduces CDi, via larger aspect ratio allowed by unsweeping of wing
- Eliminates need for LE slat, via increased CLmax from unsweeping of wing
- Configuration exploits synergy in fin stakes :
    - Functions as mounting pylons for engines and tail surfaces
    - Provides shielding of fan faces from ground observers
    - Provides usual strake's added yaw power at large beta
- Allows for small vertical tails, via small engine-out yaw moments
- Requires no typical weight penalty of T-tail, via twin pi-tail fins
    - Allows for lightweight horizontal tail, via its two-point mounting
    - Wake vortex circulation reduced by 80% from baseline through lower weight and increased aspect ratio
- Multi-segment rearward acoustic liners for noise reduction

In addition to those D8 series features advanced technology has been included in the D8.5 version in the following ways:

- Ultra high bypass ratio engines
- Advanced structural materials
- Reduced structural load margin through the use of the structural health monitoring and gust load alleviation
- Natural laminar flow on the bottom wing
- Advanced engine component efficiencies
- Advanced engine component materials
- Variable area nozzle for noise reduction at takeoff and fan operability
- Rearward acoustic liners for noise reduction
- Undercarriage fairings for noise reduction
- Approach procedures to reduce noise
- Lean Direct Injection (LDI) advanced combustor

Advanced technology insertion has partially "flattened" the PFEI vs. Mach dependence curve (compared to D8.1), primarily via the smaller weight penalty of thinner airfoils allowed by improved materials. This has allowed us to trade fuel burn for more speed, while still meeting the N+3 fuel burn goal.

Additional speed increases might be feasible, but are deemed unfavorable because of two other reasons which are not explicitly contained in a PFEI vs. Mach curve. The required sweep would make wing-bottom laminar flow much more difficult to achieve. Also, the amount of engine inlet diffusion required would introduce deleterious secondary flows in the BLI system.

In addition to the general configuration of the D8 series aircraft several technologies are central to achieving the final performance of the D8.5 aircraft. The detailed modeling and impact of each of these technologies as they are incorporated in the aircraft is included throughout the rest of the report. The following list of the technologies describes in general the technology and the level to which they are included in the D8.5 aircraft.

- *Boundary Layer Ingestion (BLI):* The D8.5 aircraft includes the effects of boundary layer ingestion of 40% of the boundary layer of the fuselage through the aft embedded engines.
- *Faired undercarriage:* These effects reduce the noise from the undercarriage.
- *Airframe advance materials and processes:* Structures technologies that are included in the design of the concepts include advanced materials and load reduction technologies such as gust load alleviation, flight envelope protection, predictive path planning, and structural health monitoring. The vehicle concept will use carbon fiber reinforced polymer (CFRP) for the entire structure, for which the constituent material properties have increased due to technological achievements by government and industry. The carbon composite material will include short carbon nanotubes (CNTs), which project to increase the compression after impact strength of the carbon fiber.
- *Airframe design load reduction (Gust load alleviation and Health monitoring):* Load reduction technologies will allow the vehicle concept to be designed to lower loading and still operate safely throughout the life of the vehicle. Gust load alleviation reduces the magnitude of gust loading on the wing through deflection of control surfaces to counteract the gust. Envelope protection and predictive path planning help limit the aircraft response to safe levels within the flight envelope. Structure and load monitoring technologies, which includes structural health monitoring, reduce the uncertainty in load and residual strength, all of which lead to a lighter and more efficient airframe.
- *Secondary Structures:* A variety of secondary structures are modeled as a factor applied to the total payload of the aircraft. This included all payload proportional factors carried on board the

aircraft. This factor is reduced from 0.35 to 0.3 for the D8.5 vehicle. This is done through the assumption that economic factors will drive the reduction in weight in items such as in seat entertainment and seats.

- *Ultra high bypass ratio engines (high efficiency small cores):* The D8.5 has a BPR ratio of 20 compared to 5 for the baseline B737 and 7 for the D8.1.
- *Advanced combustor technology (LDI):* The LDI combustor is used to model the mixing in the combustor for control of the generation of NOx.
- *Metal material allowable temperatures and cooling effectiveness:* Increased metal temperatures of the hot sections of the engine as well as increased film cooling effectiveness are taken into account. This was done to the extent that the total cooling flow was able to be reduced, by allowing a metal temperature of 1500 K and a film cooling effectiveness of 0.4.
- *Component efficiencies (Fan, Compressor, Turbine):* Continuation in the development and improvement of the component efficiencies of the turbofan engine is taken into account and bracketed to the extent that could be done within the timeframe of the program.
- *Advanced Engine Materials:* Advanced engine materials including CMC's and Titanium aluminum alloys, are included through a 10% reduction in the engine mass correlations developed for the engine.
- *Natural Laminar Flow on bottom wings*: Laminar flow is modeled for the D8.5 vehicle for the bottom surface of the wing only at a 60% laminar flow extent. This is modeled as a natural laminar flow with no boundary layer control mechanisms.

5.2.1 Design Modification Sequence from B737-800 to D8.1

In this section we illustrate the major reasons for the large fuel burn reduction of the D series aircraft by examining an aluminum-technology D8.1 configuration compared to B737-800 baseline aircraft. The features of the design will be shown by introduction of the various changes into the TASOPT design procedure on a one by one basis, so that, as the B737-800 gradually "morphs" into the D8.1 the various performance metrics can be observed. This allows us to determine the physical origins of the benefits, and to gauge their feasibility for being achieved in practice. Starting with the B737-800 as Case 0, the modifications will be introduced in eight steps, giving Cases 1-8, with the D8.1 being Case 8.

The following mission and optimization objective is specified for all Cases:

- 180 passengers x 215 lb / passenger = 38700 lb passenger payload (with luggage)
- 3000 nm range, landing with a 5% fuel reserve
- Cruise M=0.8 for Cases 0-2, M=0.76 for Case 3, M=0.72 for Cases 4-8
- Minimize fuel burn
- Balanced field length < 8000 ft for Cases 0-7, 5000 ft for Case 8

The (numerous) other inputs, such as material properties, added weight fractions, etc., are kept the same for all cases, unless specifically described.

Note that *in all of the different cases, the aircraft has been re-optimized for the change in conditions*. For example, in evaluating the effect of the change in cruise Mach number, it is not "just" slowing down, but includes the capability for a lighter wing. The point is that the different cases show the effect of changes in overall aircraft design rather than "only" the changes in aerodynamics, structures, and propulsion systems, i.e. the different include the interaction of those changes in allowing increased performance of an aircraft optimized to best take account of the changes. For reference the initial and final values of PFEI are 7.43 for the B737 Case 0, and 3.8 for the D8.1 Case 8, a 49% reduction.

Figure 38 through Figure 41 summarizes the evolution of key aircraft parameters for Cases 0-8 in sequence.
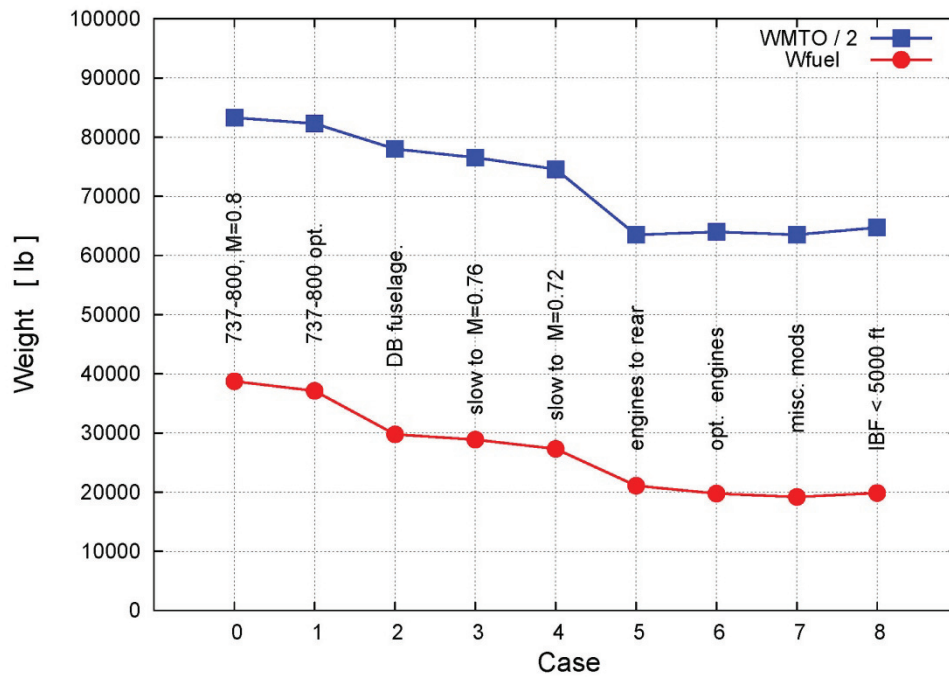
Figure 38: Aircraft parameter evolution; maximum takeoff weight, fuel weight.
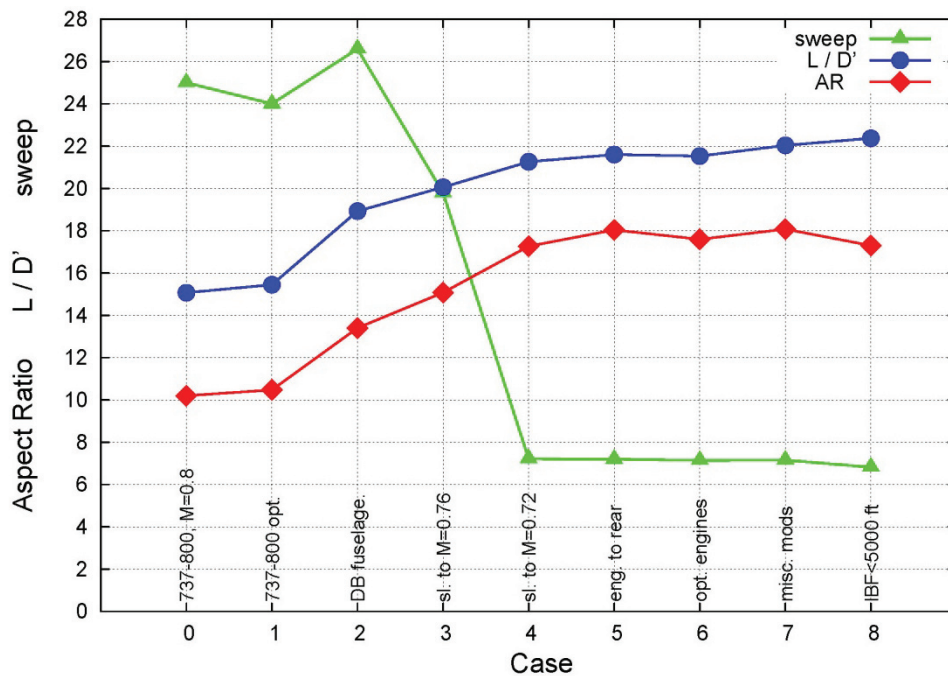
Figure 39: Aircraft parameter evolution; sweep, L/D, aspect ratio.
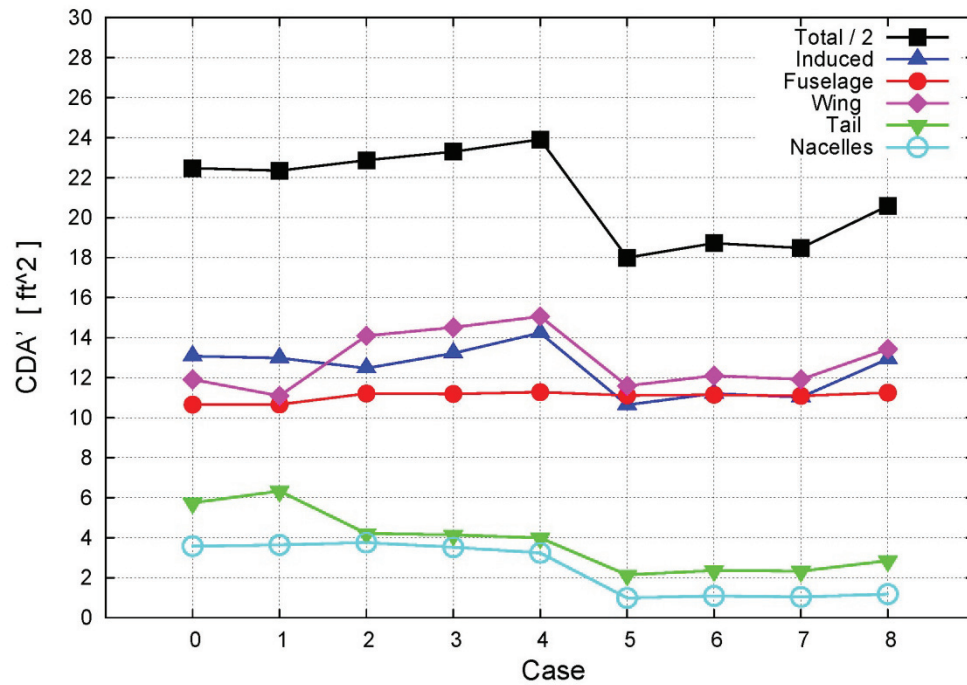
Figure 40: Aircraft parameter evolution; CDA's.
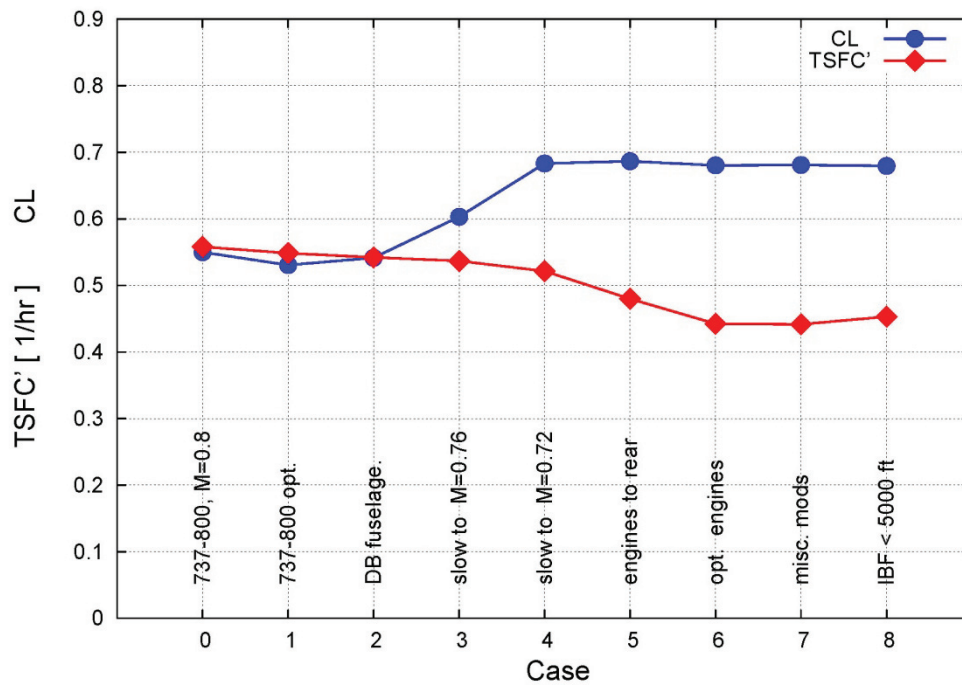
Figure 41: Aircraft parameter evolution; CL, TSFC.

5.2.1.1 Description of Modification Sequence

The different cases are described below:

Case 0: M = 0.80

This is the stock Boeing 737-800, as configured and sized by TASOPT for the design mission. This case has also been used to "calibrate" the handful of empirical added-weight fractions which have been used for all subsequent configuration studies. This case is NOT optimized, in that the usual design variables such as cruise CL, aspect ratio, sweep airfoil, t/c (wing airfoil thickness/chord), engine BPR and FPR, etc., are simply set to their known values for the B737. TASOPT is used here only to determine the key sizing parameters, in particular the wing span and area, the engine fan diameter and mass flow, and the numerous airframe gauges and weights. The fact that ALL of these sizing parameters (and not just the few used for calibration) closely match the actual values for the B737, gives considerable confidence that the overall TASOPT model well captures the aircraft features and capabilities.
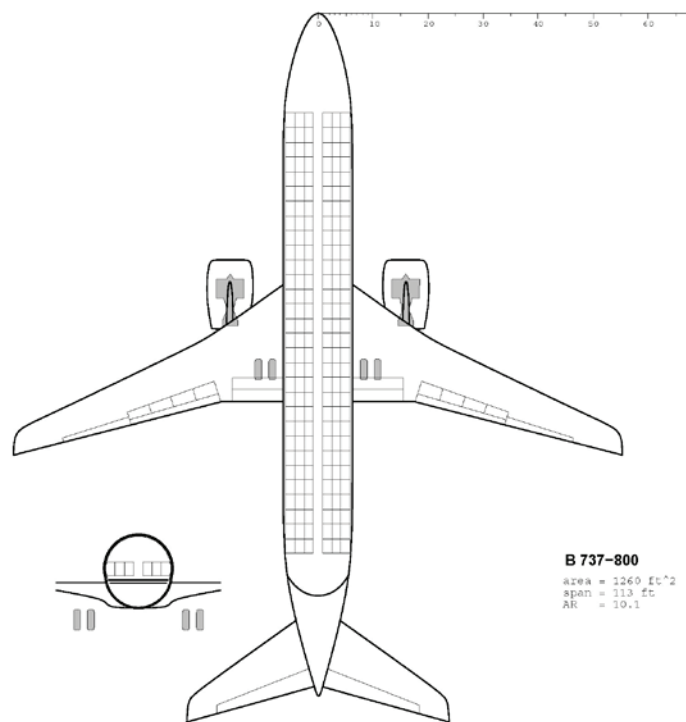
Figure 42: Boeing 737-800, for comparison with D8.1 in Figure 43.

Case 1: M = 0.80

This is close to the B737-800, except that now most of the usual optimization variables are determined by optimization rather than being explicitly prescribed:

- CL cruise lift coefficient
- AR aspect ratio
- Lam wing sweep
- t/c wing airfoil thickness/chord
- hCR1 start-of-cruise altitude
- Tt4TO takeoff turbine inlet temperature
- Tt4CR cruise turbine inlet temperature

The following remaining optimization variables were NOT optimized for this case, but were held at their known values for the CFM56-7 engine used on the B737-800:

- FPR fan pressure ratio
- BPR bypass ratio
- OPR overall pressure ratio

The reason is that a larger-BPR, larger-diameter engine, which would result from optimization would not fit under the B737 wing without modifications to the landing gear. Figure 38 through Figure 41 show that little changed during the optimization from Case 0 to Case 1, providing validity for the TASOPT model (assuming the B737 aircraft has also been optimized by Boeing). The main changes are

- +4.2% span
- +2.7% AR
- -1.2% MTOW
- +2.5% L/D
- -3.3% fuel burn, mainly via lower induced drag.

These changes are reassuring, since transport aircraft are typically designed to be slightly smaller than optimum[59] with a slight amount of fuel burn sacrificed for a smaller, lighter, and cheaper airframe so as to minimize total operating cost to the airline.

Case 2: M = 0.80

For this case, the B737 fuselage is replaced with the *double-bubble D8 fuselage*. The horizontal tail is now specified indirectly via a static margin of 0.20 at the aftmost CG case, in lieu of the previous B737's tail volume specification. This is done so that the nose-up trimming moment of the D8 fuselage can be properly exploited. The new fuselage gives very substantial benefits:

- +28% AR
- -5.2% MTOW
- -15.4% L/D
- -19.7% fuel burn

The lower weight and improved L/D result from numerous interacting effects. Ironically, the D8 fuselage itself has a slightly larger drag area by about 5% than the B737-800 fuselage, and it is only about 4% lighter than the B737 fuselage. Hence, all its benefits come from secondary effects on the rest of the aircraft. The most dominant of these is the front nose loading which allows the horizontal tail (HT) to be shrunk for the same overall pitch trimming power and static margin. Furthermore, the D8 fuselage's larger overall lift fraction and reduced HT download reduce the wing loads, which the optimizer exploits this by stretching the span and aspect ratio, thus producing the large L/D increase. Additional weight savings come from the 2-point support of the HT, which greatly reduces its bending moments and weight over the usual 1-point supported cantilever HT.

Case 3: M = 0.76

The difference between this case and Case 2 is that the cruise Mach has been reduced and the airplane re-optimized, giving the following benefits:

- +12.5% AR
- -2.9%   MTOW

---

[59] Liebeck R.H., personal communication

- +6%   L/D
- -1.0%   TSFC
- -3.0%   fuel burn

The larger Aspect Ratio is of course the direct result of the reduced sweep of 19.8 degrees, from 26.6 degrees of Case 1. In addition, the nacelle drag decreases somewhat, since the diffusion into the fan (from M=0.76 to 0.60) has been reduced by 20%, which reduces the nacelle loading and supervelocities on the nacelle surface. For this case, the minimum static margin has also been reduced from 0.20 to 0.15, which is considered permissible in light of the lower Mach and lower sweep which is expected to have a weaker sensitivity to transonic pitch up.

Case 4: M = 0.72

This is the same as Case 3, but cruise Mach is reduced further. A significant fuel burn reduction is produced:

- +14.5% AR
- -5.3%   MTOW
- +6%   L/D
- -2.9%   TSFC
- -5.3%   fuel burn

The Aspect Ratio increase is allowed by the now nearly unswept wing. The diffusion into the fan is now only 60% as large as in the M=0.8 case, giving further nacelle drag benefits. The minimum static margin is now further reduced to 0.10, justified by the very small sweep and no transonic pitch up issues, both due to the lower Mach number.

Case 5: M = 0.72

The CFM56-class engines are now moved from the wing to the tail and mounted flush with the top fuselage. Simultaneously, the APU and hydraulic/pneumatic power generation systems weight locations are moved from the tailcone to just behind the nose gear to help offset the rearward engine weight shift. The aircraft aft most-CG still shifts back by about 5 feet, taking the main landing gear with it. The elimination of the underwing engines allows a considerably shortening of the nose and main landing gear, which are lightened to 3.75% of gross weight from the previous 5.5%. The gear shortening is also allowed by the shorter D8 fuselage which can be seen to have no tail strike problems.

Moving the engines close to the centerline reduces the engine-out yaw moments by a factor of 5, allowing a large reduction in the required vertical tail (VT) area, weight and drag. The engine-out case is in fact no longer limiting, and instead the VT area is now sized by tail volume for the required yaw stability and damping.

With the rear flush engine mounting, a large fraction of the fuselage boundary layer is now ingested into the fans, although the cores still take in clean flow -- the ideal situation. This change is considerably enabled by the Mach number reduction from the previous two cases, in that the potential-flow Mach number at the engine inlet locations is close to the M=0.60 value required by the engine fans. Hence the fuselage boundary layer sees little or no deceleration going into the fans, avoiding development of streamwise vorticity and leaves the distortion more uniformly spread out over the fan face rather than being highly concentrated. This should considerably improve the fan's ingestion performance and stall resistance.

In summary, the lower-Mach cruise, the rear-mounted engines, and the BL ingestion all combine in a very synergistic manner to give a large overall aircraft performance improvement. The net benefits are as follows:

- +4.4% AR

- -14.9% MTOW
- -8.0% TSFC'
- +1.6% L/D'
- -22.8% fuel burn

Several observations on the drag reductions can be made:

1. The reduction in L/D appears modest but is misleading. The drag area of the entire aircraft shrank by 25%, but the lifting wing area also shrank by 24%, so the ratio changed little. The real benefit of the drag-area decrease in the case appears entirely in the reduced weight.

2. The fuselage mounting allows more than half of the nacelle wetted area (and weight) to be eliminated, since the rear fuselage in effect doubles as a flow-aligning nacelle and also acts as an acoustic shield. So the nacelles themselves have almost no aerodynamic load in cruise, see no flow misalignment at low speed and high alpha, and have lesser noise shielding demands, so that they can have a smaller chord than a typical underwing nacelle. In addition, they have surface velocities below the freestream value, all which combine to produce the extremely low nacelle drag, as can be seen in Figure 43.

Case 6: M = 0.72

This is the same as Case 5, except that the engine OPR is increased from 30 to 35, and the fan, compressor, and turbine efficiencies are increased by 1%, all to reflect realistic 15-year engine technology improvements from the CFM56 baseline. Furthermore, FPR and BPR are now optimized instead of being held fixed at the CFM56's values of FPR=1.65, BPR=5.1. The result is:

- FPR = 1.68
- BPR = 7.5
- -6.7% MTOW
- -7.8% TSFC'
- -6.7% fuel burn

Most of the benefits are from the increased component efficiencies. The changes in FPR and BPR and their benefits are small, due to the CFM56 engine parameters fortuitously being not too far from the optimum in this case. The main reason is that because of the substantial BLI, the fan must perform extra work just to bring the BL fluid back up freestream total pressure, so it optimizes to a larger FPR than expected. The corresponding BPR must also be modest, otherwise the core could not drive the fan at the large FPR. For advanced technology cores, with e.g. improved cooling or turbine materials, the additional core power would naturally optimize to a significantly lower FPR and larger BPR.

Case 7: M = 0.72

This is the same as Case 6, except that the slats are removed along with their weight. This is considered feasible since the elimination of sweep has inherently improves CLmax. The excrescence profile drag factor has also been correspondingly reduced by 3%, from 1.08 to 1.05. The following benefits are obtained:

- +2.7% AR
- -2.9% MTOW
- -0.2% TSFC'
- +2.4% L/D'
- -2.9% fuel burn

The gain is modest but not insignificant, and perhaps the simplicity and lower cost of a slatless wing would be a stronger consideration for the impact of this improvement as well as a reduction in noise.

Case 8: M = 0.72

This is the D8.1 configuration. It is the same as Case 7; except that a 5000 ft balanced field length constraint is now imposed, as opposed to the 8000 ft constraint assumed previously. The net result is perhaps a tolerable but certainly not insignificant penalty.

- -4.3%   AR
- +3.6%   MTOW
- -2.6%   TSFC'
- +1.5%   L/D'
- +3.5%   fuel burn

Dfan = 49 in
FPR = 1.58
BPR = 7.1
OPR = 35.8

optional thrust reverser

22,23 rows
180 seats
19"x33"

Sh=252 ft^2
Sv=134 ft^2

N+3 D8.1

Mach = 0.72
Area = 1298 ft^2
Span = 150 ft
MAC   = 10.6 ft
AR   = 17.3
L/D   = 22.1
MTOW = 126920 lb
Wfuel= 19820 lb
Range= 3000 nmi
Field= 5000 ft
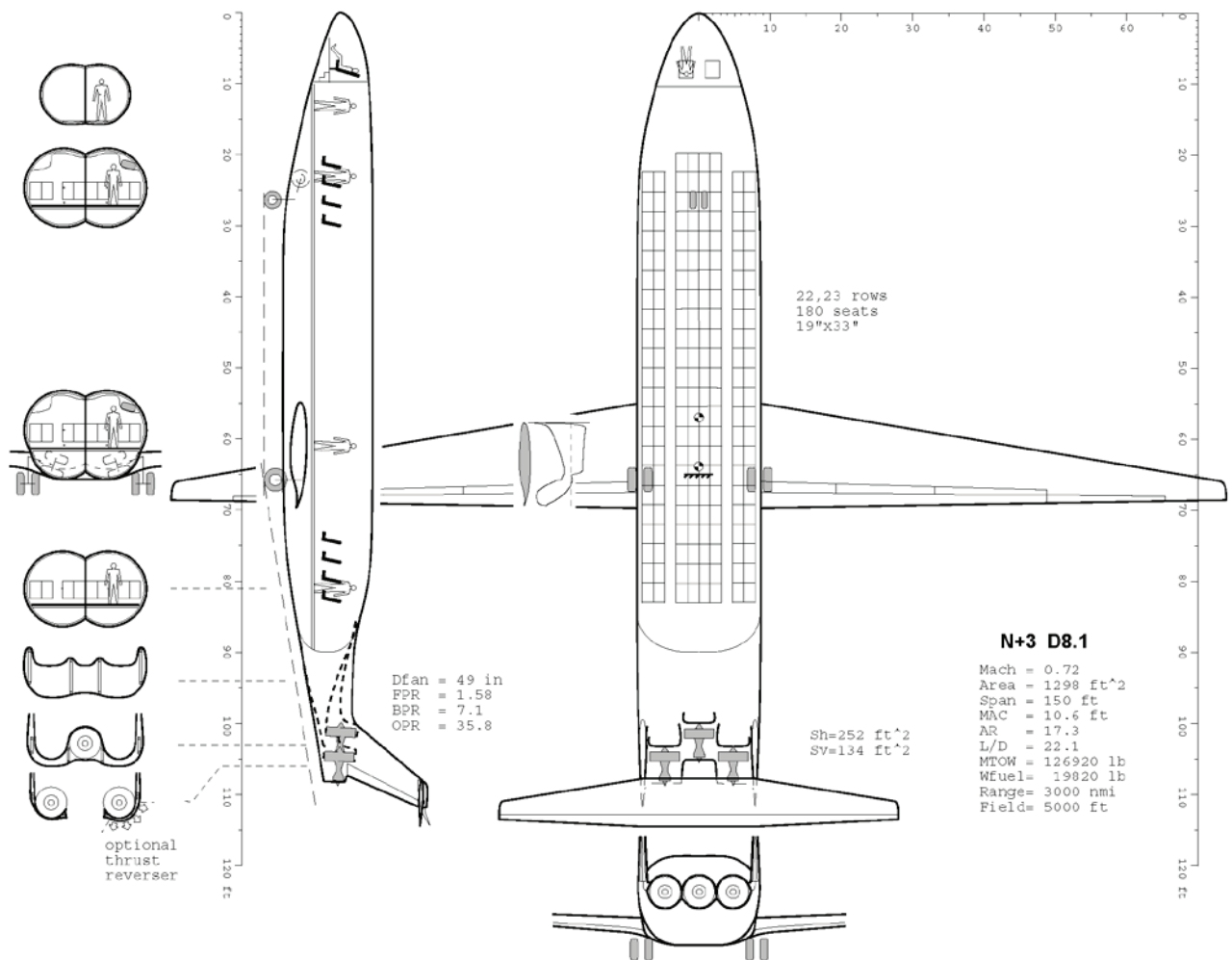
Figure 43: D8.1 layout.

5.3 Configuration Geometry / Dimensions

Section 5.1 and Section 5.2 provided an overall description and overview of the D8 series aircraft configuration. In this section the detailed geometry, dimensions, performance parameters and weights of both the D8.5 aircraft will be documented.

Table 9 describes the overall physical geometry and dimensions of the D8.5 aircraft.

Table 9: D8.5 Aircraft Geometry and Dimensions

Aspect Ratio, AR	24.85
Span (feet)	170
Sweep (deg)	12.6
Cabin width (feet)	16.7
Fuselage width (feet)	17.4
Cabin height (feet)	7.4
Fuselage height (feet)	12.7
Fuselage length (feet)	107
Horizontal tail AR	13.0
Horizontal tail span (feet)	50

5.3.1 Aerodynamic Parameters
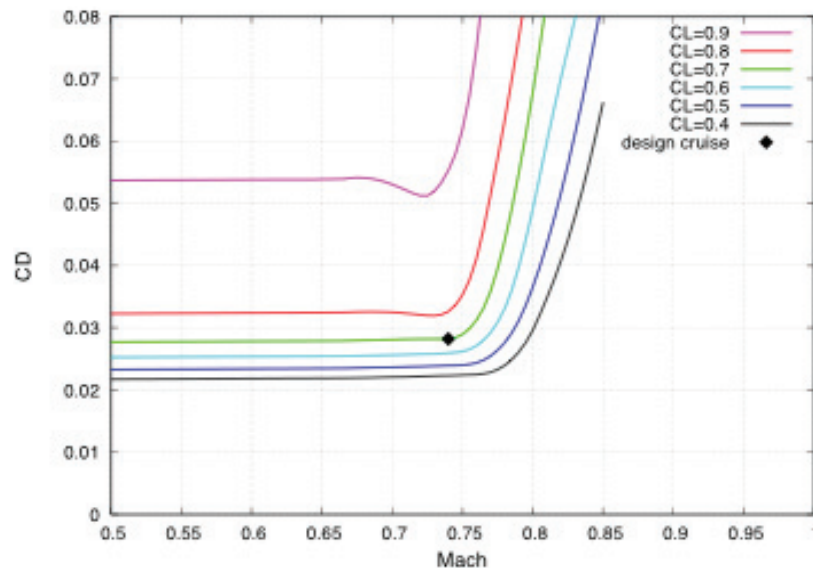
Figure 44: D8.5 transonic drag rise polars.
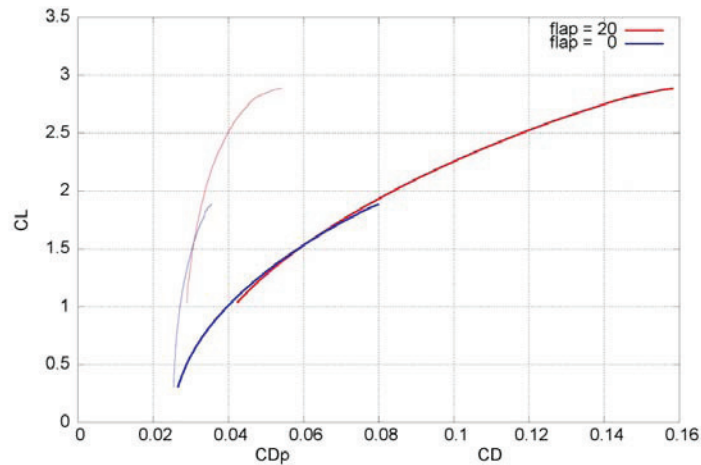
Figure 45: D8.5 low speed drag polar.

Table 10: D8.5 Engine Performance Parameters

Parameter	Sea Level Static	Rolling / Rotation	Takeoff	Cutback	Top of climb	Cruise	Approach
Net thrust (kN)	37.7	29.0	27.7	14.2	5.9	5.9	1.9
Ram drag (kN)	N/A	9.2	11.8	9.2	11.7	11.7	4.1
TSFC' (lb/lb h)	0.174	0.228	0.239	0.243	0.370	0.370	0.418
Engine mass flow (kg/s)	201.9	207.8	210.3	163.0	57.6	57.4	78.7
BPR	22.8	23.3	23.5	25.7	20.0	20.0	23.6
Cooling flows (kg/s)	0.125	0.126	0.126	0.090	0.040	0.040	0.047
OPR	33.7	33.4	33.2	21.4	50.2	50.0	9.0
TT4/TT2	5.6	5.6	5.5	2.57	6.63	6.62	2.98
Fan efficiency (%)	96.5	96.5	96.5	97.3	95.1	95.1	98.0
High compressor efficiency (%)	90.0	90.0	90.0	90.0	90.0	90.0	90.0
Low compressor efficiency (%)	93.0	93.0	93.0	93.0	93.0	93.0	93.0
High turbine efficiency (%)	92.5	92.5	92.5	92.5	92.5	92.5	92.4
Low turbine efficiency (%)	90.4	90.5	90.5	86.9	93.0	93.0	80.5
Fan pressure ratio	1.25	1.24	1.24	1.14	1.43	1.42	1.04
Low pressure compressor pressure ratio	1.92	1.92	1.92	1.62	2.27	2.27	1.22
High pressure compressor pressure ratio	17.56	17.40	17.33	13.24	22.07	22.0	7.36
Low Pressure Turbine Pressure Ratio	0.14	0.14	0.14	0.20	0.08	0.09	0.47
High Pressure Turbine Pressure Ratio	0.25	0.25	0.25	0.25	0.25	0.25	0.25
Core Inlet Pressure Recovery	0.995	0.995	0.994	0.994	0.962	0.962	0.994
Core Exhaust Duct Recovery	0.995	0.995	0.995	0.995	0.995	0.995	0.995
Fan Exhaust Duct Recovery	0.985	0.985	0.985	0.985	0.985	0.985	0.985

Propulsion System Weight and Dimensions

The propulsion system is comprised of three embedded high bypass ratio geared turbofans located in the aft pi-tail of the aircraft. Table 11 lists the propulsion system components and materials for the D8.5 aircraft.

Table 11: Propulsion System Component Mass Breakdown

Engine Length (in)	59.9
Engine Diameter (in)	51.9
Nacelle, Reverser, VAN Weight (lb)	236.2
Pylon Weight (lb)	105.7
Fan Weight (lb)	630.8
Low Pressure Compressor Weight (lb)	18.3
Core Weight (lb)	282.4
Low Pressure Turbine Weight(lb)	240.5
Accessories Weight (lb)	388.7
Fan Drive Gearbox Weight (lb)	146.2
Nacelle Material	Advanced Carbon Composites, Titanium
Fan Material	Advanced Carbon Composites, Titanium
Compression System Material	Titanium Matrix Composite Disks, Ti front stages, Ni rear stages
Turbine Material	Ceramic Matrix composites, Nickel Alloys, TiAl
Accessories Material	10% Improvement over current SOA

The engine accessories weight includes the FADEC, wiring harness, accessories gearbox, and other associated miscellaneous engine accessories. The engine nacelle weight includes the noise liner and nacelle mounting pylons as well as containment structure.

5.3.2 D8.5 Series Weight Buildup

The following definitions are important when discussing the weight buildup of the aircraft concept and will help to define the different groups to which the structural mass has been allocated.

Operating Empty Weight (OEW)
Operating Empty Weight (OEW) is the basic weight of an aircraft including the crew, all fluids necessary for operation (such as engine oil and engine coolant) and all the gear required for flight but not including the fuel and the payload.

Maximum Takeoff Weight (MTOW)
The Maximum Takeoff Weight (MTOW) of an aircraft is the maximum weight at which the pilot of the aircraft is allowed to attempt to take off, due to structural or other limits. The MTOW includes the Operating Empty Weight (OEW), as well as fuel and payload.

Material Properties

The table below gives a list of the material properties used in the design. The variables that correspond to these material properties are directly inserted into the TASOPT structural sizing code. Definitions of the variables can be found in the TASOPT documentation. The D8.5 Concept will use carbon fiber reinforced polymer (CFRP) for the entire structure, with improved constituent material properties have improved due to technological achievements from government and industry. The carbon composite material will include short carbon nanotubes (CNTs), which project to increase the compression after impact strength of the carbon fiber.

Table 12: Material Properties

Variable[60]	Value	Units	Justification
sigskin	29800	psi	59.6ksi compression after impact (2.0 typical factor of safety for fuselage)
sigbend	49500	psi	99ksi unnotched compression 50/40/10 layup (2.0 typical factor of safety for fuselage)
sigcap	39700	psi	59.6ksi compression after impact (1.5 typical factor of safety for wing)
tauweb	21300	psi	64ksi unnotched compression 10/40/50 layup (1.5 typical factor of safety for wing)
sigstrut	66000	psi	198ksi unnotched tension 50/40/10 layup (3.0 stress concentration factor to simulate open hole tension)
rhoskin	0.056	lb/in^3	CFRP (62% fiber volume fraction)
rhobend	0.056	lb/in^3	CFRP (62% fiber volume fraction)
rhocap	0.056	lb/in^3	CFRP (62% fiber volume fraction)
rhoweb	0.056	lb/in^3	CFRP (62% fiber volume fraction)
rhostrut	0.056	lb/in^3	CFRP (62% fiber volume fraction)
Ecap	18.2	Msi	50/40/10 bias layup
Eweb	7.5	Msi	10/40/50 bias layup

The structural sizing code performs basic panel sizing using the material properties listed in Table 12. At interfaces of components, weight fractions are used to account for additional structure weight of all fasteners, non-load bearing materials, etc. These weight fractions are calibrated to the baseline B737-800 aircraft, and scale with the weight per the TASOPT documentation. Thus, the D8.5 concept structure interface weight is reduced in magnitude (but not ratio) from the baseline B737-800. This reduction in weight is projected to be achieved primarily from use of unitized structure manufacturing and assembly techniques.

The D8.5 concept will have a reduced part count due to the ability to lay up complex parts as a co-cured structure requiring fewer fasteners and fittings. Out-of-Autoclave (OOA) resins also enable larger components to be cured without the size restriction of an autoclave. Processes like Resin Transfer Molding (RTM) and Vacuum-assisted Resin Transfer Molding (VaRTM) allow increased out-time for complex layups prior to curing. Pultruded Rod Stitched Efficient Unitized Structure (PRSEUS) and similar processes allow for the combination of skin, stringer, and frame elements into a common

---

[60] These variables are TASOPT density and material strength scaling factors and are defined in the TASOPT documentation.

structure. These techniques and others allow for weight savings at details and interfaces to match weight savings in the structure itself.

The component weights shown next were obtained entirely via sizing using the predicted loads and assumed material properties.

5.3.3 D8.5 Operating Empty Weight (OEW)

Table 13 – Operating Empty Weight (OEW) Breakdown

Component	Weight, lbs
Structure	35,652
Fixed Equipment	3,000
Propulsion	6,659
Landing Gear	6,096
Total	**51,406**
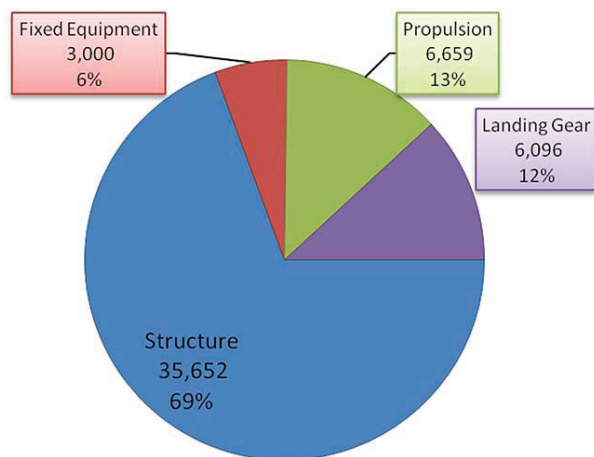
Figure 46: Operating Empty Weight (OEW) breakdown.

Fixed Equipment includes:
- Miscellaneous Fixed Equipment
  - Pilots
  - Cockpit windows
  - Cockpit seats, furnishing, mechanisms
  - Flight Instrumentation
  - Navigation and communication equipment, antennas, etc.
  - Cockpit power-related weight (power generation, wiring

5.3.4 *D8.5 Maximum Takeoff Weight (MTOW)*

Table 14: Maximum Takeoff Weight (MTOW) Breakdown

Component	Weight, lbs
Structure	35,652
Fuel	11,486
Fixed Equipment	3,000
Payload	38,700
Propulsion	6,659
Landing Gear	6,096
Total	**101,592**
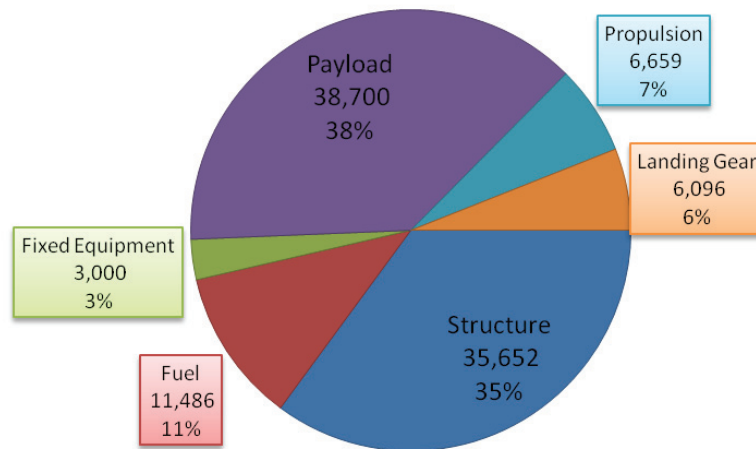
Figure 47: Maximum Takeoff Weight (MTOW) breakdown.

Fixed Equipment includes:

- Miscellaneous Fixed Equipment
    - Pilots
    - Cockpit windows
    - Cockpit seats, furnishing, mechanisms
    - Flight Instrumentation
    - Navigation and communication equipment, antennas, etc.
    - Cockpit power-related weight (power generation, wiring)

5.3.5 *D8.5 Structure Weight Breakdown*

Table 15: Structure Weight Breakdown

Component	Weight, lbs
Fuselage	24,774
Wing	13,439
Horizontal Tail	259
Vertical Tail	173
Total	**38,646**
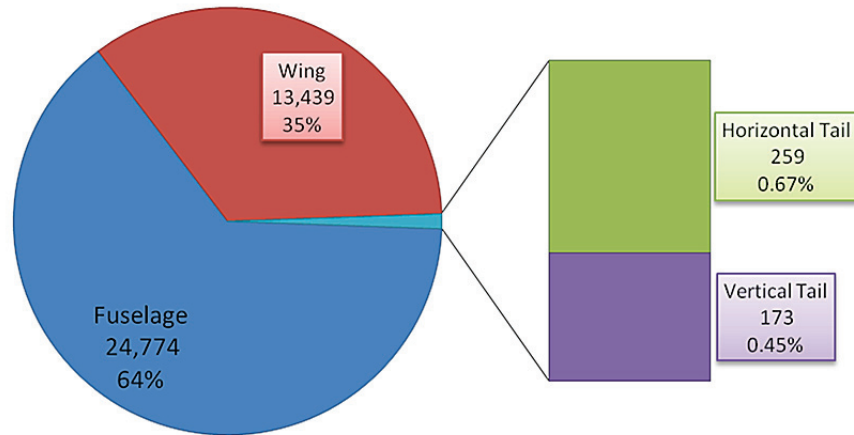
Figure 48: Structure weight breakdown.

5.3.6 D8.5 Fuselage Weight Breakdown

Table 16: Fuselage Weight Breakdown

Component	Weight, lbs
Fixed Equipment	3,000
APU	1,355
Fuselage Fixed	11,610
Shell	1,366
Tail Cone	76
Additional Side Material	118
Additional Vertical Material	-
Windows	626
Insulation	1,024
Floor	1,729
Seats	3,870
Total	**24,774**
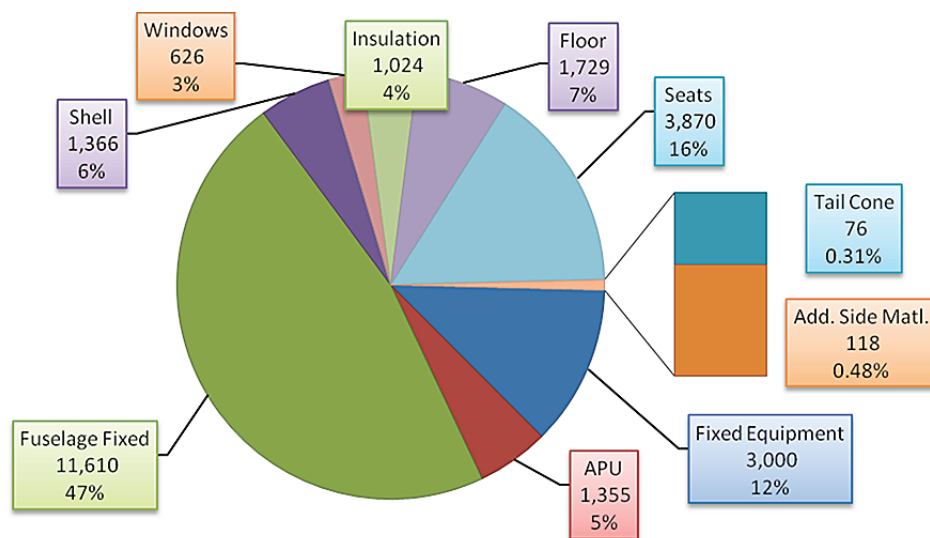
Figure 49: Fuselage weight breakdown.

Fuselage Payload Proportional Equipment includes:
- Flight Attendants
- Galleys
- Toilets
- Doors and emergency exits
- In-Flight Entertainment Systems
- Overhead Luggage Compartments
- Interior Furnishings, soundproofing, and lighting
- Floor Decking and Carpeting
- Emergency Oxygen System
- Other Emergency Equipment (slides, lifeboats…)
- Food and water

5.3.7 D8.5 Wing Weight Breakdown

Table 17: Wing Weight Breakdown

Component	Weight, lbs
Skin and Spar Caps	8,490
Spar Webs	237
Flaps	1,745
Slats	-
Ailerons	349
Leading/Trailing Edges	873
Ribs	1,309
Spoilers	175
Wing Fixed	262
Total	**13,439**
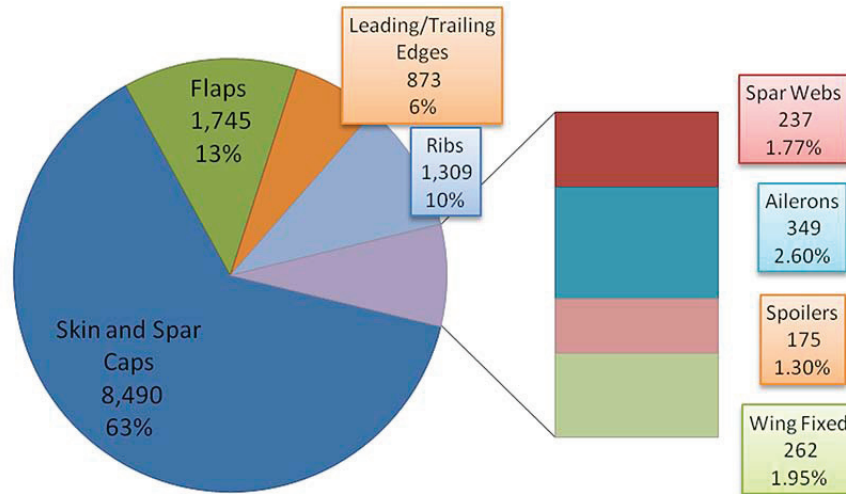
Figure 50: Wing weight breakdown.

Wing Fixed Equipment includes:
- Hydraulics
- Wiring
- Etc.

5.3.8 D8.5 Engine Weight Breakdown

Table 18: Engine Weight Breakdown

Component	Weight, lbs
Bare Engine	5,121
Engine Fixed	512
Nacelle	709
Pylon	317
Total	**6,659**
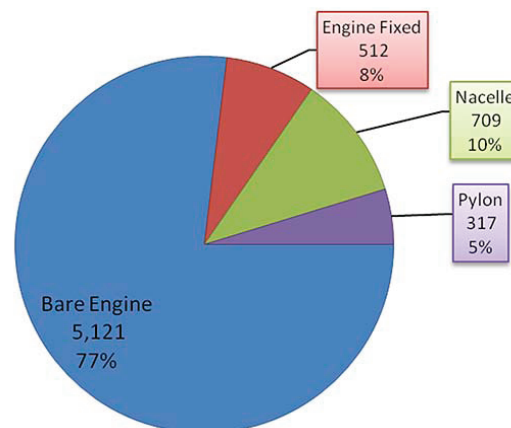
Figure 51: Engine weight breakdown.

Engine Fixed Equipment includes:
- Fuel System
- Accessories

5.3.9 D8.5 Landing Gear and Actuation System Weight Breakdown

Table 19: Landing Gear and Actuation System Weight Breakdown

Component	Weight, lbs
Actuation Systems	1,016
Node Landing Gear	1,016
Main Landing Gear	4,064
Total	**6,096**
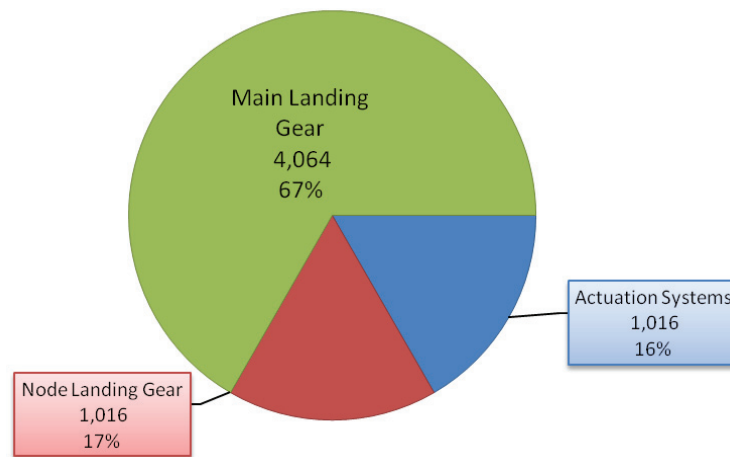
Figure 52: Landing gear and actuation system weight breakdown.

5.4 D8.5 Performance

This section outlines the detailed performance of the D8.5 aircraft concept in regards to the metrics identified for evaluation of the transport aircraft both in regards to the NASA goals as well as climate and other factors.

Table 20: D8.5 Important Mission Performance Parameters

MTOW (lb)	101591.5
Total fuel burn (lb)	11485.5
Fuel burn at roll (lb)	15.2
Fuel burn at climb (lb)	2147.6
Fuel burn at cruise (lb)	8126.3
Fuel burn at approach (lb)	664.4
Reserve Fuel (lbs / %)	546.9 / 5%
Cruise altitude beginning (feet)	44,653
Cruise altitude end (feet)	46,415
Cruise L/D	25.25
Noise at sideline (EPNdB)	75.6
Noise at flyover (EPNdB)	63
Noise at approach (EPNdB)	74.4
Cumulative EPNdB	213
LTO emissions % Below CAEP 6	87.26
LTO emissions (g/kN)	10.5
Cruise emissions (NOx) (g/kg)	4.22

5.4.1 D8.5 Noise

Aircraft noise is dominated by the loudest noise source and, *all* noise sources must be addressed to have an aircraft that meets the N+3 noise goal. With informed decisions about engine placement, airframe configuration, and aircraft operations, one can reduce noise from both airframe and engine sources. This is not an optimization process, rather it is a design process that relies on understanding how noise scales with parameters such as those defining geometry and velocity. As such, we have chosen a configuration with low noise attributes, then optimized the configuration to minimize fuel consumption, and then re-evaluated and iterated based on these results.

The low noise configuration chosen for the D8.5 configuration has the following features and enabling technologies for noise reduction:

- Advanced, aerodynamically clean and efficient airframe design

- Augmented lift on takeoff and approach from single slotted flaps
- Elimination of leading edge slats due to increased airframe lift at low speeds from reduced wing sweep
- Faired undercarriage, which is also shortened because of improved tail strike clearance
- High bypass ratio engines with low fan pressure ratio and near sonic tip speeds
- Boundary layer ingestion that reduces jet dissipation and jet velocity
- Low engine idle thrust on approach to reduce engine noise and reduce drag requirement to achieve trim
- Aft mounted distributed propulsion system with fin strakes to enable more effective airframe shielding of fan forward noise
- Variable area exhaust nozzle for high thrust but low jet velocity
- Multi-segment extended rearward acoustics liners
- Displaced runway threshold at approach
- Steep approach trajectory of 4 degrees

Figure 53 through Figure 55 show Overall Sound Pressure Level (OASPL) values as a function of the axial distance between the aircraft and the observer. The results are presented for the three certification points: sideline, flyover and approach.

5.4.1.1 Aircraft Noise at Sideline

Figure 53 shows the aircraft noise at sideline. The loudest point for the sideline certification point corresponds to the observer being located 450 meters to the side of the runway and at the axial rotation position. Engine noise sources are reduced due to low fan pressure ratio values and subsonic tip speeds. Furthermore, the fan noise sources are attenuated; the forward fan noise due to acoustic shielding and the rearward fan noise through extended acoustic liners. The dominant noise source is from the jet. At this location, forward noise is reduced due to acoustic shielding. Fan rearward noise is attenuated through extended acoustic liners. The ratio of bypass exhaust duct length to fan diameter is 1.25 and lining is used along the outer and inner section of the exhaust duct. Peak fan rearward noise attenuation has been calculated using results from Law and Dowling[61].

---

[61] Law, T.R., Dowling, A.P., "Optimization of Annular and Cylindrical Liners fro Mixed Exhaust Aeroengines," AIAA-2007-3546, 13th AIAA/CEAS Aeroacoustics Conference (28th AIAA Aeroacoustics Conference), 2007.
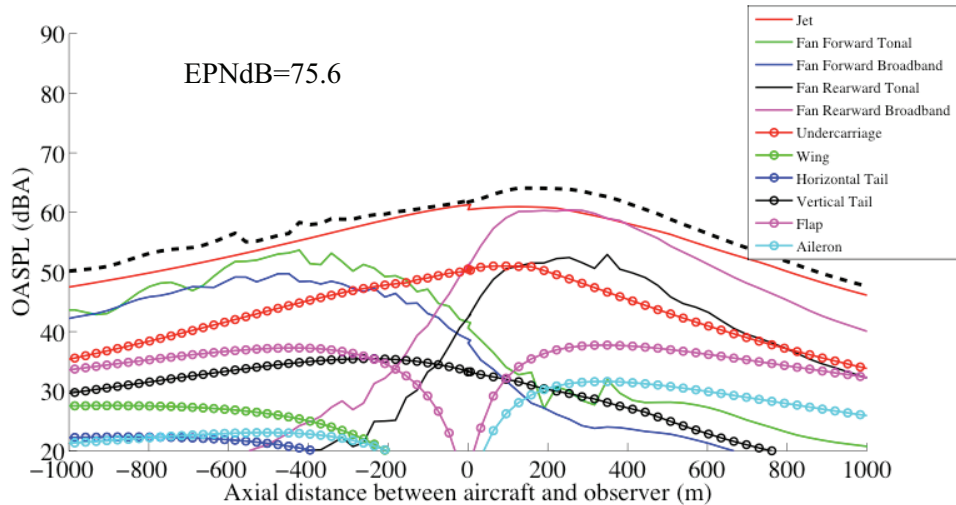
Figure 53: Overall Sound Pressure Level values for the D8.5 configuration at the sideline measurement point.

5.4.1.2 Aircraft Noise at Flyover

Figure 54 shows the aircraft noise at flyover. The aircraft achieves ultra low noise levels at flyover because it reaches an altitude of 626 m prior to cutback because of the 8.2 degree climb angle. The angle of attack is 9.0 degrees, thus the aircraft cabin angle does not exceed 20 degrees. The climb angle after cutback is 3.0 degrees, which exceeds the engine-out climb angle requirement for a 3 engine configuration (Crichton et al., 2007)[62]. The trajectory relies on a takeoff thrust of 27.7 kN and a post-cutback thrust of 14 kN. This operation procedure ensures low noise at cutback because of the thrust reduction and the large distance from the aircraft to the observer. Furthermore, the fan noise is attenuated through acoustic shielding of the forward source and extended acoustic lines for the rearward source.
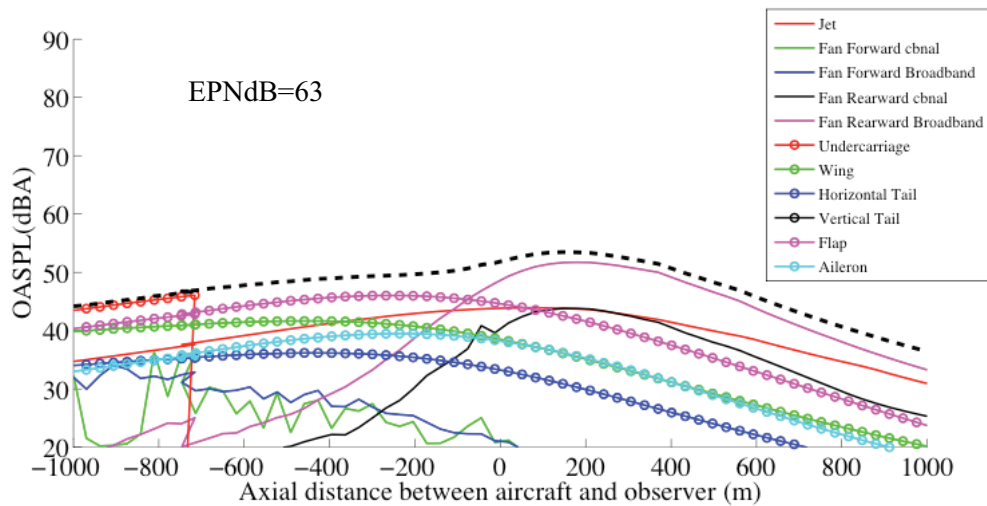
Figure 54: Overall Sound Pressure Level values for the D8.5 configuration at the flyover measurement point.

---

[62] Crichton, D., De la Rosa Blanco, E., Law, T., and Hileman, J., "Design and Operation for Ultra Low Noise Take-Off," AIAA 2007-0456, 45th AIAA Aerospace Sciences Meeting and Exhibit, Reno, NV, January 2007.

5.4.1.3 Aircraft Noise at Approach

Figure 55 shows the aircraft noise at approach. For the D8.5 configuration, the high lift system is greatly simplified, the aircraft is assumed to be aerodynamically clean and the "sailplane" airfoil noise coefficient is used to estimate wing noise for all three noise measurement locations. The engine noise is reduced by airframe shielding of fan forward and rearward noise, liners for fan rearward noise and low engine idle thrust. A trimmed approach Mach number of 0.178 with a flight path angle of 4 degrees is possible with a 20 degree flap deflection, low engine idle thrust and windmilling of the middle engine. The undercarriage noise is reduced by the use of fairings. In terms of aircraft procedure, displacement threshold together with a steep descent trajectory allow for reduced noise. The dominant noise source is flap noise.
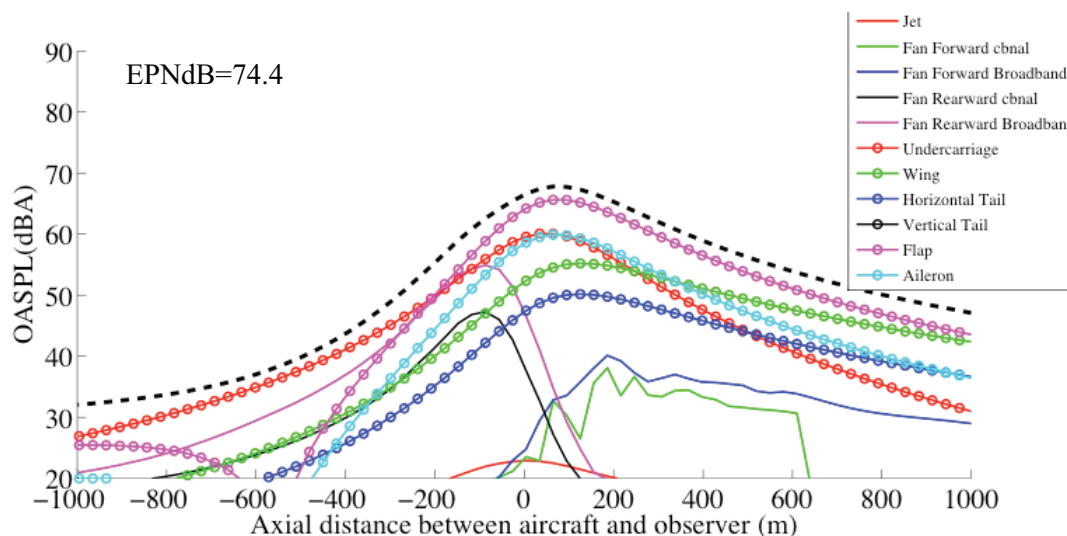
Figure 55: Overall Sound Pressure Level values for the D8.5 configuration at the approach measurement point.

5.4.2 D8.5 LTO NOx

Landing/takeoff (LTO) NOx emissions are characterized by CAEP 6 as grams produced during a standardized cycle versus the maximum engine thrust. The low LTO NOx emissions, with respect to CAEP 6 standards, of the N+3 concept aircraft are enabled by two key technologies, high bypass ratio and the Lean Direct Injection (LDI) combustor. The low fan pressure ratio associated with the increased bypass ratio of the N+3 engine concept increases the engine propulsive efficiency, creating more thrust per unit heat released without increasing the combustor operating temperature. Increasing thrust without changing the temperature, and thus without negatively impacting NOx production, is a powerful tool for reducing emissions and can on its own lead to a 60% reduction in regulated NOx on its own.

The Lean Direct Injection combustor, currently under development at NASA Glenn, is another enabler for meeting the N+3 emissions goals. The LDI combustor injects fuel into multiple flame zones, enabling lean combustion while minimizing local hotspots. This allows the LDI combustor in the N+3 concept engine to meet the N+3 NOx goal while retaining the fuel burn and carbon emissions advantages.

The NOx production of the N+3 concept engines has been estimated using published correlations from experiments with the NASA LDI combustor[63]. Cycle parameters from the N+3 engine model simulating

---

[63] Tacina, R., Mao, C., Wey, C., "Experimental Investigation of a Multiplex Fuel Injector Module for Low Emissions Combustors," AIAA 2003-0827, 2003.

relevant operating conditions from the LTO cycle (100%, 85%, 30%, and 7% SLS max thrust) are used as inputs to the correlation. A limit of 4 grams of NOx per kg of fuel was used to represent the minimum NOx production based on existing engine data at idle, as suggested by Dr. Chi-Ming Lee at NASA GRC. The percentage of CAEP 6 NOx produced by each engine concept is determined by integrating the predicted NOx production over the time specified by the CAEP LTO cycle. Cruise NOx was estimated based on the calculated engine conditions at cruise with the same combustor correlations and limits.

Table 21: D8.5 NOx Performance Results

LTO emissions % Below CAEP 6	87.26
LTO emissions (g/kN)	10.5
Cruise emissions (NOx) (g/kg)	4.22

5.4.3 D8.5 PFEI

The reference mission for the D8 series aircraft was selected in order to have the greatest impact if this aircraft were inserted into the fleet. A 180 passenger B737 type aircraft would provide the D8.5 an opportunity to replace a significant portion of the currently operating fleet. The choice of a 3000 nm mission with reserves would allow the D8.5 aircraft to complete a North American transcontinental route such as Seattle to Miami. This combination of a 180 passenger payload with a 3000 nm mission puts the total aircraft productivity outside of that of the currently operated B737-800 configurations. To validate the design/optimization code for the D8 aircraft a B737-800 class aircraft was designed and run through the optimization process (See Figure 42). Once the design code output matched that of the B737-800 stated performance, the code was rerun with a single class 180 passenger configuration, at a range of 3000 nm. This optimized design output was used as the baseline for comparison for the NASA N+3 goals. For reference the calculated PFEI was 7.43 kJ/kg-km and the PFEI of a B737-800 presented in the 12 month review and shown in Figure 30 in Section 3.1.4, was 7.1 KJ/kg-km.

Table 22: Payload Fuel Energy Intensity Performance

D8.5 PFEI (kJ/kg-km)	2.17 (-70.8%)[64]
D8.1 PFEI (kJ/kg-km)	3.79 (-48.9%)
737-800 TASOPT Baseline (kJ/kg-km)	7.43 (-0%)
NASA N+3 Goal PFEI (kJ/kg-km)	2.23 (-70%)

Although aircraft may be designed to meet a specific range and payload capacity, airlines fly their aircraft over a wide variety of distances to meet the needs of their route structures. To this variation, the Bureau of Transportation Statistics (BTS) database was examined to find the actual variation in payload carried and range flown. The result is shown in Figure 56, which contains a map of operation-weighted contours of payload and range for U.S. operations of the Boeing 737-800 in 2006. Darker colors indicate more operations flown for a given payload-range combination. The payload range diagram is given for comparison.

The average distance flown was 1096 nm with standard deviation 556 nm. As is typical for all aircraft types, the Boeing 737-800 was generally operated at a range well below R1 (defined here as the

---

[64] Percent reduction from B737-800 baseline as calculated from validated TASOPT B737 case.

maximum range at maximum structural payload weight) with just more than half of its structural payload capacity as discussed in Section 2.3.1.5, this is also typical. To ensure that the aircraft concepts are efficient at distances where they will typically be used, the fuel efficiency was also examined for shorter flight distances.
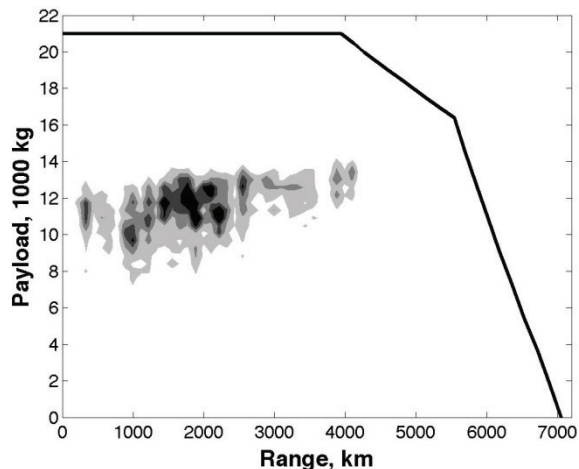
Figure 56: Operation-weighted distribution map of U.S. operations in 2006 for the Boeing 737-800 aircraft with comparison to the payload range diagram for the aircraft. Information derived from U.S. BTS Form 41 database (2006).

In addition to aircraft PFEI over a single mission as optimized through the TASOPT code, an aircraft's performance can be assessed against other missions to see how the aircraft performs when used on a mission other than the design mission. TASOPT allows for the option to calculate a specific aircraft without re-optimizing the aircraft for the mission selected. Figure 57 shows the performance of the D8.5 aircraft operated at a range from 500 nm to the design 3000 nm mission.
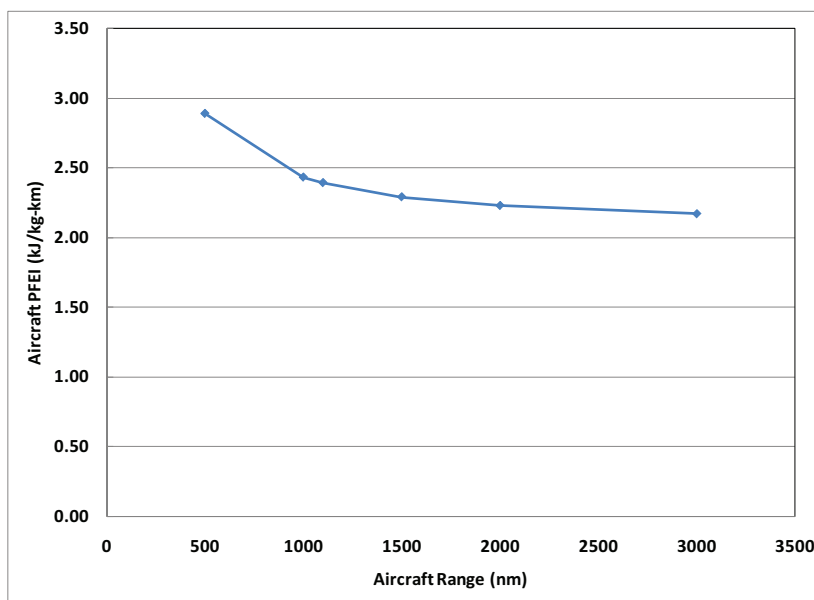
Figure 57: PFEI Variation of D8.5 assessed against changes in vehicle range.

In addition to designing and optimizing a single aircraft TASOPT allows for the option of driving the optimization function to the minimization of a fleet of aircraft in terms of the global PFEI of the fleet. To assess how this might change the D8.5 aircraft configuration we examined what would happen if the aircraft were designed to minimize the fleet PFEI when the fleet is operated 50% of the time at full capacity over a distance of 1100 nm and 50% of the time over a distance of 3000 nm. The performance of a fleet of aircraft under those optimization and operation requirements is calculated at 2.33 kJ/kg-km as compared to the D8.5 performance of 2.17 kJ/kg-km for an increase in PFEI of 2.3%. The small reduction obtained shows that the longer design range is the driving design case for the optimization and any mission is bracketed by this choice of the design range.

5.4.4 D8.5 Balanced Field Length

The following table outlines the balanced field length performance as well as the landing distance performance of the D8.5 vehicle. The details behind the balanced field length calculations are discussed in the Figures of Merit discussion in Section 3. The landing distance is calculated for two CLmax configurations as well as under various braking coefficient conditions (wet and dry) to bracket the performance.

Table 23: D8.5 Aircraft Mission Parameters

Takeoff distance balanced field length (feet)	5000
Dry landing distance (CLmax =3) (feet)	2768[65]
Dry landing distance (CLmax =2) (feet)	3555
Wet landing distance (CLmax =3) (feet)	4185
Wet landing distance (CLmax =2) (feet)	5684

5.4.5 D8.5 Climate

As discussed in Section 3.2, our climate metric of interest is globally-averaged time-integrated surface temperature change, normalized by aircraft productivity (payload × distance), calculated in the APMT-Impacts Climate Module. For the D8 series, we have assessed the climate impact of four different cases. We began with two baseline cases: the Boeing 737-800 and a hypothetical aircraft that meets the NASA N+3 goals flying the same mission as the B737-800 (-70% fuel burn and -75% LTO NOx). We then assessed the climate performance of the D8.1 and D8.5 concepts. For each case, we accounted for the following climate impacts: production and combustion CO_2, well-to-tank methane (WtT CH_4), short- and long-lived effects of NOx on ozone, NOx on methane, clouds (contrails and contrail-induced cirrus), sulfates, soot, and water vapor (H_2O). These impacts are calculated based on fuel usage and the amount of CO_2 and NOx emitted for a given flight. The temperature breakdown for the B737-800 baseline mission is shown for these effects in Figure 58.

---

[65] Assumes 3 deg approach path over 50 foot obstacle, plus 3 second delay to full braking.
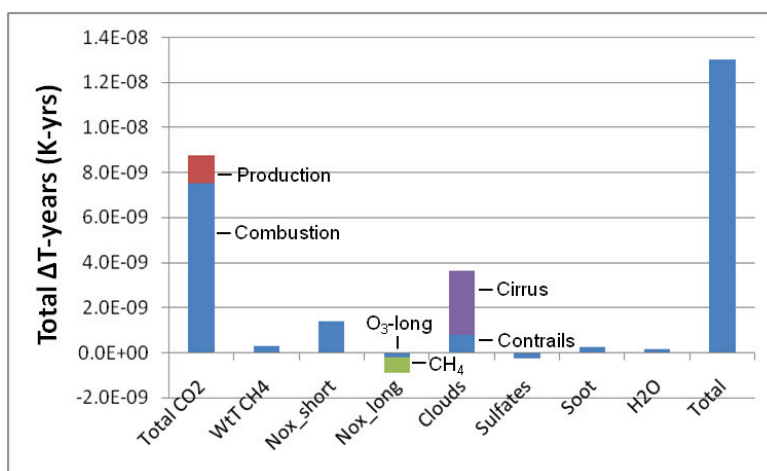
Figure 58: Climate impact (by effect) of Boeing 737-800 for a sample mission

Figure 58 depicts which impacts have a warming effect and which impacts have a cooling effect on the global climate as well as the relative magnitude of the impacts. The figure shows that carbon dioxide is the dominant climate impact of aircraft activity, with aviation-induced cloudiness having the second most significant impact. NOx emissions result in warming and cooling effects that nearly balance out over the lifetime of impacts. The remaining species—well-to-tank methane, sulfates, soot, and water vapor—have a smaller influence on temperature change.

The results of our climate analysis of all four cases are detailed in Table 24. The impact metric that was used for comparing the different aircraft is shown in the last column as normalized climate impact.

Table 24: Climate impact of D8 series cases

Vehicle	Payload (kg)	Distance (km)	ΔT-years (°K-yrs)	Normalized Climate Impact (°K-yrs / (kg x km))
B737-800	19958	3723	1.37E-08	1.84E-16
N+3 Goals	19958	3723	4.07E-09	5.48E-17
D8.1	38700	5556	7.61E-09	3.54E-17
D8.5	38700	5556	4.33E-09	2.01E-17

Using the N+3 Goals case as the target level for climate impact, it is clear that both D8 configurations exceed the climate goal. The D8.1 results in an 81 percent climate improvement from the B737-800 baseline case while the D8.5 results in an 89 percent improvement. The improvement in terms of climate impact of the D8-series is mostly attributable to fuel burn savings. These concepts also benefit from reduced cloud formation due to a cruise altitude in excess of 40,000 feet. At this altitude, forcing due to contrails and contrail-induced cirrus is greatly reduced relative to that which occurs at the typical cruise altitude of the B737-800.

5.4.6 D8 series round trip time

One change between the B737 baseline and the D8 series aircraft is the reduction in Mach cruise number from Mach 0.80 to Mach 0.74. The major impact of this change is the perceived increase in round trip

time for the passengers and aircraft when operated. This effect was not ignored when considering the design of the D8 aircraft. When considering total round trip time of the aircraft from gate to gate including the loading and unloading time the D8 aircraft can provide a reduction in block time for an operating airline. The primary method for this is the decrease in loading time and unloading time through the two aisle shortened row configuration. Figure 59 details the B737-800 and D8 round trip flight times for a variety of missions.

737-800
30 x 6 per aisle
(35 minutes load,unload)

D8.x
23 x 4 per aisle
(20 minutes load,unload)

	Flight times [hr]		Trip times [hr]		
	737	**D8.5**	**737**	**D8.5**	
NYC–LAX	4.81	5.29	5.98	5.96	(–1 minutes)
NYC–ORD	1.55	1.73	2.71	2.40	(–19 minutes)
BOS–DCA	0.93	1.06	2.09	1.73	(–22 minutes)
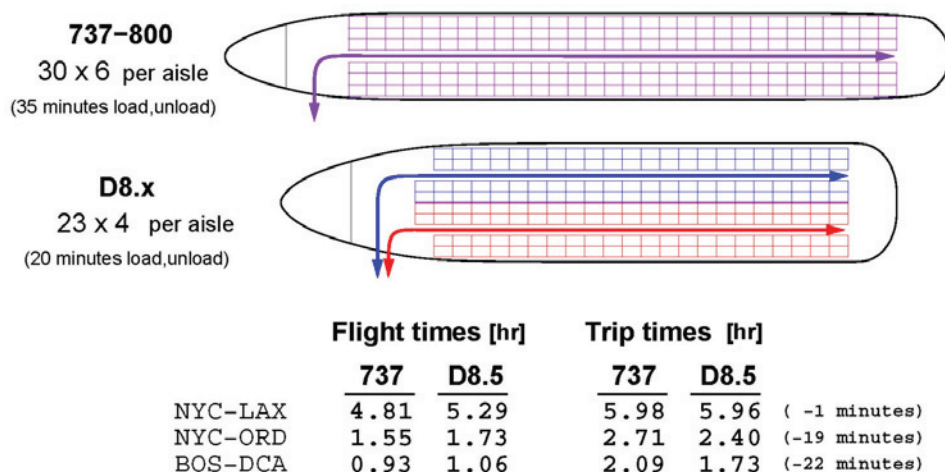
Figure 59: Comparison of D series to B737 round trip time

5.4.7 D8 Series Aerodynamic Performance

This discussion presents sample calculations showing some key aerodynamic features of the D8 configurations. (D8.1 results shown here.) The calculations were performed using AVL[66].

Cruise condition

Figure 60 shows the delta (Cp) loading vectors with the CG in the middle of the allowable range. Note the substantial loading on the fuselage nose, which alleviates much of the usual tail download for pitch trim. The usual fuselage carryover lift is also present at the wing location. The forward and over-wing loads combine to make the fuselage carry 18.5% of the total lift, in contrast to the 6-8% typically carried on the conventional B737 fuselage. The greater fuselage lift has considerable structural weight benefits for the entire airframe. Figure 61 shows the spanwise loading and the spanwise Cl distributions for this case. The fuselage lift and the modest tail download are apparent, resulting in a good overall span efficiency.

---

[66] http://raphael.mit.edu/avl

CG-Forward Landing Condition

Figure 62 shows the delta-Cp loading vectors with the CG in the forward limit, which is the case that sizes the horizontal tail. Again, the large upload on the fuselage nose considerably alleviates the download required from the horizontal tail to achieve pitch trim. Figure 63 shows the spanwise loading and Cl distributions for this case. The Cl values on the horizontal tail are the chosen limit so as to leave sufficient remaining nose-up pitch authority for control.
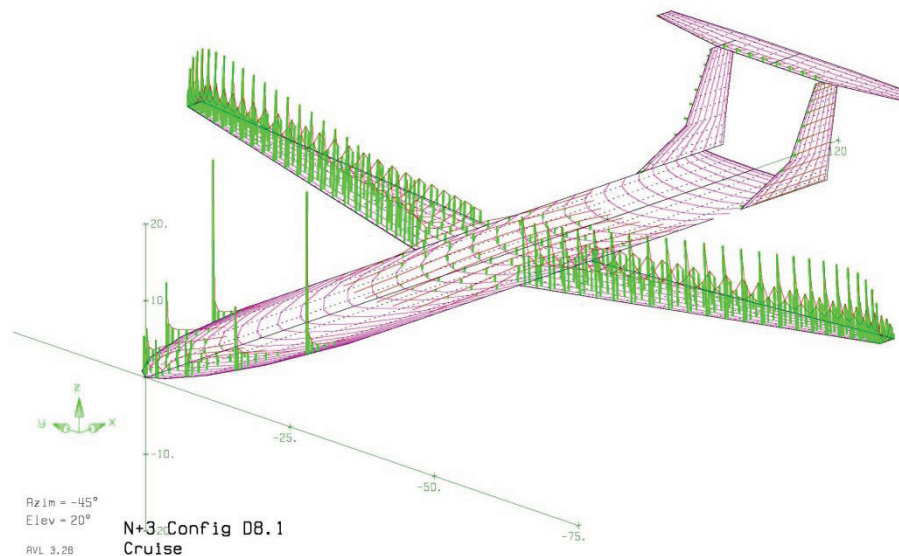
Figure 60: Delta-Cp load vectors on D8.1 configuration at cruise.
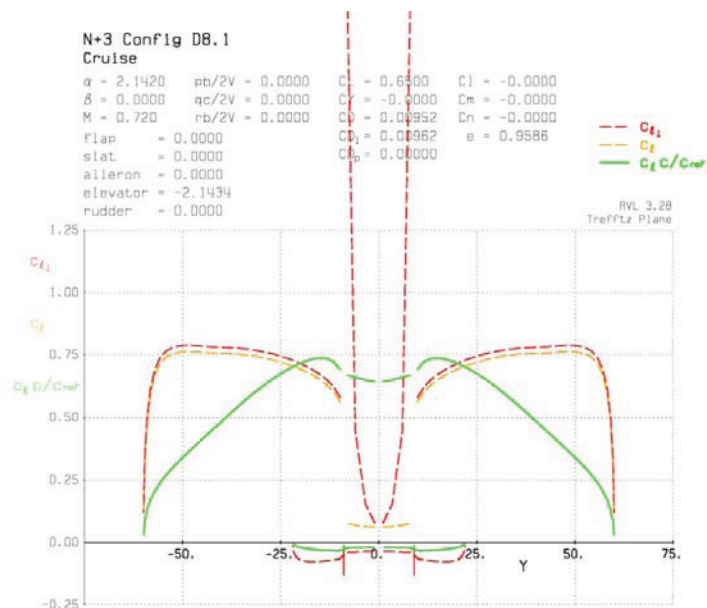
Figure 61: Spanwise loading (green) and section Cl (red) distributions on the D8.1 at cruise.
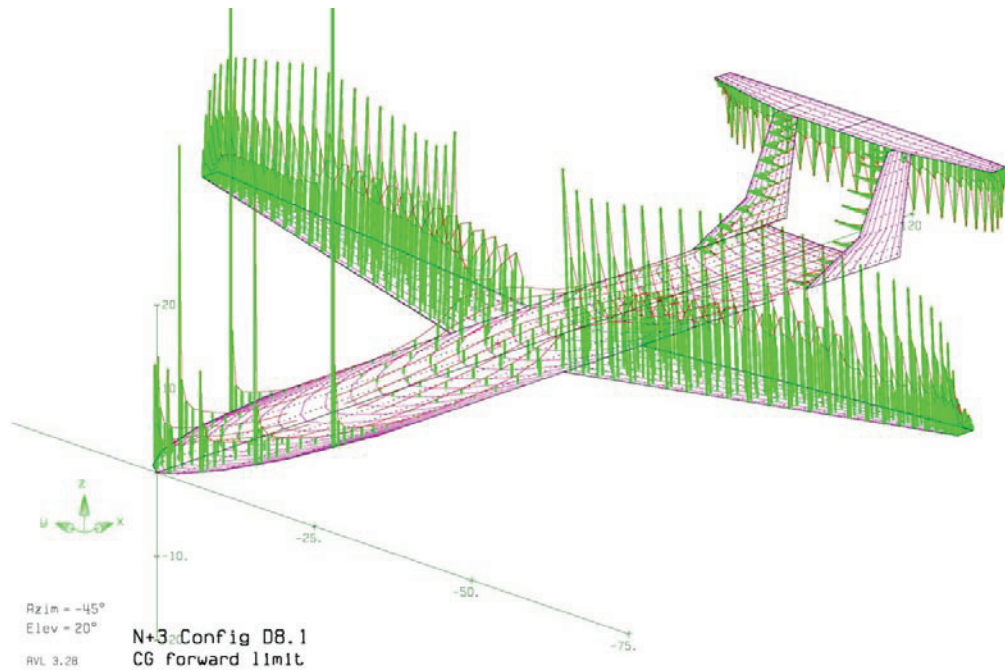
Figure 62: Delta-Cp load vectors on D8.1 configuration with CG at forward limit at landing.
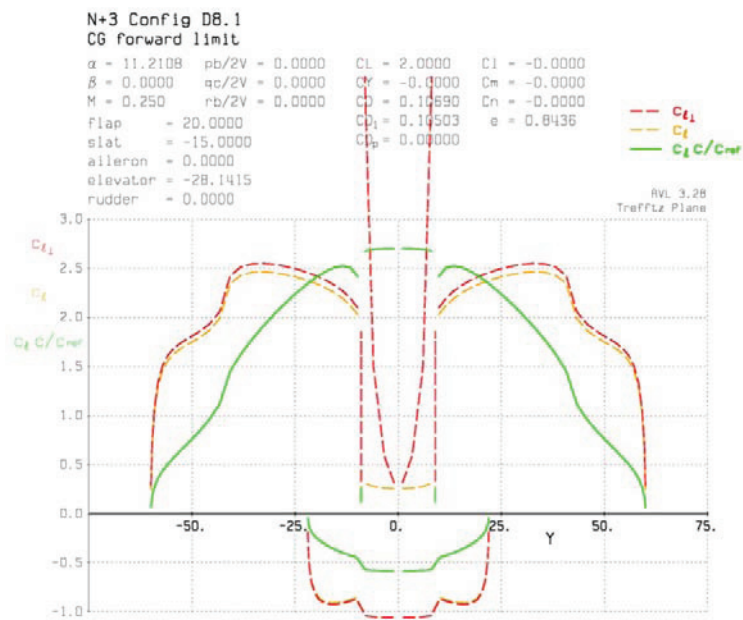
Figure 63: Spanwise loading (green) and section Cl (red) distributions on the D8.1 with CG at forward limit at landing.

5.4.8 Preliminary Flutter Study for D8.5

A preliminary flutter study has been performed for the D8.5 configuration using the structural/aero/control ASWING code. Its flutter prediction capability has been validated against Theodorsen theory in the primary reference[67], and independently versus NASTRAN by Love et al[68].

5.4.8.1 ASWING model

The physical ASWING model consists of a set of connected beams allowing arbitrarily large deformations. The beams have distributed mass and inertia representing the structure, payload, and fuel, and also point masses representing the engines, landing gear, and other major items. The aero loads are modeled with a compressible unsteady lifting-line formulation and slender-body formulation. Flutter predictions are computed by an eigenmode analysis of the full linearization of the nonlinear model taken about any solution state. Analysis over a set of states, over increasing flight speeds for example, gives a root locus.

5.4.8.2 D8.5 flutter case examined

The examined flutter case is flight at max weight at 20 kft altitude, where maximum indicated airspeeds reach the expected Mach buffet boundary $M \approx 0.8$, presumably in a dive. Figure 64 shows the ASWING system eigenvalues for eight indicated airspeeds from 160 to 188 m/s (311 to 365 kt). No roots cross over the imaginary axis, which indicates that no static and no dynamic instabilities are present.

---

[67] Drela, M., "Integrated simulation model for preliminary aerodynamic, structural, and control-law design of aircraft," AIAA 40th SDM Conference, Paper 99-1394, April 1999. Also at http://raphael.mit.edu/aswing/.

[68] Love, M., Zink, P., Wieselmann, P., Youngren, H., "Body freedom flutter of high aspect ratio flying wings," AIAA 46th SDM Conference, Paper 05-1947, April 2005.

D8.5

	Ω_x	Ω_z	$\beta°$	$\alpha°$	V_{ref}	C_L	C_D	e
1	0.0	0.0	0.00	-0.02	160.0	0.265	0.0229	0.651
2	0.0	0.0	0.00	-0.13	164.0	0.252	0.0227	0.629
3	0.0	0.0	0.00	-0.22	168.0	0.240	0.0224	0.607
4	0.0	0.0	0.00	-0.31	172.0	0.229	0.0222	0.584
5	0.0	0.0	0.00	-0.40	176.0	0.218	0.0221	0.560
6	0.0	0.0	0.00	-0.47	180.0	0.209	0.0219	0.535
7	0.0	0.0	0.00	-0.54	184.0	0.200	0.0217	0.509
8	0.0	0.0	0.00	-0.61	188.0	0.191	0.0216	0.483
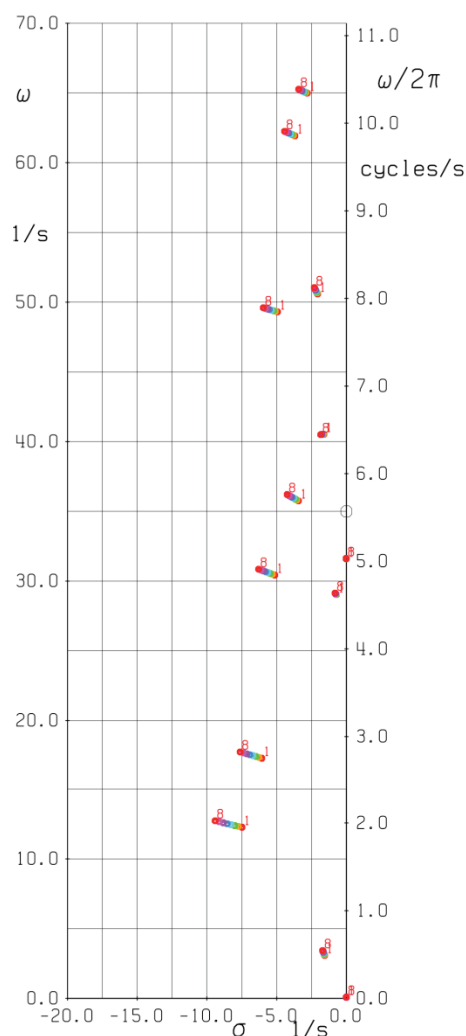
Figure 64: ASWING eigenmode analysis Root locus for D8.5 configuration over a range of high airspeeds. No unstable roots are observed.

5.4.8.3 Artificially-induced flutter case

To determine the sensitivity of flutter to mass distribution, and to gain confidence that ASWING can in fact predict flutter for such an aircraft, the ASWING model was modified by mounting a fictitious 300 lb mass cantilevered 5 feet behind the wing's structural axis near each wingtip. This gives a substantial rearward shift in the local CG. The artificial modification does indeed induce flutter as expected, indicated by the roots crossing the imaginary axis in Figure 65. The most unstable mode turns out to be

the classic antisymmetric torsion/bending flutter, and is shown in Figure 66. The other nearby unstable mode seen in Figure 65 has the same basic shape, but is symmetric.

```
D8.5   (+ tip masses)

     Ωx      Ωz      β°      α°      V_ref    C_L     C_D      e
1    0.0     0.0     0.00    -0.03   160.0   0.266   0.0229   0.664
2    0.0     0.0     0.00    -0.13   164.0   0.253   0.0227   0.643
3    0.0     0.0     0.00    -0.23   168.0   0.241   0.0224   0.622
4    0.0     0.0     0.00    -0.32   172.0   0.230   0.0222   0.599  ← flutter speed
5    0.0     0.0     0.00    -0.41   176.0   0.220   0.0220   0.575    (172m/s=335kt)
6    0.0     0.0     0.00    -0.48   180.0   0.210   0.0219   0.551
7    0.0     0.0     0.00    -0.55   184.0   0.201   0.0217   0.526
8    0.0     0.0     0.00    -0.62   188.0   0.192   0.0216   0.500
```
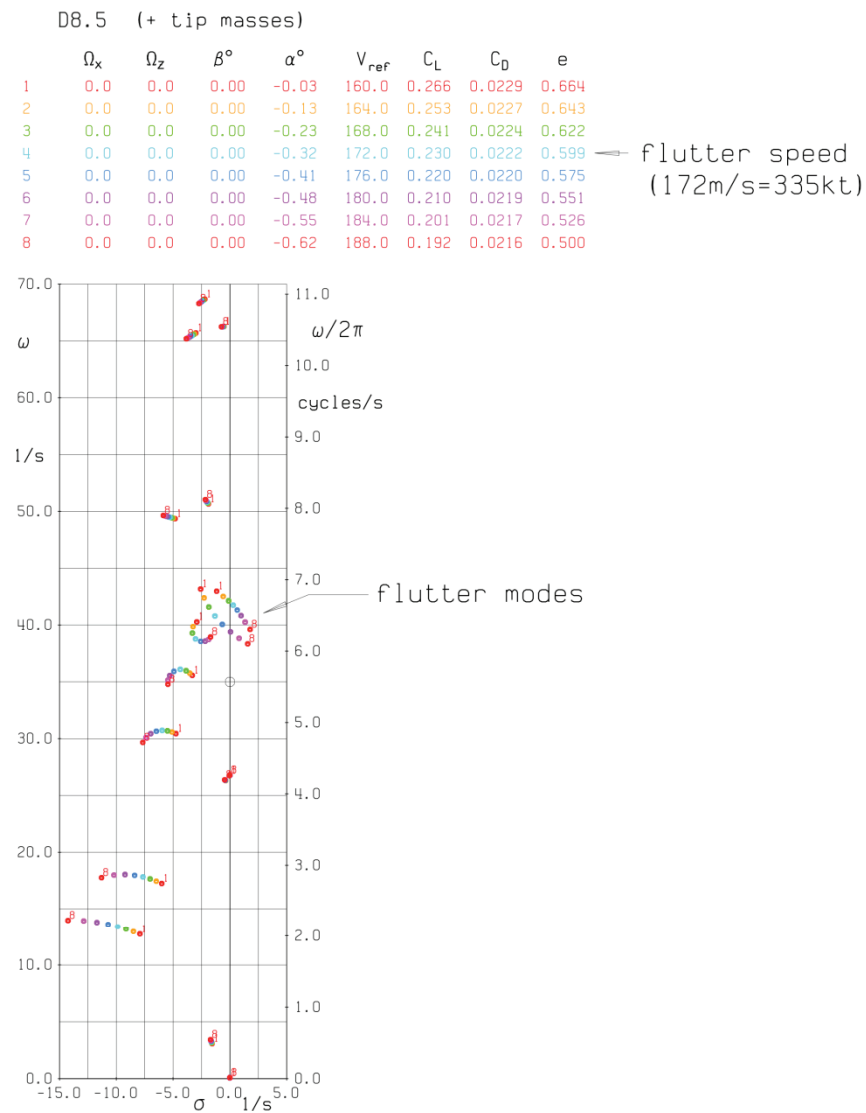
Figure 65: ASWING eigenmode analysis Root locus for D8.5 configuration modified with artificial masses near the wingtip. Flutter is now induced at 335 kt indicated airspeed.
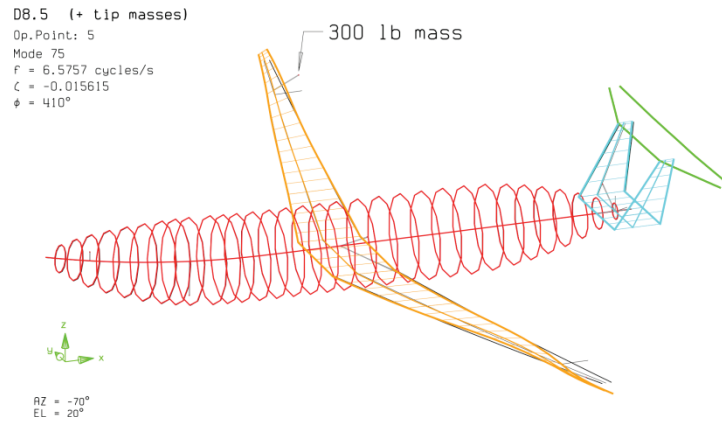
Figure 66: Asymmetric torsion/bending flutter mode cantilevered 5 ft behind the wing near the tips.

5.4.8.4 Conclusions

The study carried out indicates that the D8.5 does not have a flutter problem. Although a relatively modest amount of added mass (0.6% of gross) did cause instability, the converse is also true that modest mass mounted forward in the wing will have a strong stabilizing effect. Passive flutter suppression via small amounts of ballast is a plausible flutter risk mitigation strategy.

5.4.9 Strut-braced Configurations

5.4.9.1 Summary

Strut-braced-wing versions of the D8 aircraft, denoted as SD8.1 and SD8.5, were also laid out and optimized. These provided additional 4.2% and 2.1% PFEI improvements, relative to the baseline B737-800, compared to the cantilever-wing versions. However, the strut configurations also incur additional risks, primarily with linear and nonlinear aero elasticity, and inevitably greater development and manufacturing costs because of their more complex structure, larger wingspans, and extreme aspect ratios. For these reasons, the cantilever design was judged to be more attractive for future development.

5.4.9.2 Approach

To investigate the possible benefits of a strut-braced wing, the cantilevered wings of the D8.1 and D8.5 were replaced with strut-braced wings in their TASOPT definitions. Other changes were made as itemized below.

- Cantilever wing changed to a strut-braced wing. The strut material is assumed to be the same as the wing sparcaps.

- The strut cross-sectional area, and hence weight, is set by the specified material stress at the N_{lift} pull-up load factor. Downward-load buckling was not considered for this preliminary investigation, but it is a concern for any future work.

- The strut was assumed to be a 15% thick hollow-shell airfoil, with a wall thickness of 1.5% chord, which together with the cross-sectional area determines its chord size and wetted area. A minimum-size strut of solid cross section was found to be unworkable due to insufficient bending and torsional stiffness.

- The main landing gear weight fraction was increased from 4.0% to 5.5% of max gross weight. This is the estimated weight penalty for the additional structure needed to cantilever the gear strut attachments sideways from the fuselage, rather than having them in the wing directly over the gear. Additional weight would also be needed to reinforce the few fuselage frames, which connect the low main gear with the high wing and prevent the wing from crushing the cabin (the 6g landing impact requirement).

- The center wingbox was excluded from the available fuel volume. This is considered necessary to reduce the possibility of flooding the cabin with fuel in the event of a wingbox rupture caused by a crash.

The aircraft were subsequently re-optimized in TASOPT with these changes. The resulting changes were mostly in wing size and weight, with only minor changes in the engine and tail sizes and weights. The major design features are described below.

5.4.9.3 SD8.1 Results

The optimized SD8.1 aluminum-technology aircraft is shown in Figure 67. Its key parameters are compared against those of the D8.1 in Table 25. The fuel burn benefit is 4.2% compared to the baseline, or 8% compared to the cantilevered version. Most of this due to the *L/D* improvement, and the rest due to the weight improvement.

The configuration changes generated by the TASOPT optimizer are as expected. The wing airfoils end up thinner than for the cantilever wings, which allow a slight increase in the CL and a slight decrease in the sweep. The inner wing airfoil has an inverse taper, with the maximum thickness at the strut attachment.

The SD8.1 has the field length constraint active at the specified 5000 ft, which makes the wing larger than the unconstrained optimum would be. The oversized wing also means that the airplane is not fuel-volume limited.

Table 25: Comparison of cantilever D8.1 and strut-braced SD8.1 aluminum aircraft

Parameter	D8.1	SD8.1	Units
MTOW	126,900	123,310	Lb
W_{fuel}	19,820	18,270	Lb
Span	150	182	Ft
Area	1298	1282	ft^2
Sweep	5.8	0	Deg
AR	17.3	25.9	
t/c_o	0.144	0.100	
t/c_s	0.131	0.126	
$C_{L_{CR}}$	0.684	0.772	
L/D	22.1	23.9	
BFL	5000	5000	Ft
$PFEI$	3.79	3.48	kJ/kg-m
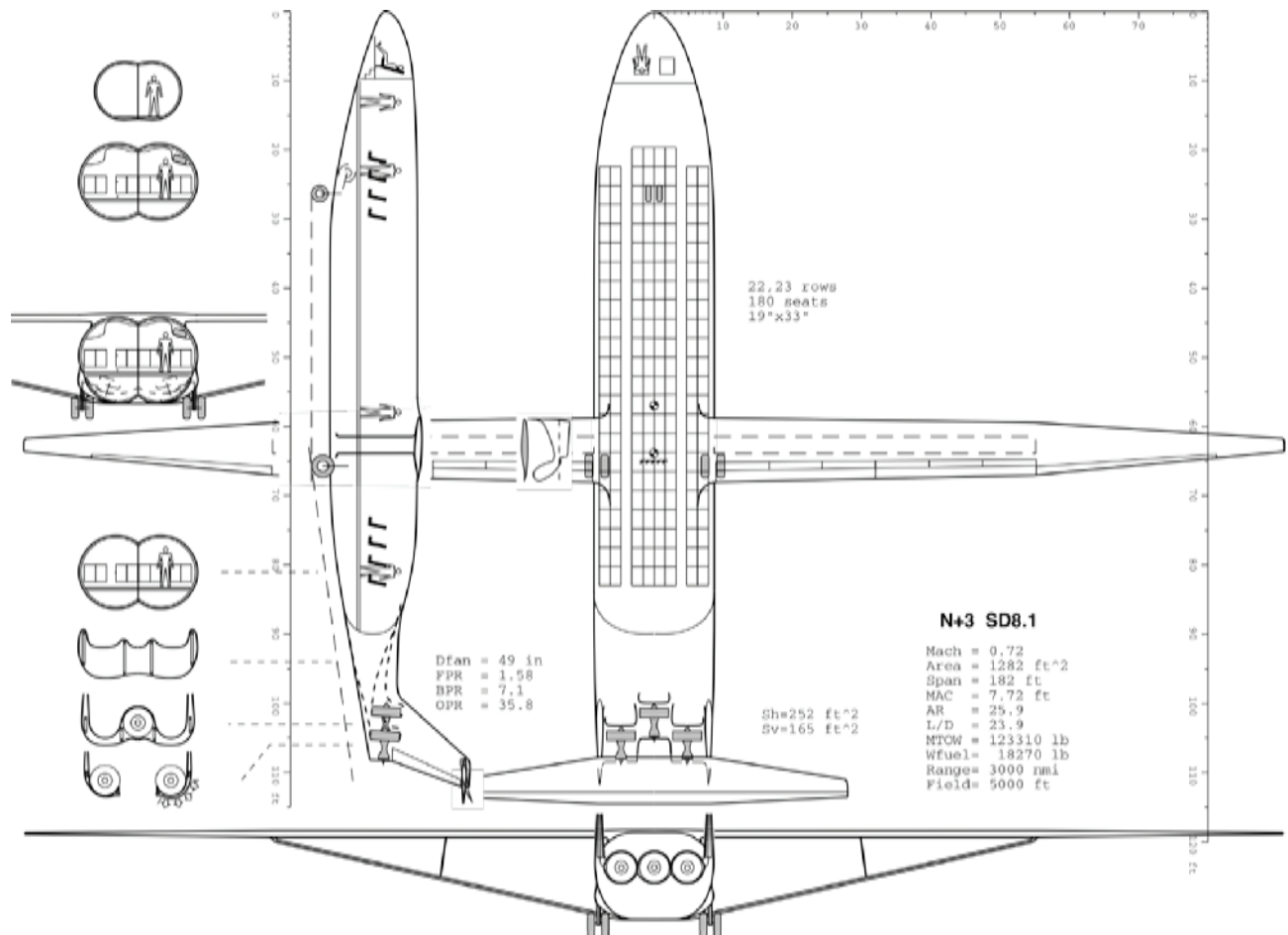
Figure 67: SD8.1 aircraft with strut-braced wing, aluminum technology.

5.4.9.4 SD8.5

The optimized SD8.5 advanced-technology aircraft is shown in Figure 68. Its key parameters are compared against those of the D8.5 in Table 26. The fuel burn benefit is 2.1% relative to baseline, or 7% relative to the cantilevered configuration. The *L/D* improvement from 25.3 to 26.1 is surprisingly modest given the large increase in *AR*. Most of this is because the profile drag, especially the fuselage, dominates the induced drag in these aircraft, so large increases in the aspect ratio bring only modest benefits. Also the added strut drag offset some of this gain.

The SD8.5 is fuel volume limited, so that the wing is slightly larger/thicker than what an unconstrained design would have. The oversized wing is why its 4860 ft field length is less than the 5000 ft constraint.

5.4.10 Powered high lift device using electric propulsors

Powered high lift device using electric propulsors was another technology evaluated in this project. The main idea behind this technology is to replace conventional high lift devices such as slats and flaps with small electric propulsors embedded in the wing. Although these electric propulsors are heavier than conventional high lift devices, they can also be used as a boundary layer ingesting propulsion system

during cruise, which might compensate for the added weight. The use of this powered high lift devices helps in reducing the takeoff field length, and might also have additional benefits in reducing the takeoff and landing noise by allowing the aircraft to take off and land at a lower velocity.

Limited analysis was conducted for this technology, as this technology is not applicable to H3.2 aircraft because of stability problems, as the D8.5 did not have a problem taking off at a short field length it was chosen not to pursue this technology further at this point.

Table 26. Comparison of cantilever D8.5 and strut-braced SD8.5 advanced-technology aircraft

	D8.5	**SD8.5**	
MTOW	101,590	97,970	lb
W_{fuel}	11,486	10,653	lb
Span	170	182	ft
Area	1162	1040	ft^2
Sweep	12.6	9.1	deg
AR	24.9	33.9	
t/c_o	0.125	0.097	
t/c_s	0.118	0.112	
$C_{L_{CR}}$	0.706	0.792	
L/D	25.3	26.1	
ℓ_{BF}	5000	4860	ft
$PFEI$	2.17	2.01	kJ/kg-m
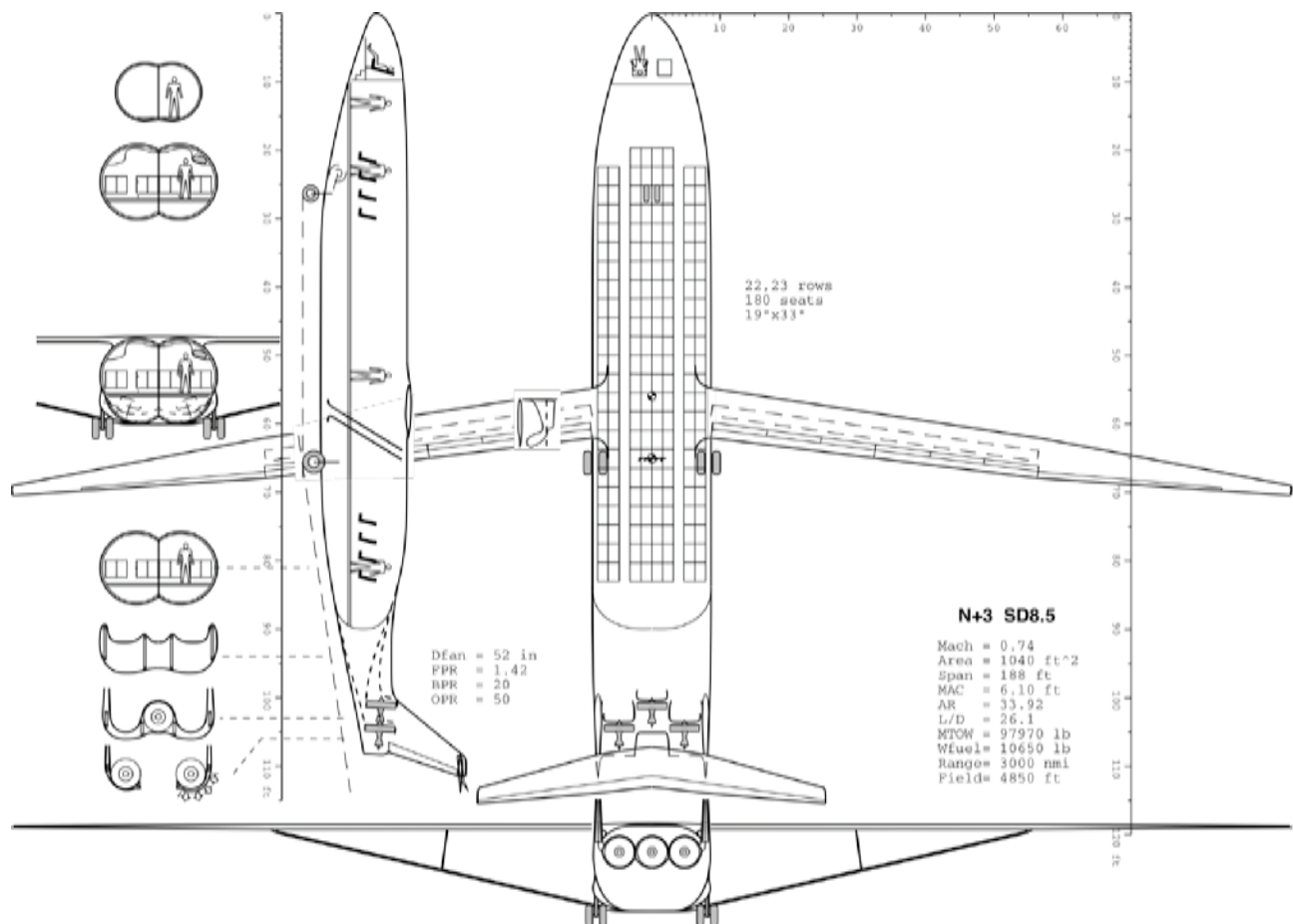
Figure 68: SD8.5 aircraft with strut-braced wing, advanced technology.

5.4.10.1 ASWING aeroelastic analyses of strut-braced configurations

The strut-braced configurations have the potential for aeroelastic problems due to their more complex geometry and much higher aspect ratios than their cantilever counterparts. To diagnose any potential problems with aeroelasticity, the SD8.1 and SD8.5 configurations were analyzed in ASWING. The added strut is treated as a beam/surface, and is assumed to be rigidly connected at its ends to the fuselage and wing beams.

Figure 69 shows the SD8.1 system root locii for a range of speeds at an intermediate altitude of 20,000 ft, which were the same conditions chosen for the previous D8.5 aeroelastic analysis. No significant instability problems are evident. However, many of the modes have flexing and axial stressing of the strut, which will buckle if the excitation is strong enough. Strut buckling is a nonlinear effect which cannot be captured by any eigenmode analysis and which may conceivably cause nonlinear instabilities with sufficiently strong elastic excitation. This is difficult to rule out by analysis, and hence must be considered an aeroelastic risk for the strut-braced configuration.

Figure 70 shows the SD8.5 system root locii. Again, no instability is immediately apparent. However, there are now numerous low-frequency modes with near-zero damping, all associated with in-plane wing flexing, which appears only because of the extreme aspect ratio that has led to unavoidably low in-plane stiffness. The lowest such mode is shown in Figure 71. Its frequency is 2.17 Hz, which is nearly the same as the first out-of-plane symmetric bending mode, also indicated in Figure 70.

The in-plane bending modes are unlikely to be unstable, but do give concern. They are readily excited by fluctuating leading edge suction in a vertical gust encounter. Because of the low damping, they will persist after excitation and be sensed by the passengers as fore-aft accelerations at 2 Hz, which is likely to be unpleasant. Also, the in-plane bending also causes in-plane bending in the strut, which can cause it to bend/twist buckle even for modest deflections. Again, this is a nonlinear effect, which cannot be captured by eigenmode analyses and thus carries risk.

SD8.1 Strut-braced

	Ω_x	Ω_z	$\beta°$	$\alpha°$	V_{ref}	C_L	C_D	e
1	0.0	0.0	0.00	4.05	100.0	0.747	0.0352	0.914
2	0.0	0.0	0.00	3.04	110.0	0.617	0.0317	0.899
3	0.0	0.0	0.00	2.34	120.0	0.519	0.0294	0.873
4	0.0	0.0	0.00	1.85	130.0	0.442	0.0279	0.826
5	0.0	0.0	0.00	1.53	140.0	0.381	0.0269	0.756
6	0.0	0.0	0.00	1.36	150.0	0.331	0.0265	0.650
7	0.0	0.0	0.00	1.31	160.0	0.291	0.0263	0.512
8	0.0	0.0	0.00	1.40	170.0	0.257	0.0266	0.359
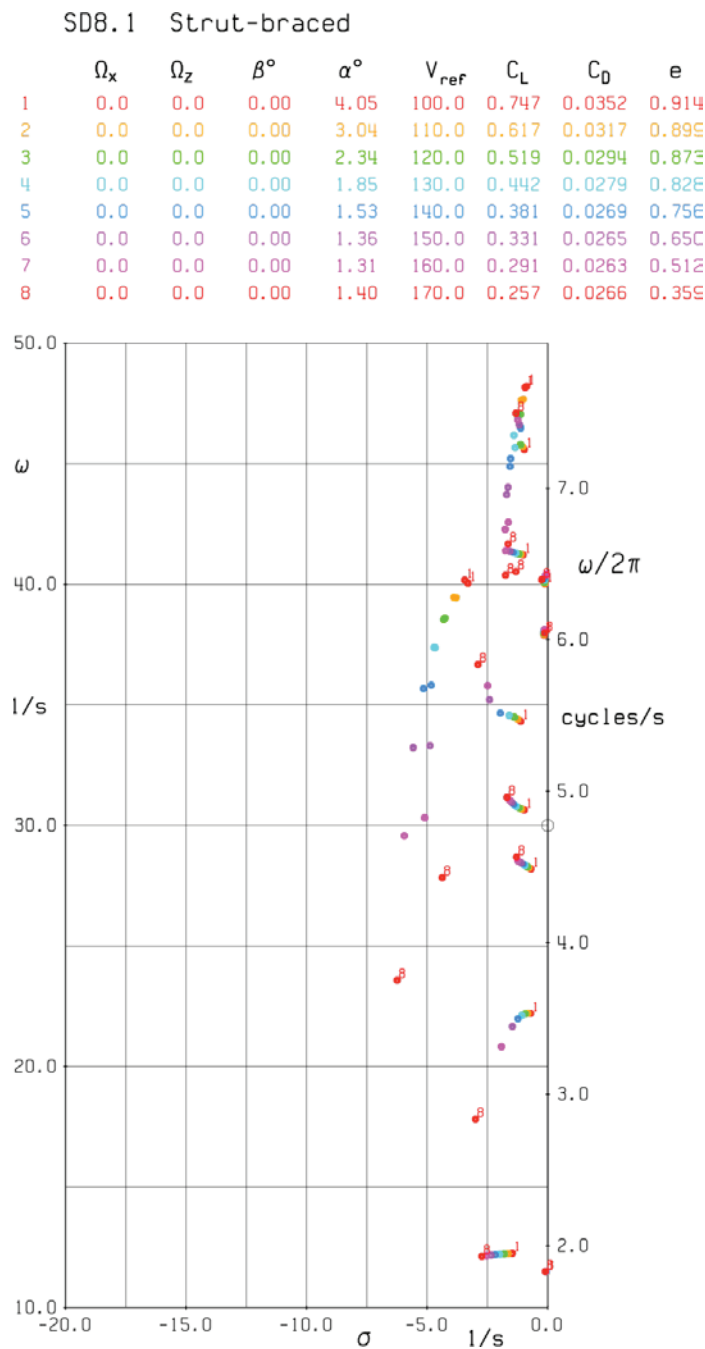
Figure 69: ASWING eigenmode analysis Root locus for SD8.1 configuration over a range of high airspeeds. No unstable roots are observed.

SD8.5

	Ω_x	Ω_z	$\beta°$	$\alpha°$	V_{ref}	C_L	C_D	e
1	0.0	0.0	0.00	3.77	100.0	0.733	0.0366	0.884
2	0.0	0.0	0.00	2.75	110.0	0.606	0.0332	0.854
3	0.0	0.0	0.00	2.02	120.0	0.509	0.0310	0.812
4	0.0	0.0	0.00	1.48	130.0	0.434	0.0294	0.754
5	0.0	0.0	0.00	1.10	140.0	0.374	0.0284	0.678
6	0.0	0.0	0.00	0.83	150.0	0.325	0.0277	0.582
7	0.0	0.0	0.00	0.67	160.0	0.286	0.0273	0.472
8	0.0	0.0	0.00	0.59	170.0	0.253	0.0271	0.357

1st asymm. in-plane bending

1st symm. in-plane bending

1st symm. out-of-plane bending
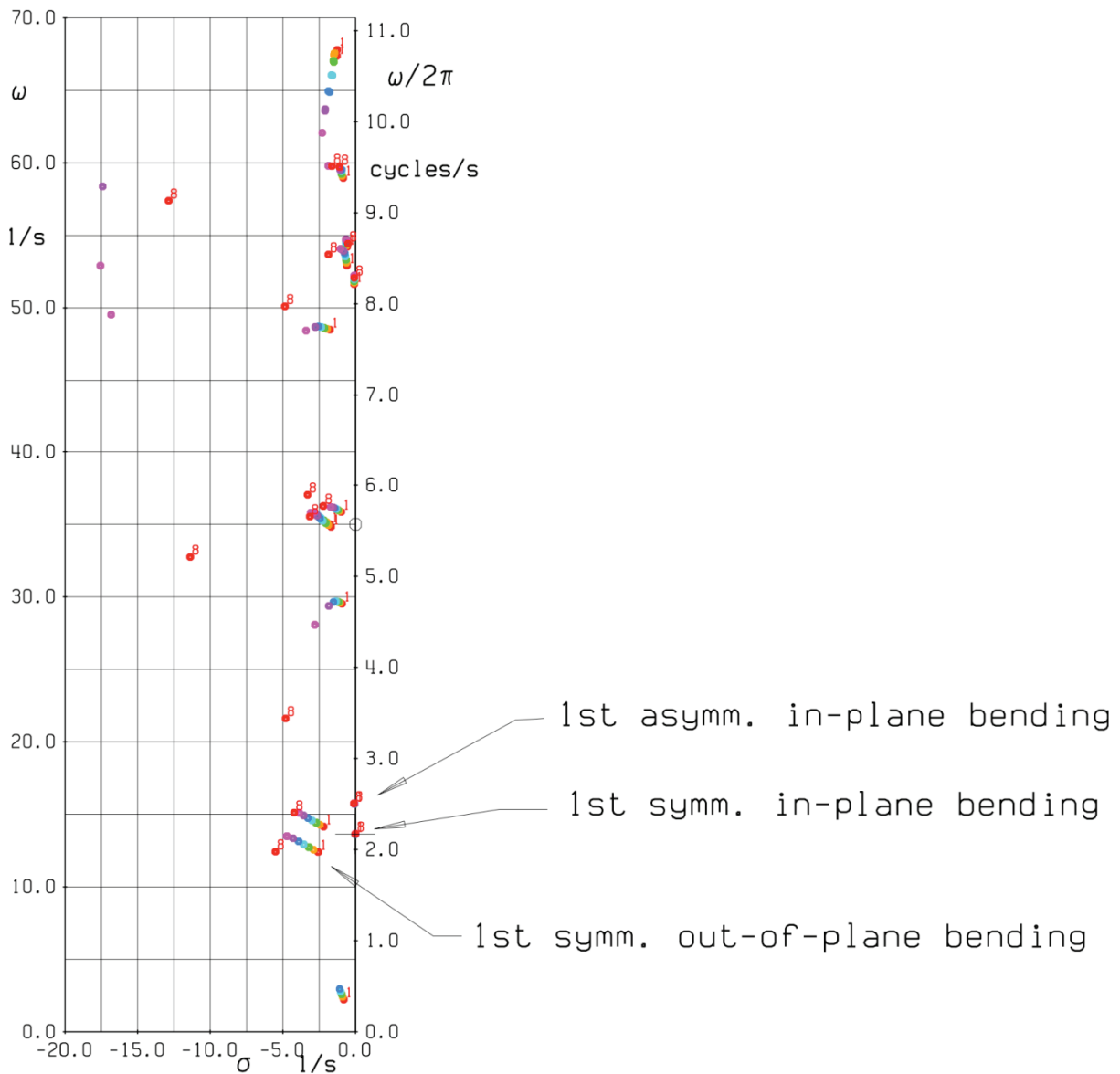
Figure 70: ASWING eigenmode analysis Root locus for SD8.5 configuration over a range of airspeeds. No unstable modes are observed, but many low frequency modes with minimal damping are present.
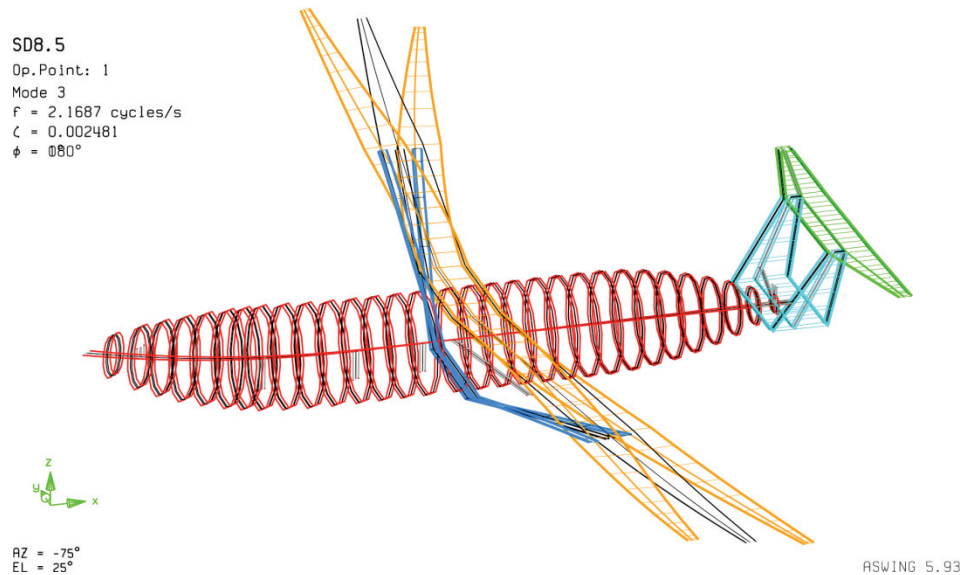
Figure 71: First in-plane bending mode with near-zero damping. Two snapshots (colored) are superimposed at 0° and 180° phase. Center black snapshot is the baseline state of the eigenmode analysis. The fore/aft fuselage acceleration is visible.

5.5   Technology Contributions to NASA N+3 Goals for the D8 Series Aircraft

In this section we analyze the contributions of each of the aircraft's technologies to the NASA N+3 goals. According to the D8 technology choices identified during the design phase (see Section 5.2); we sought to quantify the relative contribution *of the aircraft configuration* (D8.1), as well as *each of the advanced concepts* (which cumulatively result in the D8.5 configuration). For each of the program metrics (fuel burn, noise, and emissions) we defined the percent contribution using the following procedure. "Value" indicates the value of the metric (e.g. PFEI for fuel burn, dB for noise, NOx for emissions.)

1. The percent change from a Boeing 737 due to the *configuration only* is:

$$\alpha = \frac{Value(D8.1) - Value(B737)}{Value(B737)}, \tag{1}$$

   where α = percent change due to configuration only

2. The percent change from a Boeing 737 due to *the full N+3 configuration, including advanced technologies,* is:

$$\beta = \frac{Value(D8.5) - Value(B737)}{Value(B737)}, \tag{2}$$

   Where *β* = percent change of the full N+3 configuration, including advanced technologies

3. Next, we sought to find the contribution of each of the advanced technologies described in the roadmaps in Section 8.2. To do this, we began with the D8.5 configuration, and removed various advanced technologies, listed in Figure 72 through Figure 74 (that is, set that value of the variable affected by that metric to its D8.1 value, which is equivalent to the B737 value). We then ran the calculations with this one variable altered from the D8.5 value to the D8.1 value. We could thus identify the difference in the metrics (fuel burn, noise, and emissions) for an aircraft with and without the advanced technology, with all other technologies still optimized to their advanced values (D8.5 configuration). The contribution of each of the i individual technologies is:

$$\phi_i = \frac{Value(D8.5) - Value(D8.5\_no\ tech_i)}{Value(D8.5) - Value(D8.1)}, \tag{3}$$

where ϕ_i = percent change due to technology i, relative to the overall difference between D8.1 and D8.5.

4. If the ϕ_i value for all of the advanced technologies are added together, they will result in some total sum percentage $\sum_{i=all}\phi_i$. However, we have already found, from items 1 and 2 above, that the *actual* percentage difference (relative to a B737) between the D8.1 (no advanced technologies) and the D8.5 (with all advanced technologies) is equal to $\beta - \alpha$. We therefore define a scaling factor that allows us to translate the percent change for each technology (calculated in Equation 3) to the percent change for each technology relative to the B737. This scaling factor S is equal to:

$$S = \frac{\text{Percentage difference in value between D8.5 and D8.1}}{\text{Unscaled sum of all advanced technologies' percentage differences}} = \frac{\beta - \alpha}{\sum_{i=all}\phi_i} \tag{4}$$

5. This scaling factor allows us to determine the relative percent contribution of each advanced technology:

$$\Phi_i = S(\phi_i), \tag{5}$$

where Φ_i is equal to the relative percent contribution of each technology.

6. To summarize, the total percent change in value between the D8.5 and the B737 is thus the sum of each of these individual components:

%change(N+3 concept) = %change(due to configuration) + %change(due to advanced technologies), or

$$\beta = \alpha + \sum_{i=all}\Phi_i, \tag{6}$$

where Φ_i is defined in equation (5), α is defined in Equation 1, and β is defined in Equation 2.

5.5.1 Technology Contributions to Noise

Figure 72 shows the contribution of the most relevant technologies to the NASA N+3 noise goal, 71 EPNdB below Stage 4. For the D8.5 configuration this corresponds to 202 cumulative EPNdB.

The technology contributors to the noise reduction are, in order of importance: the change of aircraft configuration from a conventional tube and wing to a D8 configuration, the use of ultra high-bypass ratio engines, the change of approach operations to have a steep approach trajectory at 4 degrees and a displaced runway threshold, increase in fan efficiency, and the use of faired undercarriage.

The change in configuration from a conventional tube and wing such as the B737-800 to a D8 configuration gives rise to the largest reduction in noise, -39.7 EPNdB below Stage 4. There are several reasons for this. First, the jet velocity, as a consequence the jet noise, is reduced due to the ingestion of boundary layer and the use of a variable area nozzle during takeoff. Second, the fan noise sources are attenuated. The fan forward noise is reduced through acoustic shielding and the fan rearward noise through the use of extensive multi-segment acoustic liners. This is allowed by the large exhaust duct length-to-fan diameter ratio, which is 1.25 for the D8.1 and D8.5 configurations.

The second largest technology contributor is the use of ultra high bypass ratio engines, which gives a noise reduction of -10.6 EPNdB. These engines have reduction of the FPR and as a consequence a reduction of fan and the jet noise sources. Furthermore, the engines operate with near sonic tip speeds as compared to current fans with supersonic tip speeds.

The other four technologies mentioned above show a lower impact. The changes in approach operations reduce noise because of an increase of the distance between the aircraft and the microphone at the approach certification point. The increase of fan efficiency reduces fan noise, and the faired undercarriage allows for a reduction of the undercarriage noise, one of the largest noise sources at approach, by reducing vortex shedding.
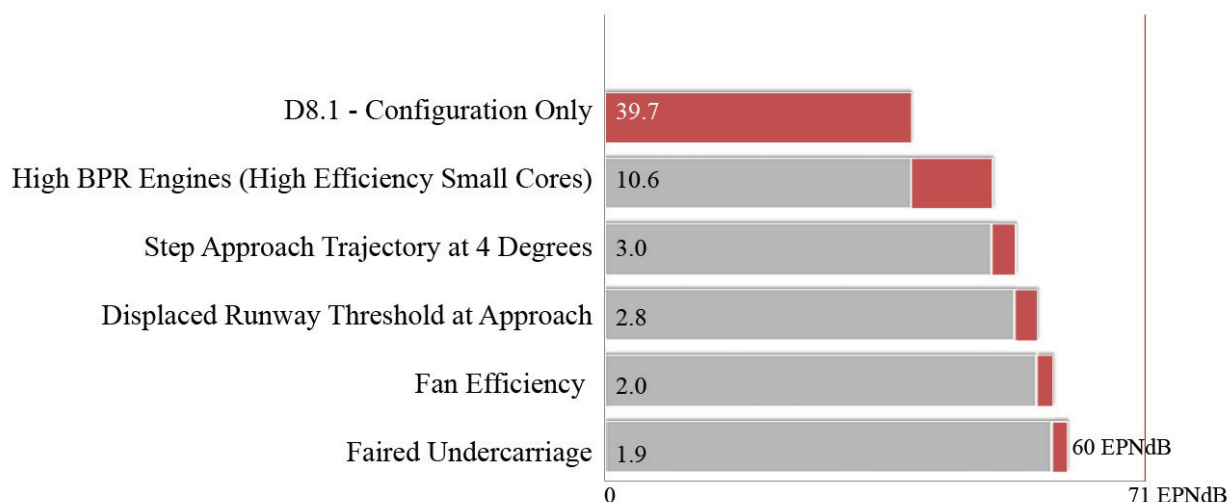
Figure 72: D8.5 Technology Contributions to NASA noise reduction goal.

5.5.2 *Technology Contributions to LTO NOx Reduction*

The same process can be carried out for the other N+3 metrics. (The methodology for evaluation of the metric's parameter is of course different for the different quantities.)

The reductions in LTO NOx are calculated utilizing the CAEP 6 standards as the reference for the baseline. The three technologies that contribute most heavily to LTO NOx reduction are, in order of importance: the D8 configuration, accounting for 51.85% reduction. This is explained by the change in the engine cycle that gives rise to a reduction in TSFC; the advanced LDI combustor technology,

accounting for 18.29% reduction; and the high bypass ratio engines with small high efficiency cores, which account for 15.55% reduction. All other technologies combined contribute 1.56% improvement, totaling 87.26% reduction from the CAEP 6 standard LTO NOx baseline (β_{NOx}). It is important to note that the D8.1 configuration has a significant increase in performance compared to the B737 in regards to LTO NOx, a difference of a reduction in 20.7% from the CAEP 6 standard.
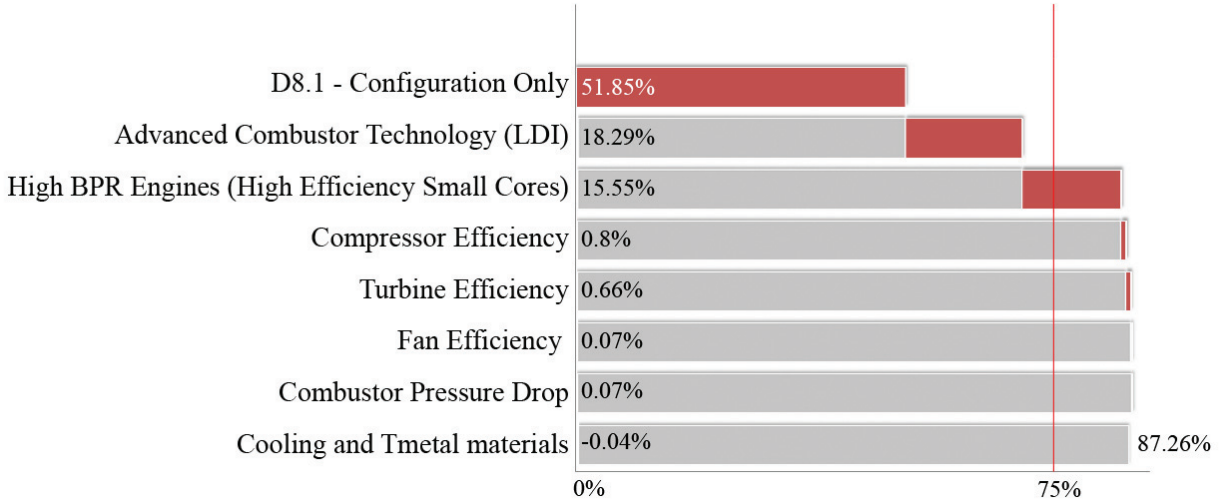
Figure 73: D8.5 Technology contributions to NASA LTO NOx reduction goal.

5.5.3 Technology Contributions to PFEI

To better understand the effect of each technology, it is helpful to connect the technology contributions to different terms of in the Breguet Range equations shown below. For the purposes of accounting for boundary layer ingestion, the Breguet range equation was modified with a term, λ, that is defined as the ratio of net required thrust to total airframe drag without BLI.

$$R = \frac{V}{SFC} \frac{L}{\lambda D} \ln\left(1 + \frac{W_F}{OEW + W_R + W_P}\right)$$
(7)

The contributions of each technology to NASA's PFEI goal are presented in Figure 74. All technologies combined achieved a 70.8% reduction in PFEI from the B737-800 baseline (β_{PFEI}, also see Section 3). As shown in the figure, the D-series airframe configuration gives the largest PFEI reduction, enabling 49.15% reduction from baseline. This large improvement in PFEI can be explained from the modification sequence of the airframe described in Section 5.2.1; in summary, the D-series airframe configuration has the following features which help improving PFEI:

- Reduction of structural weight enabled by the double bubble fuselage

- Improvement of airframe aerodynamic performance from reduced flight Mach number, lifting fuselage and boundary layer ingestion

- Reduction in TSFC with a use of higher efficiency engine.

As we can see from the range equation, the reduction of OEW is one of key parameters that affect the PFEI of an aircraft, and there are a few technologies in D8.5 that focuses on reducing this parameter. The largest contributor in the category is the airframe advanced material and processes, which gives an additional 7.55% reduction in PFEI. This is the result of reducing the weight of the aircraft structure which is the heaviest component. With this improvement, the empty weight fraction of this vehicle changed from 54% in the D8.1 to 50% in the D8.5. Although other weight reduction technologies, such as airframe design load reduction, secondary structures, advanced engine materials and cockpit fixed weight each has a relatively small impact on PFEI, it still contributes to an additional 2.5% reduction in PFEI altogether.

Another major parameter to focus on is the corrected lift to drag ratio ($L/\lambda D$) of the aircraft, which indicates the aerodynamic performance of the airframe. The D8.5 has two important technologies associated with the aerodynamics of the aircraft: Boundary Layer Ingestion (BLI) and natural laminar flow on wing bottom surface. BLI reduces the λ in the corrected lift to drag ratio, providing a reduction of 2.57% in PFEI. Applying laminar flow on wing bottom surface reduces the profile drag of the wing section, contributing to a reduction of 2.54% in PFEI.

The final important parameter that affects the PFEI is the thrust specific fuel consumption (TSFC) of the propulsion system. The propulsion system technology that gives the largest contribution to PFEI of the vehicle is the use of ultra high bypass ratio engines with high efficiency small cores, which increases the propulsive efficiency of the engine. This technology alone contributes to 4.24% reduction in PFEI. Other engine technologies such as increased hot section allowable metal temperatures, further improvements in component efficiencies, increased cooling effectiveness, and advanced combustors add another 5.11% in PFEI reduction.

In summary, the D8.5 gets an improvement of 49.15% from the airframe configuration, 10.05% from further reduction of structural weight, 2.54% in additional aerodynamic improvement, and 9.35% from improvements in engine performance.
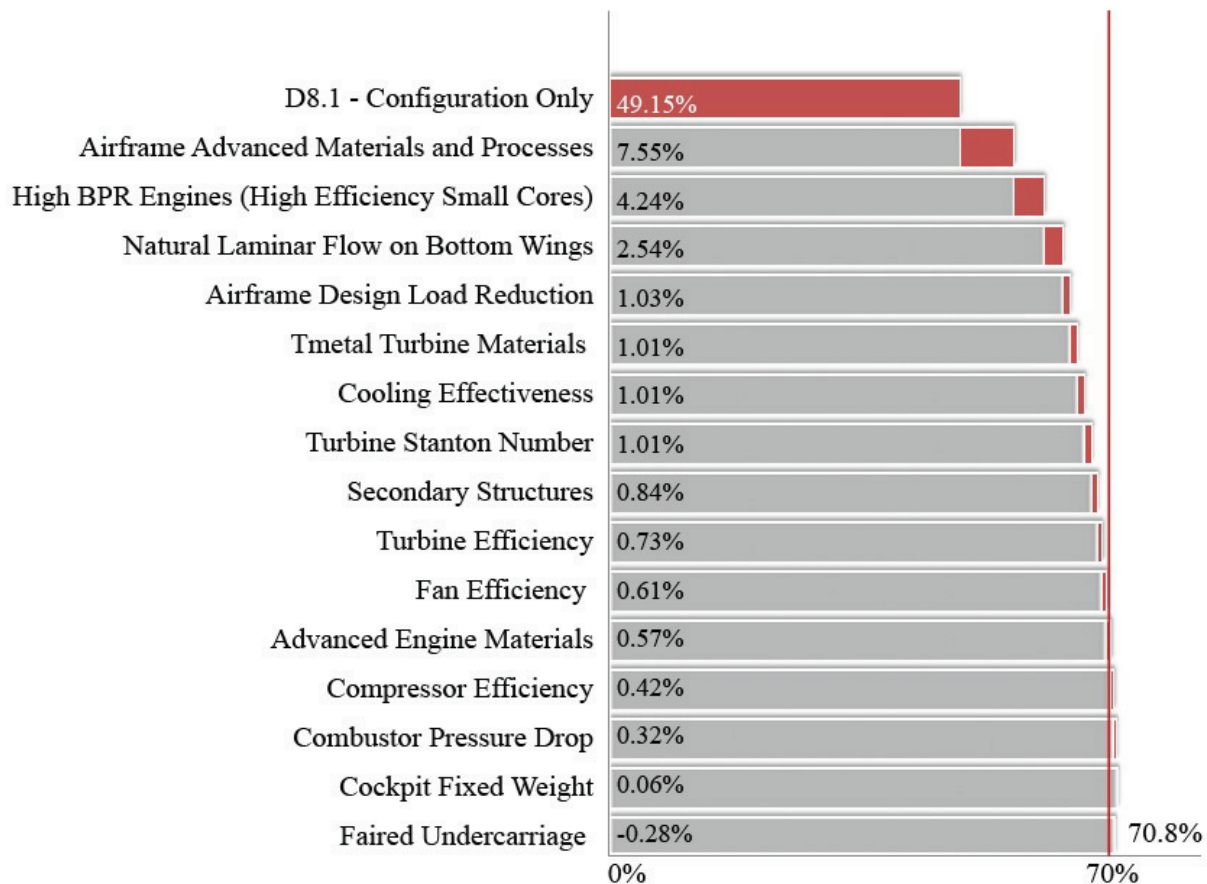
Figure 74: D8.5 Technology contributions to NASA PFEI goal.

5.6   Trades

Section 5.5 of the report discusses the contribution to the NASA N+3 metrics through a change in aircraft configuration and the inclusion of each of the technologies used in the D8.5 aircraft. In this section, a trade off study between the N+3 metrics is presented. Each of the aircraft configurations performance under investigation is the result of an aircraft design generated through an optimized design process discussed in detail in section 5.7.

Figure 75 shows the PFEI and noise trends with increasing bypass ratio (BPR). An increase in the BPR gives rise to a decrease of the fan pressure ratio (FPR) and an increase of the fan diameter. In terms of noise, this leads to lower fan noise and to lower jet velocities, which gives rise to lower jet noise. As a consequence, there is a significant decrease in the aircraft noise as shown in Figure 75. In terms of PFEI, an increase in the BPR gives rise to an increase of the propulsive efficiency, which has a beneficial effect in PFEI. This also gives rise to an increase of the nacelle size and therefore nacelle drag, which is detrimental for PFEI.   An additional effect of the increased BPR is a reduction to the core size. The decrease in core size implies a decay of the core component efficiencies due to Reynolds number effects, larger tip clearance flows and larger hub leakage flows. This has a detrimental effect on PFEI and a resulting big design challenge. As a result of all those effects, an increase of BPR produces a decrease of

the PFEI, as illustrated in Figure 75. The effect of BPR in PFEI is larger at the lower values of BPR but it tends to decay for BPR above 10 where the detrimental effects tend to compensate the benefits. The effect in noise also decays at the larger BPR but is less pronounced than the effect on PFEI. As a result of these trades a BPR value of 20 was chosen for the D8.5 final configuration.
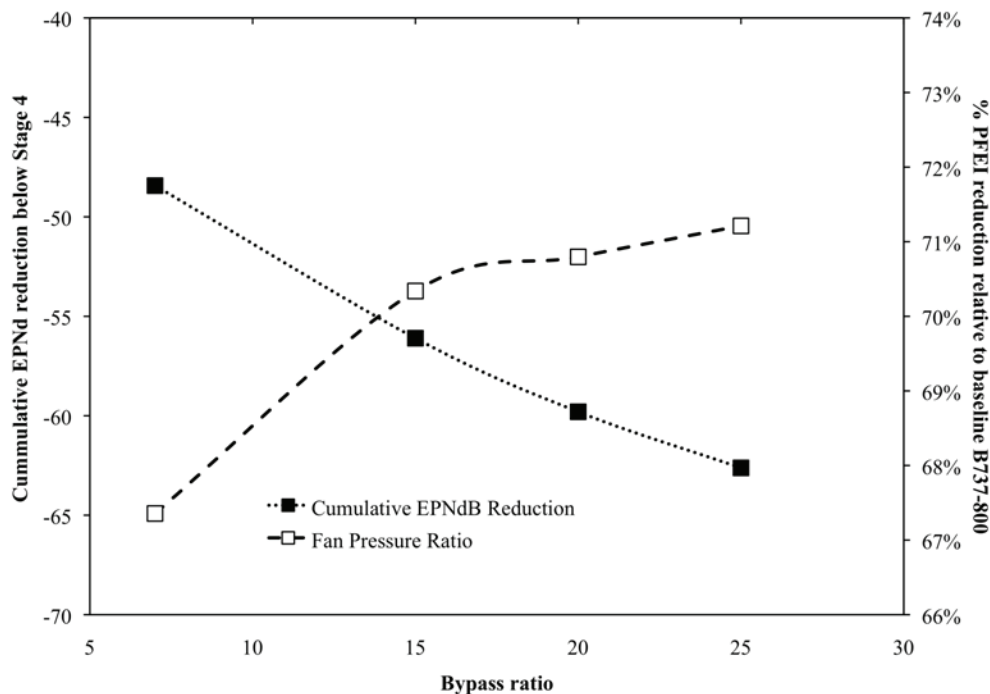
Figure 75: Percent PFEI reduction and cumulative noise reduction as a function of bypass ratio for D8.5 configuration.

Figure 76 shows the tradeoff between balanced field length, noise, and PFEI. There is not a significant effect on PFEI when changing the balanced field length (BFL). However, there is a driving influence on the noise. The noise level is lower for the case of a BFL of 3200 feet and it shows an asymptotic behavior when the BFL increases over 5000 feet. The reduced noise value for the case of 3200 feet is achieved in part by an increase of the wingspan, which has grown to 192.6 feet for this case. This large value, which is comparable to the B777 wingspan, makes the aircraft design not suitable for a metroplex environment. The reduction of noise can be explained as followed: at sideline, there is an increase of noise due to the high thrust required for takeoff; this is minor compared to the decrease of noise at flyover when compared to the cases with a longer BFL. There are several reasons for this reduction in noise. First, the distance between the aircraft and the observer at the flyover position increases significantly as the aircraft takes off further upstream from the observer and with a higher climb angle. Second, the FPR for this aircraft is lower leading to lower fan and jet noise. Finally, the flight speed after cutback is reduced causing the airframe noise to be lower. At approach, there is a decrease of noise due to a reduction of the approach speed as a consequence of the increase in the wingspan of the aircraft. A value for the BFL of 5000 feet for the final D8.5 configuration was used to ensure a metroplex aircraft while limiting the effect on PFEI and taking advantage to the reduction in aircraft noise, allowing for inclusion of a -60 EPNdB noise reduction relative to Stage 4.
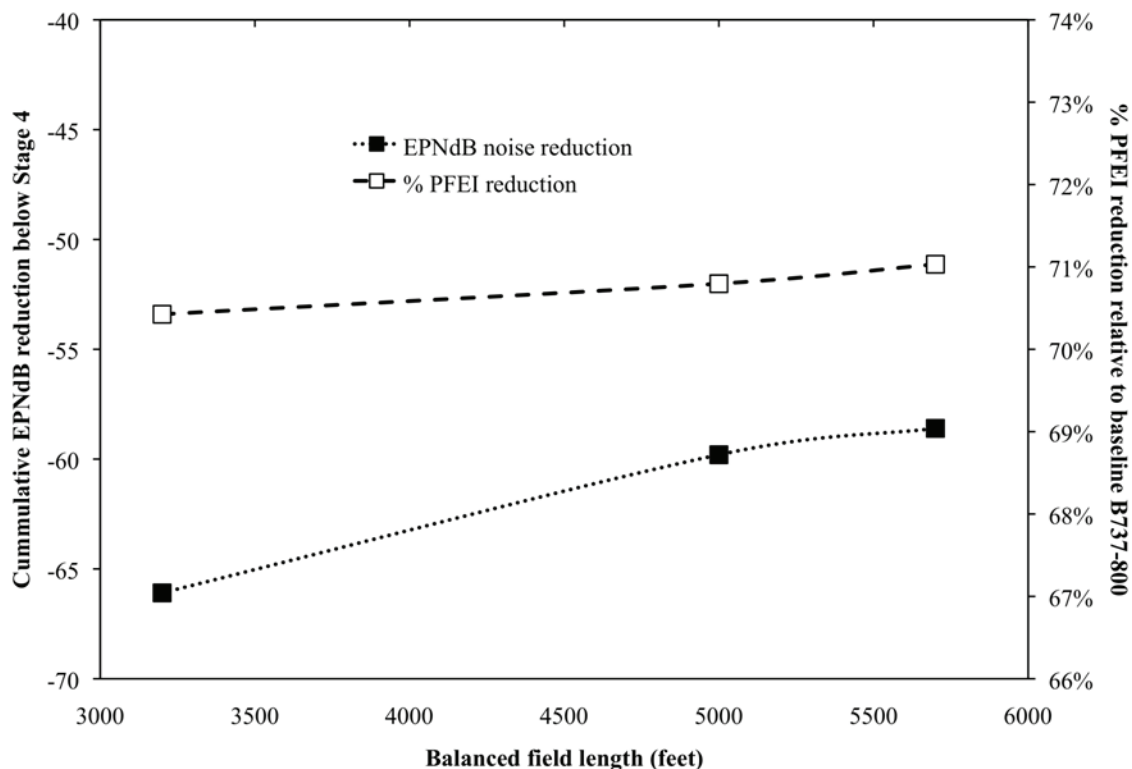
Figure 76: Percent PFEI reduction and cumulative noise reduction as a function of balanced field length for D8.5 configuration.

Figure 77 shows the tradeoff between PFEI and noise for different lengths of the exhaust duct. An increase of the exhaust duct leads to a PFEI increase due to higher engine weight and nacelle drag, and lower exhaust duct pressure recovery. Alternatively, there is a noise decrease due to an increase of the area available for the application of acoustic liners. Liner attenuation gives a reduction of -20 EPNdB for the case of a ratio of exhaust duct to fan diameter of 1.25 relative to an unlined engine. A further extension of the exhaust leads to a progressively smaller effect in noise as well as in PFEI, as shown in Figure 77. A value of 1.25 for the ratio of the exhaust duct length to fan diameter was used for the D8.5 final design.
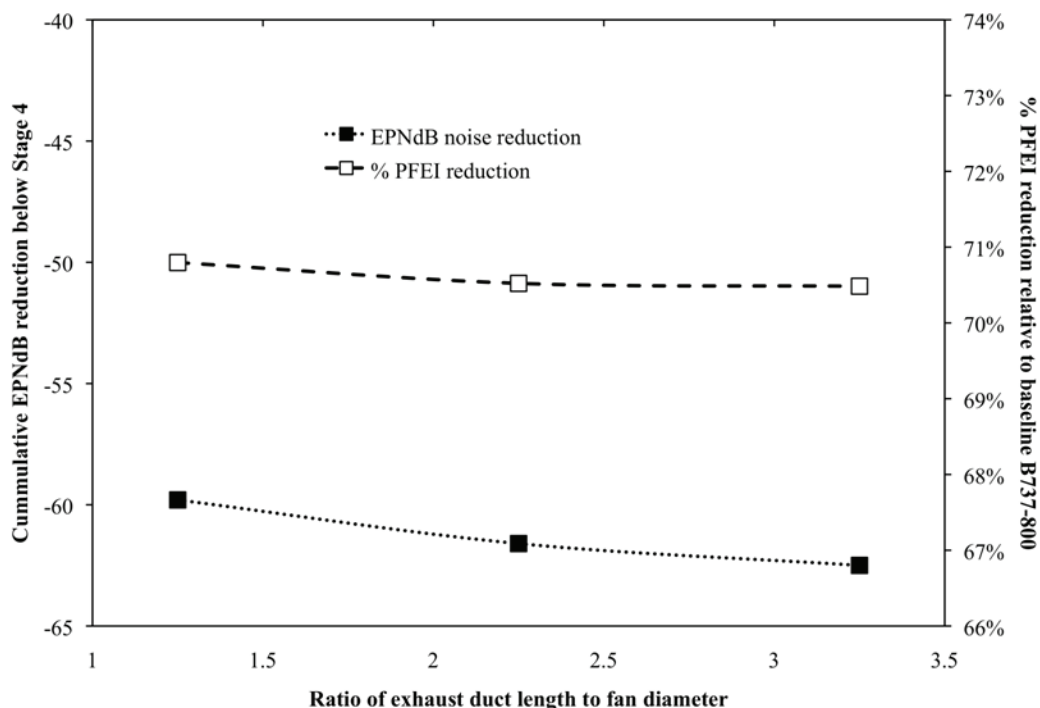
Figure 77: Percent PFEI reduction and cumulative noise reduction as a function of ratio of the exhaust duct length to fan diameter for D8.5 configuration.

Figure 78 illustrates the change in PFEI for a different amount of boundary layer ingestion (BLI) of the fuselage. PFEI decreases when applying boundary layer ingestion as a consequence of a reduction of the wake and jet dissipation. Changes in noise are not included as these are not significant, even when the ingestion of the boundary layer leads to lower jet velocities and therefore jet noise. This is due to the fan rearward noise being the dominant source in this case. A value of 40% BLI was used for the final D8.5 configuration which represents a conservative approach to ingesting the entire fuselage top surface wake defect through the engines.
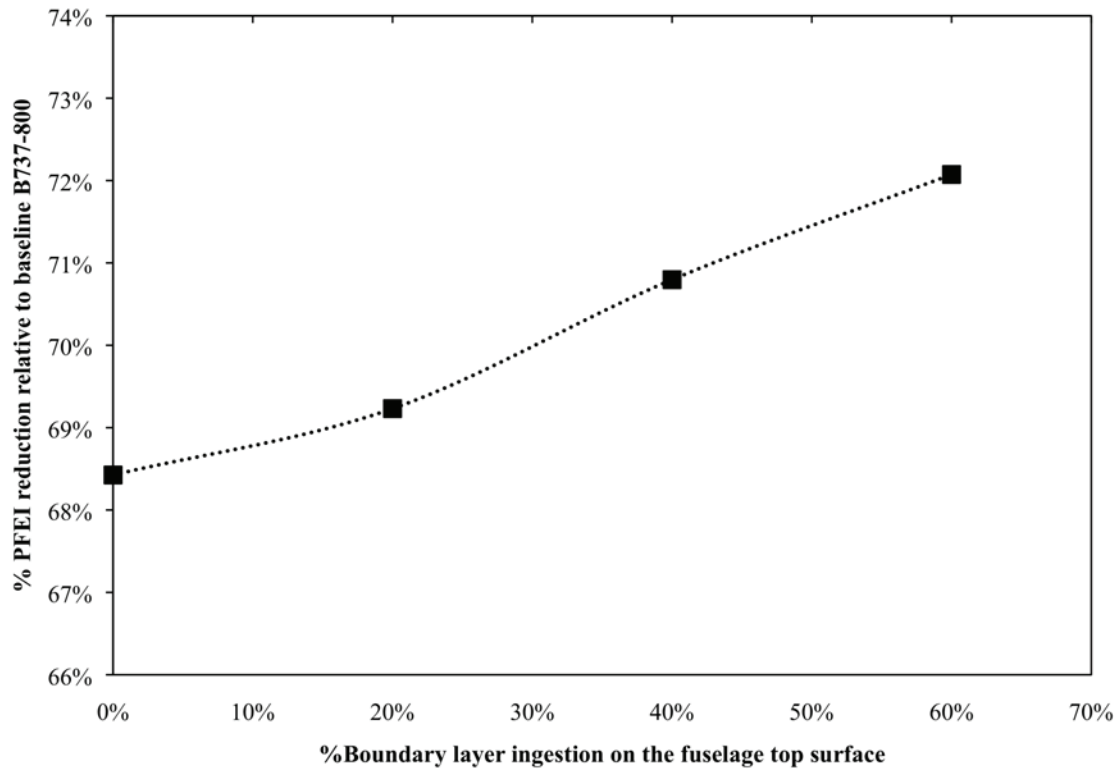
Figure 78: Percent PFEI reduction as a function of percentage of boundary layer ingestion on the fuselage top surface.

In addition to the specific technologies explored in the previous trade section several other technologies were evaluated to determine the performance difference between the conventional D series aircraft D8.1 and an aircraft which includes a specific individual advanced technology projected to the N+3 timeframe several design cases were set up which used as the baseline aircraft the D8.5 with the exception of one advanced technology reduced to the D8.1 conventional level at a time and then the vehicle was allowed to be optimized to maximize the effect of the removal of the that advanced technology (via TASOPT.) Table 27 identifies the overall change in aircraft PFEI as a result of the removal of the one specific technology under investigation at a time.

Table 27: Technology Insertion Sensitivity in Absolute PFEI

Technology	Variable Units	Current Value of Technology (D8.1)	Advanced Value of Technology (D8.5)	PFEI for the D8.5, if this variable is set to the D8.1 value	Sensitiviy Coefficients
Boundary layer ingestion	% BL ingestion (fuselage)	fBLIf=.4, fBLIw=0	fBLIf=0	2.3461	-0.1762
Faired undercarriage	fglnose, fglmain	fglnose = .0075 , fglmain = .03	fglnose = .01 , fglmain = .04	2.1531	0.0168
Airframe advance materials and processes	Material Strength, Density	Alum	2035 Table	2.6253	-0.4554
Airframe desging load reduction (Gust load alleviation and Health monitoring)	Design Load Factor	3	2.5	2.232	-0.0621
Secondary Structures	Factor	0.35	0.3	2.2204	-0.0505
High bypass ratio engines (high efficiency small cores)	BPR (Ratio)	6.7 (Optimized)	20	2.4255	-0.2556
Advanced Hot section materials and Cooling Effectiveness	K	1200	1500	2.2308	-0.0609
Component efficiencies (Fan)	% efficiency	FPRo=1.5	FPRo=1.5	2.2066	-0.0367
Component efficiencies (Compressor)(Poly)	% efficiency	H=0.89, L=0.92	H=0.90, L=0.93	2.195	-0.0251
Component efficiencies (Turbine)(poly)	% efficiency	H=0.91, L=0.92	H=0.925, L=0.93	2.2141	-0.0442
Combustor Pressure Drop	% pressure drop	0.94	0.955	2.189	-0.0191
Advanced Engine Materials	kg	Off	On	2.204	-0.0341
Natural Laminar Flow on bottom wings	C_L (unitless)	Off	On	2.3228	-0.1529
Exhaust Duct Length	Ratio nacelle area to fan area	6	4	2.1903	-0.0204

5.7 Design Methodology

5.7.1 TASOPT Summary

TASOPT (**T**ransport **A**ircraft **S**ystem **OPT**imization) is a program for simultaneously optimizing the airframe, engine, and operating parameters of a wing+tube transport aircraft. It was developed partly to support the present N+3 project, and subsequently used to develop, evaluate, and optimize the D configurations and compare them to the B737-800 baseline; it was also used for the (larger) D13 aircraft to be described in Section 7.0. The chosen figure of merit has been minimum fuel burn or equivalently PFEI for one or more given payload and range missions, possibly in the presence of field length constraints.

This section is an introduction and brief summary for the structural, aerodynamic, propulsion, and performance models which are integrated together in TASOPT. The component models and the integration are all described in complete (and voluminous) detail in the Appendices.

5.7.2 Background

There is a vast body of work on conceptual and preliminary aircraft design. Traditional approaches of e.g. (Roskam[69], Torrenbeek[70], Raymer[71]) have relied heavily on historical weight correlations, empirical drag

---

[69] Roskam, J., *Airplane Design*, DAR Corporation, Lawrence, Kansas, 2000.

build-ups, and established engine performance data for their design evaluations. The ACSYNT program[72,73] likewise relies on such models, with a more detailed treatment of the geometry. More recently, optimization-based approaches such as those of Knapp[74], the WingMOD code of Wakayama[75,76], and in particular the PASS program of Kroo[77] perform tradeoffs in a much more detailed geometry parameter space, but still rely on simple drag and engine performance models.

The recent advent of turbofan engines with extremely high bypass ratios (Pratt geared turbofan), advanced composite materials (Boeing 787), and possibly less restrictive operational restrictions (Free-Flight ATC concept), make it of great interest to re-examine the overall aircraft/engine/operation system to maximize transportation efficiency. The present NASA N+3 effort is one example of research towards this goal. In addition, greater emphasis on limiting noise and emissions dictates that such aircraft design examination should be done under possibly stringent environmental constraints.

5.7.3   General TASOPT Approach

To examine and evaluate future aircraft with potentially unprecedented airframe, aerodynamic, engine, or operation parameters, it is desirable to dispense with as many of the historically-based methods as possible, since these cannot be relied on outside of their data-fit ranges. The approach used by TASOPT is to instead rely on *low-order physical models that implement fundamental structural, aerodynamic, and thermodynamic theory and associated computational methods for all primary predictions*. Historical correlations are used only where absolutely necessary and in particular only for some of the secondary structure and for aircraft equipment. Modeling the bulk of the aircraft structure, aerodynamics, and propulsion from a fundamental basis gives considerable confidence that the resulting optimized design is realizable, and not some artifact of inappropriate extrapolated data fits. All of the details of the structural and aerodynamic models can be found in the various sections of Appendices A - F. The following descriptions are meant as an overview to explain the process.

---

[70] Torrenbeek, E., *Synthesis of Subsonic Airplane Design*, Delft University Press, 1988.

[71] Raymer, D.P., *Aircraft Design: A Conceptual Approach*, AIAA Education Series. AIAA, 1992.

[72] Jayaram, S., Myklebust, A., Gelhausen, P., "ACSYNT – A standards-based system for parametric computer aided conceptual design of aircraft," AIAA Paper 92-1268, Feb 1992.

[73] Mason, W.H., Arledge, T.K., "ACSYNT aerodynamic estimation – An examination and validation for use in conceptual design," AIAA Paper 93-0973, Feb 1993.

[74] Knapp, B., "Applications of a nonlinear wing planform design program," Master's thesis, MIT, Aug 1996.

[75] Wakayama, S., "Lifting surface design using multidisciplinary optimization," PhD thesis, Stanford, June 1994.

[76] Wakayama, S., "Blended-wing-body optimization setup," AIAA Paper 00-4740, Sept 2000.

[77] Kroo, I., PASS, program for aircraft synthesis studies, Software Package, Desktop Aeronautics, Palo Alto, CA, 2005.

5.7.4 *Weight and Structural Models*

The assumed weight breakdown is diagrammed in Figure 79.

The airframe primary structure elements are modeled as simplified geometric shapes, with the gauge-sizing loads for each element imposed at the critical loading cases listed in Table 28.

Table 28: Load Cases for Sizing Primary Structural Elements

Max $N_{lift}W_{MTO}$	wing bending spar caps and shear webs
Δp at max altitude	fuselage skin tension
Max L_{vtail} at V_{NE}	fuse and tailcone skin shear, added side stringers, tail caps and webs
Max L_{htail} at V_{NE}	added top/bottom stringers, tail caps and webs
Max $N_{land}W_{MTO}$	added top/bottom stringers, fuselage floor beams

W_{pay}

W_{padd} f_{padd}

W_{apu} f_{apu}

W_{fix}

W_{shell} : W_{skin} 1

f_{string}

f_{frame}

f_{fadd}

W_{db}

W_{window}

W_{insul}

W_{seat}

W_{floor}

W_{cone}

W_{hbend}

W_{vbend}

W_{fuse}

W_{wcap} 1   1

W_{wweb}

W_{wadd} :

W_{flap} f_{flap}

W_{slat} f_{slat}

W_{aile} f_{aile}

W_{lete} f_{lete}

W_{ribs} f_{ribs}

W_{spoi} f_{spoi}

W_{watt} f_{watt}

f_{wadd}

W_{wing}

W_{strut}

W_{htail} :

W_{hcap}

W_{hweb} 1

W_{hadd} f_{hadd}

W_{vtail} :

W_{vcap}

W_{vweb} 1

W_{vadd} f_{vadd}

W_{eng} :

W_{ebare} 1

W_{eadd} f_{eadd} 1

W_{nace}

W_{pylon} f_{pylon}

W_{fuel} :

W_{burn} 1

$W_{reserve}$ $f_{reserve}$

W_{hpesys} f_{hpesys}

W_{lgnose} f_{lgnose}

W_{lgmain} f_{lgmain}

W_{MTO} 1

Figure 79 Aircraft weights and weight fractions breakdown.

5.7.4.1 Fuselage

The fuselage, as sketched in Figure 80, is assumed to be a pressure vessel with spherical or ellipsoidal endcaps, which is subjected to bending and torsion loads at the various loading scenarios considered.
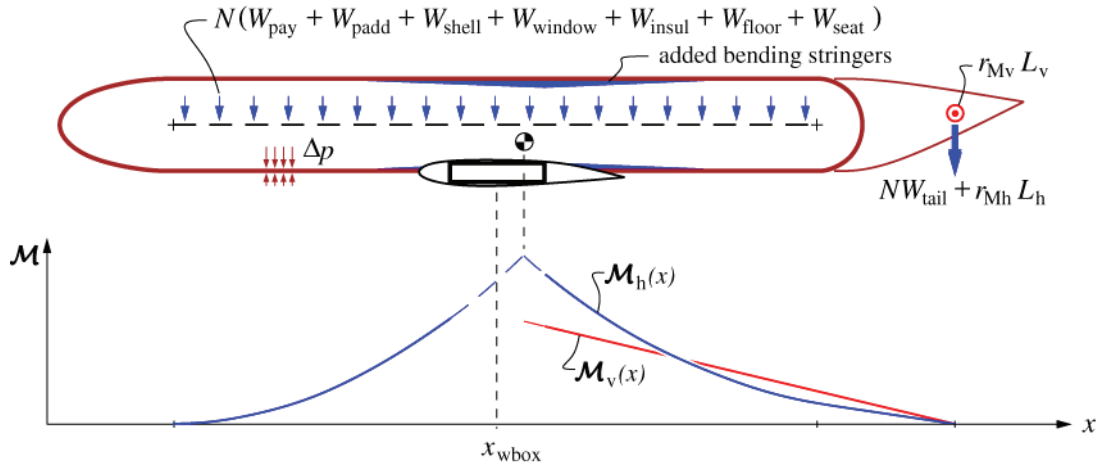
Figure 80: Fuselage layout, pressure load, and bending load.

The fuselage cross-section, shown in Figure 81, has a "double-bubble" cross-section. The usual simple circular cross-section is a special case. The skin and added assumed stringers and frames are all sized to obtain a specified stress at the specified load situations. A payload-loading analysis provides the weight of the floor. All other secondary-structure weights and interior furnishings (windows, doors, seats, insulation, galleys, etc.) are estimated using historical weight fractions and assumed to be proportional to the number of passengers, or interior area, or cabin length, as appropriate for each element.
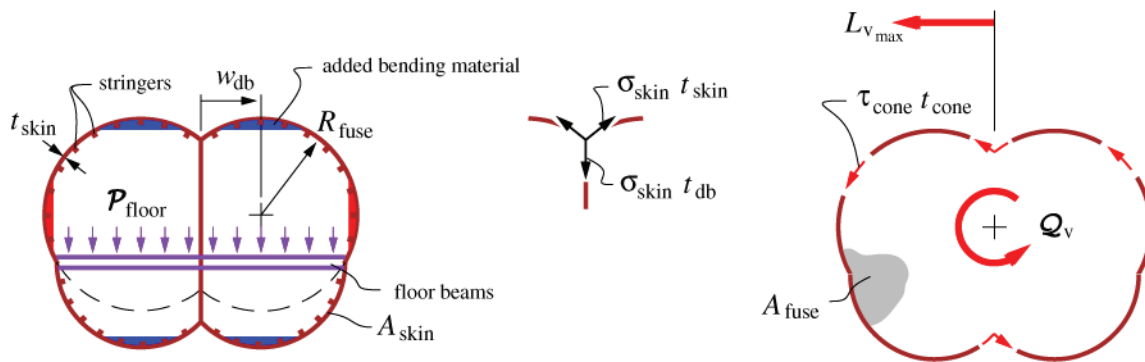
Figure 81: Fuselage cross-section, shell/web junction tension flows, and torsion shear flow from vertical tail load. Fuselage frames are not shown.

5.7.4.2 Wing

The wing, shown in Figure 82, is assumed to have a double piecewise linear taper planform at some sweep angle, and to be subjected to a double piecewise linear aerodynamic lift distribution with tip and fuselage-carryover lift modifications. The relieving of distributed weight loads of the structure and fuel are also imposed. An optional strut or engine with its structural or relieving weight load is assumed to act at the planform break as sketched.

Figure 82: Wing planform and applied aerodynamic and weight loads. An optional strut or engine can also impose added structural or weight loads.

The wing cross-section, shown in Figure 83, consists of a structural box with curved top and bottom sparcaps, with front and rear shear webs. These elements are sized to achieve specified allowable stresses due to the perpendicular-plane bending moment $M_\perp$ at the chosen critical loading condition at a maximum allowable load factor. The known structural gauges then give the wing's primary structural weight and weight moments. The internal box volume also gives the maximum fuel capacity and fuel weight. The weight of the slats, flaps, ailerons, spoilers, and other secondary structure is currently estimated using historical weight fractions.

Figure 83: Wing or tail airfoil and structure cross-section, shown perpendicular to spar axis. Leading edges, fairings, slats, flaps, and spoilers contribute to weight but not to the primary structure.

5.7.4.3 Tail Surfaces

The tail surfaces are treated using the same model as for the wing, except that struts, engines, and fuel are absent in the code implementation. Also, the sizing load case is different as given in Table 28.

5.7.5   Aerodynamic Models

The various aerodynamic models represent the lift forces which balance the weight, and the drag forces which balance the thrust. The latter is actually formulated as a *power balance* as derived by Drela[78], which is compared with the usual force balance in Figure 84a and Figure 84b. The two formulations are being entirely equivalent if there is no Boundary Layer Ingestion (BLI). In the case with BLI, sketched in Figure 84c, however, the power balance considerably simplifies the analysis. The various power components and BLI terms can also be estimated without ambiguity from the quantities in the non-BLI case, with only the BL ingestion fraction f_{BLI} required as the additional input. The overall benefits are the elimination of that fraction of the wake dissipation, and a reduction in the required engine outlet power, and hence in the engine size and weight.
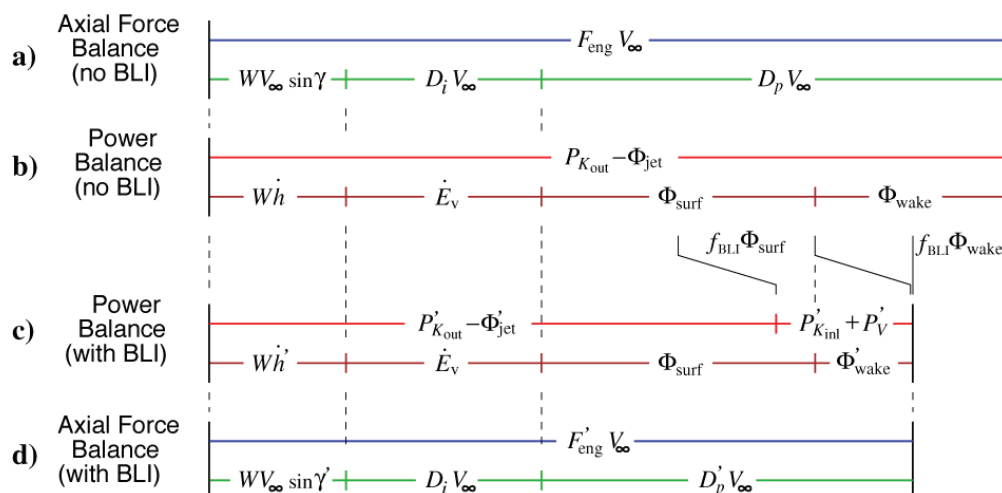
Figure 84: Force balance a) and equivalent power balance b) for the non-BLI case. The latter readily addresses the BLI case c), which can be optionally interpreted again in terms of equivalent or effective forces d). Primes ( )' denote quantities which are significantly modified by the BLI.

5.7.5.1 Wing profile lift and dissipation (profile drag power)

The wing airfoil performance is represented by a parameterized transonic airfoil family spanning a range of thicknesses, shown in Figure 85. Each airfoil has been designed and optimized for good transonic drag

---

[78] Drela, M., "Power balance in aerodynamic flows," *AIAA Journal*, 47(7):1761–1771, July 2009. Also AIAA Paper 09-3762, San Antonio Conference, June 2009.

rise behavior, which was determined by the 2D viscous/inviscid MSES code[79] for a range of lift coefficients and Mach numbers.

	NC090	NC100	NC110	NC120	NC130
area =	0.06210	0.06836	0.07464	0.08093	0.08723
thick. =	0.09001	0.10000	0.11000	0.12000	0.13000
camber =	0.02142	0.02036	0.01930	0.01826	0.01722
r_{LE} =	0.01457	0.01489	0.01522	0.01556	0.01590
$\Delta\theta_{TE}$ =	11.78°	11.74°	11.71°	11.68°	11.64°
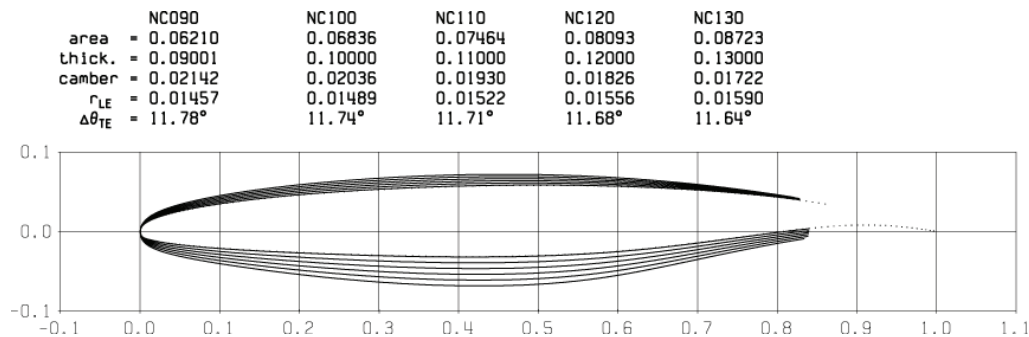
Figure 85: Airfoil family used to generate airfoil-performance database.

These predictions are interrogated and applied to the wing via standard sweep corrections, modified to account for shock unsweeping at wing root, as sketched in Figure 86. The overall model gives reliable transonic lift and drag performance predictions of the entire wing in cruise, and also in high climb and high descent.

This approach for representing the airfoil performance in effect represents an arbitrary "rubber airfoil", whose thickness can now be optimized by trading profile drag versus structural merit, together with the effects of the all the other airframe, engine, and operating parameters. It also has the advantage of eliminating the need for empirical wave drag estimates, since the wave drag has been captured by the viscous CFD calculations and hence is implicitly contained in the airfoil performance database.

2D multielement MSES calculations were also used to estimate the airfoils' and hence the wing's C_{Lmax} and viscous dissipation for takeoff predictions. The airfoil thickness is assumed to have a negligible effect here, so the coefficients can be computed offline and another airfoil database for runtime execution is not required.

---

[79] Drela, M., Giles, M.B., "Viscous-inviscid analysis of transonic and low Reynolds number airfoils," *AIAA Journal*, 25(10):1347–1355, Oct 1987.
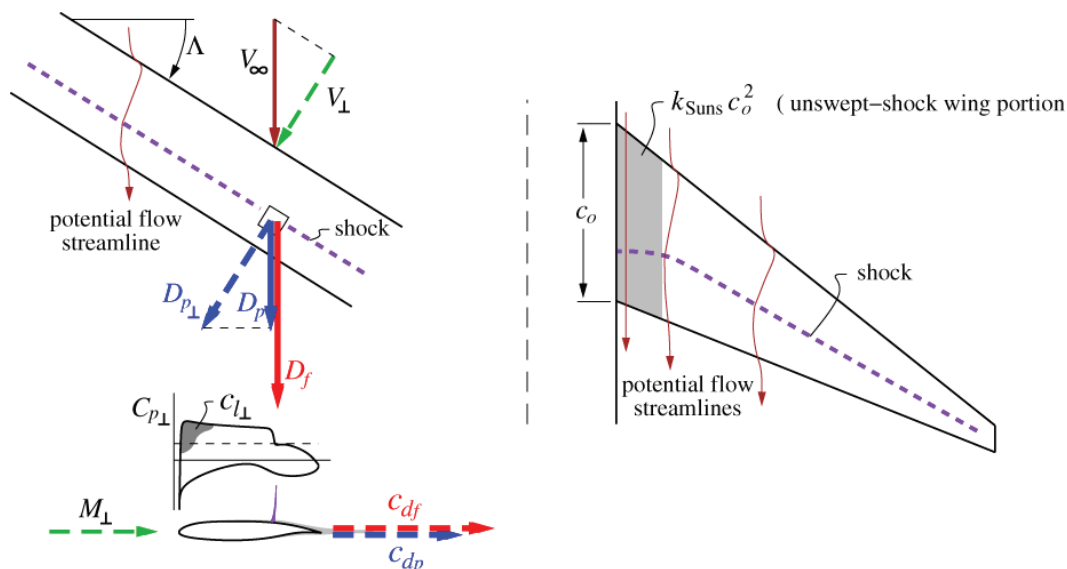
Figure 86: Application of 2D airfoil c_d and c_ℓ to an infinite swept wing, with wing root correction to account for local shock unsweep roughly over the area $k_{uns}c_o^2$.

5.7.5.2 Fuselage viscous dissipation (profile drag power)

As for the wing airfoils, the fuselage drag is obtained from compressible viscous/inviscid CFD, suitably simplified with axisymmetric-based approximations. This approach also gives a detailed definition of the fuselage boundary layer, and in particular gives the surface/wake dissipation breakdown sketched in Figure 84, which is needed to model the BLI influence on the excess power which gives the climb rate. This information would not be immediately available from traditional wetted-area drag prediction methods.

5.7.5.3 Nacelle viscous dissipation

The dissipation on the exterior of the engine nacelle is estimated using turbulent $C_f(Re_l)$ correlations, recast in power-dissipation form as for the other components. The model estimates the nacelle's exterior velocity distribution from the flight and fan-face Mach numbers, as sketched in Figure 87. This approach makes the predicted nacelle drag strongly dependent on the flight speed and the engine power setting, as is the case in reality, and thus provides realistic nacelle drag estimates over the entire flight regime.
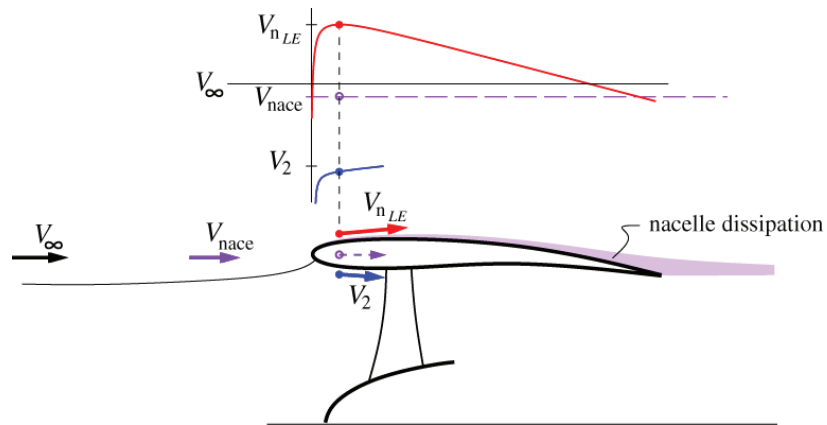
Figure 87: Velocity distribution on inside and outside of engine nacelle. Outside velocity determines nacelle dissipation and implied nacelle drag. The $V_{n_{LE}} > V_2$ case shown is for a typical cruise condition, while $V_{n_{LE}} < V_2$ will occur at low speeds and high power.

5.7.5.4 Vortex kinetic energy loss (induced drag power)

Overall aircraft induced drag is predicted by a Trefftz-Plane analysis, with the circulation in the Trefftz Plane tied directly to the spanwise wing load distribution, with corrections for wake contraction due to the fuselage, as shown in Figure 88. The tail load is also included. The overall calculation then captures trim drag and, together with the structural weight models, allows spanload shape optimization.
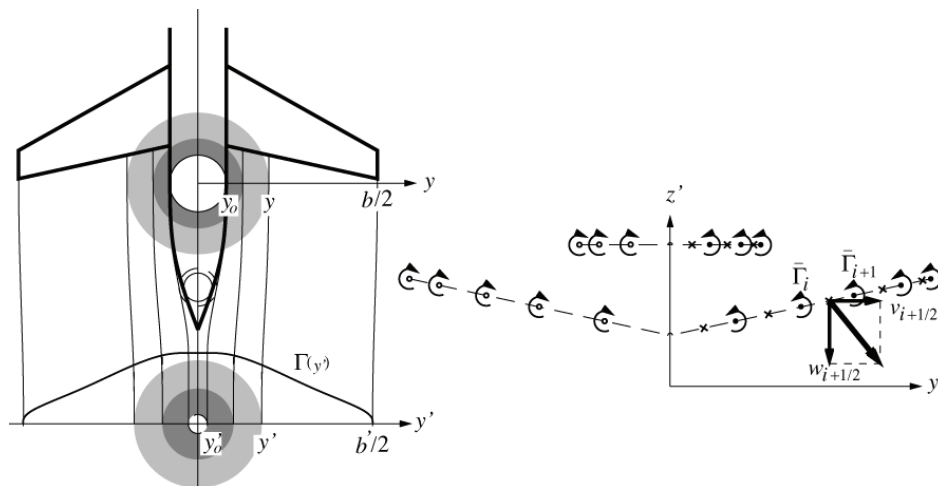
Figure 88: Wake streamline contraction due to fuselage thickness, carrying wing circulation into the wake, which is then used in the Trefftz-Plane impulse and kinetic energy calculation. The wake of the loaded horizontal tail is also included, thus capturing trim drag.

5.7.6 Engine Models

TASOPT uses a fairly detailed component-based turbofan model, sketched in Figure 89. It is based on the approach of Kerrebrock[80], with added models for turbine cooling flow and cooling loss definitions, sketched in Figure 90. Variable $c_p(T)$ effects, using constituent-based gas properties, are used to allow treating almost any common hydrocarbon or alcohol fuel without the need to estimate and input effective c_p's. The overall engine model code implementation has a *design mode* which is used to size the engines for cruise and, an *off-design mode* used to determine performance at takeoff, climb, and descent.
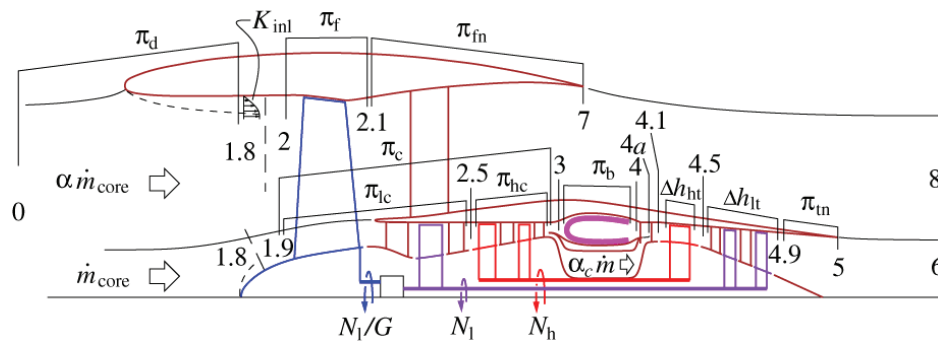
Figure 89: Engine layout and operating parameters assumed in the turbofan performance model. All gas state variables are computed at all the numbered stations.
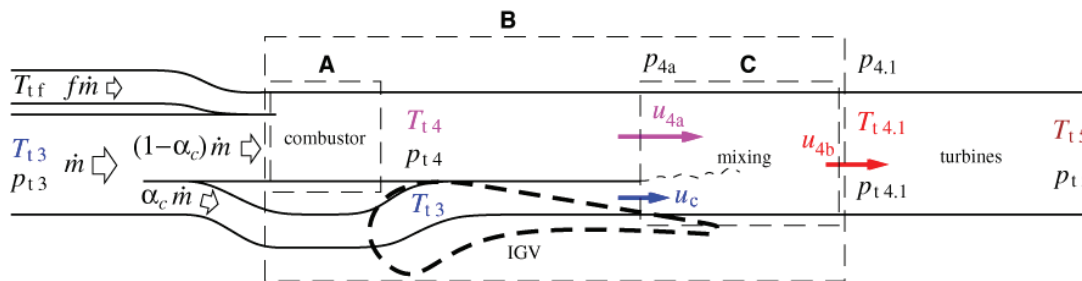
Figure 90: Control volumes and state variables used in turbofan film-cooling flow and loss prediction model.

This component-based engine simulation dispenses with the need for engine performance curve fits and correlations. This is deemed especially important for examining designs with extreme engine parameters which fall outside of historical databases, particularly if BLI is also used. The detailed turbine cooling flow model is also a key advantage, since cooling losses strongly influence the choice of engine parameters such as T_{t4} and fan pressure and bypass ratios. The inclusion of the cooling model allows optimization of these parameters simultaneously with the airframe, aerodynamic, and mission parameters, so that a global optimum can be determined. The details of the turbofan sizing and analysis can be found in Appendix B while the details of the film cooling flow loss model included in the analysis can be found

---

[80] Kerrebrock, J.L., *Aircraft Engines and Gas Turbines*, 2nd Ed., The MIT Press, Cambridge, 1996.

in Appendix C. The details of the engine weight model incorporated into the process are discussed in Appendix H.

5.7.7 Stability and trim

Each of the weight items shown in Figure 79 has an associated mass centroid, so that the weight buildup is done in parallel with a weight-moment buildup. Likewise, the spanwise lift integration for the wing and horizontal tail is performed in parallel with a pitching moment integration, including airfoil profile moment contributions. The pitching moment of the fuselage is also added, using coefficients determined via slender body theory and calibrated with off-line vortex lattice calculations for the whole configuration.

The overall weight + aerodynamic moment coefficient C_M is then used to impose two conditions: one for pitch trim and one for pitch stability, at the two extreme CG limits chosen among all possible payload and fuel load fraction and distribution situations.

$$C_M = 0 \qquad\qquad \text{(imposed at most-forward CG)} \qquad\qquad (8)$$

$$\frac{\partial C_M}{\partial C_L} + StaticMargin = 0 \quad \text{(imposed at most-rearward CG)} \qquad\qquad (9)$$

These two equations are treated as a coupled 2×2 system for two design variables: the wing box location x_{wbox} shown in Figure 80, and also for the horizontal tail area S_h. The static margin (S.M.) and the most-negative allowable horizontal-tail C_{Lh} are specified in this calculation. This procedure ensures that any aircraft which is produced by TASOPT is automatically both pitch-trimmable and stable to within the specified margins.

5.7.8 Mission profiles

5.7.8.1 Profile calculation

Integration of standard trajectory ODE's determines the weight, altitude, and thrust profiles over the specified mission. These are sketched in Figure 91 together with a few integration points. The cruise portion is assumed to be at the ideal cruise-climb angle to maintain the specified cruise Mach number and overall airplane C_L at a specified constant cruise T_{t4}. Higher T_{t4} values are specified over the climb, which then determines the climb trajectory. A constant descent angle is specified, and the resulting required T_{t4} is computed at each descent point. The integration is repeated with varying initial takeoff fuel until the specified range is obtained, thus giving the required mission fuel. The end result is a defined aircraft and engine combination which achieves the specified payload and range mission. Off-design missions can also addressed, allowing the possibility of minimizing fuel burn for a collection of fleet missions rather than for just the aircraft-sizing mission.
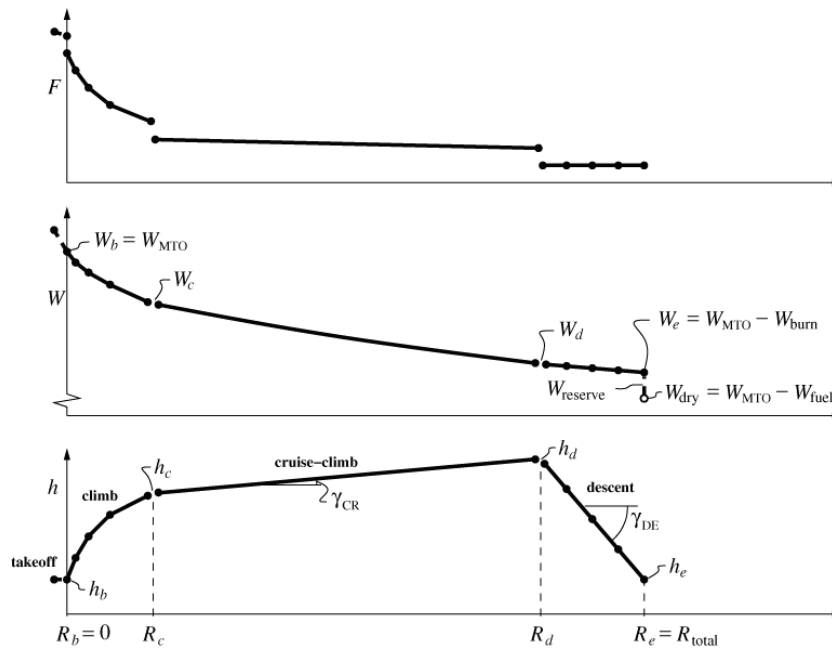
Figure 91: Computed mission profiles of thrust, weight, altitude, all versus range.

5.7.8.2 Takeoff

The takeoff performance model described earlier is used to evaluate any given design's balanced field length. This can be optionally included as a constraint in the overall combined airframe + aero + engine + operations optimization, so that the performance penalties of a field-length constraint can be directly evaluated.

5.7.9   Weight Iteration and Optimization

TASOPT has a number of calculation procedures organized as nested iteration loops.

5.7.9.1 Inner weight iteration

The primary calculation procedure starts with a number of input specifications and mission requirements, shown in violet on the left in Figure 92. These are inputs to all the physical models described above which are then recast to allow computation of the wind and tail dimensions, the loads and structural gauges, the aerodynamic performance, the engine size and performance, the mission fuel weight, and end up with all the component weights and the gross takeoff weight. Because the models also require various weights as inputs, the procedure is necessarily iterative, indicated by the loop in Figure 92. This procedure was used to "design" the B737-800 baseline, with the known B737-800 parameters used for all the inputs. In this case the weight iteration then returns an aircraft whose airframe size, engine size, weight, and performance very closely matches the actual B737-800's values in all aspects, giving confidence in the validity of the component models and overall methodology.
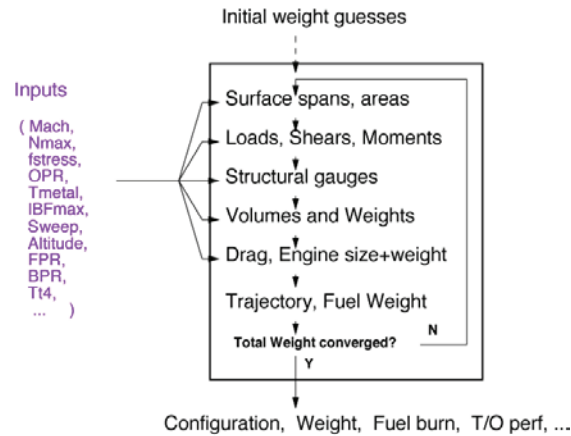
Figure 92: Weight-iteration procedure.

5.7.9.2 *Outer weight iteration*

For the design, development, and evaluation of the D8.x aircraft, the basic weight iteration described above is nested in an optional optimization procedure. For this calculation, all the inputs on the left of Figure 92 are segregated into two types:

1. *Design Variables*, whose influence on the objective fuel burn is non-monotonic. These are shown in red in Figure 93. All the available ones are listed in Table 29, but only a partial set can be chosen if appropriate.

2. *Design Parameters*, whose influence on the objective are monotonic. These are shown in blue in Figure 93.
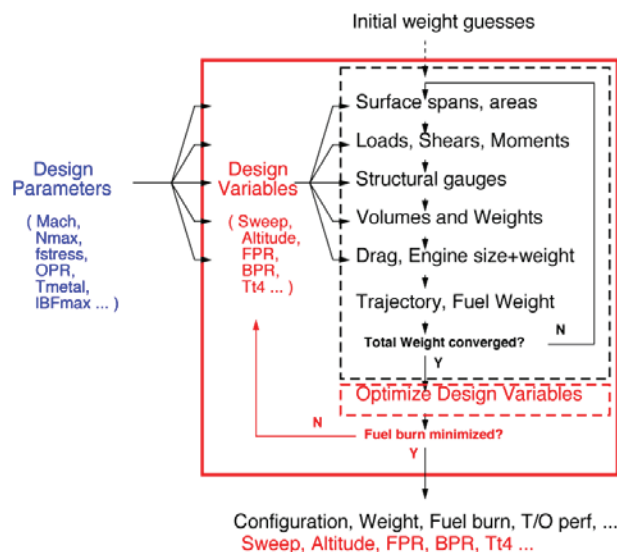
Figure 93: Inner weight-iteration procedure combined with outer optimization of design variables selected from the previous inputs. These now become outputs.

Table 29: List of Design Variables Selectable for Optimization

C_{LCR}	cruise lift coefficient
AR	overall aspect ratio
Λ	wing sweep angle
$(t/c)_o$	airfoil thickness at η_o (wing root)
$(t/c)_s$	airfoil thickness at η_s (planform break or strut-attach)
λ_s	inner panel taper ratio
λ_t	outer panel taper ratio
$r_{c_{\ell_s}}$	clean c_l at η_s (planform break)
$r_{c_{\ell_t}}$	clean c_l at 1 (tip)
FPR_D	design fan pressure ratio
BPR_D	design bypass ratio
h_{CR}	start-of cruise altitude
$T_{t4_{CR}}$	cruise turbine inlet temperature
$T_{t4_{TO}}$	takeoff turbine inlet temperature

The optimization procedure then adjusts the design variables and repeatedly invokes the weight-iteration procedure in a descent process in order to minimize the fuel-burn objective function. Constraints on balanced field length or fuel volume can be optionally imposed during this process. The chosen design variables, which were previously inputs, are now outputs and give the global design optimum which gives the minimum fuel burn.

5.7.9.3 Parametric Sensitivities

Using the optimization procedure shown in Figure 93, post-optimum sensitivities of the outputs to the inputs can be determined, for example

$$\frac{\Delta\left(PFEI_{opt}\right)}{\Delta M_{CR}}, \quad \frac{\Delta\left(PFEI_{opt}\right)}{\Delta N_{\max}}, \quad \frac{\Delta\left(PFEI_{opt}\right)}{\Delta OPR_D} \dots \tag{10}$$

These are presented in the sensitivity-study in section 5.6.

5.7.10 Restriction to wing+tube aircraft

The description of the structural and aerodynamic models above suggests why TASOPT is restricted to tube+wing configurations – most other configurations would be quite difficult or impossible to treat with

these models. For example, a joined-wing configuration[81] has a relatively complex structure with out-of-plane deformations and the possibility of coupled twist/bend buckling in the presence of eccentricity from the airloads, which requires a greatly more complex structural analysis than straightforward beam theory. A blended-wing-body configuration[82] with non-circular cabin cross sections likewise has non-obvious critical load cases and load paths, and its transonic aerodynamics are dominated by 3D effects. For these reasons such non-traditional configurations are simply outside the scope of the TASOPT methodology.

---

[81] Wolkovitch, J., "The joined wing: An overview," *Journal of Aircraft*, 23(3), Mar 1986.

[82] Liebeck, R., "Design of the blended wing body subsonic transport," *Journal of Aircraft*, 41(1), Jan 2004.

6 Hybrid Wing Body (HWB) Design Concept

6.1 Design Overview

The Hybrid Wing Body (HWB) configuration that was examined by the research team builds upon information that was first developed during the Silent Aircraft Initiative, was furthered by NASA N+2 research at MIT, and has been greatly modified to address the NASA N+3 goals. The HWB configuration employed here uses aerodynamic shaping of the centerbody leading edge to generate lift under the nose; this improves the aerodynamic efficiency of the design relative to concepts that utilize centerbody reflex camber by allowing for the use of supercritical outer wing profiles. The HWB configuration has been designed in an optimization process built up from a combination of first principles and empirical data to incorporate mission, airframe, operations, and propulsion system design and optimization. This process has as its objective the global optimization of aircraft fuel burn, but the configurations that are being optimized are inherently low in noise. For example, the engines are above the aircraft so that there is engine noise shielding, the fan pressure ratios are low so that jet noise and fan noise are low, the fan tip speed is near sonic so that the shocks (and combination tone noise) are weak, and there is ample room for acoustic liners for engine noise treatment.

The H3.2 aircraft design,[83] depicted in Figure 94, was designed with a payload and range comparable to a B777-200LR. As will be discussed in Chapter 7, this larger payload capacity was chosen to reduce the empty weight fraction of the aircraft to an acceptable level for reduced fuel consumption. A wide range of propulsion system configurations, including both podded and boundary layer ingesting engines, were considered in the design process, as was the use of cryognenic methane fuel. In addition to having higher specific energy, which improves the fuel efficiency of the aircraft, the low fuel temperature allows for the use of superconducting materials. Such materials could be used in a distributed, turbo-electric propulsion system to distribute power from the gas turbines to many engine fans without the need for gears. The low temperatures could also enable laminar flow over the pressure surface of the outer wings. However, as will be explained in Section 6.2.5 the final H3.2 design is powered by conventional jet fuel and uses a bevel gear transmission system to distribute power from two gas turbines engines to four fans.
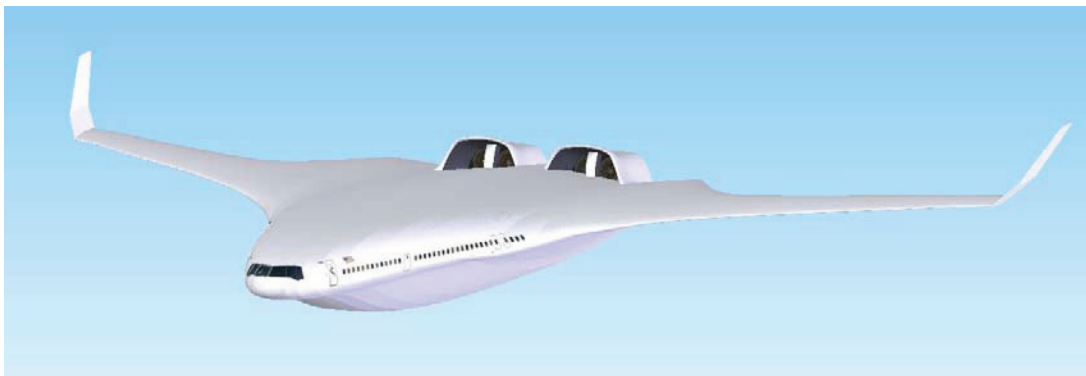
Figure 94: H3.2 conceptual aircraft design.

---

[83] The nomenclature H3.2 refers to the second iteration of the Class 3 Hybrid Wing Body design. The H3.1 design was presented in the January 2010 interim report. As will be discussed in Chapter 7, three different sizes were considered for the HWB concept: a B737 size with 180 passengers which is denoted as H1.2, a 767 size with 256 passengers, plus cargo, which is denoted as H2.2, and a B777 size aircraft which is denoted H3.2.

Each of the design features used for the H-Series of aircraft is discussed below:

- HWB configuration with lifting nose:
    - Allows for supercritical outer wing profiles and improved aerodynamic performance through built-in nose-up trimming moment, via fuselage lift on nose region.
    - Includes coach cabin and cargo capacity designed according to Boeing 777-200LR rules
    - Allows for shorter landing gear via better tail clearance
    - Improves propulsive efficiency via fuselage boundary layer ingestion (BLI)
    - Incorporates an assumed 30% reduction in structure weight, using structural weight based on Boeing WingMOD based response surface model (used for NASA N2A aircraft design) through use of advanced materials and manufacturing techniques
    - Incorporates drooped leading edge device to increase CLmax during takeoff and approach for reduced velocities, and airframe noise, during takeoff and approach
    - Uses faired undercarriage for reduced noise

- Embedded aft engines:
    - Improve propulsive efficiency via fuselage boundary layer ingestion
    - Provides reduced susceptibility to bird strike, since engines are invisible head-on, especially at takeoff angle of attack
    - Provide complete shielding of fan faces from ground observers
    - Allow for extensive acoustic liners, for reduced noise

- Distributed propulsion system:
    - Includes two gas turbine cores powering four fans providing a high bypass ratio of 20
    - Provides a reduced fan diameter to allow for longer effective acoustic liners for reduced noise, higher fan RPM (also to reduce fan noise) and lower engine speeds during approach while meeting go-around maneuver requirements
    - Incorporates a bevel gear transmission system, which distributes power from low pressure turbine to fans
    - Requires fan design development concerning the need to cope with distortion caused by ingested boundary layer flow

- Thrust vectoring, variable area nozzle:
    - Allows for reduced jet noise during takeoff, optimum cruise performance, and enables operation at low fan speed.
    - Provides pitch trim during cruise to minimize profile drag
    - Allows increase in induced drag for aircraft trim on approach using thrust vectoring combined with elevon

In addition, multiple other features were considered but ultimately not chosen in the final design. Each of these design features are discussed below:

- Cryogenic methane fuel:
    - Well suited to large wing volume of HWB configuration
    - Can be practical if methane hydrates are developed as a fuel source
    - Increases energy efficiency of aircraft system as fuel weight is reduced
    - Reduces life cycle greenhouse gas emissions as fewer greenhouse gases are produced per unit of energy in the aircraft tank
    - Promotes laminar flow on lower wing surface through lower temperature

- Eliminates need for a cryocooler required for superconducting turbo-electric propulsion system cooling
- Allows for intercooler regenerator engine cycle
- Can be contained in integrated fuel wing tanks with minimal insulation, on the order of a few mm thick, where rate of boil-off equals fuel flow

- Turbo-electric, distributed propulsion system
  - Includes three gas turbine cores powering twenty-three fans thus yielding a high bypass ratio, roughly 25 at takeoff.
  - Provides a reduced fan diameter to allow for longer effective acoustic liners for reduced noise, higher fan RPM (also to reduce fan noise) and lower engine speeds during approach while meeting go-around maneuver requirements
  - Incorporates an electrical transmission system, which splits power from low pressure turbine to fans decoupling power source from propulsive force giving flexibility on fan location
  - Enables low loss electrical power distribution using high temperature super conducting materials and cryocooler
  - Raises an issue in fan design concerning the need to cope with distortion caused by ingested boundary layer flow
  - Allows for aircraft control through different fan operation

The key performance metrics for the H3.2 aircraft are summarized in Table 30. Although the final design did not achieve either the N+3 noise or PFEI goals, it does achieve the fuel efficiency N+2 goals, and it does so with a relatively conventional propulsion system. As the D8 design has a field length that is well suited for a metroplex, the HWB concept was not required to meet this constraint. In addition to the H3.2 design that is presented herein, configuration studies are presented in Section 6.7 to understand the trade off in fuel performance encountered when noise was reduced further.

Table 30: Performance of H3.2 Relative to N+2 and N+3 Program Metrics

Metric	777-200LR Baseline	N+2 Goals % of Baseline	N+3 Goals % of Baseline	HWB
Fuel Burn (PFEI) [KJ/kg-km]	5.94[84]	3.58 (40% Reduction)	1.79 (70% Reduction)	2.75 (54% Reduction)
Noise [EPNdB] (EPNdB below Stage 4)	288	246 (-42 EPNdB Below Stage 4)	217 (-71 EPNdB Below Stage 4)	242 (-46 EPNdB Below Stage 4)
LTO NOx [g/kN] (% Below CAEP 6)	67.9	75% Reduction of CAEP 6	>75% Reduction of CAEP 6	18.6 (81% Reduction of CAEP 6)
Field Length [ft]	10,000	4375 (-50%)	metroplex	9,000

[84] Data from Piano-X for B777-200LR operated at maximum range with maximum structural payload (R1 of the payload range curve).

Table 31. H3.2 Aircraft Mission Parameters

Range (nm) (Plus 5% fuel reserves)	7600
Payload (lb)	134,431
Cruise Mach number	0.83
Takeoff distance balanced field length (feet)	9000
Landing distance (feet)	4966
Cruise altitude beginning (feet)	34,921
Cruise altitude end (feet)	40,850

6.2 Technologies

6.2.1 Airframe

The airframe architecture uses an all-lifting hybrid wing body (HWB) with control and low speed lift augmentation being provided by outer wing elevons, drooped leading edge, thrust vectoring and winglets. The wide all-lifting centerbody houses the passenger cabin while also providing forward shielding of engine noise and enabling extensive boundary layer ingestion. The large internal volume also enables the use of alternative fuels with low volumetric energy density such as LNG. The HWB centerbody uses a forward cambered airfoil developed during the Silent Aircraft Initiative (SAI) for the SAX-40 aircraft concept[85,86] which was also used on the NASA N2A/N2B[87,88] designs. This airfoil has a carved leading edge producing forward lift to trim the aft lift from the supercritical outer wing at cruise[89]. The tailless aircraft can be trimmed in other flight segments using the elevons and thrust vectoring. Parameterization of the twist distribution allows design for trimmed flight at start of cruise in a clean configuration along with elliptical span loading to minimize induced drag. This also results in a non-elliptical lift distribution with increased induced drag for a quiet, trimmed approach.

As was demonstrated with the SAX-40 and the N2A/N2B designs, the HWB configuration offers the opportunity for low noise emission. In addition to shielding forward radiating engine noise, the large centerbody of the HWB design provides ample room for high bypass ratio engines and extensive exhaust liners. These *airframe* features combine to enable a dramatic reduction in *engine* noise. The large lifting surface eliminates the need for flaps to augment lift at low speeds, which removes a dominant noise source on conventional aircraft, while also enabling the use of a drooped leading edge to augment lift on

---

[85] Hileman J., Z. Spakovsky, M. Drela, and M. Sargeant. "Airframe design for 'Silent Aircraft'," AIAA-2007-0453, 45th AIAA Aerospace Sciences Meeting and Exhibit, Reno, NV, 2007.

[86] Hileman J., Z. Spakovsky, M. Drela, M. Sargeant, and A. Jones. "Airframe Design for Silent Fuel-Efficient Aircraft," accepted to Journal of Aircraft, 2010.

[87] Ng, L., "Design and Acoustic Shielding Prediction of Hybrid Wing-Body Aircraft," Master of Science Thesis, Massachusetts Institute of Technology, Cambridge, Massachusetts, 2009.

[88] Tong, M., S. Jones, and J. Haller. "Engine Conceptual Design Studies for a Hybrid Wing Body Aircraft," NASA TM-2009-215680, Nov. 2009.

[89] Sargeant, M., T. Hynes, W. Graham, J. Hileman, M. Drela, and Z. Spakovszky. "Stability of Hybrid-Wing–Body-Type Aircraft with Centerbody Leading-Edge Carving," accepted to Journal of Aircraft, 2010.

takeoff and approach. The drooped leading edge does not add to the airfoil noise[90] thus allowing for decreased approach speeds without additional noise being incurred. Decreased approach speed is desirable as all airframe noise sources scale with velocity to the 5th or 6th power. Because of this, there is an incentive to design for reduced stall speed since approach speed is set as 1.23 x stall speed. Because increased wing area, which increases drag, can also be used to lower the aircraft stall speed there is a tradeoff between airframe noise and cruise performance, which is discussed in detail in Section 6.7. Because of this implicit tradeoff, the HWB optimization was optimized for both PFEI and approach noise. The HWB concept employed here was designed with fairings on the landing gear to reduce undercarriage noise; it must be noted that this is not a unique feature to the HWB concept as it can be used on any aircraft concept[91].

6.2.2 Airframe Structure and Materials

Structures technologies that are included in the design of the H3.2 configuration include advanced materials and load reduction technologies such as gust load alleviation, flight envelope protection, predictive path planning, and structural health monitoring.

The airframe concept will use carbon fiber reinforced polymer (CFRP) for the entire structure, assuming improved constituent material properties. The carbon composite material will include short carbon nanotubes (CNTs), which project to increase the compression after impact strength of the carbon fiber. Safety factors have been added to the material properties to account for ultimate loading and residual strength requirements. If 60% of the structure could realize this weight fraction while the other 40% of the air vehicle structure would be unchanged due to sizing not based on strength then the overall structural weight fraction would be approximately 0.7 of present day composite technology. It should be noted that at interfaces of structural components are also reduced in weight by primarily using the unitized structure manufacturing and assembly techniques. The HWB concept will have a reduced part count due to the ability to layup complex parts as a co-cured structure requiring fewer fasteners and fittings. Out-of-Autoclave (OOA) resins enable larger components to be cured without the size restriction of an autoclave. Processes like Resin Transfer Modeling (RTM) and Vacuum-assisted Resin Transfer Molding (VaRTM) allow increased out-time for complex layups prior to curing. Pultruded Rod Stitched Efficient Unitized Structure (PRSEUS) and similar processes allow for the combination of skin, stringer, and frame elements into a common structure. These techniques and others would allow for weight savings at details and interfaces to match weight savings in the structure itself. Additional details are provided in Appendix G.

Load reduction technologies will allow the vehicle concept to be designed to lower loading and still operate safely throughout the life of the vehicle. Gust load alleviation reduces the magnitude of gust loading on the wing through deflection of control surfaces to counteract the gust. Envelope protection and predictive path planning help limit the aircraft response to safe levels within the flight envelope. Structure and load monitoring technologies, which includes structural health monitoring, reduce the uncertainty in load and residual strength, all of which lead to the ability to design a lighter more efficient airframe.

---

[90] Andreoum, C., W. Graham, and H. Shin. "Aeroacoustic comparison of airfoil leading-edge slat and droop," AIAA-2007-0230, 45th AIAA Aerospace Sciences Meeting and Exhibit, Reno, NV, 2007.

[91] Quayle A., A. Dowling, H. Babinsky, W. Graham, H. Shin, and P. Sijtsma. "Landing Gear for a Silent Aircraft," AIAA-2007-0231, 45th AIAA Aerospace Sciences Meeting and Exhibit, Reno, NV, 2007.

6.2.3   Boundary layer ingestion

Boundary layer ingestion (BLI) is one of the technologies used for the H3.2 design. BLI by the engines could benefit the vehicle aerodynamic performance by eliminating kinetic energy dissipation in the wake and by reducing dissipation in the mixing of engine exhaust jet. The first effect comes from the elimination of the wake defect itself through ingestion, while the second effect comes from the reduction of jet kinetic energy required associated with the first effect. Detailed analysis on benefits of boundary layer ingestion is described in Appendix F.

Although boundary layer ingestion improves the aerodynamic performance of the aircraft, there are drawbacks associated with this technology, such as the degradation of the propulsion system performance. The ingestion of low kinetic energy flow (and hence low total pressure flow) increases the specific fuel consumption of the engine. Furthermore, inlet pressure non-uniformity and distortion coming into the fan gives rise to additional aero-mechanical vibration, a decrease on the stability margin and reduction of fan efficiency, further increasing the specific fuel consumption. These issues can be alleviated through innovative inlets designs. The rise in specific fuel consumption increases with the amount of boundary layer ingested by the propulsion system, which leads to a tradeoff between aerodynamic performance of the vehicle and the efficiency of the propulsion system. Due to the wide fuselage that is characteristic of HWB configurations, the propulsion system can be distributed covering the whole centerbody, which makes the tradeoff between boundary layer ingestion and propulsion system performance very relevant for this type of aircraft.

6.2.4   Propulsion System

The H3.2 concept uses an advanced geared distributed turbofan propulsion system with major improvements in material technology and flowpath aerodynamics. It has also been equipped with an advanced combustor to allow for significant reduction in specific fuel consumption and emissions.

The use of distributed propulsion in the H3 configuration enhances the ingestion of the vehicle boundary layer to improve propulsive efficiency. This also allows for a more effective packaging of very high bypass ratio engines without the subsequent increase in wetted area and resulting drag. There is also a benefit in noise associated with the H3 propulsion system. The reduction of the fan diameter leads to narrower exhaust duct (higher length-to-diameter ratio) that, when lined with acoustic liners, are more effective at attenuating fan rearward noise. In addition, smaller fans have higher rotational speed giving rise to an increase in the blade passing frequency, which results in noise that is more readily attenuated.

Advanced materials with higher allowable hot section temperatures, more efficient turbine cooling schemes – such as improved cooling hole design, and prime reliant thermal barrier coatings will enable turbine operation at higher burner exit temperatures, allowing for higher bypass ratios and better propulsive efficiency. Cruise fuel consumption is also reduced due to a reduction in the required turbine cooling air flow at takeoff.

Evolutionary gains in component performances are assumed. In particular, new design and machining processes will be necessary to create efficient high pressure turbines with small blade heights. As core size (measured by the corrected flow leaving a compressor) decreases, current machines experience a large degradation of efficiency below certain values (3 lbs/s). High efficiency at core sizes lower than this is critical in reaching higher overall pressure ratios for increased thermal efficiency.

Advanced Lean Direct Injection (LDI) combustors, currently under development at NASA Glenn, were assumed to be in use to enable the N+3 emissions goal. The LDI combustor injects fuel into multiple flame zones, enabling lean combustion while minimizing local hotspots. This allows the LDI combustor

in the N+3 concept engine to meet the LTO N+3 NOx goal while retaining the fuel burn and carbon emissions advantages.

During this research effort, the range of propulsion system configurations that are listed in Table 32 were examined. Figure 95 graphically depicts some of the propulsion system configurations with their corresponding transmission systems.

Table 32: H3 Propulsion System Configuration Options

Number of Fans	Number of Cores	Type of transmission system
3	3	Direct / Planetary gears
4	4	Direct / Planetary gears
6	2	Bevel Gears
8	4	Bevel Gears
9	3	Bevel Gears
12	4	Bevel Gears
5	3	Electric
7	3	Electric
10	3	Electric
11	3	Electric
12	3	Electric
N	3	Electric
Maximum span coverage	3	Electric
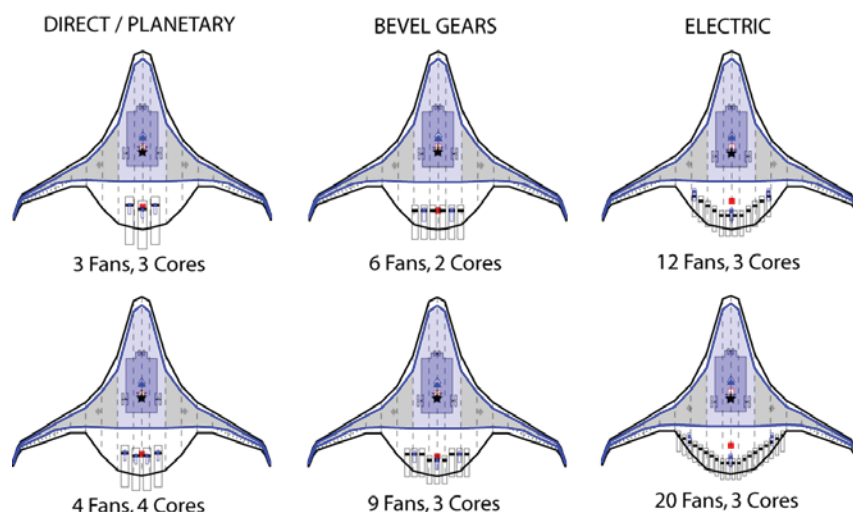
Figure 95: Example propulsion system configuration on the H3 design.

6.2.5 Choice of H3.2 propulsion system and fuel

As a result of the airframe and propulsion system optimization, a propulsion system using four fans and two cores was selected for the H3.2 aircraft design.

This choice of propulsion system was largely a result of a tradeoff between boundary layer ingestion and propulsion system performance. The chord length decreases rapidly with increasing spanwise distance from the aircraft centerline, the gain in boundary layer ingestion decreases as the span covered by the propulsion system increases. This results in the optimal being a relatively small value of 45%, which can be covered with relatively few fans. This spanwise coverage translates to the engines ingesting 60% of the boundary layer on the top fuselage surface. The final design has a mechanical transmission system (beveled) because these tend to be lighter and less complex as compared to electrical transmission systems. A mechanical design also further drove the propulsion system to a design with fewer fans. Finally, a propulsion system with two cores was chosen over three cores because of the higher engine component efficiencies that are associated with larger core size.

Because the optimization process led to a design with a mechanical transmission system, instead of an electrical transmissions system, the research team selected conventional jet fuel over LNG to power the H3.2. Although the use of LNG did result in a few percentage points of improvement in PFEI relative to conventional jet fuel, which was a result of the improved specific energy of the fuel, the improvement was not deemed to be sufficiently large to merit the large risks that would be incurred in having two airport fueling systems.

6.3 Design Methodology

6.3.1 Overview

The hybrid wing body (HWB) design methodology utilizes a modular design framework packaged into the HWBOpt Matlab program. The methodology consists of a complete aircraft system design loop wrapped in a global optimization routine. As shown in Figure 96, the design loop is organized to be modular by discipline to accommodate continuous evolution of the program, while minimizing feedback loops.
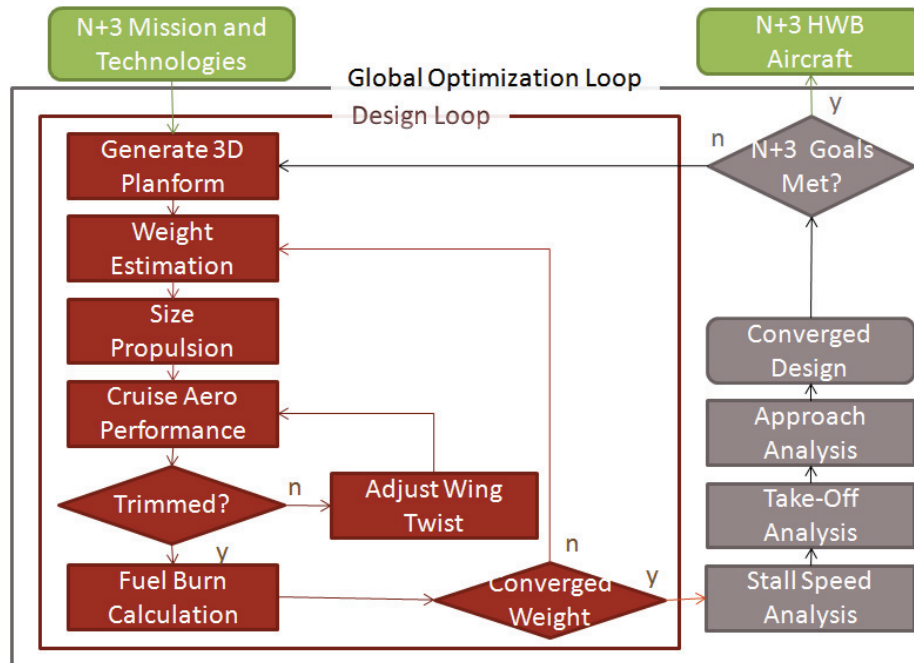
Figure 96: HWBOpt program flow chart.

The analysis begins with the specification of mission and technologies. The design variables that are fed into the global optimization loop describe the airframe planform, propulsion configuration, engine cycle and operating environment. For each input vector, the design process begins by lofting the planform into a 3D airframe that contains a pre-configured cabin, which for the H3.2 design is described in Section 6.3.2. As is discussed in Section 6.3.3, the aircraft weight is estimated and along with initial aerodynamic analysis, is used to size the propulsion system to meet the top-of-climb thrust requirements. The propulsion system performance module, which is discussed in Section 6.3.4, is then input into the cruise aerodynamic analysis to compute fuel burn, which is discussed in Section 6.3.5. The cruise analysis also requires adjustment of the wing twist to trim the aircraft at the start of cruise without control surface deflection or thrust vectoring. The new fuel estimate feeds back to the initial weight estimate and the design loop iterates until a converged stable design is achieved. This is followed by off-design analysis that involves stall speed calculations for takeoff and approach analysis, as is required to compute the N+3 metrics, and is discussed in Section 6.3.6. The inability to trim the aircraft or close the engine cycle at any off-design condition also results in a non-convergent design. The global optimizer, which is discussed in Section 6.3.7, iterates on the design variables with the objective function being defined by airframe noise and PFEI targets. The output of the process was a Pareto front of aircraft concepts that have a minimal weighted combination of airframe noise and PFEI.

6.3.2   Cabin Design

During the initial trade studies, historical values of passenger per unit area and passenger per unit volume were used to estimate the passenger capacities. Later, structural and interior ground rules were established from similar short and long range aircraft, such as the B737-800 and B777-200LR, to determine if the HWB internal volume provided the expected capacities. One significant initial requirement was that structural walls were periodically located along the width of the cabin, running in the fore-aft direction. These walls allowed the wing to more efficiently react to internal pressure loads and were estimated to be 6 inches wide, which includes 4 inches structural width and 1 inch of insulation/paneling on either side.

A trade study was performed to determine the number of seats between the structural walls that led to the most efficient arrangement. Economy seat combinations of 2-3 (e.g. MD-80) and 3-3 (e.g. B737, A320), where the values signify the number of seats on either side of the aisle, were found to be the most efficient grouping to be placed between the evenly spaced structural walls; thus the layouts could use either combination to maximize passenger capacity within the cabin. For long range aircraft, economy seat widths were based on the publicly available values of A350 XWB (Extra Wide Body), while short range aircraft were based on the A320. These are the widest of any commercial aircraft in their class.

The H3.2 cabin accommodates 354 passengers in a three-class configuration utilizing five groupings of 2-3 seating in economy class (see Figure 97). The cabin is divided into two compartments with First and Business Class in the forward section and Economy Class in the aft section. A cross-aisle is located at the front of economy class, which provides for evacuation and a secondary ground servicing point for galley carts in addition to the forward servicing point for First and Business class. A centerline group of seats is utilized instead of a centerline wall dividing the forward compartment because the latter would make it difficult to locate galleys, lavatories and aisles in the nose section.
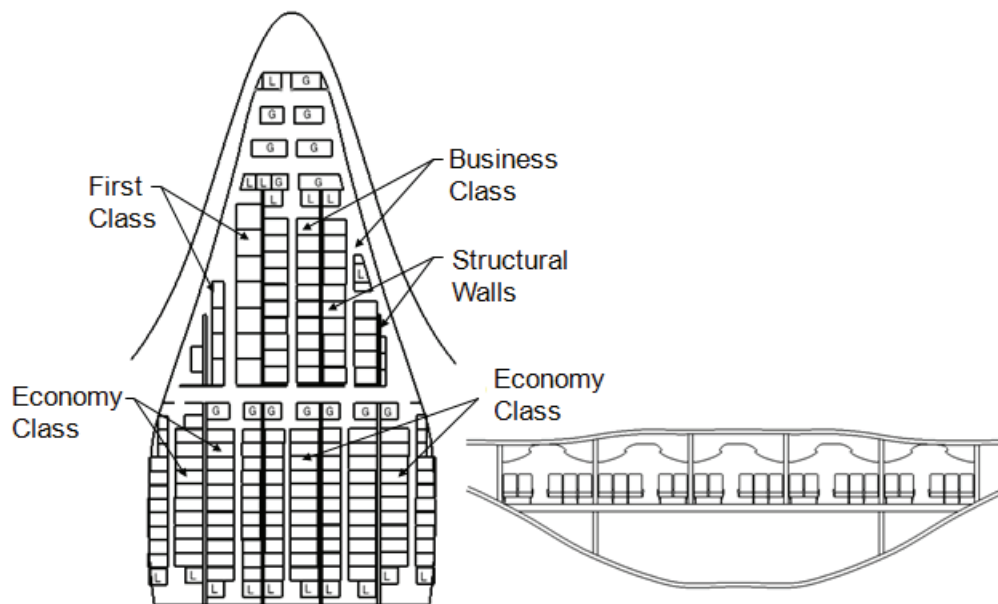
Figure 97: H3.2 cabin layout.

Wide body aircraft utilize their belly capacity to carry revenue cargo (see Figure 12 in Section 2.3); as such, the H3.2 cargo compartment was designed to accommodate 194 m^2 of revenue cargo volume using standard cargo containers (22 LD3 containers + 8 LD7 Long Pallets which could accommodate 25,628 kg of revenue cargo in the belly of the aircraft (using typical cargo densities). The cargo capacity corresponds to 43% of the maximum structural payload, which as shown in Figure 98 is in line with the current fleet of tube-wing aircraft.
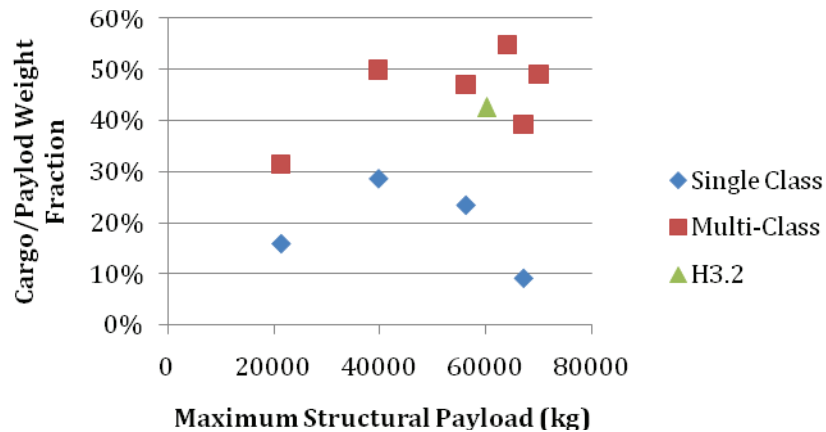
Figure 98: Revenue cargo capacity as a fraction of maximum structural payload for varied aircraft sizes from single aisle to wide body aircraft.

6.3.3 Airframe and Propulsion System Weight Buildup

The weight buildup within HWBOpt is based on the models that were used to create the SAX-40 designs.[85,86,92] Because of a lack of publicly available data for HWB designs, the structural weight model for the HWB is based on a Response Surface Model (RSM) based on WingMod,[93] a multidisciplinary design and optimization code that has been used by Boeing for blended wing body aircraft design. Some of the HWB aircraft concepts that were created fall outside of the design range for the RSM as it was originally intended. The RSM results are scaled by 70%, assuming an optimistic improvement in material properties by the N+3 time frame, as discussed in Section 6.2.2 and Appendix G.

The payload for the H3 consists of 354 passengers with 215 lbs per passenger (180 lb per passenger with 35 lb of check baggage) with additional cargo payload of 56,500 lb.

The landing gear weight is estimated as a fixed 4% of the MTOW with additional fixed weight for the fairings. The weight of fixed equipment and furnishings on the aircraft is estimated using Roskam's correlations[94] for a Class II commercial transport aircraft, based on the planform, cabin/cargo dimensions and payload. Fuel weight is computed using mean cruise SFC with continuous cruise climb with climb fuel weight being estimated as a fixed 2% of MTOW. Reserve fuel for an hour of flight at the end of cruise condition and unusable fuel is also accounted.

The propulsion system weight buildup uses various empirical weight models and weight scaling laws. The weight of a bare engine is calculated based on diameter and thrust scaling of the Granta-3401 engine[95] from the SAX-40 aircraft. The engine components in the Granta engine are separated into the

---

[92] Jones, A., "Multidisciplinary optimization of aircraft design and takeoff operations for low noise," S.M. Thesis, Massachusetts Institute of Technology, 2006.

[93] Wakayama, S. and I. Kroo. "The challenge and promise of blended wing body optimization," 7th AIAA/USAF /NASA/ISSMO Symposium on Multidisciplinary Analysis and Optimization. AIAA 1998-4736, Sep. 1998.

[94] Roskam, J. "Airplane Design, Part V: Component Weight Estimation," 2nd ed., Roskam Aviation and Engineering Corporation, Ottawa, Kansas, 1989, pp. 97–112.

[95] de la Rosa Blanco, E., C.A. Hall, and D. Crichton. "Challenges in the Silent Aircraft Engine Design," AIAA Paper 2007-0454, 2007.

fan and the core. The weight of the fan is scaled based on its diameter, and the weight of the core is scaled based on the design thrust generated by the engine at cruise. The weight of the nacelle and the exhaust duct is computed based on an empirical correlation[96], which is based on fan diameter, duct length to diameter ratio, and the inlet geometry.

Since different transmissions were assessed, different weight correlations were established for each engine transmissions system. The weight calculation of planetary gears uses the correlation from NASA GRC WATE++[97] model. This correlation relates the weight of the transmission system with the fan mass flow and core shaft power output at takeoff condition. The weight of bevel gear transmission is based on scaling the torque carried by the transmission system, using the transmission weight of the Granta-3401 as a baseline. Finally, the weight calculation of the electric transmission system, which includes the HTSC generator and motor, cryocooler, inverter was conducted using the weight correlation developed by the research team (Appendix K.) This model uses core shaft power and torque to compute the weight of each component in the electric transmission system.

6.3.4 Engine Design

Engine cycle performance and sizing calculations were conducted using a semi-perfect gas cycle model. Engine flows are assumed to be a mixture of semi-perfect gases with tabulated specific heat data (the specific heat of each constituent is temperature-dependent). This provides higher fidelity than a perfect gas model with a minimum of added complexity. It also has the benefit of eliminating the need for fuel heating values, since the fuel is also treated as a semi-perfect gas (so the heat released in combustion is a function of the state of both the air and fuel prior to burning); this is particularly useful when analyzing LNG as a fuel, since fuel temperature may have a significant effect on cycle performance and thermal management of the entire aircraft system. Details of the gas model and cycle performance calculations can be found in the Appendices B, C, and D.

Figure 99 illustrates the aircraft design procedure for the H3.2 design. For a given aircraft design, the design model sizes the propulsion system to meet the cruise thrust requirement of the airframe. Because of the close coupling between the propulsion system and the airframe, multiple iteration loops were required to match the propulsion system and the airframe. Because of the coupling between the inlet pressure recovery and engine size, one iteration loop was required to match the inlet pressure recovery assumed by the engine cycle calculation and the physical inlet pressure recovery calculated from the size of the propulsion system. The H3.2 final engine design assumes clean flow in the engine core. Furthermore, another iteration loop was required to solve for the required aircraft cruise thrust, which was closely coupled with the propulsion system weight and its fuel consumption. The sizing of propulsion system was only conducted at cruise condition, assuming that the propulsion can meet other off-design requirements such as takeoff and top of climb. Detailed off-design calculations were conducted using the commercial software package Gasturb with the finalized aircraft design to check that the propulsion system met all operational requirements.

---

[96] Raymer, D., Aircraft Design: A Conceptual Approach AIAA Education Series, New York, NY, 2006. ISBN 1-56347-829-3.

[97] Tong M. and B. Naylor. "An Object-Oriented Computer Code for Aircraft Engine Weight Estimation," NASA/TM—2009-215656, 2009.
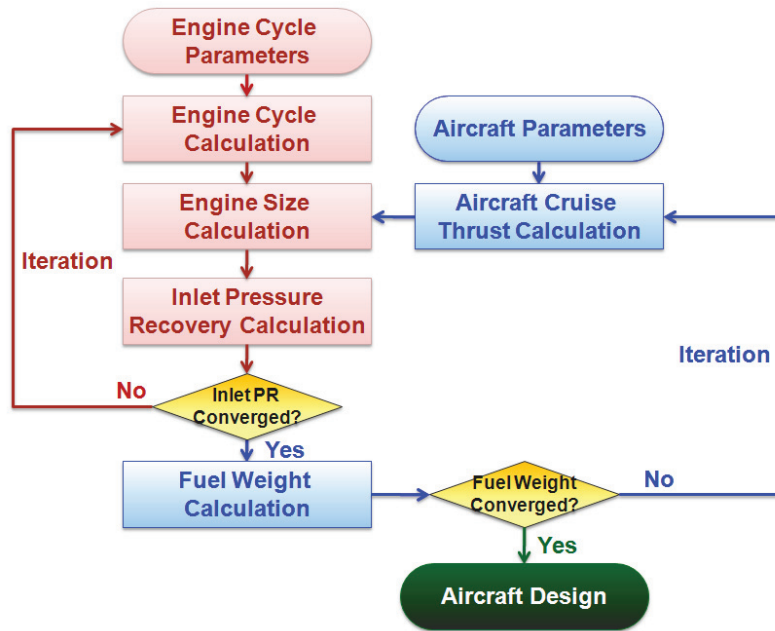
Figure 99: HWBOpt engine design process.

6.3.5 Airframe Aerodynamics

The Quasi-3D aerodynamic analysis methodology developed and validated to assess SAX-40[85,86] and N2A/N2B[87,88] airframes was expanded to create HWBOpt. The cruise Mach number of the HWB aircraft was fixed to Mach 0.83 based on a Boeing CFD study using CFL3Dv6[98] Navier-Stokes analysis to identify the drag divergence Mach number for the SAX-40 and N2A/N2B airframes, which has a similar airframe to the N+3 HWB design.

The airframe lift distribution, induced drag and neutral point were computed for each lofted airframe (including twist and control surface deflection) using a vortex-lattice analysis performed using AVL[99]. AVL uses a Prandtl-Glauert correction to capture compressibility effects but is limited to wing-perpendicular Mach numbers below the transonic regime. The twist distribution is parameterized to meet static margin limits (>5%) while PFEI optimization results in a near elliptical span loading (including the centerbody) at cruise. Profile, viscous and wave drag for the outer wing 9% thick supercritical airfoil was computed offline using MSES[100] at the cruise Mach number and a representative Reynolds number. The resulting drag polar is integrated as a lookup table as a function of sectional lift and sweep. This 2-D approach is not applicable for the centerbody due to the 3-D nature of the flow field, where aerodynamic performance is estimated using Hoener[101]. The centerbody profile and viscous drag was computed using Hoerner correlations for bodies of revolution with lift coefficient dependence. Results from the Boeing CFD study of the Silent Aircraft and NASA SAX-40F designs were used to validate this analysis methodology; details are provided in Appendix I.

---

[98] CFL3D Version 6, NASA Langley Research Center.

[99] Athena Vortex Lattice, Drela, M., MIT, Cambridge, MA. http://Raphael.mit.edu/avl.

[100] Multi-Element Airfoil Design/Analysis Software, Drela, M., MIT, Cambridge, MA.

[101] Hoerner S., "Fluid-Dynamic Drag," Hoerner Fluid Dynamics, 1965.

6.3.6   Aircraft Operations

The flight segments assessed as part of the design include takeoff, balanced field takeoff, begin cruise, end cruise, approach, and landing.

The takeoff field length and balanced field length calculation assumes quadratic dependence of thrust on velocity in order to analytically relate takeoff velocity to distance. The force balance results in a system of first order ODE's as discussed in Appendix I. The drag for the airframe is computed using the aerodynamic model discussed above, assuming a typical takeoff Mach number of 0.2. Balanced field length calculation is based on FAR-25 regulations, accounting for the additional wind-mill drag[102] and trim drag required to balance the spanwise asymmetric thrust moment from engine-out. Configurations with electrically distributed propulsion are assumed to circumvent the latter by redistributing thrust as required. The takeoff analysis for noise is based on a first order time marching solution assuming three segments: ground roll, instantaneous rotation, and initial climb, using thrust vectoring for pitch trim.

The cruise analysis considers start of cruise and end of cruise with continuous cruise climb between the two states assuming NextGen operations. The former governs the twist distribution by requiring pitch trim without elevon deflection or thrust vectoring. The altitude for the latter is adjusted to maintain the same lift coefficient as start of cruise and requires the aircraft be trimmable using thrust vectoring. The static margin increases through the cruise segment as the fuel weight is reduced and the CG moved forward, hence the start of cruise point is used to ensure static stability and cabin angle of attack limits. The fuel weight is computed using the average SFC assuming linear variation from start to end of cruise.

The HWB design is trimmed at approach using a combination of thrust vectoring and elevator deflection[103]. In addition to trimming the pitching moment, the combination is used to increase the induced drag being generated by the airframe, which enables a steeper approach path. Directing thrust downward requires increasing elevator deflections to pitch trim the aircraft and this requires a larger angle of attack because the aft section of the outer wings are unloaded and the thrust opposes lift. The increased lift is accompanied by an increase in induced drag, and a steeper approach path is necessary for trim thus increasing the distance between the aircraft and the ground and reducing noise impact. Regulations require the approach speed to exceed 1.23 times the stall speed in the approach configuration. Hence the stall characteristics are enhanced using deployable drooped leading edges instead of flaps to reduce noise from the shedding of turbulence. In addition, the engines operate at idle thrust to lower noise and reduce the amount of drag that needs to be generated to trim the aircraft. Aircraft trim analysis is based on steady approach conditions with aerodynamic forces computed using the HWBOpt aerodynamic model.

6.3.7   Optimization Routine

The design philosophy employed for the HWB aircraft, like the D series, is to optimize the airframe, propulsion and operations simultaneously to capture all interactions. Since the HWB design space is diverse as it also includes considerable variation in propulsion system configurations, the approach focuses on global optimization. The objectives functions include both PFEI and noise. The noise calculation for optimization was limited to airframe noise at approach due to computational constraints in terms of estimating off-design engine parameters. The airframe planform and twist distribution were parameterized as shown in Figure 100 and constrained to accommodate the cabin box and cargo. The engine cycle was parameterized using the FPR, BPR, T_{t4}/T_{t2} at cruise for a given propulsion configuration.

---

[102] Kroo, I. and R. Shevell. "Aircraft Design: Synthesis and Analysis," Desktop Aeronautics Inc., 2006.

[103] Hileman J., T. Reynolds, E. de la Rosa Blanco, T. Law, and S. Thomas. "Development of Approach Procedures for Silent Aircraft," AIAA-2007-451, 45th AIAA Aerospace Sciences Meeting, Reno, NV, 2007.

For the purpose of optimization, T_{t4}/T_{t2} at takeoff was set to its cruise value assuming the use of variable area inlets. This assumption was relaxed post-optimization to reduce takeoff noise. The propulsion configurations that were examined included all permutations on number of fans, cores and transmission systems being considered. As previously mentioned, cruise Mach was fixed, leaving operational considerations to the altitude at the start of cruise.

$$x_{airframe} = \begin{bmatrix} span \\ xle3 \\ xle5 \\ ale1 \\ cho5 \\ cho9 \\ twst0 \\ twst1 \\ twst2 \end{bmatrix}$$

$x_{operation} = [h_{CBN}]$ Cruise Begin Altitude

$$x_{engine} = \begin{bmatrix} FPR \\ OPR \\ T_{t4}/T_{t2} \\ Prop \end{bmatrix} \begin{matrix} \text{Fan Pressure Ratio} \\ \text{Operating Pressure Rati} \\ T_{t4}/T_{t2} \text{ Take-Off and Cru} \\ \text{Propulsion System Configuration} \end{matrix}$$
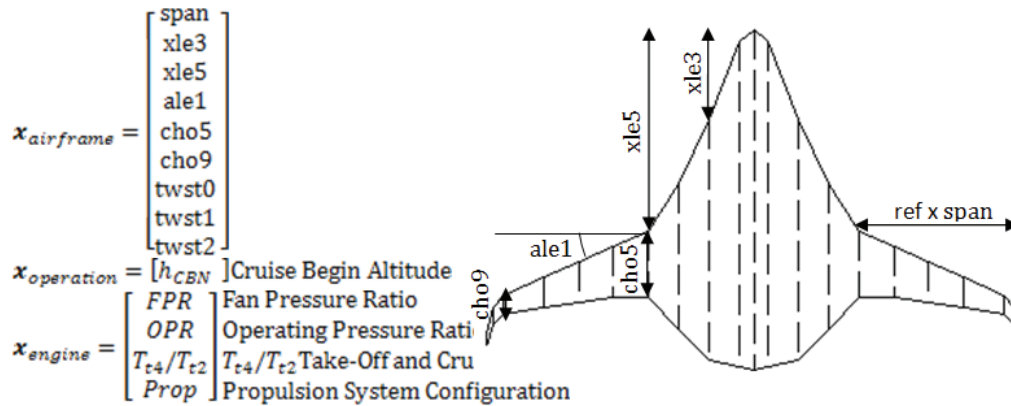
Figure 100: HWB optimization parameters.

Constraints on the design include static stability and passenger comfort based on cabin angle during cruise. Additional geometric constraints were imposed due to operational restrictions on aircraft span (<65m), based on ICAO Annex 14 code E airports regulations, and balanced field takeoff length (<9000ft). The resulting design space was vast with islands of feasibility created by imposing stability and sizing constraints on the airframe combined with the exploration of an exhaustive set of propulsion configurations and cycles. Also, the inclusion of discrete propulsion configuration choices resulted in a multi-objective mixed-integer programming problem. The lack of *a priori* knowledge of the target design space favored the use of a stochastic approach. In particular a hybrid multi-objective genetic algorithm was utilized with initial designs chosen using uniform Monte Carlo sampling of the design space. Details of the optimization problem formulation and algorithm are provided in Appendix I.

6.4   H3.2 Configuration

The sections that follow present the key features and parameters that describe the H3.2 design.

6.4.1   *Physical Geometries Dimensions*

Table 33 presents the overall physical geometry and dimensions of the H3.2 aircraft. A three-view diagram of the aircraft concept is given in Figure 101 with details of the internal layout illustrating cabin, cargo, fuel tanks, spars, propulsion system, and undercarriage.

Table 33: H3.2 Aircraft Geometry and Dimensions

Aspect Ratio, b^2/S	4.47
Span, b (feet)	213
Mid Chord Sweep (degree)	31.7
Fuselage Length (feet)	147.96
Cargo Volume (cubic feet)	6851
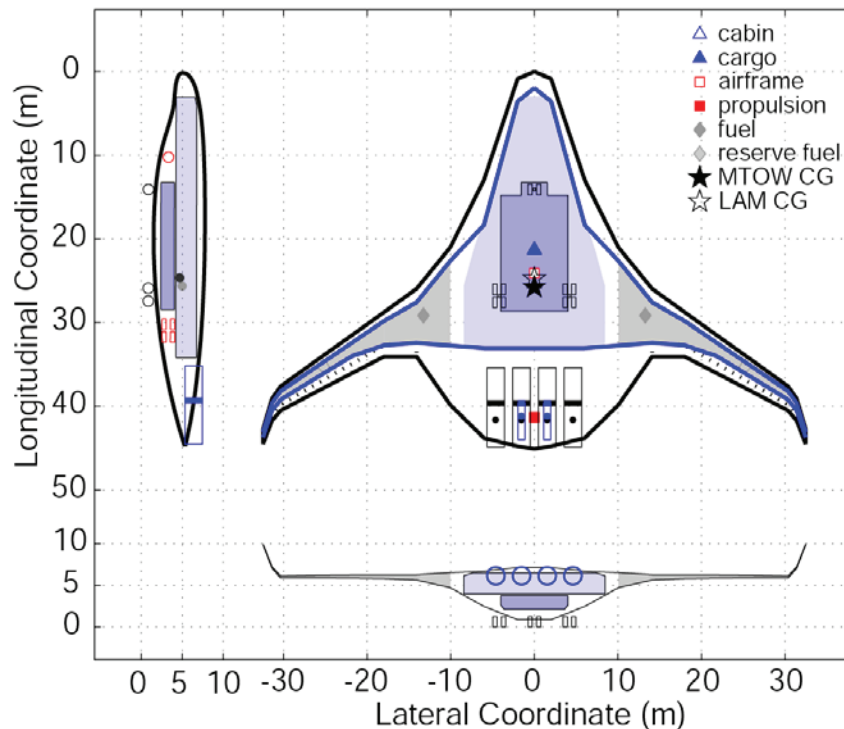
Figure 101: Three views of the H3.2 design with details for the cabin, cargo, engines, undercarriage, and internal spars. Centers of gravity given for each of the internal components as well as the overall center of gravity for the entire mission from takeoff with maximum takeoff weight (MTOW) to landing approach (LAM).

6.4.2   Aerodynamics and Drag Polar

Results from a vortex lattice analysis, performed using AVL, were used to illustrate the aerodynamic performance and control surface deflections for the H3.2 configuration during the beginning of cruise, end of cruise, and landing approach. Table 34 lists the conditions for each of these. The outer wing twist is set such that the aircraft is trimmed at the beginning of cruise while thrust vectoring is used to trim the aircraft at the end of cruise.

Table 34: Aircraft Parameters for Begin Cruise, End Cruise, and Approach

	Begin Cruise	End Cruise	Approach
Angle of Attack (deg)	3.0	3.2	10.4
Thrust vector angle (deg)	0	16.3	-17.7
Elevon Deflection (deg)	0	0	-14.5
Static margin (percent)	6.9	12.8	8.9
Droop leading edge angle (deg)	0	0	27.0

The delta-Cp plots for the H3.2 configuration, given for cruise and landing approach in Figure 102, shows that considerable lift is generated under the nose of the fuselage during cruise. This balances the lift created from the outer wings.
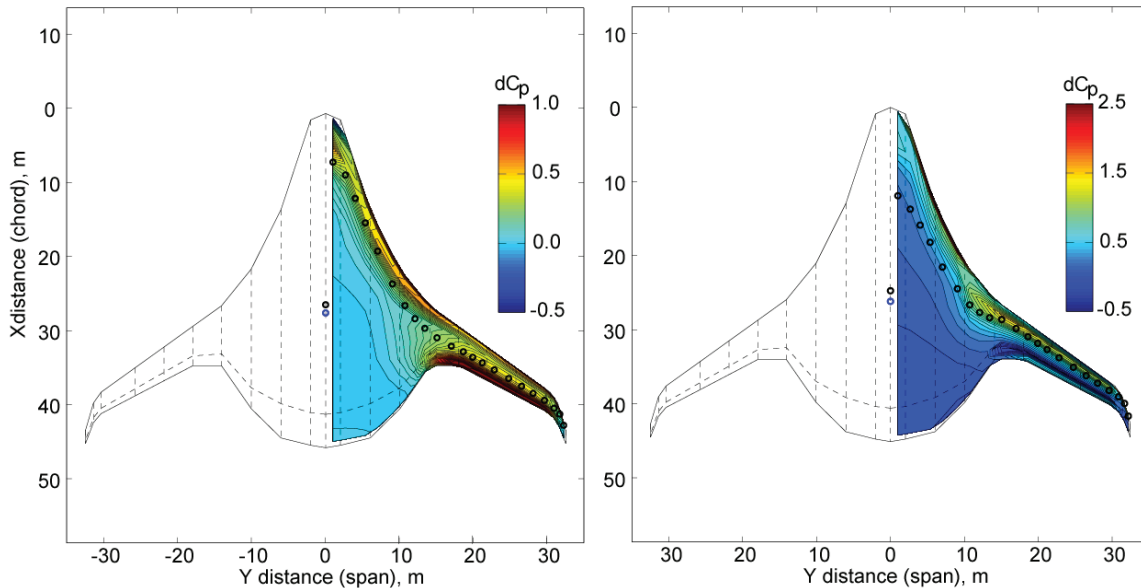
Figure 102: Delta-Cp for the H3.2 configuration during cruise (left) and approach (right).

During approach, a combination of elevon deflection and thrust vectoring unloads the aft section of the outer wings. As shown by Figure 103, the span loading of the H3.2 configuration for cruise and landing approach indicates that this change in elevon setting results in a considerable deviation from the elliptical loading present throughout cruise. The elevon deflection results in sufficient induced drag being generated to trim the aircraft for a 4.4° approach path.
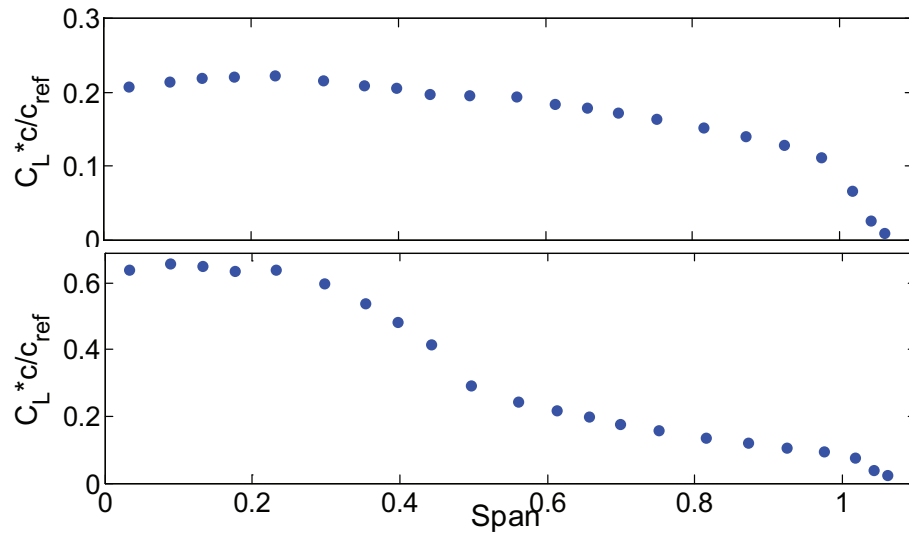
Figure 103: Spanload for cruise (top) and landing approach (bottom).

The drag polar for the H3.2 configuration is shown in Figure 104 for the takeoff and landing configurations as well as for cruise.
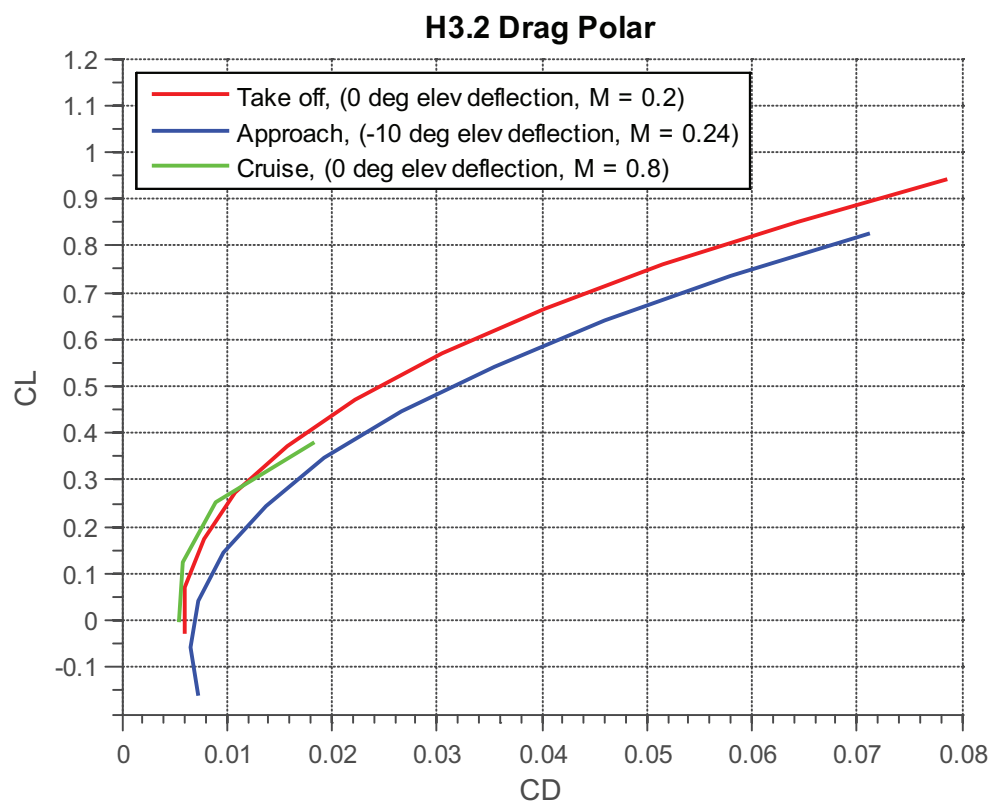
Figure 104: H3.2 drag polars.

6.4.3 Vehicle Component Weight Statement

6.4.3.1 Maximum Takeoff Weight (MTOW) Breakdown

The *Maximum Takeoff Weight (MTOW)* of an aircraft is the maximum weight at which the pilot of the aircraft is allowed to attempt to take off, due to structural or other limits. The MTOW includes the Operating Empty Weight (OEW), as well as fuel and payload.

The breakdown of MTWO is given in Table 35 and Figure 105.

Table 35: Maximum Takeoff Weight (MTOW) Breakdown

Component	Weight (lbs)
Structure	93104
Fuel	126159
Fixed Equipment	56417
Cabin Payload (incl. crew)	65520
Cargo Payload	68911
Propulsion System	40178
Landing Gear and Fairings	20277
Total	**470566**
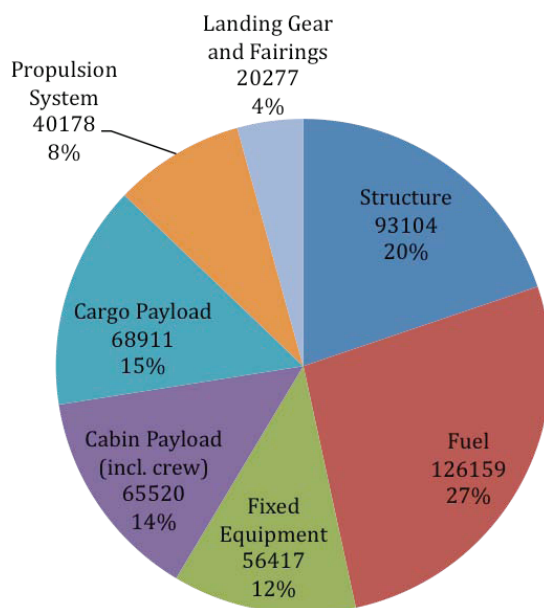
Figure 105: Maximum Takeoff Weight (MTOW) breakdown.

6.4.3.2 Operating Empty Weight (OEW) Breakdown

The *Operating Empty Weight (OEW)* is the basic weight of an aircraft including the crew, all fluids necessary for operation such as engine oil, engine coolant, and all the gear required for flight but not including fuel and the payload.

The OEW breakdown is presented in Table 36 and Figure 106 with the fixed equipment being further broken out in Table 37.

Table 36: Operating Empty Weight (OEW) Breakdown

Component	Weight (lbs)
Structure	93104
Fixed Equipment	56417
Propulsion System	40178
Landing Gear and Fairings	20277
Total	**209976**
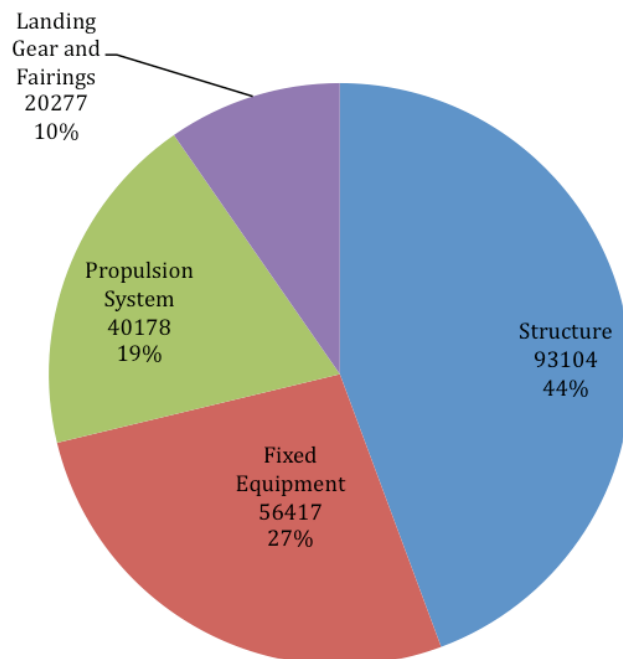
Figure 106: Operating Empty Weight (OEW) breakdown.

Table 37: Fixed Equipment Breakdown

Component	Weight (lbs)
Air conditioning, pressurization, de-icing	2058
Electrical system	1042
Instrumentation, avionics, and electronics	4887
Auxiliary Power Unit	1500
Hydraulic and pneumatic systems	5646
Baggage handling - cargo bay	3843
Flight control systems	3872
Auxiliary gear	2100
Paint	2118
Penalty for Unconventional slats	1000
Oxygen system	35
Food and water	8796
Seats - Passengers	11328
Galleys	3000
Lavatories plus water	2829
In-flight entertainment	1770
Miscellaneous	363
Seats - Cabin crew	120
Seats - Flight Deck Crew	110
Total	**56417**

6.4.3.3 Propulsion System Weight and Dimensions

The propulsion system is comprised of four fans driven by two cores through a beveled gear transmission system. The high bypass ratio propulsion system is embedded into the aft section of the aircraft fuselage to ingest some of the boundary layer that forms over the upper centerbody.

The details of the propulsion system in terms of weights, materials and performance parameters are presented in Table 38 and Table 39 as well as Figure 107.

Table 38: Propulsion System Information and Component Mass Breakdown

Number of cores	2
Number of fans	4
Engine core length (in)	102.64
Engine diameter (D) (in)	82.80
Intake duct length (L/D)	2
Bypass exhaust duct and nozzle length (L/D)	2
Fan nacelle weight (lb)	2464
Core nacelle weight (lb)	134
Fan weight (lb)	3840
Core weight (lb)	23695
Fan nozzle weight (lb)	4646
Engine support and accessories weight (lb)	3635
Total transmission weight (lb)	1764
Nacelle material	Aluminum, Carbon Composites
Fan material	Titanium Alloys
Compression system material	Titanium front stages, Nickel alloy rear stages
Turbine material	Nickel Superalloys
Engine support and accessories	Current SOA: steels, Aluminum alloys
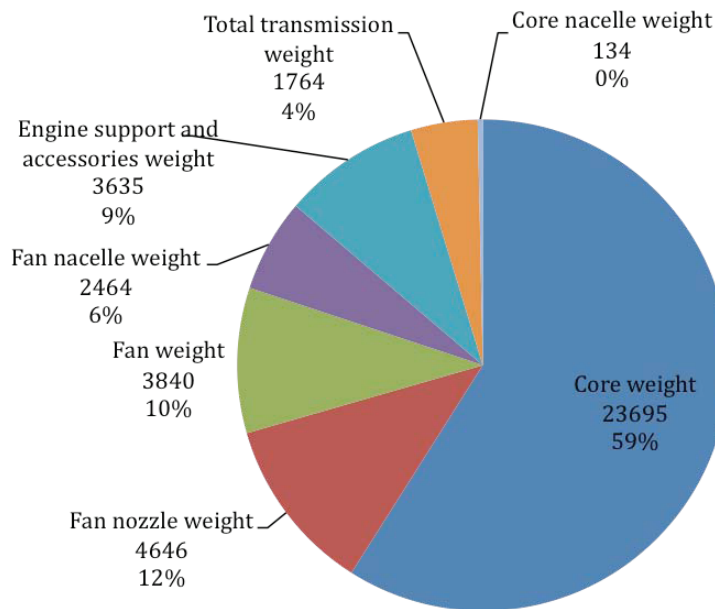
Figure 107: Propulsion system weight breakdown.

Table 39: H3.2 Engine Performance Parameters

Parameter	Sea Level Static	Takeoff	Cutback	Top of climb	Cruise	Approach
Net thrust (kN)	261.4	181.7	109	44	36.9	3.0
SFC (g/kN-s)	6.12	8.91	9.32	14.47	14.00	72.5
Engine mass flow (kg/s)	1119	1308	1105	512	484	648
BPR	18.86	21.04	24.11	19.44	19.97	44.08
Cooling flows (kg/s)	4.54	4.75	3.52	2.01	1.85	1.15
OPR	52.8	46.7	34.0	55.2	50.0	9.2
T_{t4}/T_{t2}	6.6	6.3	5.7	7.0	6.6	4.1
Fan efficiency	0.921	0.953	0.959	0.928	0.944	0.928
High compressor efficiency	0.921	0.931	0.902	0.912	0.930	0.715
Low compressor efficiency	0.926	0.930	0.933	0.925	0.930	0.878
High turbine efficiency	0.936	0.943	0.939	0.944	0.935	0.908
Low turbine efficiency	0.941	0.955	0.937	0.956	0.938	0.918
Intake pressure recovery	0.99	0.972	0.972	0.943	0.943	0.972
Exhaust duct pressure recovery	0.973	0.975	0.977	0.975	0.975	0.989
Fan pressure ratio	1.43	1.39	1.27	1.46	1.41	1.06
Low pressure compressor pressure ratio	2.66	2.55	2.26	2.69	2.61	1.34
High pressure compressor pressure ratio	13.88	13.19	11.89	14.03	13.57	6.51
Burner pressure ratio	0.956	0.955	0.954	0.956	0.955	0.953
High pressure turbine pressure ratio	3.32	3.21	3.21	3.22	3.22	2.81
Low pressure turbine pressure ratio	10.43	10.47	7.99	11.60	10.94	2.82

6.5   Performance

This section outlines the detailed performance of the H3.2 aircraft concept against the metrics identified for evaluation of the transport aircraft both with regard to the NASA goals as well as climate and other factors.

Table 40: H3.2 Important Mission Performance Parameters

MTOW (lb)	470566
Total fuel burn (lb)	126159
Fuel burn at climb (lb)	9411
Fuel burn at cruise (lb)	109287
Reserve fuel (lb) (%)	6211 (5)
Cruise altitude beginning (feet)	34921
Cruise altitude end (feet)	40850
Cruise L/D (w/ and w/o BLI)	27.8 / 24.2
Noise at sideline (EPNdB)	82
Noise at cutback (EPNdB)	77.4
Noise at approach (EPNdB)	82.6
Cumulative EPNdB	242
LTO emissions (% below CAEP 6)	81
LTO emissions (g/kN)	18.6
Cruise emissions (NOx) (g/kg)	5.6

6.5.1 H3.2 Noise

Aircraft noise is defined by the loudest noise source; therefore, all noise sources must be addressed for the aircraft to meet the N+3 noise goal. With informed decisions about engine placement and airframe configuration, one can reduce noise from both airframe and engine sources. This is not an optimization process; instead, it is a design process that relies on understanding how noise scales with parameters such as those defining geometry and velocity. As such, we have chosen a configuration with low noise attributes, then optimized the configuration to minimize fuel consumption, with multiple iterations to refine the results to reach an optimal combination of low noise and low fuel consumption.

The low noise configuration chosen for the H3.2 design has the following features and enabling technologies for noise reduction:

- Advanced, aerodynamically efficient airframe centerbody design that eliminates flaps
- Deployable drooped leading edge instead of slats to augment lift on takeoff and approach
- Faired undercarriage
- Increased induced drag on approach to trim the aerodynamically clean aircraft without additional noise generation
- High bypass ratio engines with low fan pressure ratio and subsonic tip speeds
- Boundary layer ingestion that reduces jet dissipation and jet velocity
- Low engine idle thrust on approach to reduce engine noise and reduce drag requirement to achieve trim
- Embedded and aft mounted distributed propulsion system to enable more effective airframe shielding and more extensive acoustic lining
- Bypass variable area exhaust nozzle for high thrust but low jet velocity
- Airframe shielding of fan forward noise enhanced by engine embedding
- Extended multi-segment rearward and forward acoustics liners

- Displaced runway threshold at approach
- Steep approach trajectory of 4.4 degrees

Figure 108 through Figure 110 show OASPL values as a function of the axial distance between the aircraft and the observer. The results are presented for the three certification points: sideline, flyover and approach.

6.5.1.1 Aircraft noise at sideline

Figure 108 shows the aircraft noise at sideline. The loudest point for the sideline certification point corresponds to the observer being located 450 meters to the side of the runway and at the axial rotation position. Fan engine noise sources are reduced due to subsonic tip speeds. Furthermore, the fan noise sources are attenuated through extended acoustic liners. The ratio of bypass exhaust and inlet duct lengths to fan diameter is 2, and lining is used along the outer and inner sections of the exhaust duct. Peak fan noise attenuation has been calculated using results from Law and Dowling[104]. Even with this attenuation, the dominant noise source is from the fan-rearward broadband as the FPR required for takeoff is 1.4, which is relatively high for a low noise configuration.
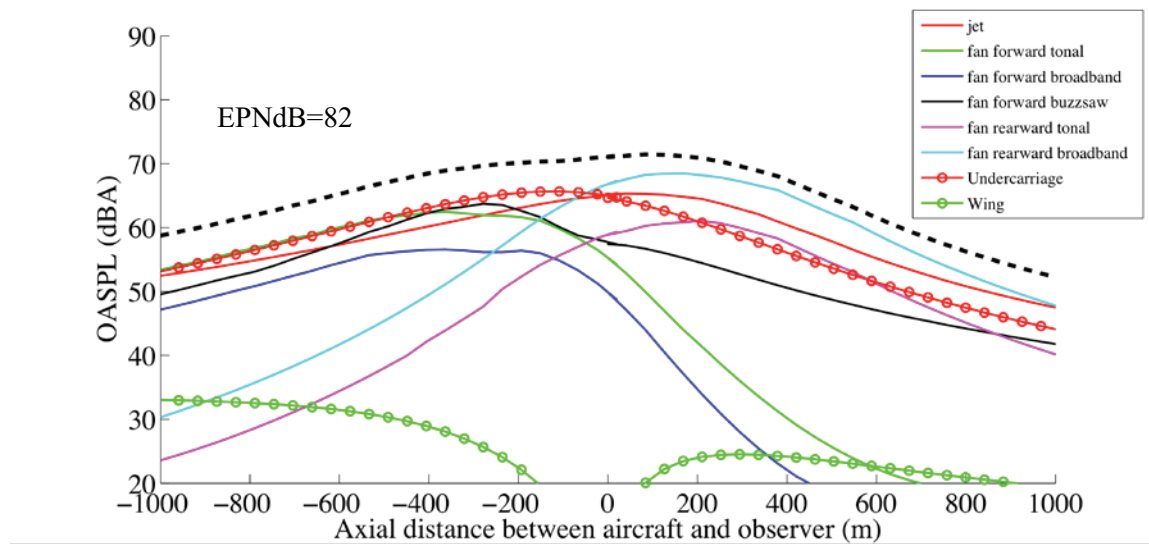
Figure 108: Overall Sound Pressure Level values for the H3.2 configuration at the sideline measurement location.

6.5.1.2 Aircraft noise at flyover

Figure 109 shows the aircraft noise at flyover. The aircraft achieves an altitude of 330 m prior to cutback through a 7 degree climb angle. The climb angle after cutback is 3.0 degrees, which exceeds the engine-out climb angle requirement for a two engine configuration (Crichton et al., 2007)[105]. The trajectory relies on a takeoff thrust of 182 kN and a post-cutback thrust of 109 kN. This operation procedure allows for

---

[104] Law, T.R., and A.P. Dowling. "Optimization of Annular and Cylindrical Liners fro Mixed Exhaust Aeroengines", AIAA-2007-3546, 13th AIAA/CEAS Aeroacoustics Conference (28th AIAA Aeroacoustics Conference).

[105] Crichton, D., E. de la Rosa Blanco, T. Law, and J. Hileman. "Design and Operation for Ultra Low Noise Take-Off," AIAA 2007-0456, 45th AIAA Aerospace Sciences Meeting and Exhibit, Reno, NV, January 2007.

noise reduction at cutback because of the thrust reduction. Furthermore, the fan noise is attenuated through acoustic shielding of the forward source and extended acoustic lines for the rearward source.
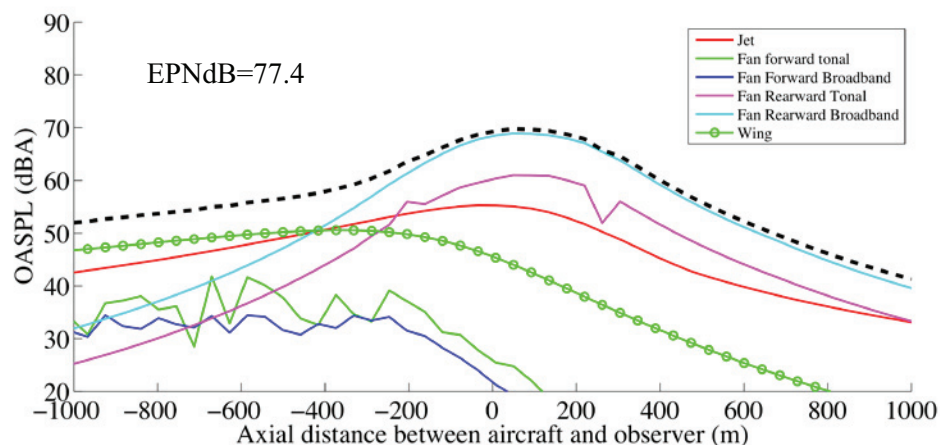
Figure 109: Overall Sound Pressure Level for the H3.2 configuration at the flyover measurement location.

6.5.1.3 Aircraft noise at approach

Figure 110 shows the aircraft noise at approach. The airframe noise at approach was reduced by the elimination of flap and slats through the use of all lifting body and deployable dropped leading edge and undercarriage fairing. Because the high lift system is greatly simplified, the aircraft is aerodynamically clean and the "sailplane" airfoil noise coefficient was used to estimate wing noise for all three noise measurement locations. The engine noise is reduced by airframe shielding of fan forward noise, extensive liners for fan rearward noise and low engine idle thrust. A trimmed approach Mach number of 0.25 with a flight path angle of 4.4 degrees was possible with a 20° flap deflection, and low engine idle thrust. A displaced threshold of 849 m was also used to increase the aircraft height. The dominant noise source is the undercarriage. Increasing the lifting area of the aircraft could reduce the noise from the undercarriage and wings, because it would result in reduced approach speed, but there will be a performance penalty. The tradeoff between noise and fuel burn is explained in section 6.7. In terms of aircraft procedures, a displaced threshold combined with a steep descent trajectory allowed for a further reduction in noise.
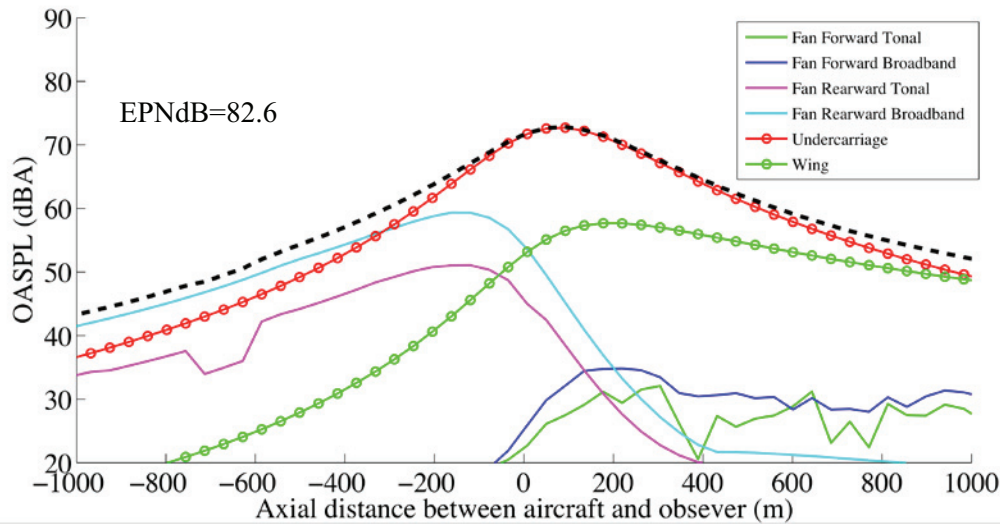
Figure 110: Overall Sound Pressure Level for the H3.2 configuration at the approach measurement location.

6.5.2 H3.2 LTO NOx

Landing/takeoff (LTO) NOx emissions are characterized by CAEP 6 as grams produced during a standardized cycle versus maximum engine thrust. The low LTO NOx emissions, with respect to CAEP 6 standards, of the N+3 concept aircraft are enabled by two key technologies: high bypass ratio and the Lean Direct Injection (LDI) combustor. The low fan pressure ratio associated with the increased bypass ratio of the N+3 engine concept increases the propulsive efficiency of the engine, creating more thrust per unit heat released without increasing the combustor operating temperature. Increasing thrust without changing the temperature, and thus without negatively impacting NOx production, is a powerful tool for reducing emissions and can lead to 60% reductions in regulated NOx on its own.

The LDI combustor, currently under development at NASA Glenn, is another important technology for meeting the N+3 emissions goals. The LDI combustor injects fuel into multiple flame zones, enabling lean combustion while minimizing local hotspots. This allows the LDI combustor in the N+3 concept engine to meet the N+3 NOx goal while retaining the fuel burn and carbon emissions advantages.

The NOx production of the N+3 concept engines is estimated using published correlations from experiments with the NASA LDI combustor[106]. Cycle parameters from the N+3 engine model simulating relevant operating conditions from the LTO cycle (100%, 85%, 30%, and 7% SLS max thrust) are used as inputs to the correlation. A limit of 4 grams of NOx per kg of fuel was used to represent the minimum NOx production based on existing engine data at idle, as suggested by Dr. Chi-Ming Lee at NASA GRC. The percentage of CAEP 6 NOx produced by each engine concept is determined by integrating the predicted NOx production over the time specified by the CAEP LTO cycle. Cruise NOx was estimated based on the predicted engine conditions at cruise with the same combustor correlations and limits.

---

[106] Tacina, R., C. Mao, and C. Wey. "Experimental Investigation of a Multiplex Fuel Injector Module for Low Emissions Combustors," AIAA 2003-0827.

Table 41: H3.2 NOx Performance Results

LTO emissions % Below CAEP 6	81
LTO emissions (g/kN)	18.6
Cruise emissions (NOx) (g/kg)	5.6

6.5.3 H3.2 PFEI

The reference mission for the H3 series aircraft was selected to overlap with the wide body portion of the ircraft fleet with a capacity over 300 passengers (see Figure 20 in Section 2.4.) Wide body aircraft utilize their belly capacity to carry revenue cargo (see Figure 12 in Section 2.3); as such, the H3 design has a capacity for 354 passengers in a three-class configuration as well as 25,628 kg (194 m^2) of revenue cargo in the belly of the aircraft. The cargo thus corresponds to 43% of the maximum structural payload, which is discussed in Section 6.3.3 and is in line with similar sized tube-wing aircraft. The discussion of payload is important to PFEI as this metric includes the entire payload, including revenue cargo, of the aircraft.

As shown in Figure 111, the payload and range of the aircraft correspond to the long range B777-200LR. This range would allow the H3.2 aircraft to complete most routes worldwide including those over the Atlantic and Pacific.
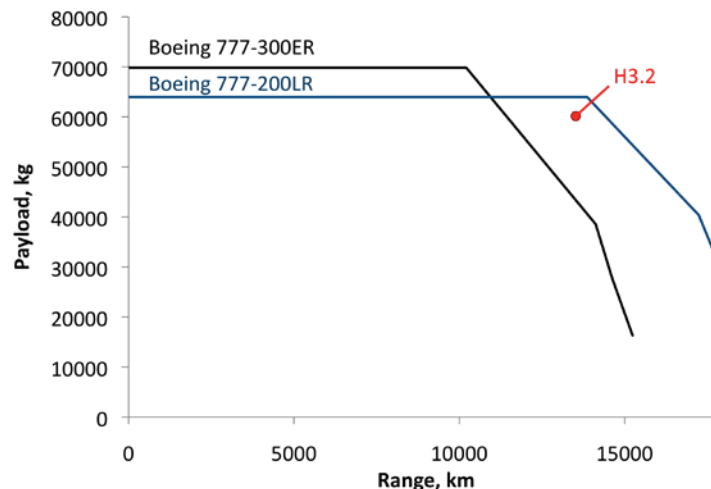
Figure 111: Payload range diagrams for the Boeing 777-300ER and B777-200LR with comparison to the design point for the H3.2.

Unlike aircraft concepts that are created from TASOPT, the PFEI values from HWBOpt cannot be validated against existing aircraft as there are no commercial HWB aircraft in operation. Instead, as is discussed in the HWBOpt Aero Model Validation Appendix, the aerodynamic performance predictions were validated against higher fidelity models. The reference aircraft for comparison was the Boeing 777-200LR due to its similar mission and the reference PFEI of 5.94 kJ/kg-km was computed for the Boeing 777-200LR at the maximum range with maximum structural payload. This reference is compared to the value of 2.75 kJ/kg-km for the H3.2 design in Table 42.

Table 42: Payload Fuel Energy Intensity Performance

H3.2 PFEI (kJ/kg-km)	2.75
B777-200LR Baseline (kJ/kg-km)	5.94
NASA N+3 Goal PFEI (kJ/kg-km)	1.79

6.5.4 H3.2 Balanced Field Length

Table 43 outlines the balanced field length performance as well as the landing distance performance of the H3.2 conceptual aircraft design. The details behind the balanced field length calculations are discussed in Section 3.1.2. Figures of Merit.

Table 43: H3.2 Aircraft Mission Parameters

Takeoff distance balanced field length (feet)	9000
Landing distances (feet) (CLmax = 0.81, mu=0.3)	4966

6.6 HWB Technology Contributions to NASA PFEI Goal

The purpose of this section is to analyze the contributions of the different technologies used in H3.2 to NASA's PFEI Goal. According to the H3.2 technology choices identified during the design phase (see Section 6.2), the research team calculated the contribution of each technology utilizing the same procedure described in Section 5.6.

The H3B (H3 baseline) configuration is analogous to the D8.1 configuration (configuration change only, without advanced technologies). The engines do not have an advanced cycle and they are placed in a conventional podded configuration without boundary layer ingestion. The engines have a high bypass ratio of 13. As with the D8 methodology, each advanced technology was systematically removed from the final H3.2 configuration to determine its relative contribution; however, unlike TASOPT, HWBOpt did not re-optimize the aircraft without this technology, it simply recalculated the PFEI.

To better understand the effect of each technology, it is helpful to connect the technology contributions to different terms in the Breguet Range equation shown below. For the purposes of accounting for boundary layer ingestion, the Breguet range equation was a modified with a term, λ, that is defined as the ratio of net required thrust to total airframe drag without BLI.

$$R = \frac{V}{SFC} \frac{L}{\lambda D} \ln\left(1 + \frac{W_F}{OEW + W_R + W_P}\right)$$

(1)

The contributions of each H3 technology to NASA's PFEI goal are presented in Figure 112. The combination of all technologies achieved a 53.9% reduction in PFEI from the B777-200LR baseline. Out of these technologies, the combination of the H3 airframe configuration with the high bypass ratio engines was the most important contributor to PFEI reduction, enabling a 31.3% reduction from the baseline. This large improvement mainly comes from two contributions: increased airframe lift to drag ratio (L/D) due to aerodynamic improvements, and the decreased engine specific fuel consumption due to the improved propulsive efficiency of the high bypass ratio engines.
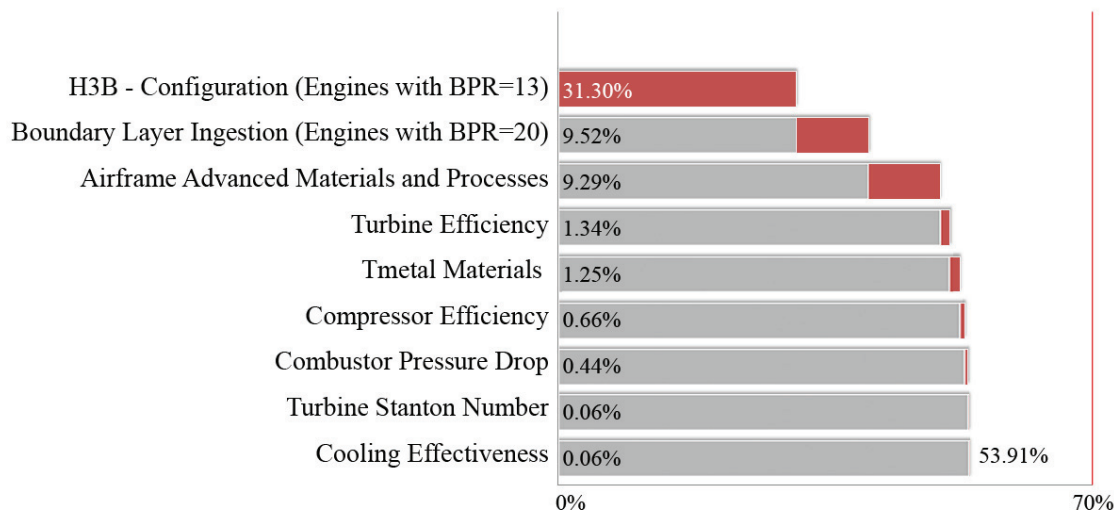
Figure 112: H3.2 technology contributions to PFEI goal.

Another significant contributor to PFEI improvement was the boundary layer ingestion (BLI), which gave an additional 9.5% reduction in PFEI. This improvement not only comes from the direct effect of BLI, which improves the airframe aerodynamic performance (through improvements in λ), but also from the change in propulsion system configuration. By using a distributed propulsion system configuration, a higher bypass ratio engine design is possible without large penalties from the nacelle drag. This decreases the engine specific fuel consumption, which further reduces PFEI.

Finally, advanced material and processes (30% reduction in structural weight) also gives large improvements in PFEI (9.3% reduction in PFEI). The main effect of this technology is the reduction of Operating Empty Weight (OEW) due to the reduced structural weight of the airframe, which improves the empty weight fraction (OEW / MTOW) of the vehicle.

All of the remaining technologies combine for a further 3.8% reduction in PFEI. This is associated with the improvement of various engine component efficiencies. Among the technologies considered for the engine, the largest contribution comes from the improvement of turbine efficiency, followed by the increase in allowable metal temperature in the turbine, which have a combined 2.6% reduction in PFEI.

6.7   PFEI – Noise Tradeoff

For the HWB configuration, it appears that there are design tradeoffs between low noise and fuel efficiency relating to planform shape and propulsion system configuration. To explore these tradeoffs, the low noise HWB aircraft (H3.2Q), which is depicted in Figure 113, was designed. It has features specifically chosen for noise reduction that were proven effective with the SAX-40 design concept. The SAX-40 aircraft concept was designed to meet a stringent noise requirement, similar to that of the NASA N+3 goals. One difference that needs to be kept in mind with this design comparison is that the H-series designs used 9% thick airfoils in the outer wing and had a cruise speed of Mach 0.83, as compared to 7% for the SAX-40 with a Mach 0.8 speed. The thicker airfoils were chosen to improve the structural integrity of the outer wings. With the thicker airfoil, the H-series designs have a larger sweep, relative to the SAX-40 design, to mitigate drag during cruise.

The H3.2Q aircraft has a larger wing area than the H3.2 to reduce the wing loading. This allows the aircraft to approach the airport at a lower velocity, reducing the airframe noise. Lower wing loading also

helps to reduce takeoff noise, with the capability to takeoff at lower thrust and to climb faster than the H3.2. To reduce rearward propagating fan broadband noise, the H3.2Q design features a higher exhaust duct length to fan diameter ratio. The added length allows for a total exhaust length of 4 L/D, which allows for increased liner attenuation. The result of these changes is a 12 EPNdB reduction in cumulative noise.

These design features, however, degrade the fuel burn performance of the aircraft. Increased wing area generates additional drag, penalizing the aerodynamic performance of the aircraft. The longer exhaust ducts require a propulsion system configuration with 3-cores driving 9-fans to enable adequate packaging. This leads to a smaller engine core, which degrades the engine component efficiency, and adds weight as well as more than doubling the drag from the nacelles. The net result of these changes is a 25% increase in PFEI to a value of 3.45 kJ/kg-km.
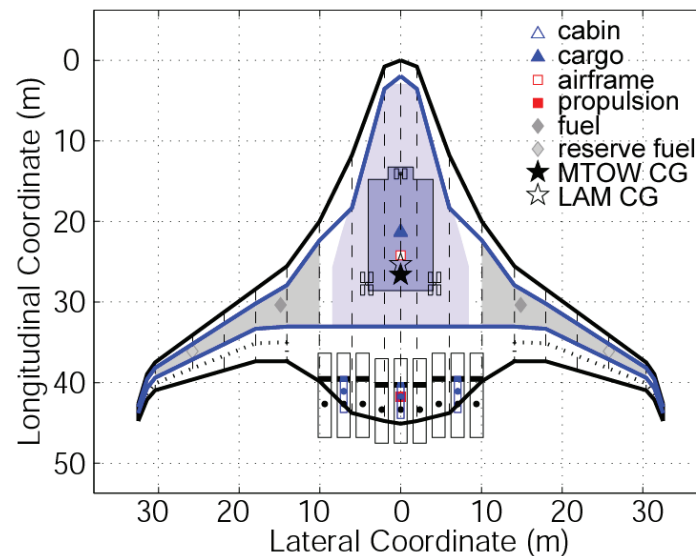
Figure 113: Quiet HWB (H3.2Q) configuration.

To quantify the noise - fuel burn tradeoff, the terms within a the modified form of the Breguet range equation from Section 6.6 were considered in Table 44 for each of three HWB conceptual aircraft designs.

Table 44: Comparison of Key Fuel Efficiency Parameters for the Three Hybrid Wing Body Aircraft Concepts

	OEW/ MTOW	L/D	TSFC (kg/N-hr)	λ	TSFC*λ (kg/N-hr)	PFEI (kJ/kg-km)
SAX-40	62%	25.1	0.0617	0.81	0.0500	5.90
H3.2Q	45%	21.8	0.0538	0.83	0.0481	3.45
H3.2	44%	24.2	0.0504	0.85	0.0428	2.75

The PFEI of SAX-40 is higher than the other concepts because of the poor empty weight fraction (OEW/MTOW) while the H3.2Q suffers relative to the H3.2 because of differences in L/D and engine

SFC. SAX-40 has a high engine TSFC due to its relative lack of advanced engine technology, while the H3.2Q's low SFC relative to the H3.2 comes from the lower inlet pressure recovery that is associated with larger boundary layer ingestion. This is also reflected in the λ values, with the H3.2Q being lower than the H3.2. Overall, H3.2 has the lowest value for TSFC* λ, indicating that the TSFC benefits of higher intake pressure recovery overcome the penalty of less boundary layer ingestion.

The dominant noise source on the HWB aircraft during takeoff is either jet exhaust or fan rearward while during approach it is either airframe-derived or fan rearward. Airframe noise is proportional to u^n/r^2, where u is the approach velocity and n is either 5 or 6 depending on whether it is turbulence scattering or vortex shedding that is the noise source, respectively. From the engine side, fan rearward noise is correlated to fan pressure ratio and it can be mitigated with extensive exhaust lining. Furthermore, if the runway is sufficiently long, then the aircraft can be operated with reduced thrust, or continuously managed as was utilized with SAX-40, to gain additional noise reductions. With these relationships in mind, one can see the importance of approach speed, fan pressure ratio, exhaust liner length, and runway length to noise levels. To quantify the tradeoffs in terms of noise, these parameters have been compared in Table 45 and Table 46 while the planforms are compared in Figure 114.

Table 45: Comparison of Key Noise Parameters for the Three Hybrid Wing Body Aircraft Concepts

	Balanced Field Length (ft)	Mid chord Sweep	Approach Wing Loading (kg/m^2)	Approach Speed (m/s)	Takeoff Fan Pressure Ratio	Exhaust Liner L / D
SAX-40	9,843	19.1°	140	60	1.19	4
H3.2Q	9,000	27.1°	158	69	1.31	4
H3.2	9,000	31.7°	166	80	1.39	2

Table 46: Comparison of Noise Levels at Three Certification Points for the Three Hybrid Wing Body Aircraft Concepts

	Cumulative Noise (EPNdB)	Sideline Noise (EPNdB)	Flyover Noise (EPNdB)	Approach Noise (EPNdB)
SAX-40	210	68.8	69.3	71.9
H3.2Q	230	80	75	75
H3.2	242	82	77.4	82.6
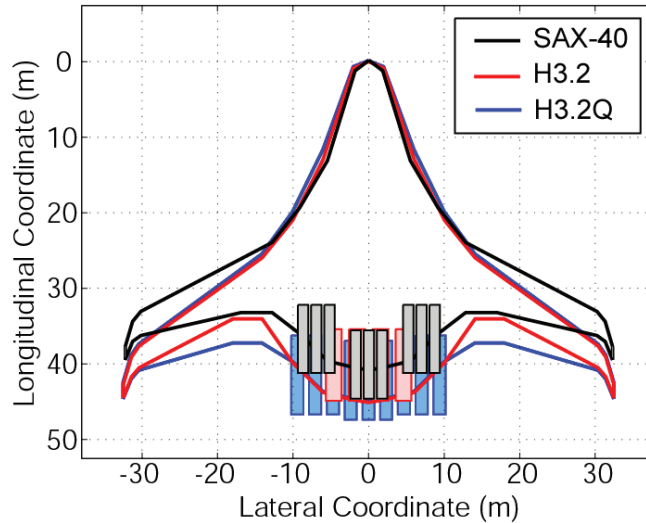
Figure 114: Planform comparison of three HWB design concepts.

Current regulations require the minimum approach speed of an aircraft to be 1.23 times the stall speed, which in turn is proportional to the square root of the wing loading, W/S, and inversely proportional to the square root of the maximum lift coefficient:

$$u = \sqrt{\frac{2}{\rho} \frac{W}{S} \frac{1}{C_L}}$$

(2)

As such, a minimum approach speed, and therefore minimum approach noise, is achieved by having low wing loading and large maximum lift coefficient. Because the maximum lift coefficient is proportional to the cosine of the mid-chord sweep squared, greater sweep leads to lower maximum lift coefficient, and by extension increased approach velocity.

The increased maximum lift coefficient, from decreased wing sweep, and decreased wing loading, from increased wing area, of the H3.2Q design lead to decreased stall speed relative to the H3.2 concept, as well as decreased approach noise. One of the main differences in the planforms is the position of the trailing edge. This extra area helps to decrease wing loading allowing for reduced approach speed. These same features led to the decreased L/D and worse PFEI of the H3.2Q relative to the H3.2. The SAX-40 concept used a large lifting area, relative to the relatively small payload being carried, to get reduced approach wing loading relative to the H3.2 designs. The penalty for this is a substantial increase in empty weight fraction, which in turn corresponds to decreased PFEI performance.

Aircraft noise originates not only from airframe sources, but also those from the engine. For the HWB concept used here, low fan pressure ratio and exhaust liner length are being used to reduce fan broadband noise. The SAX-40 concept uses relatively high L/D values for the exhaust duct and a low fan pressure ratio at takeoff to achieve its noise objective. The H3.2 utilizes lower L/D values for the exhaust duct and a higher fan pressure ratio. The result is increased engine noise at takeoff relative to the other conceptual designs.

6.8   Potential for Further PFEI Improvements on the H3.2 Design

As described in the previous section, although the H3.2 achieved a significant reduction in fuel burn, as compared to the baseline, this design could not meet the N+3 goals in either PFEI or noise. In this section, we will go over potential improvements that could be introduced.

During the analysis, it was found that this design had "white space" that could be eliminated. Figure 115 describes suggested modifications to the H3.2 planform. The section that has been cut out from the original planform could possibly be eliminated, since that section does not carry an aerodynamic load. This section was left to give room for more boundary layer ingestion; however, the tradeoff between boundary layer ingestion and engine performance drove the propulsion system to a limited amount of BLI, leaving that particular section unused. The removal of this section would reduce skin friction drag and structural weight, increasing the performance of this aircraft. Furthermore, the winglet could also be removed. It is on the current configuration for yaw control, but it is conceivable that this could be supplied with thrust vectoring. The winglet removal would eliminate wetted surface area and weight, thereby reducing fuel consumption.

A first order analysis have been conducted to quantify the aerodynamic benefit of removing the fuselage outer trailing edge and the winglets by scaling the skin friction drag of the aircraft with the surface area reduction. Table 47 shows the performance changes between the original design and the modified design. While these estimates are crude, clear benefit can be observed in the modified designs.
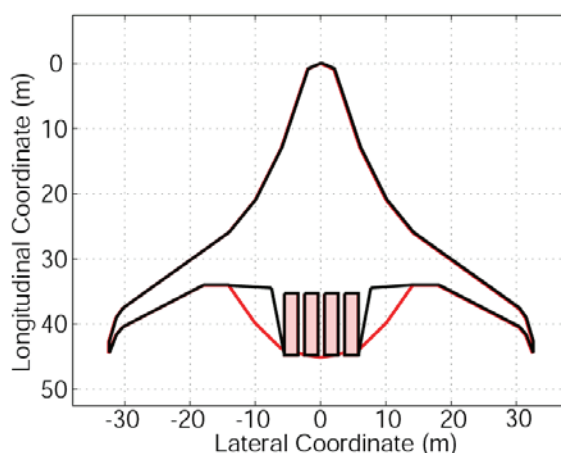
Figure 115: Suggested improved planform (black) and original design (red).

Table 47: Performance Estimates of Modified H3.2 Design

	H3.2	**Modified**
CD	0.0078	0.0071
L/D	24.2	25.7
PFEI	2.75 kJ/kg-km	2.57 kJ/kg-km

6.9 Discussion on Technologies Explored But Not Selected

In addition to the technologies previously discussed in this section there are a few technologies that have been evaluated and modeled for integration into the H series aircraft. As a result of either a determination that the technology will not be mature in the target timeframe of the N+3, the technology was not compatible with other technologies selected for inclusion in the concepts or the final aircraft performance was not optimal when the technology was included, these technologies have not been used in the final aircraft performance reported previously. In most cases an extensive amount of modeling analyses was completed towards the exploration of these technologies. This section is to provide a brief description of those technologies. In some cases detailed information in regards to these technologies is included in the Appendix.

6.9.1 Liquefied Natural Gas (LNG)

6.9.1.1 LNG as Aircraft Fuel

The evaluation of alternative fuels focused on conventional Liquefied Natural Gas (LNG) which is natural gas (~90% methane) liquefied to -162°C at 1 atm. It was considered as a viable fuel for future aviation based on the following comparison relative to conventional jet fuel:

- 16% lower well-to-wake lifecycle carbon emissions for conventional extraction methods (refer to Appendix K on LNG)
- 16% higher specific energy, in addition to 33% lower energy density
- Large potential resource base. The U.S. Department of Energy estimates natural gas from methane hydrates sources to have tremendous supply potential[107], though research on extraction viability and costs is ongoing.

Integration of the cryogenic fuel imposes additional thermal, structural and volumetric constraints and risks. The use of non-integral tanks was evaluated and shown to impose more than 3% tank/fuel weight penalty for typical thermal loads and structure sized for emergency landing. Additional penalties would be incurred due to increased wing bending moments for relocating the fuel from the wings to the fuselage. However, assuming adequate wing design, fuel storage in the wing box eliminates the structural loading requirements. Additionally, with minimal insulation on O (mm), the boiling point of LNG is well matched to promote laminar flow using wall cooling on the lower wing surface at typical cruise speeds. Wall cooling results in a viscosity gradient in air at the wall, reducing the boundary layer shape factor and increasing the critical Reynolds number. Additionally, for Tollmien-Schlichting instabilities that typically dominate transition at cruise, wall cooling is also seen to diminish the range of linearly amplified frequencies and their growth rate[108]. Overall, delayed transition is favored resulting in an estimated ~17% skin friction drag reduction with a minimal ~1% insulation/fuel weight penalty. The onboard heat sink also enables the use of alternative engine cycles such as chiller-regenerator cycle and regenerator cycles. These cycles have the benefit of higher thermal efficiency and core power than the standard Brayton cycle. Detailed description of the benefit of alternative cycles is given in Appendix K. Not considered herein are details regarding the heat management system and additional requirements to disable the system at low altitude due to humidity and icing considerations. Details on tank sizing for both tank architectures are included in the Appendix K on LNG.

---

[107] U.S. Department of Energy, "Methane Hydrate - Future Energy Within Our Grasp."

[108] Reshotko, E. "Drag Reduction by Cooling in Hydrogen-Fueled Aircraft," Journal of Aircraft, Vol. 16, No. 9, Article No. 79-4112, Feb. 1979.

6.9.1.2 LNG-Enabled Electric Distributed Propulsion System

Another technology evaluated over the course of this project is an electric transmission system. The main feature of this technology is to replace the mechanical transmission system between the low pressure turbine and the fan to an electric transmission system, consisting of High Temperature Super Conductor (HTSC) generator and motor, cryocooler and inverter. Major benefits of this technology to the performance of the aircraft include:

- Large boundary layer ingestion enabled by the flexible distribution of propulsors,
- Mechanical decoupling between fan and core,
- Thrust redistribution between propulsors for vehicle control.

One of the main penalties associated with this technology is the increase in weight of the transmission system. By coupling this technology to the use of LNG, the power to weight ratio of the electric transmission system can be improved, mainly from the weight reduction of cryocoolers required to maintain superconductivity in the windings of generators and motors.

In order to quantify the benefits of this technology, the performance and weight model of the electric transmission system was first developed. Details of electric transmission system models and aircraft system level analysis are included in Appendix K. This model was then applied to the airframe system designs, and compared to aircraft designs with various propulsion system configurations with different transmission systems (details are given in section 6.2.4 above). Although the electric distributed propulsion gave better performance than podded propulsion system, the optimal amount of boundary layer ingestion was found to occur at a much lower fuselage span coverage, which could be obtained using beveled gear transmission system with lower weight than the electrical system.

6.9.1.3 Climate Impact of LNG Use as Aircraft Fuel

We explored the potential climate benefit of using liquefied natural gas in a Boeing 777-300ER using our climate metric of globally-averaged time-integrated surface temperature change, normalized by aircraft productivity (payload × distance), calculated in the APMT-Impacts Climate Module. In order to determine fuel usage of the LNG case, we assumed equivalent energy consumption across the baseline Jet A case and the LNG aircraft concept. We then used emissions indices specific to LNG for lifecycle CO_2 and CH_4 emissions and combustion NOx emissions. We also assumed zero SO_X or particulate matter emissions for the LNG case. While there would also likely be differences in emissions of water vapor in moving from Jet A to LNG, for the purposes of this analysis, we assumed these emissions to be unchanged across the cases. The results of the fuel comparison are shown in Table 48.

Table 48: Climate impact of Jet A vs. LNG Fuel (Boeing 777-300ER)

Vehicle	Payload (kg)	Distance (km)	ΔT-years (°K-yrs)	Normalized Climate Impact (°K-yrs / (kg x km))
Jet A	34785	11908	1.11E-07	2.69E-16
LNG	34785	11908	9.96E-08	2.40E-16

The expected climate benefit of an LNG aircraft comes primarily from a reduction in combustion CO_2 emissions of approximately 25 percent on the basis of fuel energy consumed. This benefit is mitigated somewhat, however, by increased production CO_2 and life cycle methane emissions. In total, the LNG aircraft improves upon Jet A in terms of climate impact by approximately 11 percent for the same aircraft flying the same mission.

7 Concept Trades – Impact of Payload and Range on D and H Configuration

The PFEI of the D and H configurations exhibit different trends with changes to aircraft mission in terms of design payload and range. While the D series exhibits large reductions in PFEI relative to conventional tube-and-wing configurations over a wide range of payloads, the H series has relatively little benefit over tube-wing configurations at smaller payloads.

7.1 Assessment of H-Series Aircraft Configuration for Varied Mission and Payload

The effective use of the unconventional internal volume of an HWB aircraft design represents a challenge to the fuel efficiency of the design as unused, "white" space needs to be avoided. This challenge is exacerbated with reduced payload. To examine the potential tradeoff in performance with payload capacity, a number of aircraft cabins were created to span the passenger capacities of narrow-body aircraft, such as the Boeing 737-800, to wide body aircraft, such as the Boeing 777-200LR. These cabins were created with the guidelines presented in Section 6.3. For simplicity, the cabins were designed based on the SAX-40 outer mold line (OML) as the SAX-40 centerbody was used for all of the H-series aircraft. Details of the cabins are presented in Table 49 while the layouts are compared in Figure 116.

Table 49: HWB Cabin Design Comparison

Class	SAX40 OML Scale	Total Cabin Width (m)	Total Seat Capacity	Type
H1	0.86	11.28	180	All Economy
H2	1.00	11.73	256	3 Class
H3	1.10	16.99	354	3 Class
H4	1.20	19.69	450	3 Class
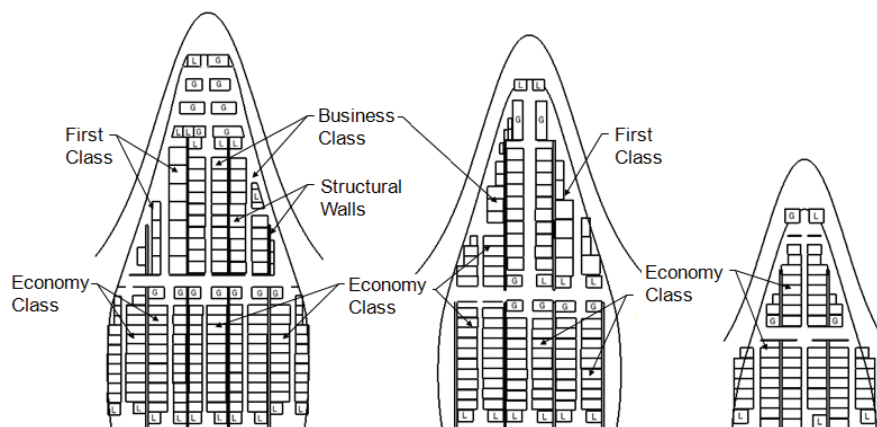
Figure 116: HWB cabin design comparison: H3 (left), H2 (middle), H1 (right).

The first cabin design was based on a 0.86 scaling of the SAX-40 OML (Option 1 in Table 49), which yielded 180 passengers in an economy-class arrangement. This configuration was based on short range interior rules. This cabin was the basis for the H1 class of aircraft.

A second cabin, the basis for the H2 class of aircraft, was designed based on original SAX-40 cabin, but with 256 passengers in a three class configuration (Option 2 in Table 49). This arrangement was inefficient because the cabin was not sufficiently wide to allow an additional grouping of seats in the left and right sides of the economy section. Available cargo volume of 143 m^2 (22 LD3 containers and 4 LD7 Long Pallets) was utilized for revenue cargo payload.

A third cabin, the basis for the H3 class of aircraft, was created by optimizing the economy section to increase the overall seat count (Option 3 in Table 49). This resulted in a 1.1 scaling of the SAX-40 OML and an arrangement for 354 passengers in a 3-class configuration. Additionally, the cargo compartment accommodates 194 m^2 of revenue cargo volume using standard cargo containers (22 LD3 containers + 8 LD7 Long Pallets).

Although it was not used for this study, due to a lack of time, a fourth cabin was also designed for a 1.2 scaling of the SAX-40 OML (Option 4 in Table 49). The result is a configuration able to hold roughly 450 passengers.

The HWBOpt framework was used to optimize advanced aircraft for each cabin configuration for reduced PFEI. The cruise Mach for each of the aircraft was set to 0.83. A span constraint was set to an appropriate scale, which was 52, 65, 65 m respectively, for the H1, H2, and H3 cabins. The H1 design has PFEI that is 31% lower than the B737-800, the reference aircraft, whereas the H3 design has PFEI that is 54% lower than the more efficient B777-200LR.

The relatively large improvement in PFEI (H-series relative to conventional aircraft) is because at small scales, the internal volume in the outboard and aft centerbody was not adequately utilized because of cabin height requirements. The unusable whitespace resulted in a relatively high empty weight fraction, relative to both larger HWB aircraft and to comparably sized tube and wing aircraft. Since the all lifting surface of the HWB planform allows for higher L/D, the H1 performance is better than the reference aircraft. However, it does not meet the PFEI of the D series aircraft and was not pursued further. At larger scales, such as the H3 design, the cabin space was more efficiently utilized and the empty weight fraction decreased as a consequence. The PFEI improvement in going from H2 to H3 is less than that from H1 to H2 because the relative changes in empty weight fraction and L/D are less. This is a consequence of the 65 m span being the same for both and in their reaching similar reductions in white space.

Table 50: HWB Payload/Range Scaling Results

Class	PAX	Revenue Cargo (m^2)	Range (nm)	PFEI (kJ/kg-km)	OEW/ MTOW	L/D
H1	180	-	3000	4.41	61.5	20.7
H2	256	143	8300	3.07	44.7	24.0
H3	354	194	7600	2.75	44.6	24.2

7.2 Assessment of D Series Aircraft Configuration for B777 Mission and Payload

7.2.1 Approach

To assess the two different concept aircraft researched during this program across the different scenario requirements we have developed a D series configuration for a B777 baseline mission. This aircraft, denoted D13 Series, has been designed and sized through the TASOPT process. The B777 reference mission requirements included: cruise Mach number, M = 0.83, range of 7600 nm, total payload of 134,420 lbs which includes passengers (500 passengers × 215 lbs / passenger with bags for 107,500 lbs as well as cargo 26,920 lbs). These are the same design requirements that were applied to the H series aircraft. The process for the design and optimization of the D13 series was the same as that for the D8 series, where a configuration was developed, the performance was assessed with technologies corresponding to current levels, and then advanced technologies were applied to get the final N+3 timeframe performance.

Figure 117 provides a detailed 3-view of the D13.1 aircraft, which, again, is based on current technologies. As for the D8 series this is a double bubble fuselage with three aft top embedded engines. The major difference is the larger fuselage size and length to accommodate a larger payload.
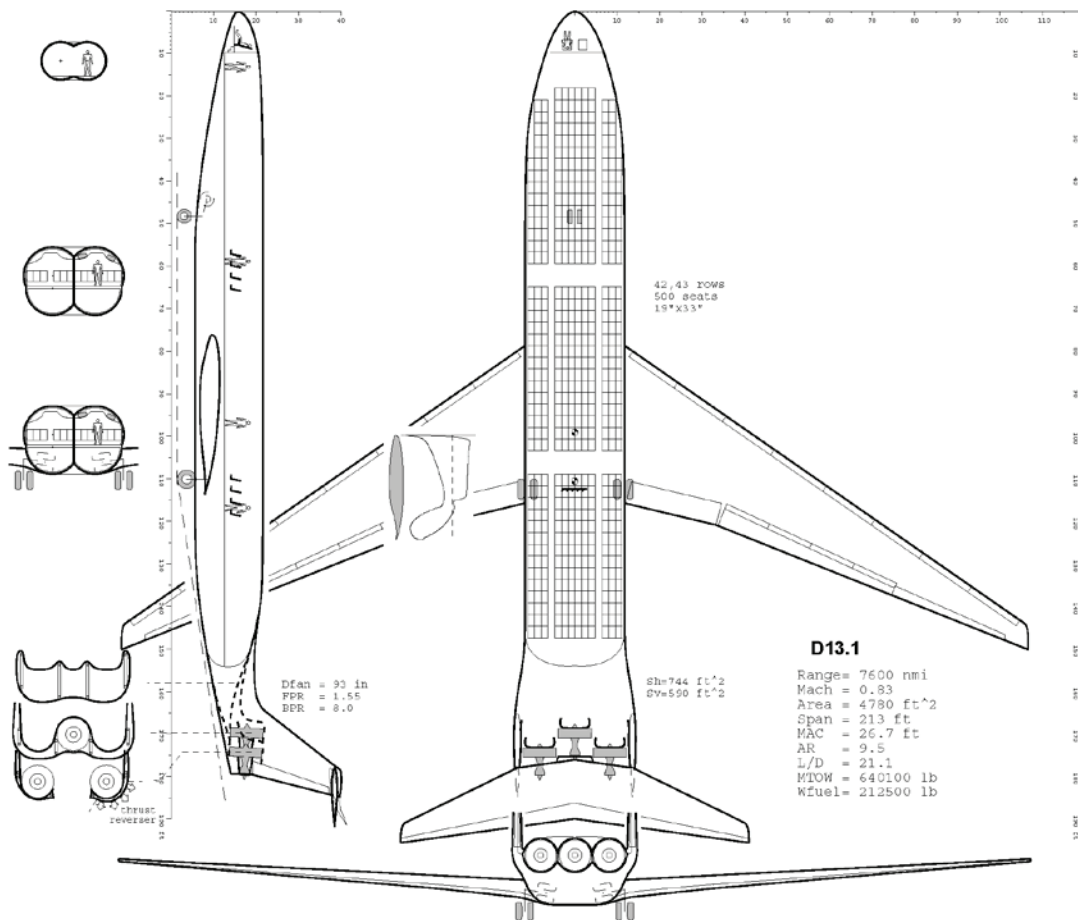
Figure 117: D13.1 series aircraft 3-view drawing.

7.2.2 Cargo Carrying Capability

A major difference in the scenario requirements of the B737 and the B777 baseline aircraft is the inclusion of cargo with the payload. The longer haul B777 mission was seen to have, as a design driver, the cargo requirement rather than just the flexibility to trade cargo for passengers as the operator desires. To address this requirement we have examined the ability of the D13 Series aircraft to accommodate the standard cargo containers used today.

Figure 118 outlines the fuselage cross sections of the D8 series, the D13 Series, the B777, the B737, and the A300 aircraft. While the LD3 container will not directly fit into either the D8 or the D13 series aircraft, there are candidate containers, denoted here as LDx and LDy, that could be developed and put into operation in the N+3 timeframe to allow the D Series aircraft to incorporate cargo. The LDy cargo container actually provides a payload volume increase over the B777 equivalent aircraft with LD3 containers. The principal finding of the container investigation is that the D series aircraft, while not required through the scenario or requirements, can accommodate the inclusion of cargo in the payload. Further, the D13 series can provide a cargo volume increase over the standard LD3 currently used on B777 aircraft.
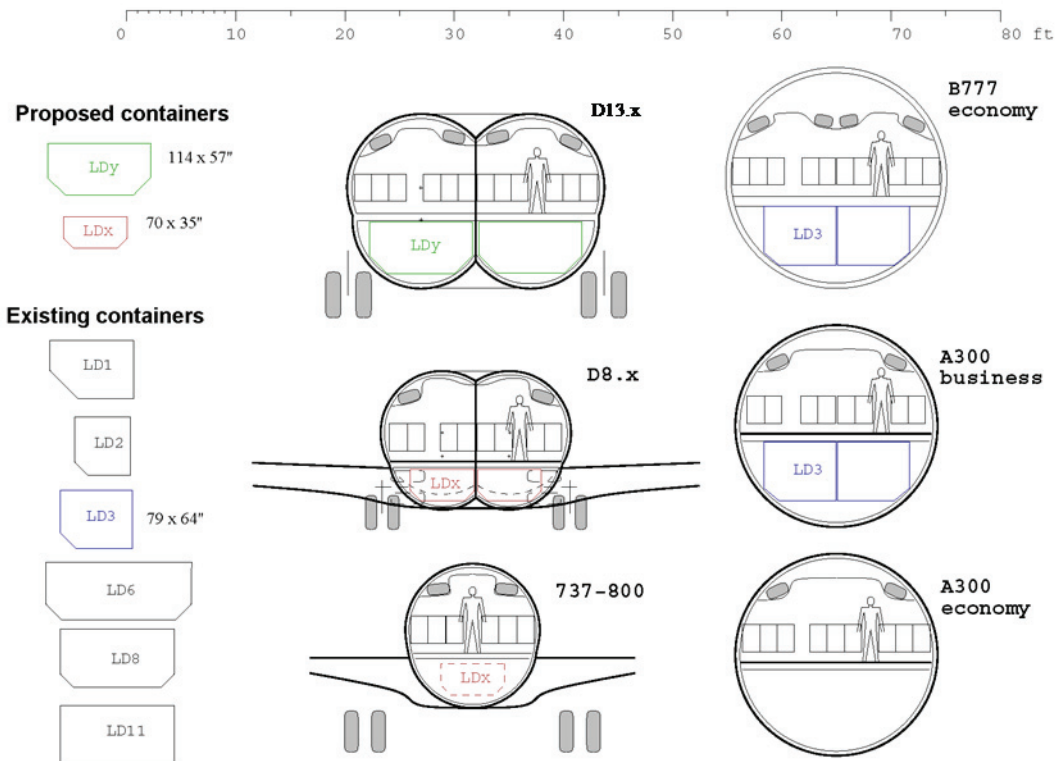
Figure 118: Cargo container cross sections compared to aircraft cross-sections.

7.2.3 D13 Series Fuel Burn Performance Compared to HWB

The development of the D13 series aircraft allows comparison, on the same missions, to the results of the H3.2 aircraft design. It is important to understand that the methods and fidelity of examination of the H series and D series aircraft are very different and the results in comparison provide an adequate sense of the trades of the performance; however, for an exact comparison, an equal level of fidelity would be

required of each configuration. In making the comparison, it should be emphasized that the D13 aircraft has been designed to operate at the same Mach number, M = 0.83, as the H series of aircraft, in other words, we have not taken advantage of a decrease in Mach number in the optimization process such that the aircraft are being compared equally in terms of the mission being performed.

Table 51 provides a list of a few of the basic mission requirements that size the design of each of the aircraft configurations as well as some of the basic aircraft geometry and performance parameters to allow for a side by side comparison.

Table 51: Comparison of D13.3 and H3.2 Aircraft Parameters

Aircraft Requirement or Parameter	D13.3	H3.2
Range (nm) (Plus 5% reserves)	7600	7600
Payload (lb)	134,420	134,431
Cruise Mach number	0.83	0.83
Takeoff balanced field length (feet)	8400	9000
Cruise altitude beginning (feet)	36,764	34,921
Cruise altitude end (feet)	42,397	40,850
Maximum Takeoff Weight (lb)	430,922	470,566
Aspect Ratio	12.75	4.47
Sweep (deg)	29.7	31.7
Span (ft)	213	213
Cruise Thrust (kN)	28.26	36.9

7.3 Comparison of Aircraft Configurations at Varied Payload

Figure 119 presents a comparison of the fuel burn, PFEI, of the D series, H series and conventional aircraft as a function of payload. As noted in Section 7.2.3, it is important to understand that the methods and fidelity of examination of the H series and D series differ considerably. With this caveat being kept in mind, one can see that the D series (double-bubble) gives a better fuel burn for the B737 size payload than for the higher payload, and H series (hybrid wing body) achieves its best fuel burn at the B777 size and payload. However, even at the larger size the double-bubble configuration gives essentially the same performance (NASA metrics) as the hybrid wing body, again with the constraint of cruise Mach number equal to 0.83. If this constraint is removed, the D13 Series aircraft will provide gains over the HWB at the larger range and payload design point as well. As a result of this we recommend continued technological development of the D series aircraft and continued conceptual development of the H series to reach the fidelity of the D series aircraft.
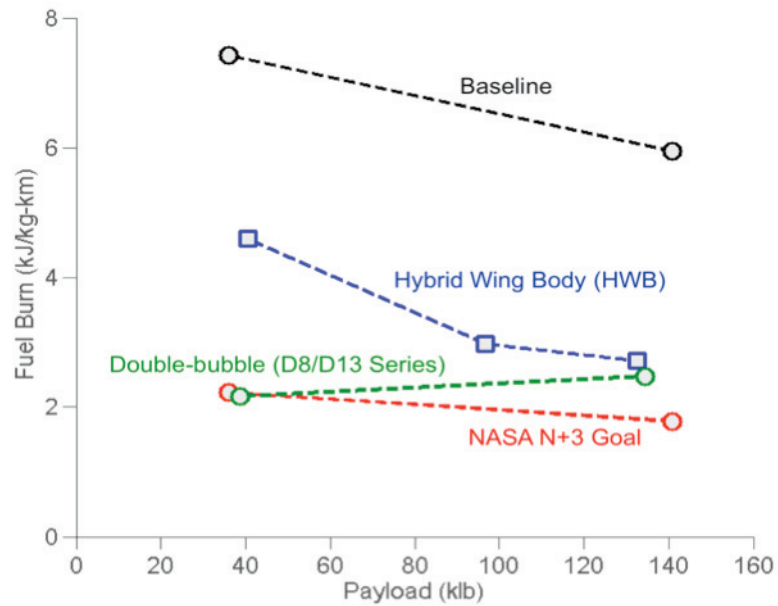
Figure 119: Fuel burn performance of double-bubble and hybrid wing body aircraft versus payload with comparison to the tube-and-wing baseline.

8 Technology Roadmaps

8.1 Risk Assessment and Technology Maturation Plans

8.1.1 Objectives and Definitions

The objective of the N+3 risk assessment activity was to quantify the risks associated with the development of each advanced vehicle concept, identify technological barriers, and provide technology roadmaps to mitigate risks and overcome these barriers.

According to the Department of Defense, risk is defined as the "measure of uncertainty in achieving program goals and objectives within defined costs, schedule and performance constraints"[109]. This definition excludes environmental, safety and occupational health hazards. Applying this same definition to the N+3 project, we interpret risk as *the measure of uncertainty in advancing an aircraft concept capable of achieving NASA N+3 goals to TRL 4 by 2025*. (TRL 4 is defined by NASA as "component and/or breadboard validation in laboratory environment"[110]). Thus, to assess this uncertainty we need to forecast the feasibility and performance of each technology by 2025.

8.1.2 Technology Forecasting Methodology

We utilized the Delphi method[111] to assess the risk of the different technologies identified during the design phase (see Sections 5.2 and 6.2). This method utilizes expert judgment to evaluate the probability of developing each technology to TRL 4 by 2025. While Delphi is a subjective method, it is useful for new technologies that lack historical data. To increase the validity of the risk assessment approach, we utilized technology trend extrapolation techniques[112] whenever data was available. This method relies on historical data and assumes the technology performance improvement will be sustained over time. The two approaches have been extensively described in the literature, and have been applied to aircraft design in the past[113].

For the Delphi method, we identified an initial set of recognized experts from industry, academia, and government agencies including NASA. To increase the reliability of their judgment, we utilized snowball sampling until each technology was covered by at least two experts (some experts covered more than one technology). Eighteen subject matter experts were consulted for the purpose of this project. They provided information on (a) the state-of-the-art of different technologies, (b) the probability of these technologies achieving at least TRL 4 by 2025, (c) the major technological barriers, and (d) technology maturation plans.

When available, we compared the experts' risk assessments with the results obtained through the technology trend extrapolation. Technologies can follow different performance improvement trends which depend on the observation period (e.g. short vs. long timeframe), the level of technology saturation

---

[109] Department of Defense, *Risk Management Guide for DOD Acuisitions,* Department of Defense, 2006, 6th Ed.

[110] Mankins, J.C., *Technology Readiness Levels*, NASA: Advanced Concepts Office/Office of Space Access and Technology, April 6, 1995.

[111] Linstone, H.A. and T. Murray. *The Delphi Method - Techniques and Applications,* Reading, MA: Addison-Wesley Publishing Company, 1975.

[112] Porter, A.L., et al., *Forecasting and Management of Technology,* New York, NY: John Wiley & Sons, Inc., 1991.

[113] Kirby, M.R. and D.N. Mavris. *Forecasting Technolgy Uncertianty in Preeliminary Aircraft Design,* World Aviation Congress. San Francisco, CA: SAE Paper 1999-01-5631.

(e.g. fan efficiency cannot reach 100%), or the presence of competing technologies (e.g. increase in turbine material temperature reduces the need for cooling technologies). Different forecasting models are recommended depending on this growth pattern. For short periods of time or slow performance growth, linear trends are useful[114], for low saturation (i.e. new technologies), exponential curves are appropriate[115], and for competing technologies or high saturation, S-shaped curves are useful[116].

$$X = \frac{A}{1 + Be^{-Ct}}$$

(1)

For S-shaped curves, A is a scaling factor (equal to 100% in case of saturation), and the parameters B and C are obtained by minimizing the standard deviation of errors between historical and forecasted data.

In case of discrepancy between Delphi and the trend extrapolation results, we solicited a second round of interviews with the domain experts, after which all answers converged. Combining the individual technology contributions to NASA goals (See Sections 5.6 and 6.6) with the results of this risk assessment, we obtained the "Risk vs. Gain" charts presented in Section 8.3. Similarly, utilizing the experts' information on technology barriers and technology maturation plans, we constructed the technology roadmaps presented in Section 8.4.

8.1.3   Vehicle Technology Risks vs. Gains Analysis

The following subsections contain risk vs. gain analyses for the different vehicle technologies and their impact on NASA N+3 goals (PFEI, NOx, and Noise reductions).

8.1.3.1 D8 Technology Risks vs. Gains Analysis

Technology Risks vs. PFEI Gains

Figure 120 shows the percentage improvement in PFEI for each of the technologies considered as a function of the probability of not developing the technology to TRL 4 by 2025. The PFEI improvement has been calculated using TASOPT. As mentioned in Section 5.6, the advancement that contributes the most to PFEI reduction is the change to the D8.1 configuration (49% reduction in PFEI). According to the experts, there is 20% of probability of not developing this configuration to TRL 4 by 2025. The risk is associated to the integration of the airframe with the propulsion system equipped with a tolerant distortion high efficiency fan. The other two technologies with the highest PFEI contribution are airframe advanced materials and processes and ultra high bypass ratio engines. They show 10% and 20% risk, respectively. In the case of the ultra high bypass ratio engines, the main concern is the development of high efficiency small cores. The technologies with highest risks correspond to further improvements on engine component efficiencies, especially the compressor given the core size. Increasing the cooling effectiveness for 0.3 to 0.4 and developing advanced engine materials have a 25% risk. All other technologies have at least 80% probability of success.

---

[114] Porter, A.L., et al., _Forecasting and Management of Technology,_ New York, NY: John Wiley & Sons, Inc., 1991.

[115] See Footnote 114.

[116] Foster, R.N., The S-Curve: A New Forecasting Tool, _Innovation, The Attacker's Advantage._ New York, NY: Summit Books, Simon and Schuster, 1986, pp. 88-111.
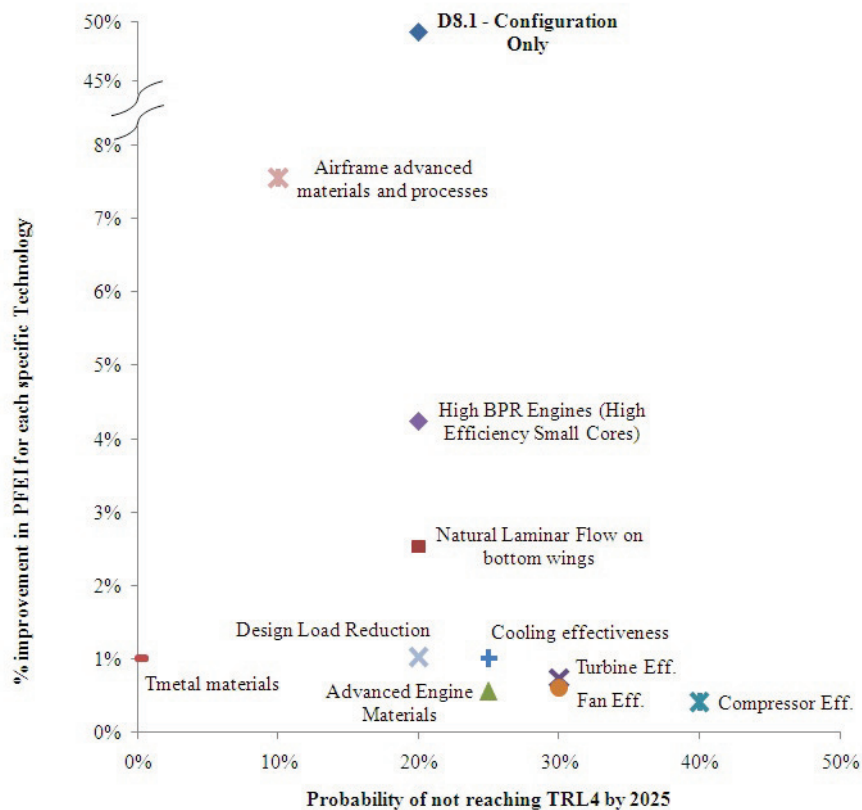
Figure 120: D8.5 technology risks vs. PFEI gains.

Technology Risks vs. LTO NOx Reduction Gains

Figure 121 shows the percentage improvement in LTO NOx for each of the technologies considered as a function of the probability of not developing the technology to TRL 4 by 2025. As mentioned in Section 5.6, the advancement that contributes the most to LTO NOx reduction is the change to the D8.1 configuration. According to the experts, there is 20% of probability of not developing this configuration to TRL 4 by 2025 for the reason given above. The second highest contributor is the development to an LDI advanced combustor. There is 100% probability of reaching TRL 4 by 2025 with this technology. For the case of the LDI combustor, however, reaching TRL 6 from TRL 4 is the most challenging step as issues related with combustor dynamics with a lean flame need to be resolved for the combustor design. The risk associated with the development of an ultra high bypass ratio engine with high efficiency small cores is 20% as explained above. The rest of the technologies show higher risk but also have lower contribution to this N+3 goal.
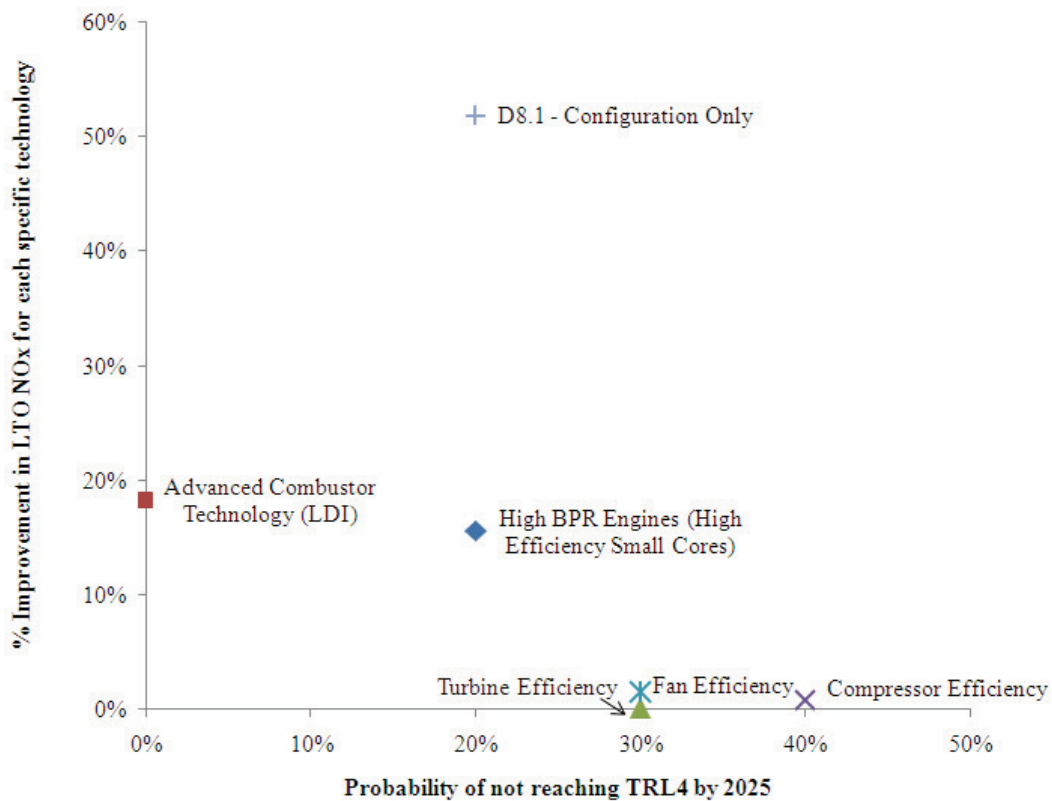
Figure 121: D8.5 technology risks vs. NOx reduction gains.

Technology Risks vs. Noise Reduction Gains

Figure 122 shows the improvement in noise reduction relative to Stage 4 of the most promising technologies as a function of the risk associated with the development of each. As mentioned in Section 5.6.3, the technology that contributes the most to noise reduction is the change of the aircraft configuration from a conventional tube and wing to the D8.1 design (-40 EPNdB reduction relative to Stage 4). According to the experts, there is a 20% risk of this aircraft configuration not being able to be developed by 2025 with TRL 4 as explained above. The second highest contributor is the development of ultra high bypass ratio engines. The development of faired undercarriages shows a 10% risk while the change in the approach trajectory could be achieved although it might imply a change on the operation procedures for the whole fleet. This should be compatible with NextGen. The displaced runway threshold at approach is a technique currently in use in some airports.
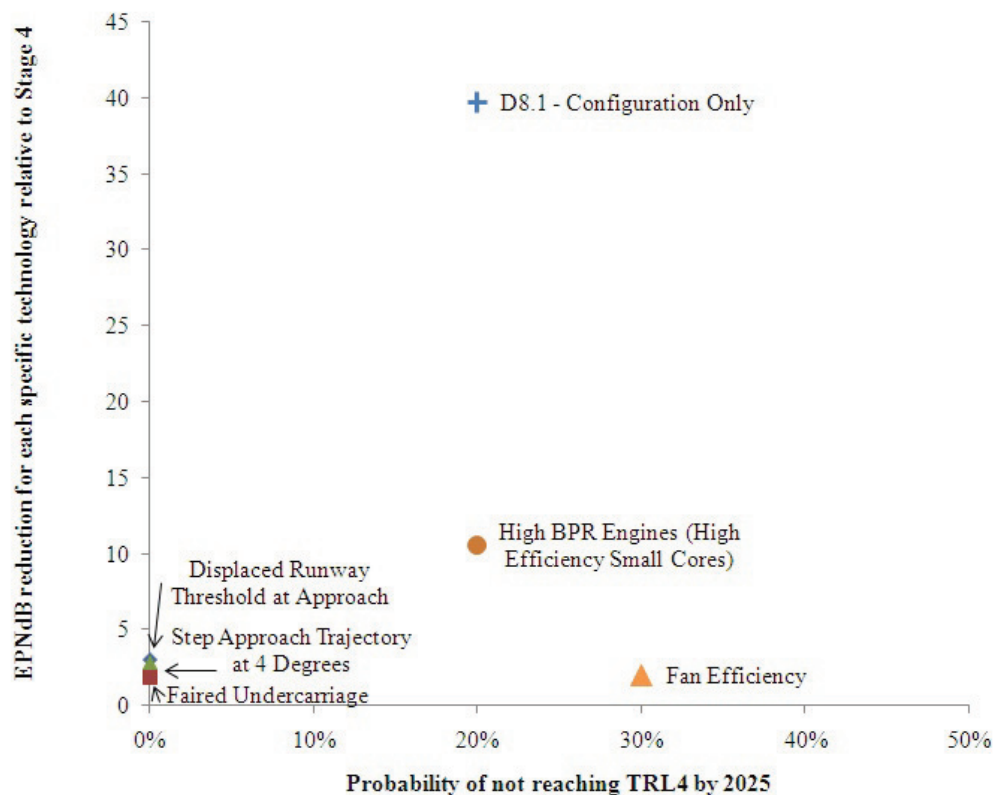
Figure 122: D8.5 Technology risks vs. noise reduction gains.

8.1.3.2 HWB Technology Risk vs. Gains Analysis

For the HWB configuration, we only performed a technology risks versus gains analysis for the PFEI goal since it was not possible to decouple the effects of the individual technologies for LTO NOx and Noise. Figure 123 presents the technology risks and their contributions to PFEI reduction. The technology that contributes the most to this goal is the H3B configuration. This is the baseline H3 configuration without advanced technologies equipped with three podded engines with a BPR of 13. According to expert judgment, there is a 10% risk of developing the airframe configuration, and a 10% risk of developing advanced materials and processes.

The development of the boundary layer ingestion has a risk of 20% because of the integration of the embedded distributed propulsion system with the airframe. Further, the engines require bevel gears, which present a higher risk than direct drive or planetary geared engines. The technologies with highest risks correspond to additional improvements on engine component efficiencies, especially the compressor given the core size. With respect to the remaining technologies for the H3.2 configuration, all have 25% or less risk of being developed to TRL 4 by 2025.
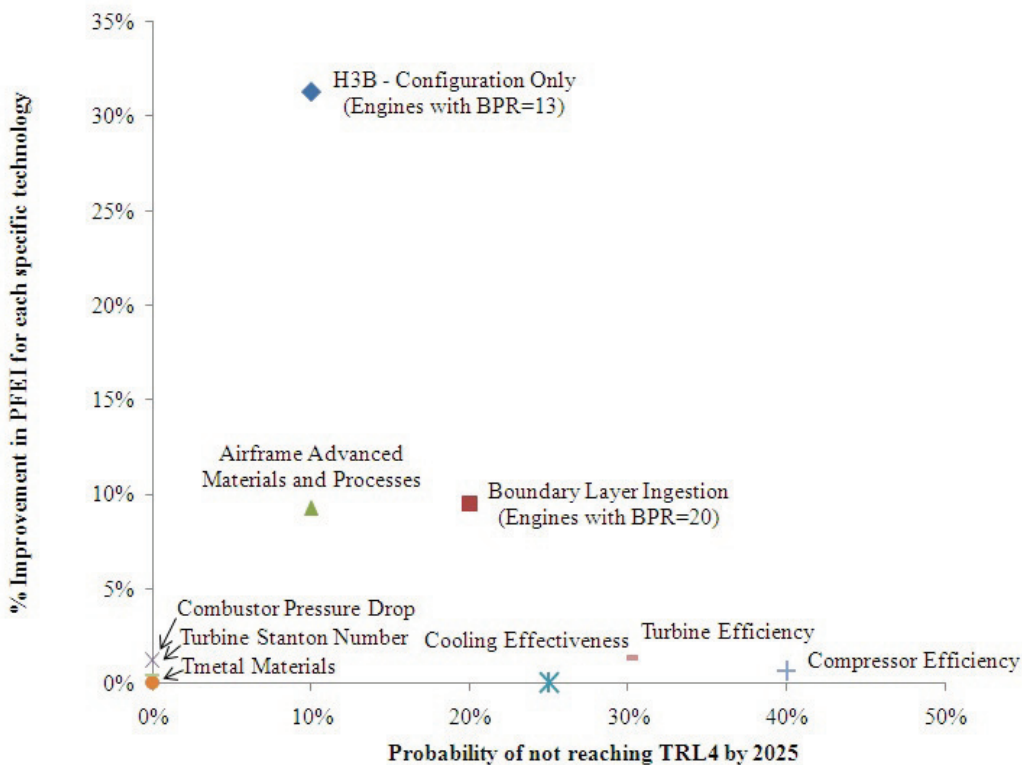
Figure 123: H3.2 technology risks vs. PFEI gains.

8.2 Technology Roadmaps

As an aid to technology planning for the step changes in air vehicle and engine performance envisioned in the N+3 program, based on the findings of this research we have developed technology maturation plans (or "technology roadmaps") for thirteen advanced technologies used in the D8 and H3 series aircrafts. The intent of the roadmaps is to provide a preliminary plan for how to carry out advancement of the technologies needed for the D8 and H3 series aircraft.

The roadmaps:

- Identify the current state of the art
- Identify the technology advancement(s) needed to achieve N+3 goals
- Asses the probability that the technology will be advanced to this state (to TRL 4) by 2025
- Explicitly lay out the development steps that will be required to advance the technology to TRL 4 by 2025

We have also included estimates of the years to reach TRL 4 for each development step.

In some cases, there are development steps that are required precursors for follow-on steps. These precursors are identified, as well as barriers to progress. In other cases, technology alternatives are provided, in the event that the recommended roadmap here is not followed – for example, ceramic matrix composites are an attractive means to reduce engine weight, but other alternatives are metal matrix

composites, or continued advancement of nickel alloys. Another example is alternative cooling techniques to film cooling.

The content of the roadmaps was primarily obtained from discussions with the 18 subject matter experts in various fields (deliberately not mentioned by name, however, their contributions are greatly appreciated), as described in Section 8.1.2. These experts estimated the probability of the technology development based on an assumption that a "reasonable" level of funding would be provided. In addition, to support the estimated probability of development, selected roadmaps provide historical data on the development of the technology, as well as extrapolated predictions of future states (see Section 8.1.2.) The historical data are not provided when either the technology had limited development history (e.g. boundary layer ingestion) or data was unavailable or inconsistent (e.g. advanced materials and processes).

The first two roadmaps in this section are *configuration roadmaps*, and are not specific to technology. "D8 Configuration" and "H3 Configuration" give overall development steps for the D8 and H3 series aircraft, primarily airframe-related development steps. The D8 Configuration roadmap also shows the crucial propulsion system integration steps for aircraft development.

The following are considered major technologies required for the D8 and H3 aircraft. Technologies 14 through 20 do not have an associated roadmap because either: (1) the technology is already developed to TRL 4, (2) information related for future development is unavailable or proprietary, or (3) it was decided that the technology would not be used for either the D8 Series or the H3 aircraft (these technologies are starred).

1. Ultra high bypass ratio engine
2. Boundary layer ingestion
3. Natural laminar flow
4. Airframe advanced materials and processes
5. Airframe design load reduction – health monitoring and gust load alleviation
6. Technologies to reduce engine weight
7. T_{metal} materials (technology roadmap included within "Technologies to reduce amount of cooling")
8. Cooling effectiveness (technology roadmap included within "Technologies to reduce amount of cooling")
9. Fan efficiency (technology roadmap included within "Boundary layer ingestion" on the development of a distortion tolerant fan)
10. Compressor efficiency
11. Turbine efficiency
12. Acoustic liners
13. Advanced combustor
14. LNG as fuel*
15. Alternative cycles*
16. Faired undercarriage
17. Secondary structures
18. Distributed turboelectric propulsion*
19. Variable area nozzles
20. Cockpit fixed weight

8.2.1 D8 Configuration

Current State: B737 tube-and-wing

Goal: D8 configuration: double bubble fuselage with lifting nose and a pi-tail, with embedded aft engines, reduced cruise Mach number, with no slats, and with natural boundary layer on the bottom wing.

Probability of reaching goal (TRL4 by 2025): 80%

	Development Steps	2010	2015	2020	2025
	PROPULSION SYSTEM AIRFRAME INTEGRATION				
1	Perform detailed design / 3D viscous CFD analysis of D8 fuselage/ engine OML at design and off design conditions	■			
2	Perform detailed design / analysis of nacelle including thrust reverses, VAN, structural mounting, and pylon	■			
3	Perform engine fan design and analysis under vertically stratified inlet distortion conditions (technology roadmap included under development of distortion tolerant fan on "Boundary layer ingestion")	■			
4	Conduct low speed wind tunnel testing		■		
5	Conduct high speed wind tunnel testing		■		
	AIRFRAME				
1	Perform detailed design / analysis of primary structures	■			
2	Conduct tests for subscale structural concept verification		■		
3	Conduct structural ground tests of large-scale primary structures		■		
	AIRCRAFT				
1	Perform sub-scale aircraft flight tests		■		
2	Conduct high fidelity noise analysis	■			

8.2.2 HWB Configuration

Current State: The Boeing 787 uses composite materials and state of the art aerodynamics in a tube and wing configuration. The B-2 bomber uses composite materials in a tail-less aircraft configuration.

Goal: Develop HWB that allows for tail-less all lifting body with improved aerodynamic performance and low structural weight with acceptable manufacturability.

Probability of reaching goal (TRL4 by 2025): 90%

Main technology development: (This roadmap does not consider propulsion system integration). Develop lightweight pressure vessel for HWB centerbody that has sufficient structural integrity and is amenable to large scale manufacture. Ensure that aerodynamic design avoids wasteful "white space" while maintaining aerodynamic performance and controllability. Combine analyses to reach optimal combination of structural and aerodynamic performance.

	Development Steps	
1	Develop conceptual structural weight model	
2	Develop rapid 3D inviscid centerbody aero optimization	
3	Develop full mission static control models	
4	Develop 3D viscous aerodynamic CFD solution	
5	Establish detailed 3D design model	
6	Conduct low speed wind tunnel testing	
7	Conduct high speed wind tunnel testing	
8	Manufacture sub-component and centerbody sections	
9	Perform ground tests of large-scale structures	
10	Conduct sub-scale aircraft flight test (X48B flight test for H3.2 design)	

2010   2015   2020   2025

8.2.3 High Bypass Ratio Engines

Current State: BPR of 11 for a geared turbofan, BPR of 8.5 for a direct drive turbofan

Goal: BPR of 20 for D8.5 and for H3.2

Probability of reaching goal (TRL4 by 2025): 100% for D8.5 by using a planetary gearbox; 80% for H3.2 by using bevel gears

Main technology development: High efficiency small cores, and bevel gears for H3.2 transmission system

	Development Steps	
	HIGH EFFICIENCY SMALL CORES	
1	Perform computational and experimental studies to mitigate the efficiency drop associated to small axial compressors and turbines (technology roadmaps included under "Small axial compressor with high efficiency" and "Small axial turbine with high efficiency")	
2	Improve design and behavior prediction of seals	
3	Develop manufacturing techniques for small HPC blades with the required tolerances	
	BEVEL GEARS FOR AIRBORNE TRANSMISSION SYSTEMS	
1	Develop reliable high power bevel gears for high rotational speed applications	

2010   2015   2020   2025

**Bypass Ratio
Historical trend graph[117]**
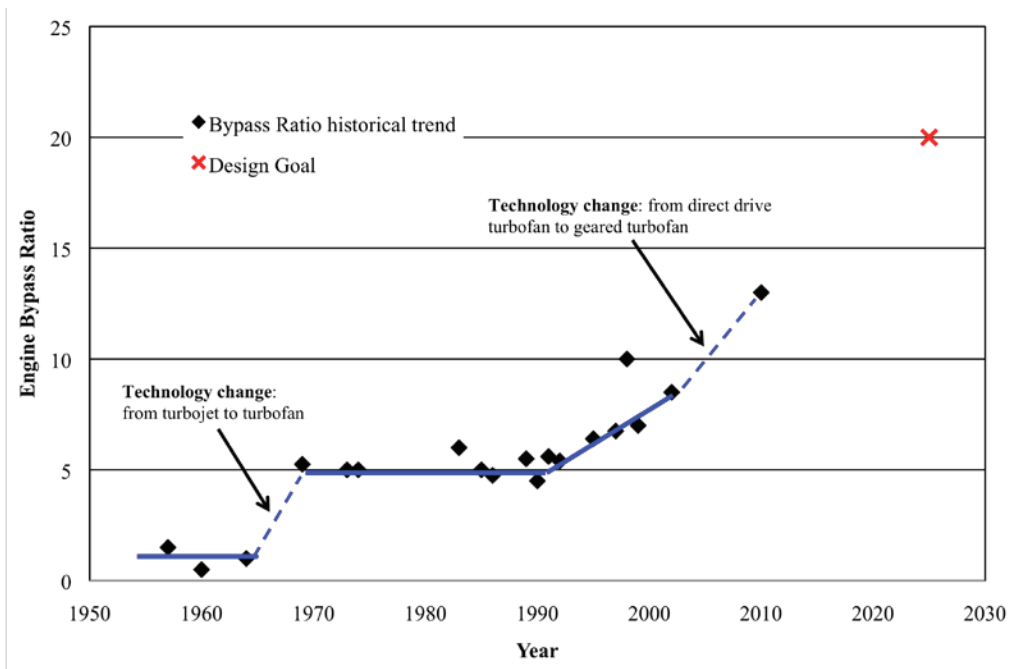
**Overall Pressure Ratio
Historical trend and forecast graph[118][119]**
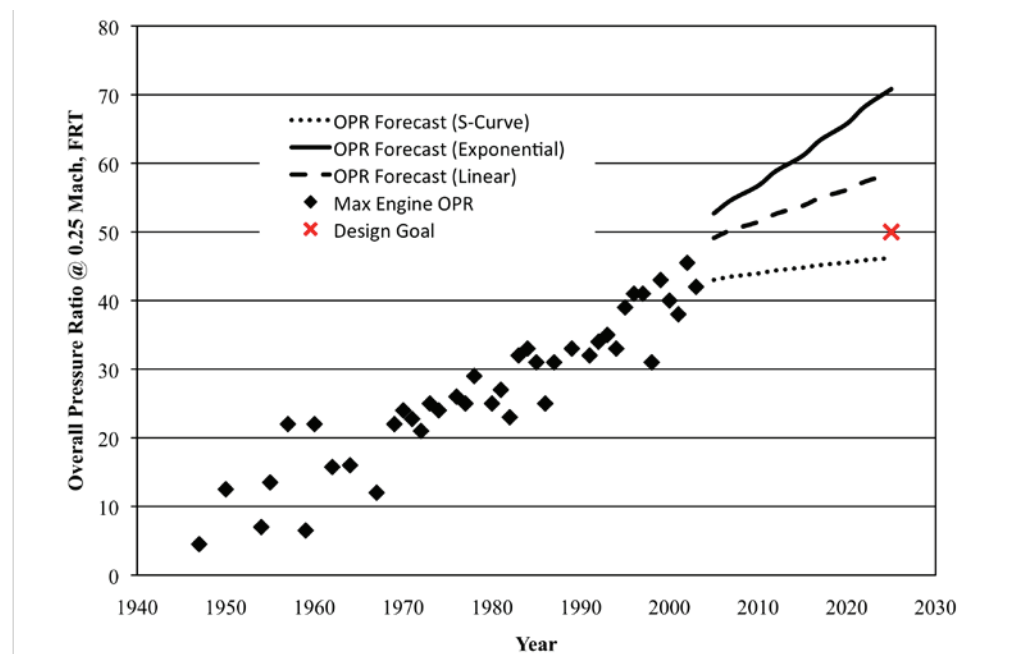
[117] Ballal, D.R. and J. Zelina. "Progress in Aeroengine Technology (1939-2003)," *Journal of Aircraft*, 41(1), 2004.

[118] Ballal, D.R., and J. Zelina. "Progress in Aeroengine Technology (1939-2003)," *Journal of Aircraft*, 41(1), 2004.

[119] Benzakein, M.J., "Roy Smith and Aircraft Engine of Today and Tomorrow" ASME IGTI Turbo Expo, June, 2009.

8.2.4 Boundary Layer Ingestion

Current State: No BLI on current civil aircraft

Goal: 40% BLI for D8.5 configuration and 30% BLI for H3.2 configuration of the fuselage. Engine with a distortion tolerant fan with rotor fan polytropic efficiency of 95%

Probability of reaching goal (TRL4 by 2025): 90% for D8.5, 80% for H3.2. The distortion tolerant fan design would require further development for the H3.2 configuration because of higher distortion levels that would occur under the presence of strong endwall flows at the fan inlet.

Main technology development: Distortion tolerant fans, and duct design to reduce distortion and losses for fully embedded engines as the ones in H3.2 configuration

	Development Steps	2010	2015	2020	2025
	DISTORTION TOLERANT FAN				
1	Perform computational studies to determine the origin of losses in a fan under the presence of distorted flows	▮			
2	Design fan rotor at low solidity and low tip relative Mach number with large choke-to-stall incidence range and high efficiency	▮			
3	Perform computational studies to determine fan operability and assess the swirl conditions at the rotor exit	▮			
4	Design fan EGV to cope with fan rotor exit swirl conditions. Explore techniques such as blade leading edge modifications as a function of EGV blade circumferential position	▮			
5	Conduct scale-model test of isolated fan system under distortion conditions to determine performance, operability, blade stress, and acoustic signature	▮			
6	Design low air side heat exchanger to operate under high distortion flows	▮			
	INLET S-DUCTS FOR EMBEDDED ENGINES				
1	Develop a distortion transformation inlet consisted of vertical and horizontal splitters that convert the vertically stratified total pressure distortion into something that approximates pure radial distortion	▮			
2	Design *alternative* flow control devices to control endwall flows development within the S-ducts	▮			

Peak Fan Efficiency
Historical Trend and Forecast Graph[120]
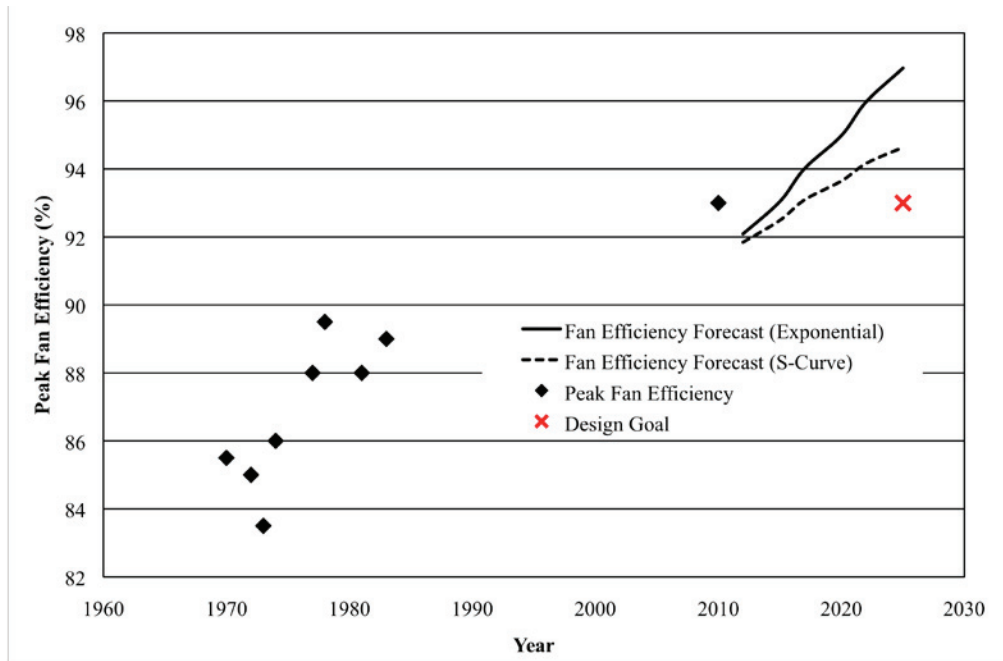
8.2.5 Natural Laminar Flow

Current State: None on civil aircrafts

Goal: Achieve natural laminar flow (NLF) on at least 60% of wing bottom surface

Probability of reaching goal (TRL4 by 2025): 80%. Note that a major part of achieving NLF is reduced Mach number to allow reduced-sweep wings, which mitigate crossflow instabilities that prevent NLF (this requires no specific technology development.)

Main technology development: Composite wings with distributed roughness elements (DRE's)

---

[120] Wisler, D.C., Advanced Compressor and Fan Systems, General Electric Aircraft Engine Business Group, Cincinnati, Ohio

	Development Steps
1	Develop advanced composite manufacturing techniques to provide adequate contour accuracy to support NLF on wings
2	Verify compatibility of DRE's with composite wing manufacturing and maintenance
3	Develop high lift technology without having leading edge slats
4	Develop wing insect protection and cleaning techniques
5	Design composite wings with DRE's and no-slats
6	Conduct high speed wind tunnels test to asses wing performance

Airframe Advanced Materials and Processes

Current State: Aluminum. AS4 and IM7 (military) and T800 (civil) carbon fibers are also used on aircraft; M65J and T1000 are the current state of the art carbon fibers. Airbus Next Generation Composite Wing (NGCW) is developing a resin system; MIT NESCT carbon nanotube program is developing short CNTs.

Goal: Use new materials and processes with unit strength of $\sigma/\rho \approx 2$ over aluminum
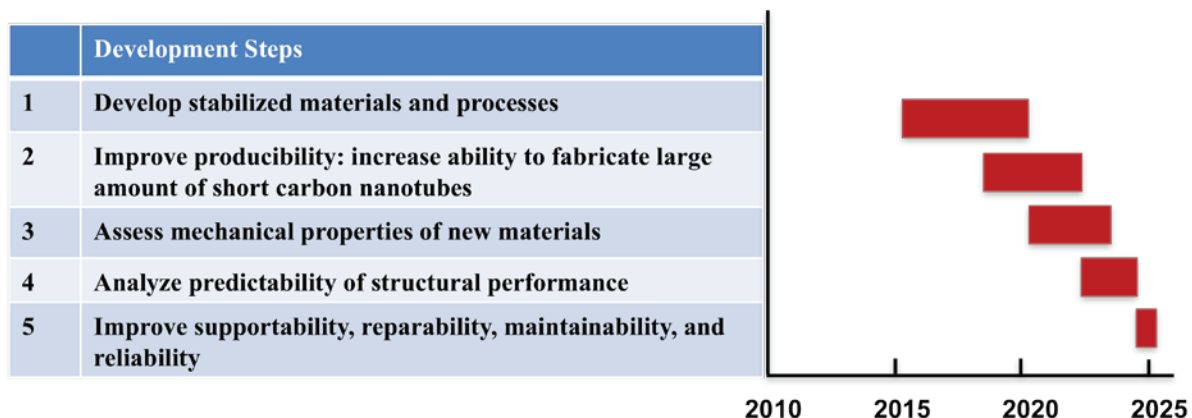
Probability of reaching goal (TRL4 by 2025): 90%

Main technology development: Develop new materials and processes such as composites including unitized bonded structures; new intermediate modulus (IM) fiber; advanced high-toughness/high-service-temperature resin; short carbon nanotubes (CNTs); unitized bonded structure techniques like PRSEUS and out-of-autoclave (OOA) curing.

	Development Steps
1	Develop stabilized materials and processes
2	Improve producibility: increase ability to fabricate large amount of short carbon nanotubes
3	Assess mechanical properties of new materials
4	Analyze predictability of structural performance
5	Improve supportability, reparability, maintainability, and reliability

8.2.6 Airframe Design Load Reduction – Health monitoring and load alleviation
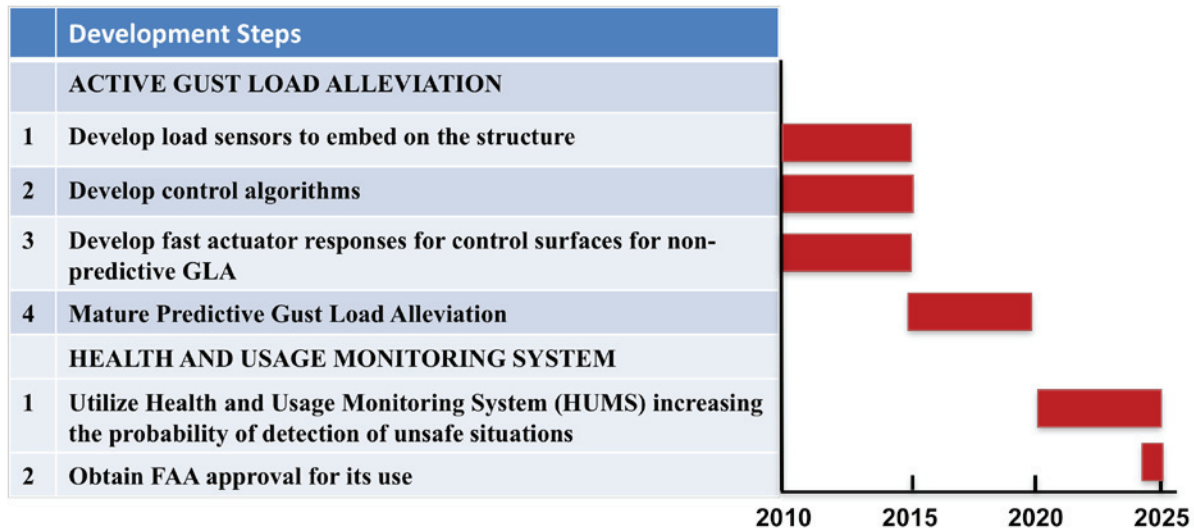
Current State: "Envelope protection" is used in Eurofighter Typhoon; Gust load alleviation is used in Boeing 777, but not designed with active load alleviation as mission-critical (primarily for passenger comfort)

Goal: Use active gust load alleviation and health monitoring to increase material unit strength. Reach maximum load factor of $N_{max} = 2.5$, which represents the maximum pull-up load factor with gust

Probability of reaching goal (TRL4 by 2025): 80-90% (gust prediction), 90% (health and usage monitoring/structural health monitoring)

Main technology development: Active Gust Load Alleviation (GLA); Health and Usage Monitoring System (HUMS) including Structural Health Monitoring (SHM).

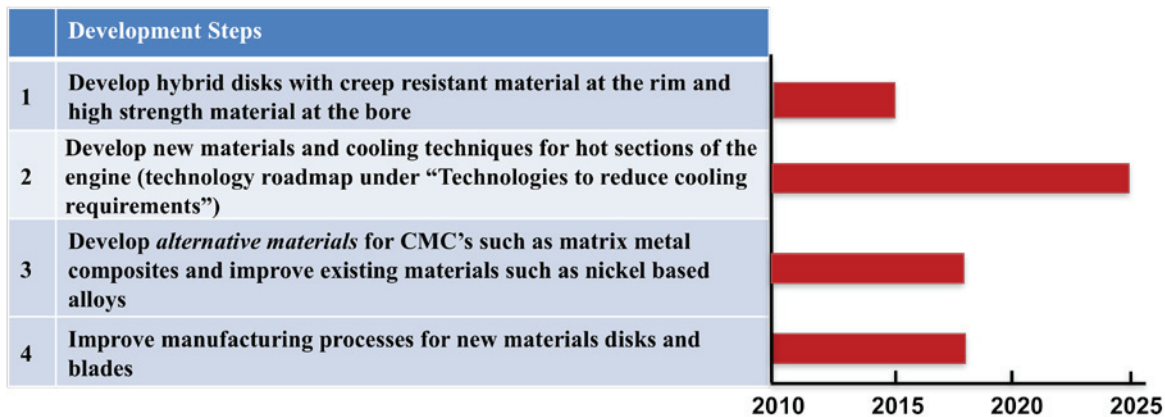| Development Steps	
ACTIVE GUST LOAD ALLEVIATION	
1	Develop load sensors to embed on the structure
2	Develop control algorithms
3	Develop fast actuator responses for control surfaces for non-predictive GLA
4	Mature Predictive Gust Load Alleviation
HEALTH AND USAGE MONITORING SYSTEM	
1	Utilize Health and Usage Monitoring System (HUMS) increasing the probability of detection of unsafe situations
2	Obtain FAA approval for its use

2010   2015   2020   2025

8.2.7 Technologies to Reduce Engine Weight. New materials.

Current State: Fan: titanium alloys; compressors: titanium front stages and nickel alloys rear stages; turbine: nickel superalloys

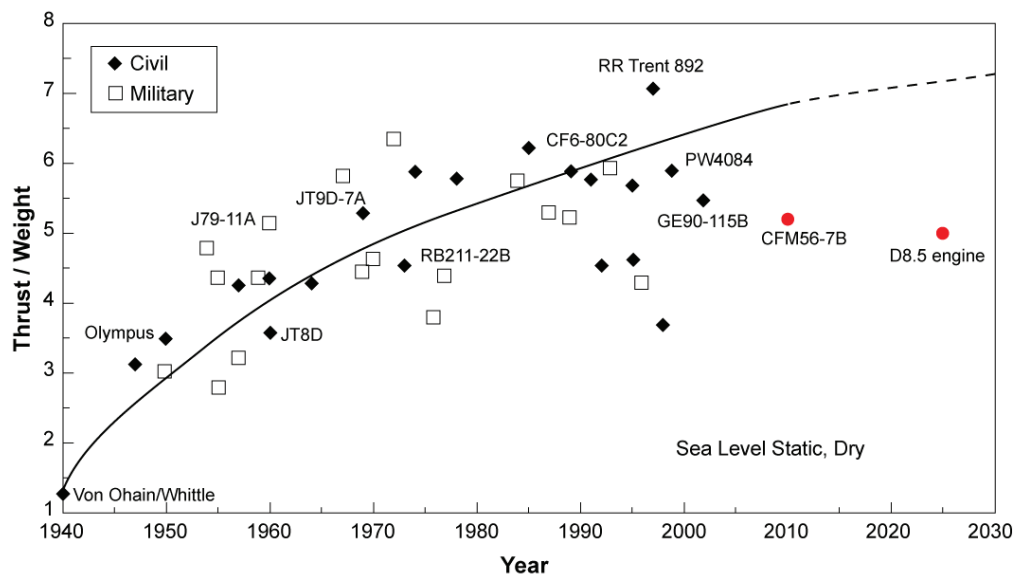**Goal:** 15-20% reduction in engine weight. Fan: advanced carbon composites and titanium; compressors: titanium matrix composite disks, titanium front stages and nickel alloys rear stages; turbines: ceramic matrix composites front stages, nickel alloys rear stages, TiAl

Probability of reaching goal (TRL4 by 2025): 75%

Main technology development: New materials for rear stages of the compressor and front stages of the turbine

	Development Steps
1	Develop hybrid disks with creep resistant material at the rim and high strength material at the bore
2	Develop new materials and cooling techniques for hot sections of the engine (technology roadmap under "Technologies to reduce cooling requirements")
3	Develop *alternative materials* for CMC's such as matrix metal composites and improve existing materials such as nickel based alloys
4	Improve manufacturing processes for new materials disks and blades

2010   2015   2020   2025

Technologies to Reduce Engine Weight
Historical Trend Graph[121]

8.2.8 Technologies to reduce cooling: T_{metal} turbine and advanced cooling techniques

Current State: Nickel based alloys with temperature capability of 1350 K with film cooling effectiveness of 0.3

Goal: Combination of new materials and thermal barrier coatings with temperature capability of 1500 K with film cooling effectiveness of 0.4 or development of new materials like ceramic matrix composites with temperature capability of 1700 K.

Probability of reaching goal (TRL4 by 2025): 75%

Main technology development: use of new materials in hot sections of the engine, and develop advanced cooling techniques

---

[121] Ballal, D.R. and J. Zelina. " Progress in Aeroengine Technology (1939-2003)", Journal of Aircraft, v41-1, 2004.

**Turbine Inlet Temperature
Historical trend and forecast graph**[122]
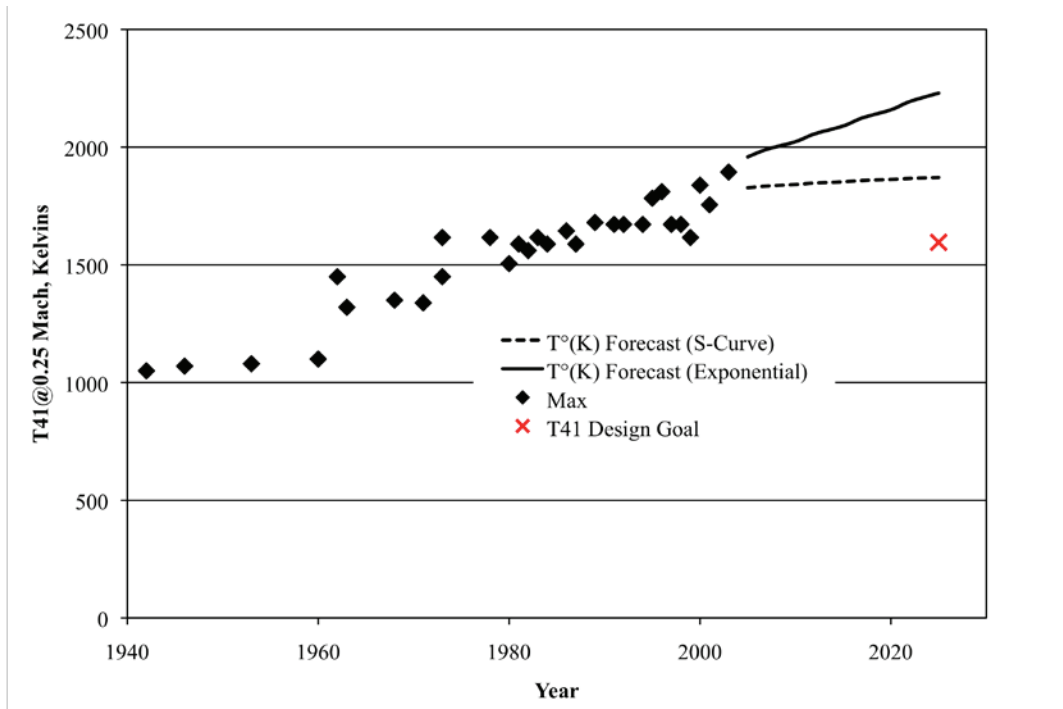
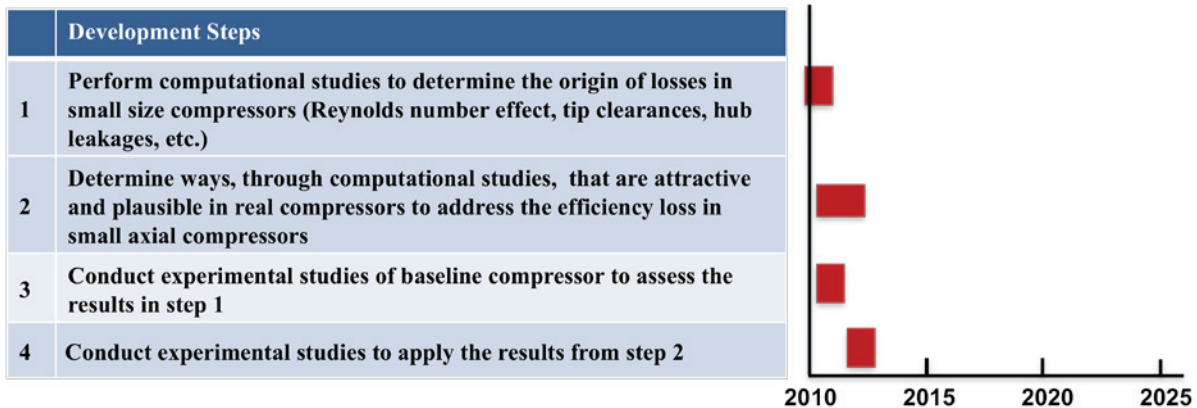### 8.2.9   Small axial compressor Efficiency

Current State: Radial compressors for corrected mass flow around 3 lb/s at the exit of the high pressure compressor

Goal: 90% for an axial high pressure compressor with exit corrected mass flow between 1-2 lb/s and 93% for low pressure compressor
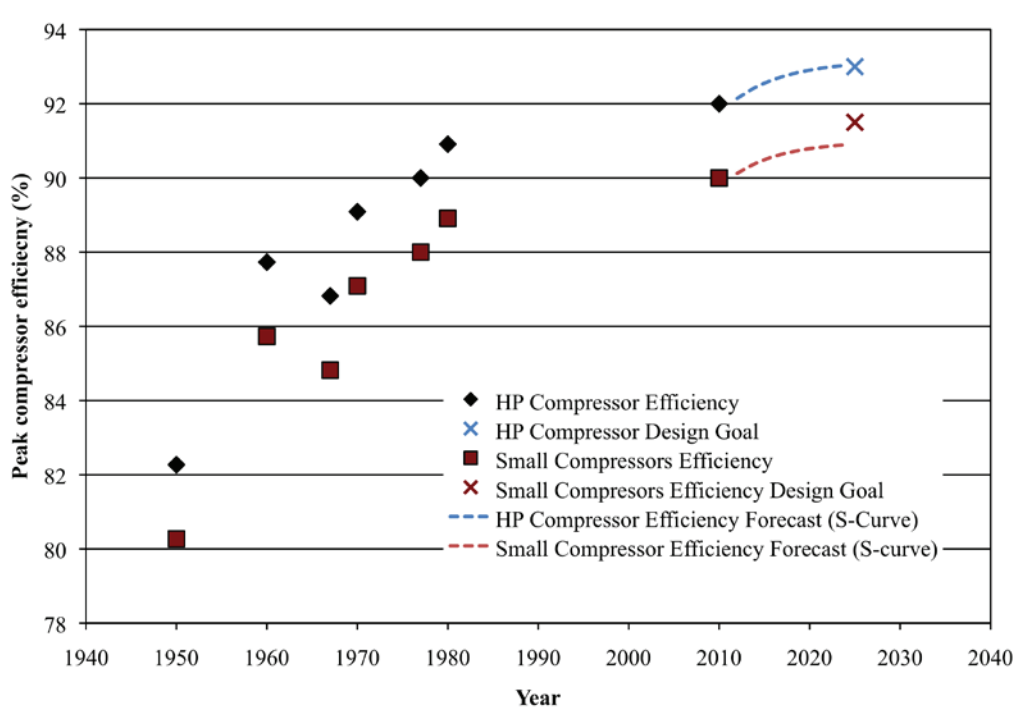
Probability of reaching goal (TRL4 by 2025): 80%

Main technology development: Reduce tip clearance and hub leakage flow losses

---

[122] Cumpsty, N. Jet Propulsion - A simple guide to the aerodynamic and thermodynamic design and performance of jet engines. Cambridge, UK : Cambridge University Press, 2003.

	Development Steps
1	Perform computational studies to determine the origin of losses in small size compressors (Reynolds number effect, tip clearances, hub leakages, etc.)
2	Determine ways, through computational studies, that are attractive and plausible in real compressors to address the efficiency loss in small axial compressors
3	Conduct experimental studies of baseline compressor to assess the results in step 1
4	Conduct experimental studies to apply the results from step 2

Peak compressor efficiency
Historical trend and forecast graph [123]
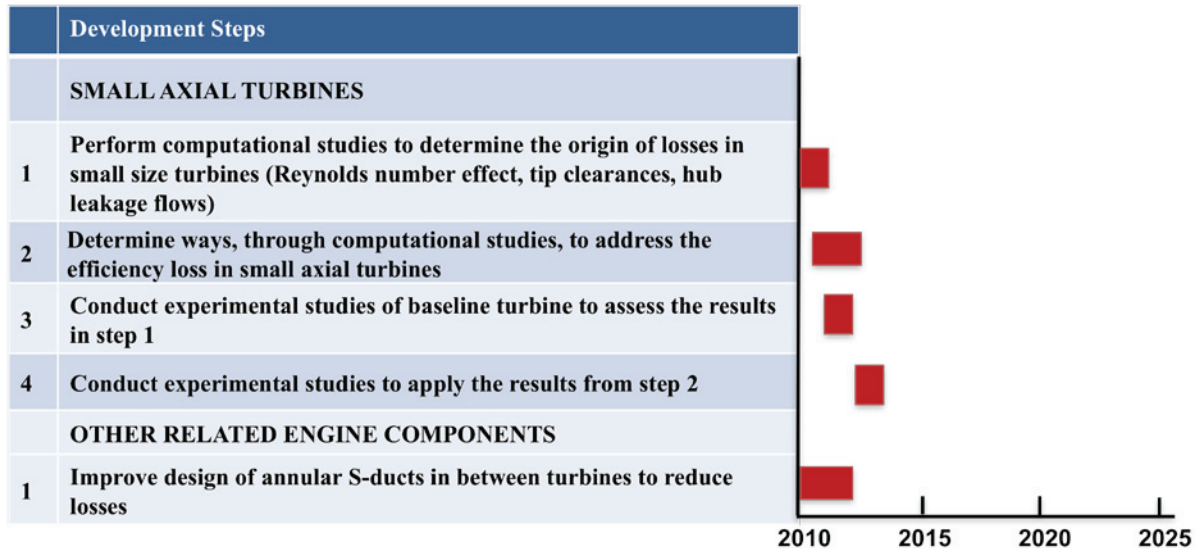

8.2.10 Small axial turbine efficiency

Current State: 91% high pressure turbine efficiency (with cooling flows of 20%), 92% low pressure turbine efficiency

Goal: 92.5% for uncooled high pressure turbine and 93% for low pressure turbine of small size

---

[123] As quoted by Cumpsty, N., "Compressor Aerodynamics", 1989 Longman Scientific and Technical, 2004 Krieger, 2004.

Probability of reaching goal (TRL4 by 2025): 80% for high pressure turbine; 90% for low pressure turbine

Main technology development: Increase efficiency for small size turbines

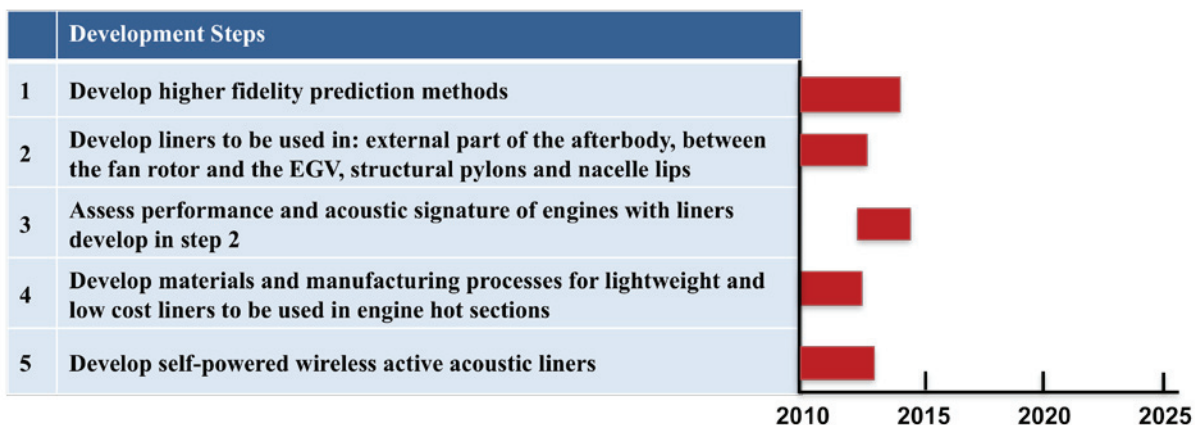|	Development Steps	
	SMALL AXIAL TURBINES	
1	Perform computational studies to determine the origin of losses in small size turbines (Reynolds number effect, tip clearances, hub leakage flows)	
2	Determine ways, through computational studies, to address the efficiency loss in small axial turbines	
3	Conduct experimental studies of baseline turbine to assess the results in step 1	
4	Conduct experimental studies to apply the results from step 2	
	OTHER RELATED ENGINE COMPONENTS	
1	Improve design of annular S-ducts in between turbines to reduce losses	

2010   2015   2020   2025

8.2.11 Acoustic Liners

Current State: -2dB for L/H of 1.

Goal: -4dB for L/H of 1 using multi-segment liners

Probability of reaching goal (TRL4 by 2025): 100%

Main technology development: Improve liner performance as bypass ratio increases.

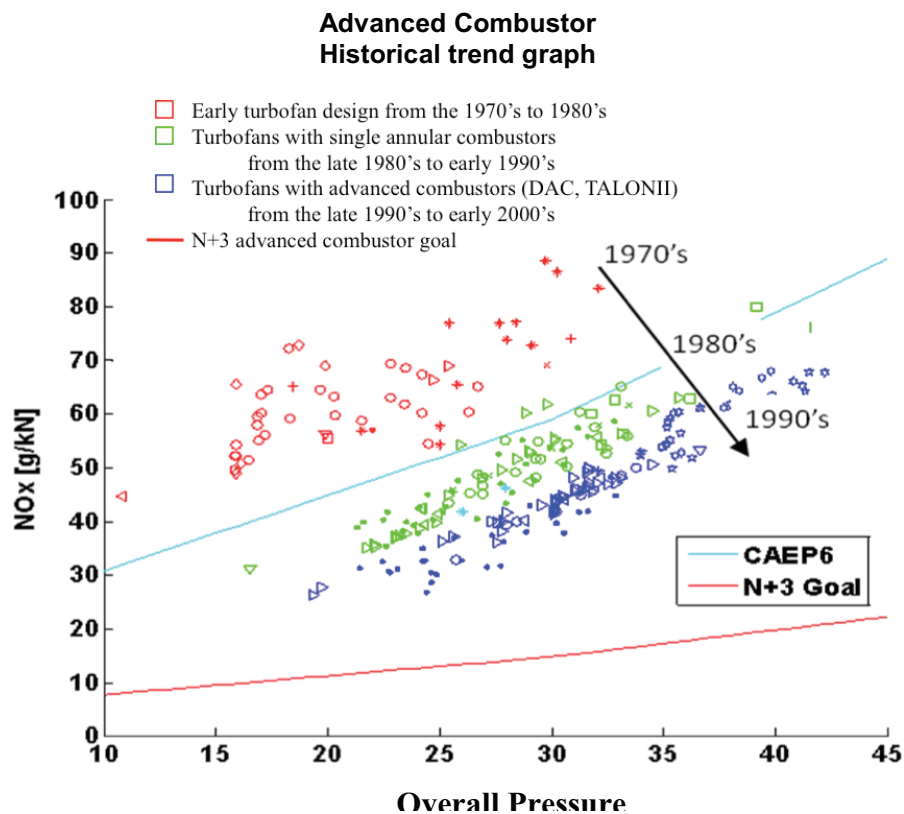|	Development Steps	
1	Develop higher fidelity prediction methods	
2	Develop liners to be used in: external part of the afterbody, between the fan rotor and the EGV, structural pylons and nacelle lips	
3	Assess performance and acoustic signature of engines with liners develop in step 2	
4	Develop materials and manufacturing processes for lightweight and low cost liners to be used in engine hot sections	
5	Develop self-powered wireless active acoustic liners	

2010   2015   2020   2025

8.2.12 Advanced Combustor

Current State: TAPs and Talon-X (from NASA's ultra-efficient engine technology program)

Goal: LDI combustor which, with more efficient engines, will reduce LTO NOx emissions to less than 25% of the CAEP6 standard

Probability of reaching goal (TRL4 by 2025): 100%. Probability of reaching TRL 6 (engine test): 75%

Main technology development: Improve combustor dynamic for lean combustion, and improve combustor cooling

Advanced Combustor
Historical trend graph

REPORT DOCUMENTATION PAGE

Form Approved
OMB No. 0704-0188

1. REPORT DATE *(DD-MM-YYYY)* 01-12-2010	**2. REPORT TYPE** Final Contractor Report	**3. DATES COVERED** *(From - To)*

4. TITLE AND SUBTITLE
N+3 Aircraft Concept Designs and Trade Studies, Final Report

Volume 1

5a. CONTRACT NUMBER

5b. GRANT NUMBER

5c. PROGRAM ELEMENT NUMBER

6. AUTHOR(S)
Greitzer, E., M.; Bonnefoy, P., A.; Blanco, E., De la Rosa; Dorbian, C., S.; Drela, M.; Hall, D., K.; Hansman, R., J.; Hileman, J., I.; Liebeck, R., H.; Lovegren, J.; Mody, P.; Pertuze, J., A.; Sato, S.; Spakovszky, Z., S.; Tan, C., S.; Hollman, J., S.; Duda, J., E.; Fitzgerald, N.; Houghton, J.; Kerrebrock, J., L.; Kiwada, G., F.; Kordonowy, D.; Parrish, J., C.; Tylko, J.; Wen, E., A.; Lord, W., K.

5d. PROJECT NUMBER
NNX08AW63A

5e. TASK NUMBER

5f. WORK UNIT NUMBER
WBS 561581.02.08.03.13.03

7. PERFORMING ORGANIZATION NAME(S) AND ADDRESS(ES)
Massachusetts Institute of Technology

8. PERFORMING ORGANIZATION REPORT NUMBER
E-17419-1

9. SPONSORING/MONITORING AGENCY NAME(S) AND ADDRESS(ES)
National Aeronautics and Space Administration
Washington, DC 20546-0001

10. SPONSORING/MONITOR'S ACRONYM(S)
NASA

11. SPONSORING/MONITORING REPORT NUMBER
NASA/CR-2010-216794-VOL1

12. DISTRIBUTION/AVAILABILITY STATEMENT
Unclassified-Unlimited
Subject Category: 05
Available electronically at http://gltrs.grc.nasa.gov
This publication is available from the NASA Center for AeroSpace Information, 443-757-5802

13. SUPPLEMENTARY NOTES

14. ABSTRACT
MIT, Aerodyne Research, Aurora Flight Sciences, and Pratt & Whitney have collaborated to address NASA's desire to pursue revolutionary conceptual designs for a subsonic commercial transport that could enter service in the 2035 timeframe. The MIT team brings together multidisciplinary expertise and cutting-edge technologies to determine, in a rigorous and objective manner, the potential for improvements in noise, emissions, and performance for subsonic fixed wing transport aircraft. The collaboration incorporates assessment of the trade space in aerodynamics, propulsion, operations, and structures to ensure that the full spectrum of improvements is identified. Although the analysis focuses on these key areas, the team has taken a *system-level approach* to find the integrated solutions that offer the best balance in performance enhancements. Based on the trade space analyses and system-level assessment, two aircraft have been identified and carried through *conceptual design* to show both the *indepth engineering* that underpins the benefits envisioned and also the *technology paths* that need to be followed to enable, within the next 25 years, the development of aircraft three generations ahead in capabilities from those flying today.

15. SUBJECT TERMS
Jet propulsion; Subsonic aircraft

16. SECURITY CLASSIFICATION OF:			**17. LIMITATION OF ABSTRACT**	**18. NUMBER OF PAGES**	**19a. NAME OF RESPONSIBLE PERSON** STI Help Desk (email:help@sti.nasa.gov)
a. REPORT U	**b. ABSTRACT** U	**c. THIS PAGE** U	UU	187	**19b. TELEPHONE NUMBER** *(include area code)* 443-757-5802

Standard Form 298 (Rev. 8-98)
Prescribed by ANSI Std. Z39-18